Strategies for intervertebral disc regeneration

Strategieën voor regeneratie van tussenwervelschijven
(met een samenvatting in het Nederlands)

Proefschrift

ter verkrijging van de graad van doctor aan de
Universiteit Utrecht
op gezag van de
rector magnificus, prof.dr. H.R.B.M. Kummeling,
ingevolge het besluit van het college voor promoties
in het openbaar te verdedigen op

maandag 3 juli 2023 des middags te 12.15 uur

door

Jie Du

geboren op 21 oktober 1989
te Sichuan, China

Promotor:

Prof. dr. M.A. Tryfonidou

Copromotoren:

Dr. L.B. Creemers
Dr. S. Grad

Beoordelingscommissie:

Prof. dr. R.L.A.W. Bleys
Prof. dr. K. Ito
Prof. dr. ir. T.H. Smit
Prof. dr. ir. J. Malda
Prof. dr. P.A.J.T. Robe

Dit proefschrift werd (mede) mogelijk gemaakt met financiële steun van:
European Union's Horizon 2020 research and innovation programme under the Marie Skłodowska-Curie grant agreement No 642414 (TargetCaRe), No 801540 (CoFund).

Table of Contents

Chapter 1

General Introduction and Outline 1

Chapter 2

Proinflammatory Intervertebral Disc Cell and Organ Culture Models Induced by Tumor Necrosis Factor-α 21

Chapter 3

Intradiscal Injection of Human Recombinant BMP-4 Does Not Reverse Intervertebral Disc Degeneration Induced by Nuclectomy in Sheep 45

Chapter 4

Functional Cell Phenotype Induction with TGF-β1 and Collagen-polyurethane Scaffold for Annulus Fibrosus Rupture Repair 79

Chapter 5

The Function of CD146 in Human Annulus Fibrosus Cells and Mechanism of the Regulation by TGF-β 107

Chapter 6

Drug Retention after Intradiscal Administration 135

Chapter 7

Summary and General Discussion 163

Appendics

Nederlands Samenvatting 184

Abbreviations 187

List of Pubications and Manuscripts 190

Acknowledgements (致谢) 192

Curriculum Vitae 196

Chapter 1

General Introduction and Outline

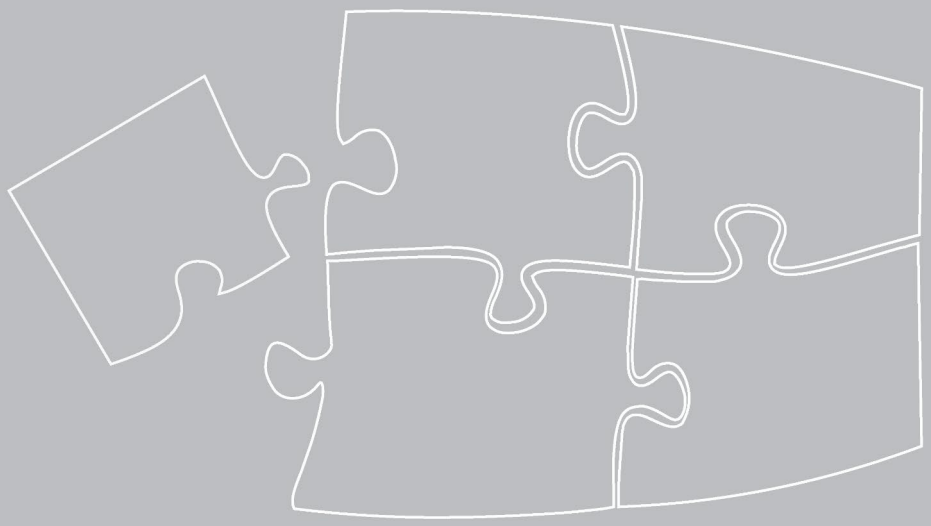

1. Chronic low back pain

Low back pain (LBP) is one of the leading causes of disability worldwide, affecting roughly 20% of the world population and causing a heavy economic burden to society and the health care system due to decreased productivity and increased healthcare costs [1]. Most people experience an episode of LBP in their lifetime [2]. About 5-10% of these patients develop chronic LBP (CLBP) defined as LBP that lasts longer than three months [3]. CLBP accounts for most of the economic burden caused by LBP, with approximately two-thirds of the total costs being associated with indirect consequences (e.g., loss of productivity) [4]. In the United States, the total cost for the management of patients with CLBP is estimated to exceed US$100 billion per year [5]. This number is estimated to be around £2.8 billion in the UK [6], € 3.5 billion in the Netherlands [7], AU$4.8 billion in Australia [8], and US$ 2.2 billion in Brazil [9].

CLBP is prevalent in almost all age groups and increases with age, where the peak prevalence ranges from 28% to 42% in people between 40 and 69 years [10, 11]. The etiology of CLBP is not well elucidated, but multiple studies suggest that intervertebral disc (IVD) degeneration is responsible for 40% of CLBP cases [12-14].

2. Intervertebral disc

IVDs are soft pads that lie between the vertebral bodies of the spine and provide stability and flexibility to the spinal column by absorbing and distributing mechanical loads [15]. IVD consists of a cartilaginous jelly-like center, the nucleus pulposus (NP), the surrounding concentric lamellae, comprising the fibrocartilaginous annulus fibrosus (AF), and inferior and superior hyaline cartilaginous endplates (EPs), which connect the IVD to the adjacent vertebral bodies. The IVD is an avascular and poorly innervated tissue. Blood vessels and nerves are only found in the peripheral AF and in the subchondral bone plate [16].

The NP contains a low density of chondrocyte-like cells (approximately 3-5×10^3 cells/mm^3) when compared with other tissues, such as cartilage (1×10^4 cells/mm^3) and liver (1×10^5 cells/mm^3) [15, 17-20]. These cells are surrounded by a highly hydrated extracellular matrix (ECM) comprising of proteoglycan, collagen type II, and little elastin. In the NP proteoglycans are the most abundant component, as opposed to hyaline cartilage, where collagen type II composes most of the matrix [21, 22]. Proteoglycans are glycosylated proteins with covalently attached highly anionic glycosaminoglycans (GAG), which provide hydration and swelling pressure [23]. The high concentration of proteoglycans results in significant binding of water which is essential to keep the fluidity and elasticity of the NP, allowing homogeneous distribution of the mechanical loading of the spine.

The cell density in the AF is approximately 3-9×10^3 cells/mm^3, similar to the NP [19, 24, 25]. The AF can be generally divided into inner and outer AF. The inner AF is a transition zone and has similar characteristics to the NP. In contrast, the outer AF is identified by well-organized concentric lamellae. From the inner to outer AF, proteoglycans and collagen type II are gradually replaced by collagen I [26, 27]. The inner AF is exposed to high hydrostatic pressures of the NP, while the outer AF is bearing tensile and torsional forces from the spine, preventing NP protrusion.

The EPs are similar to hyaline cartilage in cell type and ECM composition. They are composed of chondrocytes and ECM rich in collagen type II and proteoglycan [28]. The two EPs separate the NP and AF from the vertebral bodies and provide a firm attachment of the IVD to the boney structures. In addition, the EP represents the main nutrition route for the IVD, as in the adult disc, only the peripheral outer AF is vascularized by small capillary vessels [29, 30].

2.1. Intervertebral disc degeneration

Although the etiology of IVD degeneration is not entirely understood, it is widely accepted that multiple endogenous and exogenous factors contribute to this complex process, including age, genetic predisposition, obesity, injury, trauma, and lifestyle [10, 31-36]. Endogenous factors, such as genetic variants, may predispose the IVD to degeneration, and exogenous factors, such as injury and herniation, may be involved in the onset and/or exacerbation of degeneration. The morphological changes occurring during IVD degeneration include loss of disc height, osteophyte formation, reduced water content and fibrosis of the NP, fissures and disorganization of the AF, and sclerosis of the vertebral EPs [37, 38].

Loss and disorganization of the ECM are the prevalent features of IVD degeneration [38]. It is generally accepted that this is caused by abnormal ECM metabolism. In the degenerative IVD, the synthesis of proteoglycan and collagen II is markedly decreased in the NP, while the collagen type I content is increased in the NP and inner AF, resulting in a reduced ratio of collagen type II to I [39]. Collagen type X appears in degenerated discs and is associated with cell clustering and cleft formation, indicating abnormal cellular activity [40]. However, in the early stage of IVD degeneration, increased collagen II expression in the NP is considered an attempted repair mechanism [41].

The primary ECM degradation process is mediated by the MMPs (matrix metalloproteinases) and the ADAMTSs (a disintegrin and metalloprotease with thrombospondin motifs). During IVD degeneration, both expression and/or activity of several MMPs and ADAMTSs are increased, including MMP-1, -2, -3, -7, -9 -13, -14, and ADAMTS-1, -4, -5, -7 -15 [39, 42-46]. The degradation of the ECM components gives rise to the histological and functional degenerative changes mentioned above. Decreased levels of proteoglycans lead to dehydration of the NP, which subsequently leads to impaired mechanical properties during loading, which can further accelerate structural damage. The damage may induce inflammation and worsen IVD degeneration [47]. In addition, in a healthy IVD proteoglycans act as an inhibitor of vascularization and nerve ingrowth. Proteoglycan loss may hence lead to angiogenesis and nerve ingrowth which are highly associated with pain [48-50]. In the IVD, the production of ECM is restricted by the disc environment due to limited access to nutrients and low cell density. This condition is thought to deteriorate degeneration. Calcification of EP during IVD degeneration further decreases nutrient diffusion and increases accumulation of anaerobic glycolysis metabolites, leading to a decline in pH [51]. GAG synthesis was shown to be reduced by 80% when NP cells were cultured at pH 6.3 found in the degenerated IVD, compared to pH 7.2 [52]. Therefore, inadequate nutrient supply and waste removal can reduce ECM by decreasing production and increasing cell death. Altogether, abnormal ECM metabolism, decreasing anabolism and increasing catabolism result in IVD degeneration, and the avascular nature of IVD deteriorate this degenerative progress.

2.2. Inflammation and disc degeneration

Inflammation is another well-known factor involved in both disc degeneration and pain, although it may also play a role in maintaining the homeostasis of the disc and repair after degeneration [45]. The healthy IVD has been identified as an immune-privileged organ. Through the unique structure of the IVD, the NP is isolated from the host's immune system by a protective barrier constituted by the non-vascularized AF and the EPs [53]. However, when this protective barrier is damaged, (auto)immune responses and/or a downstream cascade of inflammation may be initiated by infiltration and activation of immune cells. Autoantibodies against collagen type I, II, V, and aggrecan have been identified in human degenerated IVD samples [54]. Studies showed that activated T and B cells were elevated upon subcutaneous implantation of autologous NP in pig [55], and immune cells, such as macrophages, neutrophils, and T cells, were recruited to degenerated IVDs in animal models and human patients [56, 57]. The immune cells aggravate disc degeneration by secreting inflammatory mediators, including IL-1β, TNF-a, IFN-γ, chemokines, and prostaglandin E2 (PGE) [45, 58]. These inflammatory mediators can amplify inflammation by further recruiting immune cells and inducing inflammation of native disc cells. For instance, TNF-α and IL-1β regulate chemokine (C-C motif) ligand 3 (CCL3) expression in NP cells and promote macrophage infiltration in degenerated, herniated discs [59]. Although immune cell infiltration causes inflammation, it is unclear whether it is the initial trigger of inflammation, as the expression of various proinflammatory mediators is upregulated in degenerated disc cells. Excessive loading for example can cause cell death and inflammatory mediator upregulation in IVD cells [65, 66]. IL-1β and TNF-α are two extensively investigated inflammatory factors in IVD degeneration [60-62]. TNF-α and IL-1β can induce disc degeneration by decreasing the synthesis of ECM proteins and promoting proteolytic enzyme production. Many studies showed that IL-1β and/or TNF-α upregulate MMP-1, -3, -9, -10, -13 and ADAMTS-4, -5, but downregulate collagen type II and aggrecan expression [43, 63-67]. Furthermore, they can induce apoptosis and accelerate senescence of disc cells [43]. In addition, these cytokines are related to nerve fiber and blood vessel ingrowth and pain processes. Also in human IVD degeneration, IL-1β expression was shown to be correlated with the expression of vascular endothelial growth factor (VEGF), nerve growth factor (NGF), and brain-derived neurotrophic factor (BDNF). Additionally, both IL-1β and TNF-α stimulation promote the gene expression of VEGF, NGF, and BDNF in NP cells isolated from patient tissues [68]. However, inflammation may also have positive effects. Inflammatory cytokines and chemokines and/or their receptors are expressed in healthy IVD cells [45, 61, 69]. Recently, a complete lack of IL-1α/β enhanced rather than prevented IVD degeneration in mice [70]. Control of inflammation has been reported to be critical in shifting the degeneration/regeneration balance towards regeneration in other vascularized tissue, such as bone [71]. Altogether, inflammatory processes may be indispensable for IVD health, however, exacerbated inflammation is undoubtedly correlated with accelerated IVD degeneration.

3. Current treatments for chronic low back pain

Non-pharmacological therapy, including supervised exercise and cognitive-behavioral therapies, are recommended as the first-line treatments for patients with CLBP [72]. Anti-inflammatory and analgesic medication is commonly used to relieve pain, such as non-steroidal anti-inflammatory drugs (NSAIDs) and opioids [73]. However, these are seldomly effective, prolonged oral intake of

NSAIDs is associated with gastrointestinal and cardiovascular adverse effects, and long-term use of opioids carries the risk of addiction [72, 74]. Recently, the use of duloxetine, an antidepressant with activity against neuropathic pain, has shown some effects as a pharmacological intervention [75]. Finally, surgical treatment is often the only alternative for patients with CLBP for whom conservative and non-invasive treatments failed. Spinal fusion is sometimes indicated. However, the effects of surgical treatment for CLBP are unsatisfactory, in contrast to patients with disc herniation resulting in the severity of pain and/or disability, where surgery yields efficient and fast relief of radiculopathy [76]. A study reported there was no difference in the outcome of chronic LBP patients randomized to lumbar fusion versus cognitive intervention and exercises in a 9-year follow-up [77]. In addition, the fusion of vertebrae has been suggested to alter the biomechanics of the rest of the spine and increase the risk of adjacent discs becoming degenerated [78]. The whole IVD replacement is another alternative, however, the long-term outcome is comparable to spinal fusion [79]. The management of complications following IVD replacement can be a daunting and challenging task [80]. Moreover, so far, all the treatments in use only focus on relieving pain, and no treatment can halt or reverse disc degeneration, which could represent a long-term solution for discogenic CLBP.

4. Prospective treatments for chronic low back pain

Several strategies have been investigated to delay IVD degeneration and induce regeneration, and thus resolve discogenic pain to meet the unmet clinical needs. These strategies can be divided into cell-based strategies and acellular strategies, like local drug delivery. Promising results have been reported in both preclinical and clinical studies, although they are still a distance from clinical application [81, 82].

4.1. Cell-based therapies

4.1.1. NP regeneration

The cell density of the NP is low, and cell viability is impaired during degeneration [15, 24]. Cell transplantation can aid in the rebuilding of cellular activity and achieve IVD regeneration. The NP is an indispensable functional center of IVD, and many pathological changes of IVDD are firstly and prominently displayed in the NP region, suggesting its crucial role in IVDD [83]. Primary studies, therefore, focused on restoring the function of the NP.

Many types of cells have been evaluated in clinical trials, including disc chondrocyte-like cells, articular chondrocytes, and several types of mesenchymal stem cells (MSCs) [84]. NP cells can produce native ECM and survive in the harsh disc microenvironment, making them a potential transplantation resource. Autologous disc-derived chondrocytes implantation following discectomy resulted in an improvement in pain and preservation of hydration two years after injection compared to discectomy alone in traumatic disc herniation patients [85]. Articular chondrocytes, as they produce ECM similar to that of NP cells, are another option. Implanting allogeneic juvenile chondrocytes in the treatment of lumbar spondylosis with LBP showed a similar outcome as disc-derived cells in the Phase I study [86]. However, the Phase II study was terminated for unrevealed reasons. Given the limited source of both disc-derived and articular

chondrocytes, their application potential, however, might be restricted. MSCs have been widely evaluated and seem to be a promising strategy for IVD regenerative therapies owing to their broad sources, self-renewal capacity, and immunosuppressive properties, although their capacity to differentiate *in vivo* is nowadays accepted to be virtually nonexistent [87]. Various clinical studies involving the delivery of autologous and/or allogeneic marrow-derived MSCs (BM-MSCs), adipose-derived MSCs (ASCs), and umbilical cord-derived MSCs (UC-MSCs) have been carried out or are ongoing [84]. The results from finished studies were promising, although the number of patients was relatively small and lacked placebo-controls [88-90]. To date, also several types of disc-derived stem cells, according to their localization within the disc, have been isolated; namely cartilage end plate-derived stem cells (CE-SCs), AF-derived stem cells (AF-SCs), and NP-derived stem cells (NP-SCs) [91, 92]. A study compared the regenerative potential of human BM-MSCs, AF-SCs, NP-SCs, and CE-SCs in a rabbit model [93]. Results indicated the CE-SC-seeded alginate construct was the most potent in inducing NP regeneration, while AF-SCs were the least potent, with NP-SCs and BM-MSCs displaying medium potency [93]. In several studies, induced pluripotent stem cells (iPSCs) have been re-differentiated towards MSC-like, notochordal cell-like, or NP-like phenotypes *in vitro* [94-96]. Cells derived from induced iPSCs represent another promising cell source for IVD regeneration when a safe, effective and reproducible process has been established.

4.1.2. AF repair and regeneration

Besides NP, AF repair and regeneration is another vital topic because an intact structure is essential for the function of the IVD. Moreover, AF injury or degeneration allows nerve ingrowth and disc inflammation related to discogenic pain [97-99]. AF regeneration even faces more challenges than NP due to the complexity of the AF structure, its cell population, and its mechanical environment [83]. Unlike NP, AF is identified as an inhomogeneous tissue, with its cellular and biochemical characteristics varying from outer to inner zones along its radial direction, which leads to region-specific biochemical and biomechanical properties [27, 100, 101]. Hence, successful IVD repair and regeneration requires the recovery of biomechanical and structural properties of healthy AF and the restoration of the behavior of resident cells [102]. In AF tissue engineering, developing an AF construct incorporating cells, bioactive molecules, and biomaterials could be a promising strategy. An appropriate cell source is the first unmet need. Both AF cells and several stem cells could be potential candidates. Cell proliferation and deposition of collagen type I and aggrecan by AF cells was achieved in an AF analogue produced by 3D printed polycaprolactone (PCL) scaffolds with angle-ply architecture *in vitro* [103]. Recently, an MSC-seeded high-density collagen gel for annular repair in a sheep model resulted in an improvement of disc height, Pfirrmann grade, and AF and NP reconstitution and organization [104], although the in situ differentiation capacity of MSCs to the AF cell type was controversial [105]. Genetically engineered silk fleece-membrane-composites enriched with GDF-6 or TGF-β3 maintained the phenotype of human AF cells and promoted IVD-like differentiation of human MSC [106]. Growth factors were used to induce cell proliferation, matrix production, and stem cell differentiation. However, to the best of our knowledge, no AF-specific differentiation protocol has been developed so far. Therefore, the AF cell may be a better alternative for AF tissue engineering until an efficient differentiation method is established. In addition, a biomaterial with appropriate biological and biomechanical compatibility is crucial for successful regeneration of the AF. Several

materials, including collagen type I, fibrinogen and thrombin crosslinked with genipin (FibGen), silk, PCL, and polyurethane, have been reported to construct AF analogs for defects repair *in vitro* and/or *in vivo*, and fabrication methods like 3D printing and electrospinning were used to mimic the native AF structure and promote mechanical properties [103, 104, 107-109]. Altogether AF tissue engineering is considered a promising strategy for AF repair and regeneration.

4.2. Local drug delivery

Access of systemic drugs to the large non-vascularized IVD is very limited. The NP drug concentrations are less than 20% compared with plasma levels after intravenous injection of drugs in rabbits [110]. A study showed it was even worse for human IVD. After intravenous administration, the concentration of cephazolin in the serum (range 31.1-148 mg/L) was much higher than in the disc (range 0-9.5 mg/L) [111]. Hence, local drug administration is increasingly considered a better strategy than systemic administration for increasing the local drug concentration while preventing side effects [112, 113].

4.2.1. Intradiscal injection of anti-inflammatory drugs

Given the vital roles of inflammation in disc degeneration and discogenic LBP, anti-inflammatory drugs have been widely investigated for suppressing the degenerative progress and/or related pain. Intradiscal injection of the traditional anti-inflammatory corticosteroids showed CLBP relief for several months in several trials [114, 115], although conflicting results were obtained [116]. Single intradiscal administration of Etanercept alleviated pain in LBP patients for up to 8 weeks [117]. Intradiscal delivery of celecoxib, a selective cyclooxygenase-2 (COX-2) inhibitor, protected IVD integrity in a puncture-induced canine disc degeneration model and reduced owner-reported pain symptoms in most animals in small cohorts of canine patients with CLBP [118-120]. Anti-inflammatory treatment could delay the progress of disc degeneration and relieve discogenic pain, but the ability to induce regeneration is limited.

4.2.2. Intradiscal injection of growth factors

Growth factors are a group of naturally occurring substances that play essential roles in regulating various cellular processes, including cell proliferation and differentiation. Several growth factors, including platelet-derived growth factor (PDGF), insulin-like growth factor-1 (IGF-1), and fibroblast growth factors (FGFs), showed beneficial effects on disc regeneration [121]. Platelet-rich plasma (PRP), a natural carrier of multiple growth factors, has been reported with encouraging effects in the field of regeneration [122]. *In vitro* studies showed PRP promoted disc cell proliferation and ECM production and was effective against apoptosis and inflammation [123, 124]. It consistently showed promising effects in retaining disc height, preserving cell density and ECM, and increasing the T2 signal intensity *in vivo* [125, 126]. In addition, several clinical trials have been conducted to evaluate the effects of PRP on LBP. LBP patients treated by intradiscal injection of PRP displayed improvement in pain [127, 128]. One component of PRP of which its levels correlated with PRP-induced NP cell-mediated IVD regeneration is TGF-β1 [123].

The transforming growth factor-beta (TGF-β) superfamily is a group of growth factors that have been widely reported in IVD regeneration studies, comprising over 30 members, including the TGF-β subfamily, the growth differentiation factors (GDFs), the inhibins and activins, and the bone morphogenetic proteins (BMPs) [129]. TGF-β signaling plays a crucial role in the development and homeostasis of IVD. Conditional deletion of the TGF-β type II receptor in collagen II expressing cells results in incomplete development of the IVD, in particular of the AF [130]. Inactivating the TGF-β signaling in inner AF cells in the IVD and surrounding growth plate chondrocytes led to the reduction in the area and length of the cartilaginous EP tissue and the increased expression of genes related to matrix degradation [131]. Additionally, TGF-β1 was shown to promote the proliferation and maintain the differentiation capacity of NP cells *in vitro* [132]. Intradiscal injection of TGF-β1 preserved disc height and increased cell proliferation and aggrecan and collagen type II expression within the NP and inner AF in a compression-induced caudal IVD degeneration mouse model [133]. Similar effects were found after intradiscal delivery of GDF-5 into degenerated IVDs in mice and rats [133, 134]. Four phase I/II clinical trials for investigating GDF-5 as a treatment for IVD degenerative disease have been completed (NCT01158924, NCT00813813, NCT01182337, NCT01124006). However, no results have been published to date. Although BMPs were initially known to be involved in osteogenesis, BMP-2 and BMP-7 have been shown to increase ECM production in IVD cells in different species [135-139]. Heterodimeric BMP-2/7 showed the potential to stimulate proteoglycan gene expression and synthesis and exerted no adverse osteogenic effect in the remaining NP after partial nucleotomy in a bovine IVD culture model [140]. The regenerative effects of BMP-2 and BMP-7 were reported in a rabbit disc degeneration model [141, 142]. However, in a goat model of IVD degeneration, intradiscal injection of BMP-2 and BMP-7 showed no evidence of IVD regeneration, similar to intradiscal administration of BMP-7 in a canine study [143, 144]. Recently, BMP-4 showed the most potent efficacy to promote ECM production *in vitro* when compared to other BMPs and TGF-β, suggesting its applicability for disc regeneration [145].

Gene therapy is a promising new strategy for IVD regeneration through the transfer of RNA or DNA to cells to, for instance, silence inflammation-related genes and over-express growth factors. The modified cell can continually express the therapeutic gene once transfection is conducted successfully [146]. Adenovirus constructs containing a human TGF-β1 gene increased TGF-β1 and proteoglycan synthesis after intradiscal injection in rabbit lumbar IVDs [147]. However, current gene therapies for IVDD are at their early stage and still face many challenges. A safe and efficient genetic delivery system should be developed, and more fundamental research on the pathogenesis of IVDD is warranted so novel potential therapeutic targets can be identified and validated.

4.2.3. Delivery system and drug retention

Bioactive molecules could be fast cleared from the IVD or/and degraded by endogenous enzymes in the IVD after bolus intradiscal delivery. Using drug delivery systems for intradiscal treatment has the potential to prolong local drug exposure and bioactivity while reducing the disadvantage of repeated injection and potential side effects [113]. Drug delivery systems are designed in various forms and shapes, including hydrogels, microparticles, and nanoparticles of biomaterials, which can be used to encapsulate small molecules, peptides and proteins, and nucleic acids

drugs, depending on their purpose [148]. Microparticles and hydrogels are explored as drug depots for local extracellular drug release and slow clearance, whereas nanoparticles can be used for intracellular and/or intratissue targeting but are faster cleared. A thermoreversible hyaluronan-poly (N-isopropyl acrylamide) (HAP) hydrogel was also shown to improve stromal cell-derived factor-1α (SDF-1α) delivery and recruitment of MSCs in an *ex vivo* model [149]. However, no evidence of IVD regeneration was observed after intradiscal injection of HAP-SDF-1α in a rat caudal IVD degeneration model [150]. In contrast, releasing of SDF-1α in an albumin/heparin nanoparticle induced stem cell migration and intervertebral disc regeneration in a similar rat model [151]. This indicates that the type of drug delivery system may affect the therapeutic results. Extended-release of triamcinolone acetonide (TAA) by poly (lactic-co-glycolic acid) (PLGA) microspheres (Zilretta®) was FDA-approved for the treatment of pain in knee osteoarthritis (OA). In addition, prolonged TAA release by a polyester amide (PEA) microsphere platform has shown potential positive effects on relieving pain in a canine IVD degeneration model and canine OA patients [152-154]. The PEA-based delivery system has been considered a better alternative for intradiscal injection than PLGA because the degradation products of PLGA decrease the local pH levels, PEA not [113, 155]. In addition, PEA degradation is mainly driven by the activity of serine protease, which is elevated in degenerated disc tissue, resulting in a degeneration tuning drug release feedback loop [156, 157]. No matter which delivery system is used, the drug retention pattern in IVD is crucial to tune and design the optimal local therapeutic strategy but is rarely investigated *in vivo*. Drug release from the delivery system is commonly evaluated *in vitro*. However, *in vivo*, multiple factors affect the release of drugs from the delivery and even the clearance of the delivery system itself [157-159]. Therefore, more fundamental knowledge on drug retention *in vivo* is needed.

5. Aims and thesis outline

This thesis aims to explore potential therapeutic strategies for NP disc degeneration and achieve NP and AF regeneration in IVD degeneration, focusing on developing tools to test these strategies to minimize the use of experimental animals.

Aim 1: To investigate anti-inflammatory treatments in IVD degeneration using an *ex vivo* organ culture model

Inflammation plays a crucial role in IVD degeneration and discogenic pain. Proinflammatory cytokine TNF-α is expressed at high levels in degenerated IVD. To bridge the gap between *in vitro* and *in vivo* studies on IVDD, an *ex vivo* organ culture model is developed to investigate the role of TNF-α in IVD degeneration in **chapter 2**. In this model, a single dose of TNF-α is intradiscally injected into bovine caudal IVD. The injected dose will need to be optimized depending on the disc size. To mimic the *in vivo* physiological mechanical conditions, IVDs will be cultured with a mechanical loading system and followed up via GAG release, inflammatory cytokine production, as well as expression of degeneration-associated genes. This model could be used to investigate the mechanisms of TNF-α in IVD degeneration and screen for therapeutic drugs targeting IVD inflammation and subsequent degeneration.

Aim 2: Evaluate the potential application of BMP-4 for IVD regeneration.

BMP-4 was shown to promote ECM production *in vitro* more strongly than other BMPs and TGF-β, suggesting its applicability for disc regeneration. In **chapter 3**, the effects of BMP-4 on IVD regeneration will be evaluated *in vitro* and *in vivo*. *In vitro,* the effects of BMP-4 on cell proliferation and ECM production will be measured in a pellet culture model of sheep NP and AF cells. If effective *in vitro*, the effects of BMP-4 will be assessed *in vivo* on a nucleotomy-induced sheep lumbar model of IVD degeneration. Anticipated outcomes to monitor regenerative effects are magnetic resonance imaging (MRI), micro-computed tomography (Micro-CT), and histological and biochemical measurements.

Aim 3: Develop a complex construct including scaffold, hydrogel, growth factor, and cells for AF repair.

To develop an AF repair strategy that can restore the mechanical and biological properties of the injured AF, a polyurethane (PU) scaffold, collagen I hydrogel, TGF-β, and AF cells will be studied in **chapter 4**. In this construct, TGF-β pre-treated AF cells with a functional AF phenotype will be encapsulated in a TGF-β-supplemented collagen I hydrogel and seeded into a porous PU scaffold. The distribution and ECM production of cells in the scaffold will be assessed *in vitro.* Then the construct will be evaluated in an *ex vivo* bioreactor-loaded organ culture AF defect model. In **chapter 4,** the functional AF phenotype induced by TGF-β is shown to be accompanied by high expression of the cell surface marker CD146. In **chapter 5** the specific function of CD146 and the mechanism of the regulation by TGF-β in AF cells will be studied. CD146 and several TGF-β related pathways will be inhibited by either short hairpin RNAs or small molecule inhibitors. After silencing of CD146 in AF cells, cell contractility and AF functional gene expression will be evaluated and further complemented with functional studies of identified key players in this signaling pathway order to clarify the potential pathways modulating CD146 after stimulation by TGF-β.

Aim 4: To study drug retention in IVD after local administration.

Local drug delivery has been considered an effective and safe strategy for IVD treatment. Knowledge regarding retention of the delivered drug *in vivo* is vital to optimize such therapeutic strategies. In **chapter 6**, a ^{19}fluorine-labelled random peptide (^{19}F-P) will be used to mimic peptide drugs. The retention of ^{19}F-P will be studied in the whole organ bovine IVD culture system and upon injection into healthy and degenerated lumbar IVDs in the sheep model of IVD degeneration (**chapter 3)** and detected by ^{19}fluorine nuclear magnetic resonance spectrum in tissue extracts. Additionally, a near-infrared (NIR) fluorescent dye, mimicking small molecule drugs, will be loaded into PEA microspheres and injected into healthy and degenerated rat caudal IVD. Retention of the dye can be detected by NIR imaging, indicating the retention of the hydrophobic small molecule drugs after intradiscal administration.

References:

[1] G.B.D. Disease, I. Injury, C. Prevalence, Global, regional, and national incidence, prevalence, and years lived with disability for 310 diseases and injuries, 1990-2015: a systematic analysis for the Global Burden of Disease Study 2015, Lancet 388(10053) (2016) 1545-1602.
[2] G.B. Andersson, Epidemiological features of chronic low-back pain, Lancet 354(9178) (1999) 581-5.
[3] A. Parthan, C.J. Evans, K. Le, Chronic low back pain: epidemiology, economic burden and patient-reported outcomes in the USA, Expert Rev Pharmacoecon Outcomes Res 6(3) (2006) 359-69.
[4] J. Kigozi, K. Konstantinou, R. Ogollah, K. Dunn, L. Martyn, S. Jowett, Factors associated with costs and health outcomes in patients with Back and leg pain in primary care: a prospective cohort analysis, BMC Health Serv Res 19(1) (2019) 406.
[5] J.N. Katz, Lumbar disc disorders and low-back pain: socioeconomic factors and consequences, J Bone Joint Surg Am 88 Suppl 2 (2006) 21-4.
[6] J. Hong, C. Reed, D. Novick, M. Happich, Costs associated with treatment of chronic low back pain: an analysis of the UK General Practice Research Database, Spine (Phila Pa 1976) 38(1) (2013) 75-82.
[7] L.C. Lambeek, M.W. van Tulder, I.C. Swinkels, L.L. Koppes, J.R. Anema, W. van Mechelen, The trend in total cost of back pain in The Netherlands in the period 2002 to 2007, Spine (Phila Pa 1976) 36(13) (2011) 1050-8.
[8] D.J. Schofield, R.N. Shrestha, R. Percival, M.E. Passey, E.J. Callander, S.J. Kelly, The personal and national costs of early retirement because of spinal disorders: impacts on income, taxes, and government support payments, Spine J 12(12) (2012) 1111-8.
[9] R.L. Carregaro, C.R. Tottoli, D.D.S. Rodrigues, J.E. Bosmans, E.N. da Silva, M. van Tulder, Low back pain should be considered a health and research priority in Brazil: Lost productivity and healthcare costs between 2012 to 2016, PLoS One 15(4) (2020) e0230902.
[10] D. Hoy, C. Bain, G. Williams, L. March, P. Brooks, F. Blyth, A. Woolf, T. Vos, R. Buchbinder, A systematic review of the global prevalence of low back pain, Arthritis Rheum 64(6) (2012) 2028-37.
[11] N.N. Knezevic, K.D. Candido, J.W.S. Vlaeyen, J. Van Zundert, S.P. Cohen, Low back pain, Lancet 398(10294) (2021) 78-92.
[12] A.J. Freemont, The cellular pathobiology of the degenerate intervertebral disc and discogenic back pain, Rheumatology (Oxford) 48(1) (2009) 5-10.
[13] A.C. Schwarzer, C.N. Aprill, R. Derby, J. Fortin, G. Kine, N. Bogduk, The prevalence and clinical features of internal disc disruption in patients with chronic low back pain, Spine (Phila Pa 1976) 20(17) (1995) 1878-83.
[14] E.S. Vasiliadis, S.G. Pneumaticos, D.S. Evangelopoulos, A.G. Papavassiliou, Biologic treatment of mild and moderate intervertebral disc degeneration, Mol Med 20 (2014) 400-9.
[15] K.A. Tomaszewski, K. Saganiak, T. Gladysz, J.A. Walocha, The biology behind the human intervertebral disc and its endplates, Folia Morphol (Warsz) 74(2) (2015) 157-68.
[16] P. Lama, C.L. Le Maitre, I.J. Harding, P. Dolan, M.A. Adams, Nerves and blood vessels in degenerated intervertebral discs are confined to physically disrupted tissue, J Anat 233(1) (2018) 86-97.
[17] T. Liebscher, M. Haefeli, K. Wuertz, A.G. Nerlich, N. Boos, Age-related variation in cell density of human lumbar intervertebral disc, Spine (Phila Pa 1976) 36(2) (2011) 153-9.
[18] Z.E. Wilson, A. Rostami-Hodjegan, J.L. Burn, A. Tooley, J. Boyle, S.W. Ellis, G.T. Tucker, Inter-individual variability in levels of human microsomal protein and hepatocellularity per gram of liver, Br J Clin Pharmacol 56(4) (2003) 433-40.
[19] A. Maroudas, R.A. Stockwell, A. Nachemson, J. Urban, Factors involved in the nutrition of the human lumbar intervertebral disc: cellularity and diffusion of glucose in vitro, J Anat 120(Pt 1) (1975) 113-30.
[20] E.B. Hunziker, T.M. Quinn, H.J. Hauselmann, Quantitative structural organization of normal adult human articular cartilage, Osteoarthritis Cartilage 10(7) (2002) 564-72.

[21] F. Mwale, P. Roughley, J. Antoniou, Distinction between the extracellular matrix of the nucleus pulposus and hyaline cartilage: a requisite for tissue engineering of intervertebral disc, Eur Cell Mater 8 (2004) 58-63; discussion 63-4.
[22] M. Venn, A. Maroudas, Chemical composition and swelling of normal and osteoarthrotic femoral head cartilage. I. Chemical composition, Ann Rheum Dis 36(2) (1977) 121-9.
[23] M. Yanagishita, Function of proteoglycans in the extracellular matrix, Acta Pathol Jpn 43(6) (1993) 283-93.
[24] K.A. Tomaszewski, J.A. Walocha, E. Mizia, T. Gladysz, R. Glowacki, R. Tomaszewska, Age- and degeneration-related variations in cell density and glycosaminoglycan content in the human cervical intervertebral disc and its endplates, Pol J Pathol 66(3) (2015) 296-309.
[25] P.J. Roughley, Biology of intervertebral disc aging and degeneration: involvement of the extracellular matrix, Spine (Phila Pa 1976) 29(23) (2004) 2691-9.
[26] P. Colombier, J. Clouet, O. Hamel, L. Lescaudron, J. Guicheux, The lumbar intervertebral disc: from embryonic development to degeneration, Joint Bone Spine 81(2) (2014) 125-9.
[27] A.J. Hayes, M. Benjamin, J.R. Ralphs, Extracellular matrix in development of the intervertebral disc, Matrix Biol 20(2) (2001) 107-21.
[28] S. Roberts, J. Menage, J.P. Urban, Biochemical and structural properties of the cartilage end-plate and its relation to the intervertebral disc, Spine (Phila Pa 1976) 14(2) (1989) 166-74.
[29] J. Naresh-Babu, G. Neelima, S. Reshma Begum, V. Siva-Leela, Diffusion characteristics of human annulus fibrosus-a study documenting the dependence of annulus fibrosus on end plate for diffusion, Spine J 16(8) (2016) 1007-14.
[30] J.P. Urban, S. Holm, A. Maroudas, A. Nachemson, Nutrition of the intervertebral disk. An in vivo study of solute transport, Clin Orthop Relat Res (129) (1977) 101-14.
[31] Y.X. Wang, J.Q. Wang, Z. Kaplar, Increased low back pain prevalence in females than in males after menopause age: evidences based on synthetic literature review, Quant Imaging Med Surg 6(2) (2016) 199-206.
[32] J.A. Miller, C. Schmatz, A.B. Schultz, Lumbar disc degeneration: correlation with age, sex, and spine level in 600 autopsy specimens, Spine (Phila Pa 1976) 13(2) (1988) 173-8.
[33] R. Shiri, J. Karppinen, P. Leino-Arjas, S. Solovieva, E. Viikari-Juntura, The association between obesity and low back pain: a meta-analysis, Am J Epidemiol 171(2) (2010) 135-54.
[34] L.A. Setton, J. Chen, Mechanobiology of the intervertebral disc and relevance to disc degeneration, J Bone Joint Surg Am 88 Suppl 2 (2006) 52-7.
[35] B. Alkhatib, D.H. Rosenzweig, E. Krock, P.J. Roughley, L. Beckman, T. Steffen, M.H. Weber, J.A. Ouellet, L. Haglund, Acute mechanical injury of the human intervertebral disc: link to degeneration and pain, Eur Cell Mater 28 (2014) 98-110; discussion 110-1.
[36] R. Shiri, J. Karppinen, P. Leino-Arjas, S. Solovieva, E. Viikari-Juntura, The association between smoking and low back pain: a meta-analysis, Am J Med 123(1) (2010) 87 e7-35.
[37] B. Vernon-Roberts, C.J. Pirie, Degenerative changes in the intervertebral discs of the lumbar spine and their sequelae, Rheumatol Rehabil 16(1) (1977) 13-21.
[38] M. Haefeli, F. Kalberer, D. Saegesser, A.G. Nerlich, N. Boos, G. Paesold, The course of macroscopic degeneration in the human lumbar intervertebral disc, Spine (Phila Pa 1976) 31(14) (2006) 1522-31.
[39] W.J. Wang, X.H. Yu, C. Wang, W. Yang, W.S. He, S.J. Zhang, Y.G. Yan, J. Zhang, MMPs and ADAMTSs in intervertebral disc degeneration, Clin Chim Acta 448 (2015) 238-46.
[40] S. Roberts, M.A. Bains, A. Kwan, J. Menage, S.M. Eisenstein, Type X collagen in the human invertebral disc: an indication of repair or remodelling?, Histochem J 30(2) (1998) 89-95.
[41] H. Takaishi, O. Nemoto, M. Shiota, T. Kikuchi, H. Yamada, M. Yamagishi, Y. Yabe, Type-II collagen gene expression is transiently upregulated in experimentally induced degeneration of rabbit intervertebral disc, J Orthop Res 15(4) (1997) 528-38.

[42] C.L. Le Maitre, A. Pockert, D.J. Buttle, A.J. Freemont, J.A. Hoyland, Matrix synthesis and degradation in human intervertebral disc degeneration, Biochem Soc Trans 35(Pt 4) (2007) 652-5.
[43] Y. Wang, M. Che, J. Xin, Z. Zheng, J. Li, S. Zhang, The role of IL-1beta and TNF-alpha in intervertebral disc degeneration, Biomed Pharmacother 131 (2020) 110660.
[44] G. Lang, Y. Liu, J. Geries, Z. Zhou, D. Kubosch, N. Sudkamp, R.G. Richards, M. Alini, S. Grad, Z. Li, An intervertebral disc whole organ culture system to investigate proinflammatory and degenerative disc disease condition, J Tissue Eng Regen Med 12(4) (2018) e2051-e2061.
[45] M. Molinos, C.R. Almeida, J. Caldeira, C. Cunha, R.M. Goncalves, M.A. Barbosa, Inflammation in intervertebral disc degeneration and regeneration, J R Soc Interface 12(104) (2015) 20141191.
[46] J. Rutges, J. Kummer, F. Oner, A. Verbout, R. Castelein, H. Roestenburg, W. Dhert, L.J.T.J.o.p. Creemers, Increased MMP-2 activity during intervertebral disc degeneration is correlated to MMP-14 levels, 214(4) (2008) 523-530.
[47] N. Boos, S. Weissbach, H. Rohrbach, C. Weiler, K.F. Spratt, A.G. Nerlich, Classification of age-related changes in lumbar intervertebral discs: 2002 Volvo Award in basic science, Spine (Phila Pa 1976) 27(23) (2002) 2631-44.
[48] J. Melrose, S. Roberts, S. Smith, J. Menage, P. Ghosh, Increased nerve and blood vessel ingrowth associated with proteoglycan depletion in an ovine anular lesion model of experimental disc degeneration, Spine (Phila Pa 1976) 27(12) (2002) 1278-85.
[49] A.J. Freemont, T.E. Peacock, P. Goupille, J.A. Hoyland, J. O'Brien, M.I. Jayson, Nerve ingrowth into diseased intervertebral disc in chronic back pain, Lancet 350(9072) (1997) 178-81.
[50] W.E. Johnson, B. Caterson, S.M. Eisenstein, S. Roberts, Human intervertebral disc aggrecan inhibits endothelial cell adhesion and cell migration in vitro, Spine (Phila Pa 1976) 30(10) (2005) 1139-47.
[51] R. Rajpurohit, M.V. Risbud, P. Ducheyne, E.J. Vresilovic, I.M. Shapiro, Phenotypic characteristics of the nucleus pulposus: expression of hypoxia inducing factor-1, glucose transporter-1 and MMP-2, Cell Tissue Res 308(3) (2002) 401-7.
[52] S. Razaq, R.J. Wilkins, J.P. Urban, The effect of extracellular pH on matrix turnover by cells of the bovine nucleus pulposus, Eur Spine J 12(4) (2003) 341-9.
[53] Z. Sun, B. Liu, Z.J. Luo, The Immune Privilege of the Intervertebral Disc: Implications for Intervertebral Disc Degeneration Treatment, Int J Med Sci 17(5) (2020) 685-692.
[54] S. Capossela, P. Schlafli, A. Bertolo, T. Janner, B.M. Stadler, T. Potzel, M. Baur, J.V. Stoyanov, Degenerated human intervertebral discs contain autoantibodies against extracellular matrix proteins, Eur Cell Mater 27 (2014) 251-63; discussion 263.
[55] A. Geiss, K. Larsson, B. Rydevik, I. Takahashi, K. Olmarker, Autoimmune properties of nucleus pulposus: an experimental study in pigs, Spine (Phila Pa 1976) 32(2) (2007) 168-73.
[56] A. Kanerva, B. Kommonen, M. Gronblad, J. Tolonen, A. Habtemariam, J. Virri, E. Karaharju, Inflammatory cells in experimental intervertebral disc injury, Spine (Phila Pa 1976) 22(23) (1997) 2711-5.
[57] Y. Kokubo, K. Uchida, S. Kobayashi, T. Yayama, R. Sato, H. Nakajima, T. Takamura, E. Mwaka, N. Orwotho, A. Bangirana, H. Baba, Herniated and spondylotic intervertebral discs of the human cervical spine: histological and immunohistological findings in 500 en bloc surgical samples. Laboratory investigation, J Neurosurg Spine 9(3) (2008) 285-95.
[58] H. Yang, B. Liu, Y. Liu, D. He, Y. Xing, Y. An, W. Tian, Secreted Factors From Intervertebral Disc Cells and Infiltrating Macrophages Promote Degenerated Intervertebral Disc Catabolism, Spine (Phila Pa 1976) 44(9) (2019) E520-E529.
[59] J. Wang, Y. Tian, K.L. Phillips, N. Chiverton, G. Haddock, R.A. Bunning, A.K. Cross, I.M. Shapiro, C.L. Le Maitre, M.V. Risbud, Tumor necrosis factor alpha- and interleukin-1beta-dependent induction of CCL3 expression by nucleus pulposus cells promotes macrophage migration through CCR1, Arthritis Rheum 65(3) (2013) 832-42.

[60] H. Takahashi, T. Suguro, Y. Okazima, M. Motegi, Y. Okada, T. Kakiuchi, Inflammatory cytokines in the herniated disc of the lumbar spine, Spine (Phila Pa 1976) 21(2) (1996) 218-24.
[61] C. Weiler, A.G. Nerlich, B.E. Bachmeier, N. Boos, Expression and distribution of tumor necrosis factor alpha in human lumbar intervertebral discs: a study in surgical specimen and autopsy controls, Spine (Phila Pa 1976) 30(1) (2005) 44-53; discussion 54.
[62] J.A. Hoyland, C. Le Maitre, A.J. Freemont, Investigation of the role of IL-1 and TNF in matrix degradation in the intervertebral disc, Rheumatology (Oxford) 47(6) (2008) 809-14.
[63] C. Shi, L. Wu, W. Lin, Y. Cai, Y. Zhang, B. Hu, R. Gao, H.J. Im, W. Yuan, X. Ye, A.J. van Wijnen, MiR-202-3p regulates interleukin-1beta-induced expression of matrix metalloproteinase 1 in human nucleus pulposus, Gene 687 (2019) 156-165.
[64] J.H. Kim, H. Choi, M.J. Suh, J.H. Shin, M.H. Hwang, H.M. Lee, Effect of biphasic electrical current stimulation on IL-1beta-stimulated annulus fibrosus cells using in vitro microcurrent generating chamber system, Spine (Phila Pa 1976) 38(22) (2013) E1368-76.
[65] S. Zhan, K. Wang, Y. Song, S. Li, H. Yin, R. Luo, Z. Liao, X. Wu, Y. Zhang, C. Yang, Long non-coding RNA HOTAIR modulates intervertebral disc degenerative changes via Wnt/beta-catenin pathway, Arthritis Res Ther 21(1) (2019) 201.
[66] J. Wang, D. Markova, D.G. Anderson, Z. Zheng, I.M. Shapiro, M.V. Risbud, TNF-alpha and IL-1beta promote a disintegrin-like and metalloprotease with thrombospondin type I motif-5-mediated aggrecan degradation through syndecan-4 in intervertebral disc, J Biol Chem 286(46) (2011) 39738-49.
[67] C.A. Seguin, R.M. Pilliar, P.J. Roughley, R.A. Kandel, Tumor necrosis factor-alpha modulates matrix production and catabolism in nucleus pulposus tissue, Spine (Phila Pa 1976) 30(17) (2005) 1940-8.
[68] J.M. Lee, J.Y. Song, M. Baek, H.Y. Jung, H. Kang, I.B. Han, Y.D. Kwon, D.E. Shin, Interleukin-1beta induces angiogenesis and innervation in human intervertebral disc degeneration, J Orthop Res 29(2) (2011) 265-9.
[69] K.L. Phillips, N. Chiverton, A.L. Michael, A.A. Cole, L.M. Breakwell, G. Haddock, R.A. Bunning, A.K. Cross, C.L. Le Maitre, The cytokine and chemokine expression profile of nucleus pulposus cells: implications for degeneration and regeneration of the intervertebral disc, Arthritis Res Ther 15(6) (2013) R213.
[70] D.J. Gorth, I.M. Shapiro, M.V. Risbud, A New Understanding of the Role of IL-1 in Age-Related Intervertebral Disc Degeneration in a Murine Model, J Bone Miner Res 34(8) (2019) 1531-1542.
[71] J. Maciel, M.I. Oliveira, E. Colton, A.K. McNally, C. Oliveira, J.M. Anderson, M.A. Barbosa, Adsorbed fibrinogen enhances production of bone- and angiogenic-related factors by monocytes/macrophages, Tissue Eng Part A 20(1-2) (2014) 250-63.
[72] N.E. Foster, J.R. Anema, D. Cherkin, R. Chou, S.P. Cohen, D.P. Gross, P.H. Ferreira, J.M. Fritz, B.W. Koes, W. Peul, J.A. Turner, C.G. Maher, G. Lancet Low Back Pain Series Working, Prevention and treatment of low back pain: evidence, challenges, and promising directions, Lancet 391(10137) (2018) 2368-2383.
[73] W.T.M. Enthoven, P.D. Roelofs, B.W. Koes, NSAIDs for Chronic Low Back Pain, JAMA 317(22) (2017) 2327-2328.
[74] P.D. Roelofs, R.A. Deyo, B.W. Koes, R.J. Scholten, M.W. van Tulder, Non-steroidal anti-inflammatory drugs for low back pain, Cochrane Database Syst Rev (1) (2008) CD000396.
[75] L. Alev, S. Fujikoshi, A. Yoshikawa, H. Enomoto, M. Ishida, T. Tsuji, K. Ogawa, S. Konno, Duloxetine 60 mg for chronic low back pain: post hoc responder analysis of double-blind, placebo-controlled trials, J Pain Res 10 (2017) 1723-1731.
[76] R.A. Deyo, S.K. Mirza, CLINICAL PRACTICE. Herniated Lumbar Intervertebral Disk, N Engl J Med 374(18) (2016) 1763-72.
[77] A. Froholdt, O. Reikeraas, I. Holm, A. Keller, J.I. Brox, No difference in 9-year outcome in CLBP patients randomized to lumbar fusion versus cognitive intervention and exercises, Eur Spine J 21(12) (2012) 2531-8.

[78] B.D. Lawrence, J. Wang, P.M. Arnold, J. Hermsmeyer, D.C. Norvell, D.S. Brodke, Predicting the risk of adjacent segment pathology after lumbar fusion: a systematic review, Spine (Phila Pa 1976) 37(22 Suppl) (2012) S123-32.
[79] J.E. Zigler, B.L. Sachs, R.F. Rashbaum, D.D. Ohnmeiss, Two- to 3-Year Follow-Up of ProDisc-L: Results From a Prospective Randomized Trial of Arthroplasty Versus Fusion, SAS Journal 1(2) (2007) 63-67.
[80] D. Franco, G. Largoza, T.S. Montenegro, G.A. Gonzalez, K. Hines, J. Harrop, Lumbar Total Disc Replacement: Current Usage, Neurosurgery Clinics of North America 32(4) (2021) 511-519.
[81] C.T. Buckley, J.A. Hoyland, K. Fujii, A. Pandit, J.C. Iatridis, S. Grad, Critical aspects and challenges for intervertebral disc repair and regeneration-Harnessing advances in tissue engineering, JOR Spine 1(3) (2018) e1029.
[82] S. van Uden, J. Silva-Correia, J.M. Oliveira, R.L. Reis, Current strategies for treatment of intervertebral disc degeneration: substitution and regeneration possibilities, Biomater Res 21 (2017) 22.
[83] O.M. Torre, V. Mroz, M.K. Bartelstein, A.H. Huang, J.C. Iatridis, Annulus fibrosus cell phenotypes in homeostasis and injury: implications for regenerative strategies, Ann N Y Acad Sci 1442(1) (2019) 61-78.
[84] A.L.A. Binch, J.C. Fitzgerald, E.A. Growney, F. Barry, Cell-based strategies for IVD repair: clinical progress and translational obstacles, Nat Rev Rheumatol 17(3) (2021) 158-175.
[85] H.J. Meisel, T. Ganey, W.C. Hutton, J. Libera, Y. Minkus, O. Alasevic, Clinical experience in cell-based therapeutics: intervention and outcome, Eur Spine J 15 Suppl 3 (2006) S397-405.
[86] D. Coric, K. Pettine, A. Sumich, M.O. Boltes, Prospective study of disc repair with allogeneic chondrocytes presented at the 2012 Joint Spine Section Meeting, J Neurosurg Spine 18(1) (2013) 85-95.
[87] A.I. Caplan, Mesenchymal Stem Cells: Time to Change the Name!, Stem Cells Transl Med 6(6) (2017) 1445-1451.
[88] C. Centeno, J. Markle, E. Dodson, I. Stemper, C.J. Williams, M. Hyzy, T. Ichim, M. Freeman, Treatment of lumbar degenerative disc disease-associated radicular pain with culture-expanded autologous mesenchymal stem cells: a pilot study on safety and efficacy, J Transl Med 15(1) (2017) 197.
[89] H. Kumar, D.H. Ha, E.J. Lee, J.H. Park, J.H. Shim, T.K. Ahn, K.T. Kim, A.E. Ropper, S. Sohn, C.H. Kim, D.K. Thakor, S.H. Lee, I.B. Han, Safety and tolerability of intradiscal implantation of combined autologous adipose-derived mesenchymal stem cells and hyaluronic acid in patients with chronic discogenic low back pain: 1-year follow-up of a phase I study, Stem Cell Res Ther 8(1) (2017) 262.
[90] X. Pang, H. Yang, B. Peng, Human umbilical cord mesenchymal stem cell transplantation for the treatment of chronic discogenic low back pain, Pain Physician 17(4) (2014) E525-30.
[91] M.V. Risbud, A. Guttapalli, T.T. Tsai, J.Y. Lee, K.G. Danielson, A.R. Vaccaro, T.J. Albert, Z. Gazit, D. Gazit, I.M. Shapiro, Evidence for skeletal progenitor cells in the degenerate human intervertebral disc, Spine (Phila Pa 1976) 32(23) (2007) 2537-44.
[92] B. Huang, L.T. Liu, C.Q. Li, Y. Zhuang, G. Luo, S.Y. Hu, Y. Zhou, Study to determine the presence of progenitor cells in the degenerated human cartilage endplates, Eur Spine J 21(4) (2012) 613-22.
[93] H. Wang, Y. Zhou, B. Huang, L.T. Liu, M.H. Liu, J. Wang, C.Q. Li, Z.F. Zhang, T.W. Chu, C.J. Xiong, Utilization of stem cells in alginate for nucleus pulposus tissue engineering, Tissue Eng Part A 20(5-6) (2014) 908-20.
[94] D. Sheyn, S. Ben-David, W. Tawackoli, Z. Zhou, K. Salehi, M. Bez, S. De Mel, V. Chan, J. Roth, P. Avalos, J.C. Giaconi, H. Yameen, L. Hazanov, D. Seliktar, D. Li, D. Gazit, Z. Gazit, Human iPSCs can be differentiated into notochordal cells that reduce intervertebral disc degeneration in a porcine model, Theranostics 9(25) (2019) 7506-7524.
[95] R.M. Guzzo, J. Gibson, R.H. Xu, F.Y. Lee, H. Drissi, Efficient differentiation of human iPSC-derived mesenchymal stem cells to chondroprogenitor cells, J Cell Biochem 114(2) (2013) 480-90.
[96] R. Tang, L. Jing, V.P. Willard, C.L. Wu, F. Guilak, J. Chen, L.A. Setton, Differentiation of human induced pluripotent stem cells into nucleus pulposus-like cells, Stem Cell Res Ther 9(1) (2018) 61.

[97] H.J. Moon, J.H. Kim, H.S. Lee, S. Chotai, J.D. Kang, J.K. Suh, Y.K. Park, Annulus fibrosus cells interact with neuron-like cells to modulate production of growth factors and cytokines in symptomatic disc degeneration, Spine (Phila Pa 1976) 37(1) (2012) 2-9.
[98] A.M.R. Groh, D.E. Fournier, M.C. Battie, C.A. Seguin, Innervation of the Human Intervertebral Disc: A Scoping Review, Pain Med 22(6) (2021) 1281-1304.
[99] D. Alexeev, S. Cui, S. Grad, Z. Li, S.J. Ferguson, Mechanical and biological characterization of a composite annulus fibrosus repair strategy in an endplate delamination model, JOR Spine 3(4) (2020) e1107.
[100] S.B. Bruehlmann, J.B. Rattner, J.R. Matyas, N.A. Duncan, Regional variations in the cellular matrix of the annulus fibrosus of the intervertebral disc, J Anat 201(2) (2002) 159-71.
[101] D.H. Cortes, W.M. Han, L.J. Smith, D.M. Elliott, Mechanical properties of the extra-fibrillar matrix of human annulus fibrosus are location and age dependent, J Orthop Res 31(11) (2013) 1725-32.
[102] G. Chu, C. Shi, H. Wang, W. Zhang, H. Yang, B. Li, Strategies for Annulus Fibrosus Regeneration: From Biological Therapies to Tissue Engineering, Front Bioeng Biotechnol 6 (2018) 90.
[103] T.R. Christiani, E. Baroncini, J. Stanzione, A.J. Vernengo, In vitro evaluation of 3D printed polycaprolactone scaffolds with angle-ply architecture for annulus fibrosus tissue engineering, Regen Biomater 6(3) (2019) 175-184.
[104] I. Hussain, S.R. Sloan, C. Wipplinger, R. Navarro-Ramirez, M. Zubkov, E. Kim, S. Kirnaz, L.J. Bonassar, R. Hartl, Mesenchymal Stem Cell-Seeded High-Density Collagen Gel for Annular Repair: 6-Week Results From In Vivo Sheep Models, Neurosurgery 85(2) (2019) E350-E359.
[105] T. Pirvu, S.B. Blanquer, L.M. Benneker, D.W. Grijpma, R.G. Richards, M. Alini, D. Eglin, S. Grad, Z. Li, A combined biomaterial and cellular approach for annulus fibrosus rupture repair, Biomaterials 42 (2015) 11-9.
[106] D.A. Frauchiger, S.R. Heeb, R.D. May, M. Woltje, L.M. Benneker, B. Gantenbein, Differentiation of MSC and annulus fibrosus cells on genetically engineered silk fleece-membrane-composites enriched for GDF-6 or TGF-beta3, J Orthop Res 36(5) (2018) 1324-1333.
[107] M.A. Cruz, W.W. Hom, T.J. DiStefano, R. Merrill, O.M. Torre, H.A. Lin, A.C. Hecht, S. Illien-Junger, J.C. Iatridis, Cell-Seeded Adhesive Biomaterial for Repair of Annulus Fibrosus Defects in Intervertebral Discs, Tissue Eng Part A 24(3-4) (2018) 187-198.
[108] N.L. Nerurkar, B.M. Baker, S. Sen, E.E. Wible, D.M. Elliott, R.L. Mauck, Nanofibrous biologic laminates replicate the form and function of the annulus fibrosus, Nat Mater 8(12) (2009) 986-92.
[109] B.K. Bhunia, D.L. Kaplan, B.B. Mandal, Silk-based multilayered angle-ply annulus fibrosus construct to recapitulate form and function of the intervertebral disc, Proc Natl Acad Sci U S A 115(3) (2018) 477-482.
[110] L. Zhang, J.C. Wang, X.M. Feng, W.H. Cai, J.D. Yang, N. Zhang, Antibiotic penetration into rabbit nucleus pulposus with discitis, Eur J Orthop Surg Traumatol 24(4) (2014) 453-8.
[111] R. Walters, R. Moore, R. Fraser, Penetration of cephazolin in human lumbar intervertebral disc, Spine (Phila Pa 1976) 31(5) (2006) 567-70.
[112] R. Walters, R. Rahmat, R. Fraser, R. Moore, Preventing and treating discitis: cephazolin penetration in ovine lumbar intervertebral disc, Eur Spine J 15(9) (2006) 1397-403.
[113] M.A. Tryfonidou, G. de Vries, W.E. Hennink, L.B. Creemers, "Old Drugs, New Tricks" - Local controlled drug release systems for treatment of degenerative joint disease, Adv Drug Deliv Rev 160 (2020) 170-185.
[114] F. Fayad, M.M. Lefevre-Colau, F. Rannou, N. Quintero, A. Nys, Y. Mace, S. Poiraudeau, J.L. Drape, M. Revel, Relation of inflammatory modic changes to intradiscal steroid injection outcome in chronic low back pain, Eur Spine J 16(7) (2007) 925-31.
[115] P. Cao, L. Jiang, C. Zhuang, Y. Yang, Z. Zhang, W. Chen, T. Zheng, Intradiscal injection therapy for degenerative chronic discogenic low back pain with end plate Modic changes, Spine J 11(2) (2011) 100-6.

[116] A. Khot, M. Bowditch, J. Powell, D. Sharp, The use of intradiscal steroid therapy for lumbar spinal discogenic pain: a randomized controlled trial, Spine (Phila Pa 1976) 29(8) (2004) 833-6; discussion 837.
[117] T. Sainoh, S. Orita, M. Miyagi, G. Inoue, H. Kamoda, T. Ishikawa, K. Yamauchi, M. Suzuki, Y. Sakuma, G. Kubota, Y. Oikawa, K. Inage, J. Sato, Y. Nakata, J. Nakamura, Y. Aoki, T. Toyone, K. Takahashi, S. Ohtori, Single Intradiscal Administration of the Tumor Necrosis Factor-Alpha Inhibitor, Etanercept, for Patients with Discogenic Low Back Pain, Pain Med 17(1) (2016) 40-5.
[118] A.R. Tellegen, I. Rudnik-Jansen, M. Beukers, A. Miranda-Bedate, F.C. Bach, W. de Jong, N. Woike, G. Mihov, J.C. Thies, B.P. Meij, L.B. Creemers, M.A. Tryfonidou, Intradiscal delivery of celecoxib-loaded microspheres restores intervertebral disc integrity in a preclinical canine model, J. Control. Release 286 (2018) 439-450.
[119] A.R. Tellegen, N. Willems, M. Beukers, G.C.M. Grinwis, S.G.M. Plomp, C. Bos, M. van Dijk, M. de Leeuw, L.B. Creemers, M.A. Tryfonidou, B.P. Meij, Intradiscal application of a PCLA-PEG-PCLA hydrogel loaded with celecoxib for the treatment of back pain in canines: What's in it for humans?, J Tissue Eng Regen Med 12(3) (2018) 642-652.
[120] T. Wiersema, A.R. Tellegen, M. Beukers, M. van Stralen, E. Wouters, M. van de Vooren, N. Woike, G. Mihov, J.C. Thies, L.B. Creemers, M.A. Tryfonidou, B.P. Meij, Prospective Evaluation of Local Sustained Release of Celecoxib in Dogs with Low Back Pain, Pharmaceutics 13(8) (2021).
[121] J.C. Kennon, M.E. Awad, N. Chutkan, J. DeVine, S. Fulzele, Current insights on use of growth factors as therapy for Intervertebral Disc Degeneration, Biomol Concepts 9(1) (2018) 43-52.
[122] Y. Chang, M. Yang, S. Ke, Y. Zhang, G. Xu, Z. Li, Effect of Platelet-Rich Plasma on Intervertebral Disc Degeneration In Vivo and In Vitro: A Critical Review, Oxid Med Cell Longev 2020 (2020) 8893819.
[123] W.H. Chen, W.C. Lo, J.J. Lee, C.H. Su, C.T. Lin, H.Y. Liu, T.W. Lin, W.C. Lin, T.Y. Huang, W.P. Deng, Tissue-engineered intervertebral disc and chondrogenesis using human nucleus pulposus regulated through TGF-beta1 in platelet-rich plasma, J Cell Physiol 209(3) (2006) 744-54.
[124] M.C. Liu, W.H. Chen, L.C. Wu, W.C. Hsu, W.C. Lo, S.D. Yeh, M.F. Wang, R. Zeng, W.P. Deng, Establishment of a promising human nucleus pulposus cell line for intervertebral disc tissue engineering, Tissue Eng Part C Methods 20(1) (2014) 1-10.
[125] K. Gui, W. Ren, Y. Yu, X. Li, J. Dong, W. Yin, Inhibitory effects of platelet-rich plasma on intervertebral disc degeneration: a preclinical study in a rabbit model, Med Sci Monit 21 (2015) 1368-75.
[126] K. Sawamura, T. Ikeda, M. Nagae, S. Okamoto, Y. Mikami, H. Hase, K. Ikoma, T. Yamada, H. Sakamoto, K. Matsuda, Y. Tabata, M. Kawata, T. Kubo, Characterization of in vivo effects of platelet-rich plasma and biodegradable gelatin hydrogel microspheres on degenerated intervertebral discs, Tissue Eng Part A 15(12) (2009) 3719-27.
[127] Y.A. Tuakli-Wosornu, A. Terry, K. Boachie-Adjei, J.R. Harrison, C.K. Gribbin, E.E. LaSalle, J.T. Nguyen, J.L. Solomon, G.E. Lutz, Lumbar Intradiskal Platelet-Rich Plasma (PRP) Injections: A Prospective, Double-Blind, Randomized Controlled Study, PM R 8(1) (2016) 1-10; quiz 10.
[128] D. Levi, S. Horn, S. Tyszko, J. Levin, C. Hecht-Leavitt, E. Walko, Intradiscal Platelet-Rich Plasma Injection for Chronic Discogenic Low Back Pain: Preliminary Results from a Prospective Trial, Pain Med 17(6) (2016) 1010-22.
[129] B. Schmierer, C.S. Hill, TGFbeta-SMAD signal transduction: molecular specificity and functional flexibility, Nat Rev Mol Cell Biol 8(12) (2007) 970-82.
[130] M.O. Baffi, E. Slattery, P. Sohn, H.L. Moses, A. Chytil, R. Serra, Conditional deletion of the TGF-beta type II receptor in Col2a expressing cells results in defects in the axial skeleton without alterations in chondrocyte differentiation or embryonic development of long bones, Dev Biol 276(1) (2004) 124-42.
[131] H. Jin, J. Shen, B. Wang, M. Wang, B. Shu, D. Chen, TGF-beta signaling plays an essential role in the growth and maintenance of intervertebral disc tissue, FEBS Lett 585(8) (2011) 1209-15.

[132] S. Ashraf, K. Chatoor, J. Chong, R. Pilliar, P. Santerre, R. Kandel, Transforming Growth Factor beta Enhances Tissue Formation by Passaged Nucleus Pulposus Cells In Vitro, J Orthop Res 38(2) (2020) 438-449.
[133] A.J. Walsh, D.S. Bradford, J.C. Lotz, In vivo growth factor treatment of degenerated intervertebral discs, Spine (Phila Pa 1976) 29(2) (2004) 156-63.
[134] J. Yan, S. Yang, H. Sun, D. Guo, B. Wu, F. Ji, D. Zhou, Effects of releasing recombinant human growth and differentiation factor-5 from poly(lactic-co-glycolic acid) microspheres for repair of the rat degenerated intervertebral disc, J Biomater Appl 29(1) (2014) 72-80.
[135] T. Hodgkinson, B. Shen, A. Diwan, J.A. Hoyland, S.M. Richardson, Therapeutic potential of growth differentiation factors in the treatment of degenerative disc diseases, JOR Spine 2(1) (2019) e1045.
[136] D.J. Kim, S.H. Moon, H. Kim, U.H. Kwon, M.S. Park, K.J. Han, S.B. Hahn, H.M. Lee, Bone morphogenetic protein-2 facilitates expression of chondrogenic, not osteogenic, phenotype of human intervertebral disc cells, Spine (Phila Pa 1976) 28(24) (2003) 2679-84.
[137] J. Li, S.T. Yoon, W.C. Hutton, Effect of bone morphogenetic protein-2 (BMP-2) on matrix production, other BMPs, and BMP receptors in rat intervertebral disc cells, J Spinal Disord Tech 17(5) (2004) 423-8.
[138] K. Takegami, H.S. An, F. Kumano, K. Chiba, E.J. Thonar, K. Singh, K. Masuda, Osteogenic protein-1 is most effective in stimulating nucleus pulposus and annulus fibrosus cells to repair their matrix after chondroitinase ABC-induced in vitro chemonucleolysis, Spine J 5(3) (2005) 231-8.
[139] Y. Imai, K. Miyamoto, H.S. An, E.J. Thonar, G.B. Andersson, K. Masuda, Recombinant human osteogenic protein-1 upregulates proteoglycan metabolism of human anulus fibrosus and nucleus pulposus cells, Spine (Phila Pa 1976) 32(12) (2007) 1303-9; discussion 1310.
[140] Z. Li, G. Lang, L.S. Karfeld-Sulzer, K.T. Mader, R.G. Richards, F.E. Weber, C. Sammon, H. Sacks, A. Yayon, M. Alini, S. Grad, Heterodimeric BMP-2/7 for nucleus pulposus regeneration-In vitro and ex vivo studies, J Orthop Res 35(1) (2017) 51-60.
[141] K. Masuda, Y. Imai, M. Okuma, C. Muehleman, K. Nakagawa, K. Akeda, E. Thonar, G. Andersson, H.S. An, Osteogenic protein-1 injection into a degenerated disc induces the restoration of disc height and structural changes in the rabbit anular puncture model, Spine (Phila Pa 1976) 31(7) (2006) 742-54.
[142] S.K. Leckie, B.P. Bechara, R.A. Hartman, G.A. Sowa, B.I. Woods, J.P. Coelho, W.T. Witt, Q.D. Dong, B.W. Bowman, K.M. Bell, N.V. Vo, B. Wang, J.D. Kang, Injection of AAV2-BMP2 and AAV2-TIMP1 into the nucleus pulposus slows the course of intervertebral disc degeneration in an in vivo rabbit model, Spine J 12(1) (2012) 7-20.
[143] M. Peeters, S.E. Detiger, L.S. Karfeld-Sulzer, T.H. Smit, A. Yayon, F.E. Weber, M.N. Helder, BMP-2 and BMP-2/7 Heterodimers Conjugated to a Fibrin/Hyaluronic Acid Hydrogel in a Large Animal Model of Mild Intervertebral Disc Degeneration, Biores Open Access 4(1) (2015) 398-406.
[144] N. Willems, F.C. Bach, S.G. Plomp, M.H. van Rijen, J. Wolfswinkel, G.C. Grinwis, C. Bos, G.J. Strijkers, W.J. Dhert, B.P. Meij, L.B. Creemers, M.A. Tryfonidou, Intradiscal application of rhBMP-7 does not induce regeneration in a canine model of spontaneous intervertebral disc degeneration, Arthritis Res Ther 17 (2015) 137.
[145] A. Krouwels, J.D. Iljas, A.H.M. Kragten, W.J.A. Dhert, F.C. Oner, M.A. Tryfonidou, L.B. Creemers, Bone Morphogenetic Proteins for Nucleus Pulposus Regeneration, Int J Mol Sci 21(8) (2020).
[146] Y. Takeoka, T. Yurube, K. Nishida, Gene Therapy Approach for Intervertebral Disc Degeneration: An Update, Neurospine 17(1) (2020) 3-14.
[147] K. Nishida, J.D. Kang, L.G. Gilbertson, S.H. Moon, J.K. Suh, M.T. Vogt, P.D. Robbins, C.H. Evans, Modulation of the biologic activity of the rabbit intervertebral disc by gene therapy: an in vivo study of adenovirus-mediated transfer of the human transforming growth factor beta 1 encoding gene, Spine (Phila Pa 1976) 24(23) (1999) 2419-25.
[148] F. Colella, J.P. Garcia, M. Sorbona, A. Lolli, B. Antunes, D. D'Atri, F.P.Y. Barre, J. Oieni, M.L. Vainieri, L. Zerrillo, S. Capar, S. Hackel, Y. Cai, L.B. Creemers, Drug delivery in intervertebral disc degeneration and

osteoarthritis: Selecting the optimal platform for the delivery of disease-modifying agents, J Control Release 328 (2020) 985-999.
[149] C.L. Pereira, R.M. Goncalves, M. Peroglio, G. Pattappa, M. D'Este, D. Eglin, M.A. Barbosa, M. Alini, S. Grad, The effect of hyaluronan-based delivery of stromal cell-derived factor-1 on the recruitment of MSCs in degenerating intervertebral discs, Biomaterials 35(28) (2014) 8144-53.
[150] C. Cunha, C. Leite Pereira, J.R. Ferreira, C. Ribeiro-Machado, S. Grad, S.G. Santos, R.M. Goncalves, Therapeutic Strategies for IVD Regeneration through Hyaluronan/SDF-1-Based Hydrogel and Intravenous Administration of MSCs, Int J Mol Sci 22(17) (2021).
[151] H. Zhang, S. Yu, X. Zhao, Z. Mao, C. Gao, Stromal cell-derived factor-1alpha-encapsulated albumin/heparin nanoparticles for induced stem cell migration and intervertebral disc regeneration in vivo, Acta Biomater 72 (2018) 217-227.
[152] I. Rudnik-Jansen, S. Colen, J. Berard, S. Plomp, I. Que, M. van Rijen, N. Woike, A. Egas, G. van Osch, E. van Maarseveen, K. Messier, A. Chan, J. Thies, L. Creemers, Prolonged inhibition of inflammation in osteoarthritis by triamcinolone acetonide released from a polyester amide microsphere platform, J Control Release 253 (2017) 64-72.
[153] I. Rudnik-Jansen, A. Tellegen, M. Beukers, F. Oner, N. Woike, G. Mihov, J. Thies, B. Meij, M. Tryfonidou, L. Creemers, Safety of intradiscal delivery of triamcinolone acetonide by a poly(esteramide) microsphere platform in a large animal model of intervertebral disc degeneration, Spine J 19(5) (2019) 905-919.
[154] A. Tellegen, M. Beukers, I. Rudnik-Jansen, N. van Klaveren, K.L. How, N. Woike, G. Mihov, J. Thies, E. Teske, L. Creemers, M. Tryfonidou, B. Meij, Intra-Articular Slow-Release Triamcinolone Acetonide from Polyesteramide Microspheres as a Treatment for Osteoarthritis, Pharmaceutics 13(3) (2021).
[155] K. Fu, D.W. Pack, A.M. Klibanov, R. Langer, Visual evidence of acidic environment within degrading poly(lactic-co-glycolic acid) (PLGA) microspheres, Pharm Res 17(1) (2000) 100-6.
[156] A.N. Tiaden, M. Klawitter, V. Lux, A. Mirsaidi, G. Bahrenberg, S. Glanz, L. Quero, T. Liebscher, K. Wuertz, M. Ehrmann, P.J. Richards, Detrimental role for human high temperature requirement serine protease A1 (HTRA1) in the pathogenesis of intervertebral disc (IVD) degeneration, J Biol Chem 287(25) (2012) 21335-45.
[157] M. Janssen, U.T. Timur, N. Woike, T.J. Welting, G. Draaisma, M. Gijbels, L.W. van Rhijn, G. Mihov, J. Thies, P.J. Emans, Celecoxib-loaded PEA microspheres as an auto regulatory drug-delivery system after intra-articular injection, J Control Release 244(Pt A) (2016) 30-40.
[158] B.S. Zolnik, D.J. Burgess, Effect of acidic pH on PLGA microsphere degradation and release, J Control Release 122(3) (2007) 338-44.
[159] J. Pradal, P. Maudens, C. Gabay, C.A. Seemayer, O. Jordan, E. Allemann, Effect of particle size on the biodistribution of nano- and microparticles following intra-articular injection in mice, Int J Pharm 498(1-2) (2016) 119-29.

Chapter 2

Proinflammatory Intervertebral Disc Cell and Organ Culture Models Induced by Tumor Necrosis Factor-α

Jie Du, Judith-J. Pfannkuche, Gernot Lang, Sonja Häckel, Laura B. Creemers, Mauro Alini, Sibylle Grad, Zhen Li

Published in JOR Spine
DOI: 10.1002/jsp2.1104

Jie Du contributed to the study design, acquisition, analysis, interpretation of data, drafting, and revising of the article, and final approval.

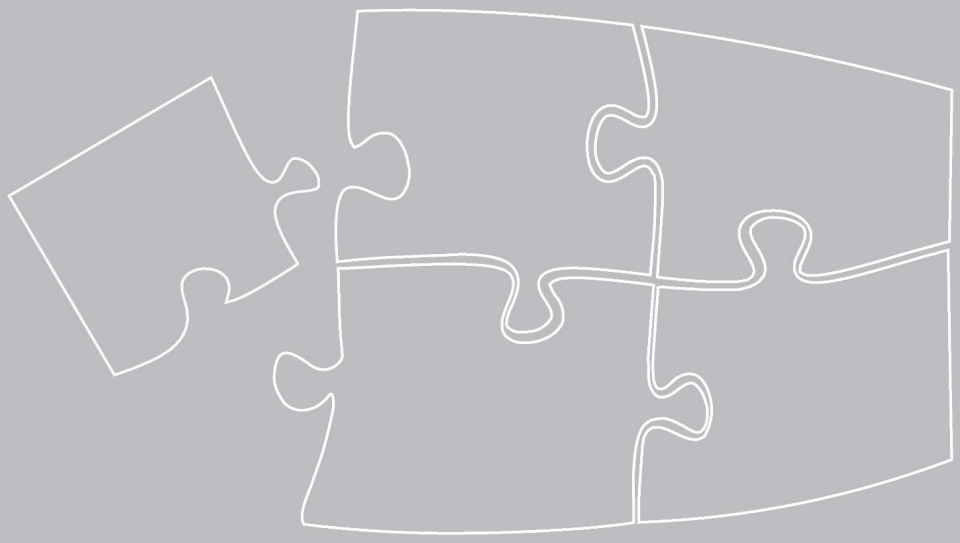

Abstract:

Inflammation plays an important role in the pathogenesis of intervertebral disc (IVD) degeneration. The proinflammatory cytokine tumor necrosis factor alpha (TNF-α) has shown markedly higher expression in degenerated human disc tissue compared with healthy controls. Anti-inflammatory treatment targeting TNF-α has shown to alleviate discogenic pain in patients with low back pain. Therefore, *in vitro* and *ex vivo* inflammatory models utilizing TNF-α provide relevant experimental conditions for drug development in disc degeneration research.

The current method article addressed several specific questions related to the model establishment. (a) The effects of bovine and human recombinant TNF-α on bovine nucleus pulposus (NP) cells were compared. (b) The required dose for an inflammatory IVD organ culture model with intradiscal TNF-α injection was studied. (c) The effect of TNF-α blocking at different stages of inflammation was evaluated.

Outcomes revealed that bovine and human recombinant TNF-α induced equivalent inflammatory effects in bovine NP cells. A bovine whole IVD inflammatory model was established by intradiscal injection of 100 ng TNF-α/cm^3 disc volume, as indicated by increased nitric oxide, glycosaminoglycan, interleukin 6 (IL-6), and interleukin 8 (IL-8) release in culture media, and upregulation of *MMP3*, *ADAMTS4*, *IL-8*, *IL-6*, and cyclooxygenase (COX)-2 expression in NP tissue. However, results in human NP cells showed that the time point of anti-inflammatory treatment was crucial to achieve significant effects. Furthermore, anti-catabolic therapy in conjunction with TNF-α inhibition would be required to slow down the pathologic cascade of IVD degeneration.

Keywords:

Intervertebral disc, Inflammation, Spine, Regeneration, 3R, Cytokines

1. Introduction

Low back pain (LBP) is the leading cause of disability worldwide [1]. One major cause for chronic LBP is symptomatic intervertebral disc degeneration (IVDD) [2-4]. IVDD is characterized by extracellular matrix (ECM) degradation, accelerated cartilaginous and bone remodeling, release of proinflammatory cytokines, altered spine biomechanics, angiogenesis and neoinnervation, altogether potentially leading to chronic LBP and disability [5-9]. IVDD can be induced by mechanical stress, trauma, infection, genetic predisposition, and inflammation [10-16].

Inflammation plays a major role in disc degeneration, as proinflammatory cytokines (i.e. tumor necrosis factor-alpha (TNF-α), interleukin-1beta (IL-1β), interleukin-6 (IL-6), interleukin-8 (IL-8), interleukin-17 (IL-17), and interferon-gamma (IFN-γ)) induce and trigger discal ECM breakdown and accelerated catabolism by stimulation of catabolic enzymes such as matrix metalloproteinases (MMPs) and a disintegrin and metalloproteinase with thrombospondin motifs (ADAMTS) [6, 17-20]. Proinflammatory cytokines have shown elevated expression in degenerative and symptomatic compared to healthy and asymptomatic IVDs [16, 21]. Since therapeutic approaches for IVDD remain limited, biological anti-inflammatory approaches to IVD regeneration have gained increasing interest. In cases of refractory LBP due to IVDD, anti-inflammatory and/or anti-degenerative therapies such as cytokine inhibition may relieve pain and slow down the progression of the disease [22-31]. Several studies indicated that cyclooxygenase-2 (COX-2) inhibitors can reduce the inflammatory response in different models [25-27]. Soluble TNF receptor type II is able to significantly attenuate the effects of TNF-α on primary human IVD cells *in vitro* [28]. Intradiscal administration of a TNF-α inhibitor, Etanercept, to LBP patient can alleviate intractable discogenic LBP for up to 4 weeks [31].

A degenerative disc exhibits increased TNF-α expression, not only produced by immunocytes, but also by disc cells themselves [15, 19, 32]. Furthermore, TNF-α can induce nucleus pulposus (NP) cells to produce other cytokines and chemokines that can further enhance the inflammatory state by recruiting and activating immune cells [33]. So far, it is widely accepted that TNF-α contribute to disc generation by decreasing the anabolism and increasing the catabolism of ECM [34]. Additionally, exogenous TNF-α induces neuropathology and sensory nerve growth into IVD, which indicated TNF-α might be the chemical mediator of discogenic pain [35, 36]. Therefore, multiple *in vitro*, *ex vivo*, and *in vivo* inflammatory IVD models have been established with TNF-α [20, 28, 37-39]. NP cells cultured with TNF-α *in vitro* showed upregulated expression of catabolic enzymes, ADAMTS 4&5 and MMP-1, -2, -3, -13, and inflammatory mediators, IL-1β, IL-6, IL-8, COX2, downregulated expression of ECM markers collagen II, aggrecan, and versican [34, 40-44]. TNF-α has been shown to induce MMP3 expression via nuclear factor κB (NF-κB) and mitogen-activated protein kinase (MAPK) pathways [45]. Intradiscal injection of TNF-α in a porcine model was sufficient to induce early-stage disc degeneration, characterized by matrix loss, annular fissure formation, and vascularization [46]. Lai et al. (2016) reported that annular puncture with TNF-α injection enhanced painful behavior with disc degeneration in a rat model [39].

Ex vivo explant culture models bridge the gap between *in vitro* and *in vivo* systems and reveal many advantages by maintaining the native tissue environment and decreasing the consumption of experimental animals. Compared with the small animals like mouse, rat and rabbit, the IVDs

from large animals such as sheep, dog and cow are more similar to human. They show comparable size and loss of notochordal cells in early adulthood as human IVD [47, 48]. Notochordal cells have been reported to present anti-inflammation and regenerative effect in IVDs [49, 50]. With those similarities, many bovine caudal IVD organ culture models were established. Bart van Dijk et al. developed a NP tissue explant culture model, and found that using polyethylene glycol to raise culture medium osmolarity was able to maintain the NP tissue specific matrix composition [25, 51]. Whole bovine caudal IVD cultured under either limited glucose condition or high-frequency loading condition led to a significant drop in cell viability, while combined treatment with limited glucose and high-frequency loading resulted in an additive increase in cell death in both the NP and annulus fibrosus (AF), and an increase in MMP13 gene expression [52]. Purmessur et al. (2013) cultured whole IVD organ excluding the endplates with exogenous TNF-α in medium, aggrecan degradation products and β-galactosidase staining were enhanced by TNF-α on day 21 without any recovery, when TNF-α was removed on day 7 [38]. Recently, our group has developed a proinflammatory and degenerative IVD whole organ culture system to investigate the proinflammatory and degenerative microenvironment operant in IVDD. Results indicated that a combination of detrimental dynamic loading, nutrient deficiency and intradiscal TNF-α injection could synergistically simulate the proinflammatory and degenerative disease condition. However, intradiscal TNF-α injection alone did not lead to a significant inflammatory effect [7].

In the present study, we sought to establish TNF-α induced *in vitro* and *ex vivo* IVD inflammation models, which would enable preclinical testing systems for screening of anti-inflammatory drugs for disc degeneration treatment. Specifically, the following questions were addressed within this study: a. Does bovine and human recombinant TNF-α have the same proinflammatory effect on bovine NP cells? b. What is the optimal dose of TNF-α when utilized within an IVD inflammation organ culture model induced by TNF-α intradiscal injection? c. Does TNF-α inhibition at different stages of inflammation have equal anti-inflammatory and/or regenerative effects on NP cells?

2. Materials and Methods

2.1. Medium selection

Alpha minimum essential medium (αMEM) has shown an advantage compared with Dulbecco's minimum essential medium (DMEM) in terms of numbers and quality of cells acquired in mesenchymal stem cells isolation and expansion [53]. In the current study, human and bovine NP cells isolation and expansion were performed with αMEM according to previous publication [54]. DMEM contains much higher amount of vitamins, amino acids and glucose than αMEM. Therefore, cells and IVD organ culture experiments with TNF-α and Etanercept were performed with DMEM, due to a much higher cell density and nutrition requirement in these experiments.

2.2. NP cells isolation and expansion

Human NP cells were isolated from traumatic IVDs (2 donors, 34/49 years old, male) with ethical approval (Cantonal Ethic Commission Bern 2016). General consent was obtained from all patients before surgery. All studies were performed in accordance with the ethical standards as laid down

in the 1964 Declaration of Helsinki and its later amendments or comparable ethical standards. The IVDs were classified as mildly degenerated by MRI (Pfirrmann grade 2-3). Bovine NP cells were isolated from caudal intervertebral discs of 6 to 12 month-old calves from local abattoirs immediately after death. NP cell isolation was performed as described previously [55]. The collected NP tissue was cut into small pieces. Human NP tissue was incubated with red blood cell lysis buffer (155 mM NH_4Cl, 10 M $KHCO_3$ and 0.1 mM EDTA in Milli-Q water) to remove the red blood cells. The chopped tissue was digested with 0.2% w/v Pronase (Roche, Mannheim, DE) in αMEM (Gibco, Paisley, UK) for 1 hour, then digested with 65 U/mL collagenase type II (Worthington, Lakewood, NL) in αMEM / 10% fetal bovine serum (FBS, PAN Biotech, Germany) in a spinner flask for 12-14 hours at 37 °C. The digested cell suspension was filtered through a 100 µm cell strainer to obtain a single-cell suspension. NP cells were expanded in αMEM supplemented with 10% FBS and 100 U/mL penicillin and 100 mg/mL streptomycin (1 % P/S, Gibco, Paisley, UK), incubated at a hypoxic condition of 2% O_2 at 37 °C. Culture medium was changed twice a week. Passage 2 and 3 NP cells were used in the current study.

2.3. Effect of human and bovine recombinant TNF-α on bovine NP cells

Bovine NP cells were seeded at a concentration of 60000/cm^2 in 12-well plates with DMEM medium (containing 4.5 g/L glucose) supplemented with 10% FBS. After cell attachment (24 hours after cell seeding), the medium was exchanged to serum-free experimental medium (DMEM supplemented with 1% ITS+, 1% nonessential amino acid (NEAA, Gibco, Paisley, UK), 50 µg/mL ascorbate 2 phosphate and 1% P/S) with or without inflammatory inducers 10 ng/mL human recombinant TNF-α (R&D systems, Zug, Switzerland) or 10 ng/mL bovine recombinant TNF-α (R&D Systems, Zug, Switzerland). After another 72 hours of culture, the cell monolayer was lysed and RNA was isolated for gene expression analysis.

2.4. Effect of human recombinant TNF-α and TNF-α inhibition on human NP cells

Human NP cells were seeded into a six well-plate at a cell density of 30000/cm^2. One day after seeding, cells were treated with 10 ng/mL (low dose) or 50 ng/mL (high dose) TNF-α in serum-free experimental medium as described above for bovine NP cells TNF-α experiments. The samples were collected at 3 timepoints, 6, 24, and 48 hours after treatment, for gene expression analysis.

To investigate the effect of TNF-α blocking with the TNF-α inhibitor Etanercept (Enbrel®, Pfizer, New York, USA), NP cells were seeded as described above and cultured for 24 hours to allow for cell attachment. Hereafter, cells were divided into 4 different groups: (1) iNP - cells were treated with 10 ng/mL TNF-α for 48 hours , (2) iNP-Eta - cells were treated with 10 ng/mL TNF-α and immediately after 1 µg/mL Etanercept was added for 48 hours, (3) iNP-24h-Eta - cells were treated with 10 ng/mL TNF-α, 24 hours after 1 µg/mL Etanercept was added, and (4) iNP-24h-FM: cells were treated with 10 ng/mL TNF-α, 24 hours after replaced to fresh medium without TNF-α. Cells treated with serum-free culture medium as described above served as negative control. All the cells were harvested for gene expression analysis at 72 hours after seeding. The concentration of Etanercept used here was selected according to previous studies, showing that Etanercept at 0.01, 0.1 and 1 µg/mL induced less than 8 % cell death in TNF-α transfected Jurkat

cells, and in human NP cells and AF cells cultured with Etanercept at 100, 250, 500, 1000, and 2000 μg/mL, cell proliferation was only suppressed with Etanercept at 500 μg/mL or higher [56, 57]. Therefore, the selected Etanercept concentration at 1 μg/mL was assumed to have no cytotoxic effect on NP cell culture in *vitro*.

2.5. IVDs dissection

Bovine caudal IVDs were collected from fresh sacrificed 6 to 12 month-old calves from local slaughterhouses. Disc dissection was performed as described previously [58]. Briefly, most of the muscle and soft tissue were removed, whole IVDs with cartilage endplates (EPs) were isolated with a band saw and redundant vertebral bone and growth plate were carefully cut off to ensure two parallel planes of discs. Disc height and diameter was then measured with a caliper. Disc volume = (long diameter + short diameter) /2)^2 × π × disc height. The surfaces of EPs were cleaned using a Pulsavac Wound Debridement Irrigation System (Zimmer, Minneapolis, USA) with Ringer's buffer to remove the cutting debris and blood clots. After prewashing in PBS with 10% P/S, IVDs were cultured in 6-well plates with 7.5 mL IVD culture medium, DMEM supplemented with 1% P/S, 50 mg/mL Primocin (Invitrogen, San Diego, CA, USA), 2% FBS, 50 μg/mL ascorbate 2 phosphate, 1% ITS+, 1% NEAA, at 37 °C, 5% CO_2.

2.6. IVD culture and intradiscal injection

IVDs having a diameter of 1.5 to 2.0 cm were selected for the current study. IVDs were cultured free swelling during the night. Dynamic loading was performed, at 0.02 to 0.2 MPa, 0.2 Hz for 2 hours per day within a bioreactor [7]. IVDs from each donor were randomly divided into three groups: PBS, TNF-α and TNF-α + Etanercept. TNF-α + Etanercept: 40 μL of TNF-α, containing 100 ng TNF-α/cm^3 of disc volume, was firstly injected into the disc, 30 minutes after 20 μL Etanercept, containing 10 μg Etanercept per 100 ng TNF-α, was injected into the disc. TNF-α: 40 μL of TNF-α, containing 100 ng TNF-α/ cm^3 of disc volume, was injected into disc 30 minutes after 20 μL PBS was injected. PBS: 40 μL and 20 μL PBS was injected into disc sequentially. The injection was performed using a 30-gauge insulin needle, after the first dynamic loading on day 1. The intradiscal injection dose of Etanercept was kept at the same ratio of TNF-α to Etanercept as *in vitro*, which is 1:100. IVDs were cultured with daily dynamic loading and free swelling recovery overnight, the disc size of IVDs was measured before and after loading [7]. Culture media were collected daily after free swelling for further analysis. The NP tissue (gel-like inner core of 6-8 mm of diameter) was collected for gene expression analysis on day 2 and day 5.

2.7. Gene expression analysis

RNA samples were collected from monolayer NP cells by adding 0.5 mL TRI reagent (Molecular Research Centre Inc., Cincinnati, OH, USA) with 2.5 μL polyacryl carrier (Molecular Research Centre Inc., Cincinnati, OH, USA) per well. RNA isolation was performed according to the manufacturer's specifications. RNA isolation from NP tissues was performed as described before [59]. NP tissues, 150 to 200 mg per sample isolated from discs, were cut into small pieces, snap-frozen in liquid nitrogen and pulverized. The pulverized tissue was carefully collected and put into 3 mL TRI reagent with 15 μL polyacryl carrier. The volume of the TRI reagent was added

according to the original NP tissue weight (3 mL TRI for 150-200 mg tissue) with a volume ratio of >10:1 to supply adequate TRI volume for RNA isolation. Samples were homogenized immediately by a tissue-lyser. After centrifugation, the supernatant was collected. Phase separation was performed by adding 100 µL bromochloropropane per 1 mL of TRI reagent and centrifugation. The aqueous phase was mixed with the same volume of 70% ethanol. The following steps were performed using the QIAGEN RNeasy MINI kit according to the manufacturer's protocol.

SuperScript VILO™ cDNA Synthesis Kit (Invitrogen) was used for cDNA synthesis with 400 ng RNA per sample. The quantitative real-time polymerase chain reaction (qRT-PCR) was conducted on QuantStudio6 PCR System (Applied Biosystems). The primers and probes used in qRT-PCR for human and bovine samples are shown in Table 1. All the data were analyzed using $2^{-\Delta\Delta CT}$ method, with *RPLP0* as an endogenous control. The *RPLP0* showed similar Ct value with different treatments, indicating TNF-α and Etanercept did not show an influence on the house keeping gene expression.

Table 1. Oligonucleotide primers and probes (bovine and human) used for qRT-PCR.

Gene	Primer/probe type	Sequence
bIL6	Primer fw (5′–3′)	TTC CAA AAA TGG AGG AAA AGG A
	Primer rev (5′–3′)	TCC AGA AGA CCA GCA GTG GTT
	Probe (5′FAM/3′TAMRA)	CTT CCA ATC TGG GTT CAA TCA GGC GATT
bCol2	Primer fw (5′–3′)	AAG AAA CAC ATC TGG TTT GGA GAA A
	Primer rev (5′–3′)	TGG GAG CCA GGT TGT CAT C
	Probe (5′FAM/3′TAMRA)	CAA CGG TGG CTT CCA CTT CAG CTA TGG
bACAN	Primer fw (5′–3′)	CCA ACG AAA CCT ATG ACG TGT ACT
	Primer rev (5′–3′)	GCA CTC GTT GGC TGC CTC
	Probe (5′FAM/3′TAMRA)	ATG TTG CAT AGA AGA CCT CGC CCT CCA T
bMMP3	Primer fw (5′–3′)	GGC TGC AAG GGA CAA GGA A
	Primer rev (5′–3′)	CAA ACT GTT TCG TAT CCT TTG CAA
	Probe (5′FAM/3′TAMRA)	CAC CAT GGA GCT TGT TCA GCA ATA TCT AGA AAA C
bADAMTS5	Primer fw (5′–3′)	GAT GGT CAC GGT AAC TGT TTG CT
	Primer rev (5′–3′)	GCC GGG ACA CAC CGA GTA C
	Probe (5′FAM/3′TAMRA)	AGG CCA GAC CTA CGA TGC CAG CC
bADAMTS4	Primer fw (5′–3′)	CCC CAT GTG CAA CGT CAA G
	Primer rev (5′–3′)	AGT CTC CAC AAA TCT GCT CAG TGA
	Probe (5′FAM/3′TAMRA)	AGC CCC CGA AGG GCT AAG CGC

bCOX2		Bt03214492_m1
bIL8		Bt03211906_m1
bRPLP0		Bt03218086_m1
hACAN	Primer fw (5′–3′)	AGT CCT CAA GCC TCC TGT ACT CA
	Primer rev (5′–3′)	CGG GAA GTG GCG GTA ACA
	Probe (5′FAM/3′TAMRA)	CCG GAA TGG AAA CGT GAA TCA GAA TCA ACT
hMMP3		Hs00968305_m1
hIL8		Hs00174103_m1
hRPLP0	Primer fw (5′–3′)	TGG GCA AGA ACA CCA TGA TG
	Primer rev (5′–3′)	CGG ATA TGA GGC AGC AGT TTC
	Probe (5′FAM/3′TAMRA)	AGG GCA CCT GGA AAA CAA CCC AGC

Note: Primers and probes with the sequence shown were custom-designed; primers and probes with the catalog number were from Applied Biosystems. Abbreviations: ACAN, aggrecan; ADAMTS4, a disintegrin and metalloproteinase with thrombospondin motifs 4; ADAMTS5, a disintegrin and metalloproteinase with thrombospondin motifs 5; COL2A1, type II collagen; FAM, carboxyfluorescein; fw: forward; Gene prefix "b" bovine, prefix "h" human; rev, reverse; IL6, interleukin 6; IL8, interleukin 8; MMP3, matrix metalloproteinase-3; RPLP0: Ribosomal Protein Lateral Stalk Subunit P0; TAMRA, tetramethylrhodamine.

2.8. Enzyme-linked immunosorbent assay

IL-6 and IL-8 content in bovine IVD organ culture media were measured with enzyme-linked immunosorbent assay (ELISA) kits (Kingfisher Biotech, St. Paul, USA). Capture antibody: anti-bovine IL-6 polyclonal antibody (KP0652B-100, Kingfisher Biotech, USA), anti-bovine IL-8 polyclonal antibody (PB1164B-100, Kingfisher Biotech, USA). Detection antibody: Biotinylated-anti-bovine IL-6 (KPB0653B-050, Kingfisher Biotech, USA), Biotinylated-anti-bovine IL-8 (PBB1165B-050, Kingfisher Biotech, USA). Experiments were performed according to the manufacturer's protocol. The results of the ELISA were presented as the original concentration in the media without normalization.

2.9. Glycosaminoglycan (GAG) and nitric oxide (NO) measurement

The amount of GAGs released in IVDs culture media was measured by using the 1,9-dimethylmethylene blue dye (DMMB) method [60]. The level of GAG release from each IVD at each time point after injection was normalized to the amount released on day 1 before injection by dividing the corresponding day's GAG release content with the amount of GAG release on day 1. The concentration of NO in the culture media of IVDs was detected as the level of its stable oxidation product, nitrite (NO^{2-}), using the Griess Reagent Kit (Promega, USA). The NO concentrations in the media are presented in the results section without normalization.

2.10. Statistical analysis

Statistical analyses were performed using GraphPad Prism 7 software (GraphPad Software, Inc., La Jolla, CA, USA). D'Agostino-Pearson omnibus normality test was used to define whether the data were normally distributed. For data that were normally distributed, unpaired t-test was used to determine differences between two groups; One-way ANOVA was used to determine differences between three or more groups. For the not normally distributed data, Mann–Whitney U test was used to determine differences between two groups; Kruskal Wallis test was used to determine differences between three or more groups. $P<0.05$ was considered statistically significant.

3. Results

3.1. Bovine and human recombinant TNF-α comprise equivalent proinflammatory potency in bovine NP cells

Bovine NP cells were treated with 10 ng/mL bovine or human recombinant TNF-α. Catabolic gene expression as well as proinflammatory mediators are illustrated in Figure1 (median and interquartile range). *COL2A1* (0.3 (0.2 to 0.5) bovine, 0.25 (0.2 to 0.7) human) expression was significantly downregulated, while *ACAN* (1.8 (0.6 to 1.9) bovine, 1.3 (0.8 to 2.2) human) expression was not changed. Degradative proteinase, *MMP3* (26.5 (21.9 to 36.8) bovine, 41.5 (34.6 to 71.8) human), *ADATMS4* (3.7 (3.1 to 6.7) bovine, 2.8 (2.3 to 5.3) human), *ADAMTS5* (12.8 (10.2 to 18.0) bovine, 12.5 (8.3 to 26.5) human), and inflammatory mediators, IL-6 (34.1 (28.0 to 66.3) bovine, 57.9 (34.6 to 121.9) human), IL8 (15.9 (6.1 to 21.9) bovine, 26.3 (20.8 to 49.6) human), COX2 (14.5 (3.7 to 16.6) bovine, 9.5 (7.1 to 11.0) human), were significantly upregulated by both types of TNF-α. There was no difference in the gene expression between treatment with human or bovine TNF-α.

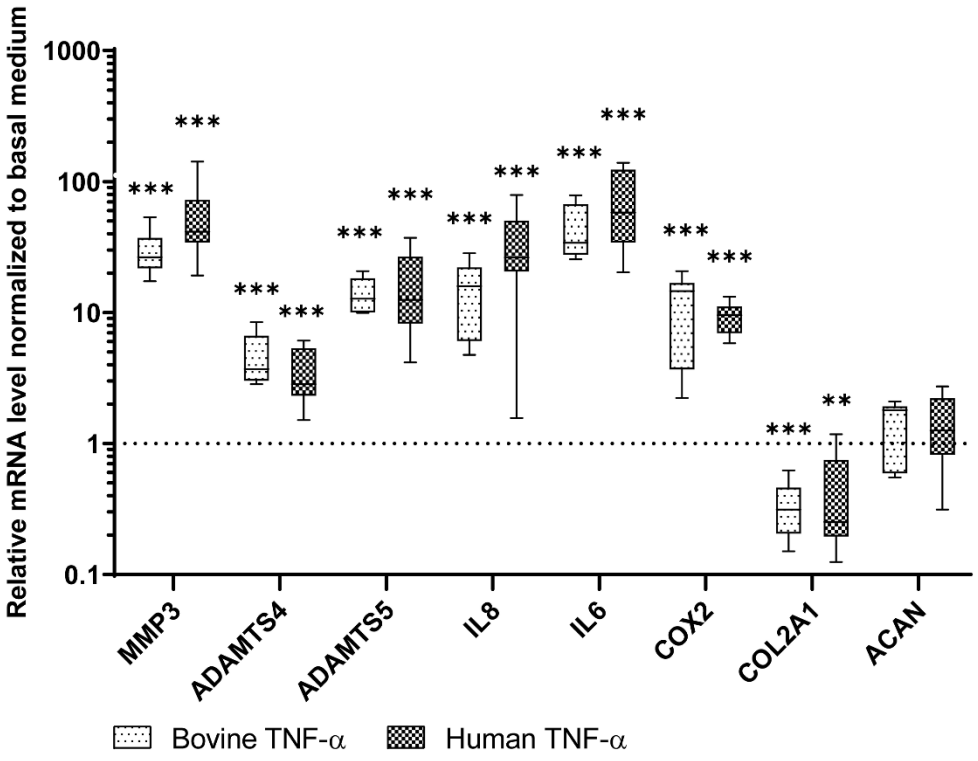

Figure 1. Relative mRNA expression level of bovine NP cells cultured with bovine or human recombinant TNF-α.

*Bovine NP cells cultured with 10 ng/mL bovine or human recombinant TNF-α for 72 hours. The mRNA expression level was normalized to the control group with basal medium. Min to Max with median and interquartile range, n = 9, **P < 0.01, ***P < 0.001 vs Basal Medium group.*

3.2. TNF-α induced inflammation in human NP cells

Human NP cells were treated with human recombinant TNF-α at a concentration of 10 ng/mL or 50 ng/mL. Samples were collected at three time points, 6, 24, and 48 hours, for gene expression analysis. As shown in Figure 2 (median and interquartile range, 10 ng: 6, 24, and 48 hours, 50 ng: 6, 24, and 48 hours respectively). *MMP3* (124.7 (106.6 to 175), 364.0 (348.4 to 403.2), 624.3 (363.5 to 765.0), 288(219.1 to 402.5), 997.1 (775.3 to 1123.0), 2222.0 (1544.0 to 3104.0)) and IL-8 (12139 (7916 to 16423), 52191(10034 to 120284), 111110 (101742 to 146623), 23167 (16714 to 25564), 155345 (35201 to 319280), 564964 (324997 to 804055)) expression were upregulated over time with a dose-dependent effect. *ACAN* (0.7 (0.7 to 1.1), 0.3 (0.2 to 0.3), 0.1 (0.8 to 0.1), 0.7 (0.7 to 0.8), 0.2 (0.2 to 0.3), 0.1 (0.07 to 0.13)) was downregulated over time independent of the TNF-α dose.

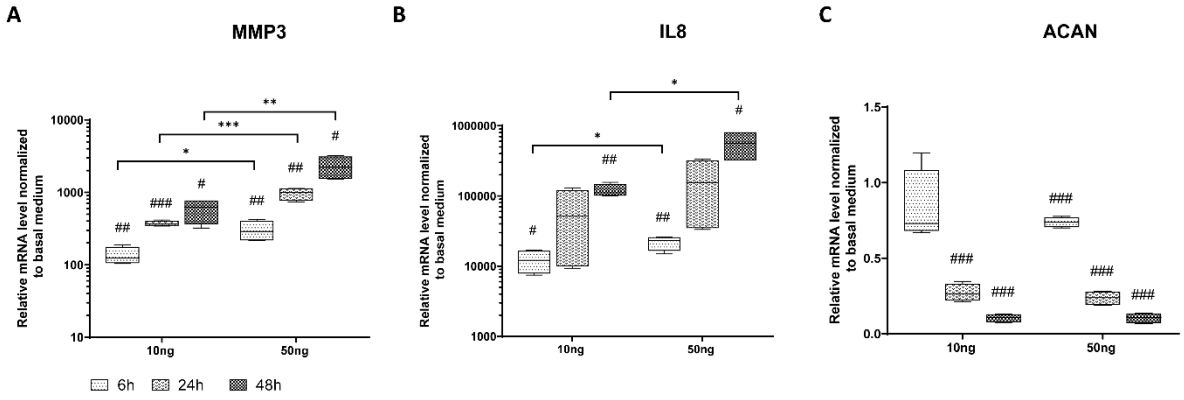

Figure 2. Relative mRNA expression of human NP cells treated with different dose of TNF-α at different time points.

*Human NP cells treated with 10 ng/mL or 50 ng/mL TNF-α for 6, 24, and 48 hours. Gene expression data of MMP3 (A), IL-8 (B), ACAN (C) were normalized to the basal medium without TNF-α as 1. Min to Max with median and interquartile range, n = 4, #P < 0.05, ##P < 0.01, ###P < 0.001 vs basal medium, *P < 0.05, **P < 0.01, ***P < 0.001, TNF-α 10 ng/mL vs 50 ng/mL at the same time point.*

To investigate the anti-inflammatory treatment with TNF-α blocking at different time points, NP cells were treated with TNF-α 10 ng/mL for 48 hours (iNP), TNF-α immediately followed by 1 µg/mL Etanercept for 48 hours (iNP-Eta), TNF-α for 24 hours followed by 1 µg/mL Etanercept for 24 hours (iNP-24h-Eta), and finally TNF-α for 24 hours then replacing to fresh basal medium without TNF-α for 24 hours (iNP-24h-FM). NP cells treated with basal medium served as control (Figure 3; median and interquartile range). Inflammation induced by TNF-α (iNP) caused an increased *MMP3* (61.7 (48.3 to 73.1)) and *IL-8* (8289 (4700 to 12572)) expression and decreased *ACAN* (0.22 (0.1 to 0.4)) expression. Etanercept applied at the beginning of the proinflammatory processes completely inhibited inflammation in iNP-Eta, as shown by decreased *MMP3* (1.5 (1.2 to 1.6)) and *IL-8* (9.3 (3.1 to 14.7)) expression and increased *ACAN* (1.0 (0.8 to 1.1)) expression compared with iNP group, but comparable to the control group. Etanercept treatment in the middle of the inflammation process can block the inflammation effect, as shown by decreased *IL-8* (19.6 (10.1 to 31.4)) expression and partly decreased *MMP3* (28.6 (24.9 to 30.0) compared with iNP. However, the *ACAN* (0.39 (0.30 to 0.41) expression was comparable with iNP. Removal of TNF-α after 24h (iNP-24h-FM) showed the similar effect as iNP-24h-Eta, partial recovery from inflammation, observed by partly decreased *IL-8* (135.6 (121.3 to 149.6) and *MMP3* (32.6 (19.5 to 46.4) expression compared with iNP, but *ACAN* (0.13 (0.11 to 0.13) expression cannot be recovered.

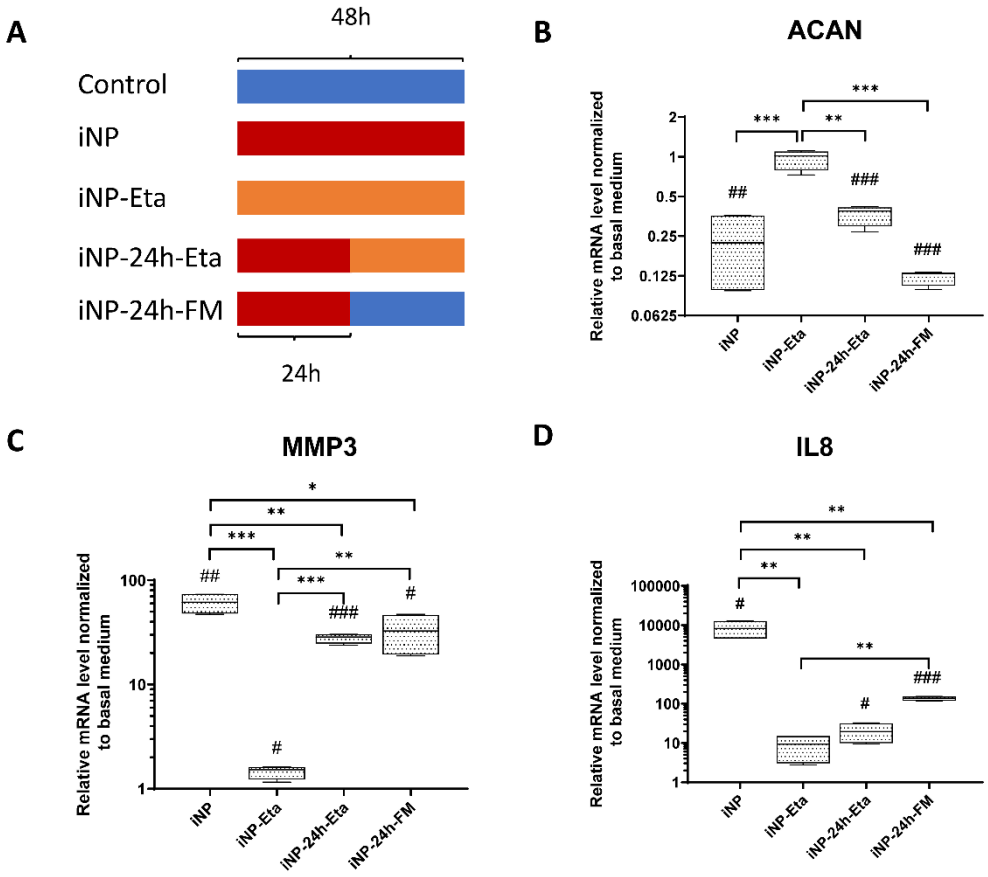

Figure 3. Relative mRNA expression levels of human NP cells.

*Human NP cells were cultured with basal medium (Control), TNF-α 10 ng/mL for 48 hours (iNP), TNF-α immediately followed by 1 μg/mL Etanercept for 48 hours (iNP-Eta), TNF-α for 24 hours followed by 1 μg/mL Etanercept added for 24 hours (iNP-24 hours-Eta), or TNF-α for 24 hours followed by fresh basal medium without TNF-α for 24 hours (iNP-24 hours-FM). (A) Scheme of treatment, blue: TNF-α free, red: TNF-α exist, orange: both TNF-α and Etanercept exist. Gene expression data of ACAN (B), MMP3 (C), and IL-8 (D) were normalized to the level of control group as 1. Min to Max with median and interquartile range, n = 4, #P < 0.05, ##P < 0.01, and ###P < 0.001 vs basal medium, *P < 0.05, **P < 0.01, and ***P < 0.001.*

3.3. Proinflammatory IVD organ culture model

According to our previous study, intradiscal injection of 100 ng human TNF-α per disc did not induce a significant inflammatory effect [7]. As shown in figure 1, both bovine and human TNF-α can induce inflammation equally in bovine NP cells. Hence, the difference in species origin of TNF-α was excluded. Therefore, we hypothesized that the dose of TNF-α may influence the results. A preliminary experiment was performed by intradiscal injection of 100, 200, or 400 ng human recombinant TNF-α into IVDs with various sizes (1.5 to 3 cm^3). Results (Figure S1) showed a trend of enhanced disc inflammation and its response with increasing TNF-α dose, evaluated by NO and GAG release in IVD culture media. When results were normalized to the injected TNF-

α amount/cm^3 disc volume, a threshold at 100 ng TNF-α/cm^3 disc volume was observed, with significant inflammatory effect above this injection dose.

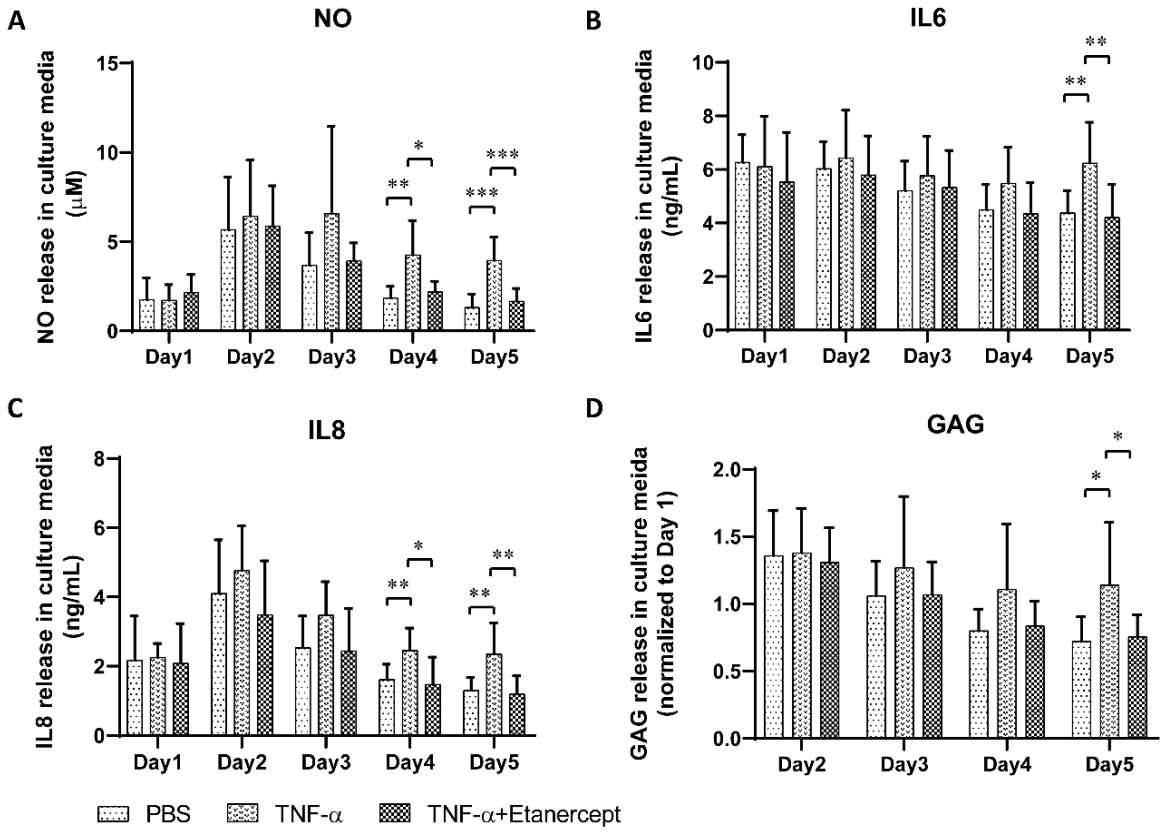

Figure 4. NO, IL-6, IL-8, and GAG release in the IVD culture medium.

*NO (A), IL-6 (B), IL-8 (C), and relative GAG (D, normalized to day 1) release in the conditioned medium of IVDs with PBS injection (PBS), TNF-α injection (TNF-α), and TNF-α plus Etanercept injection (TNF-α + Etanercept). Intradiscal injection performed after day 1 loading. Mean + SD, n = 9, *P < 0.05, **P < 0.01, and ***P < 0.001.*

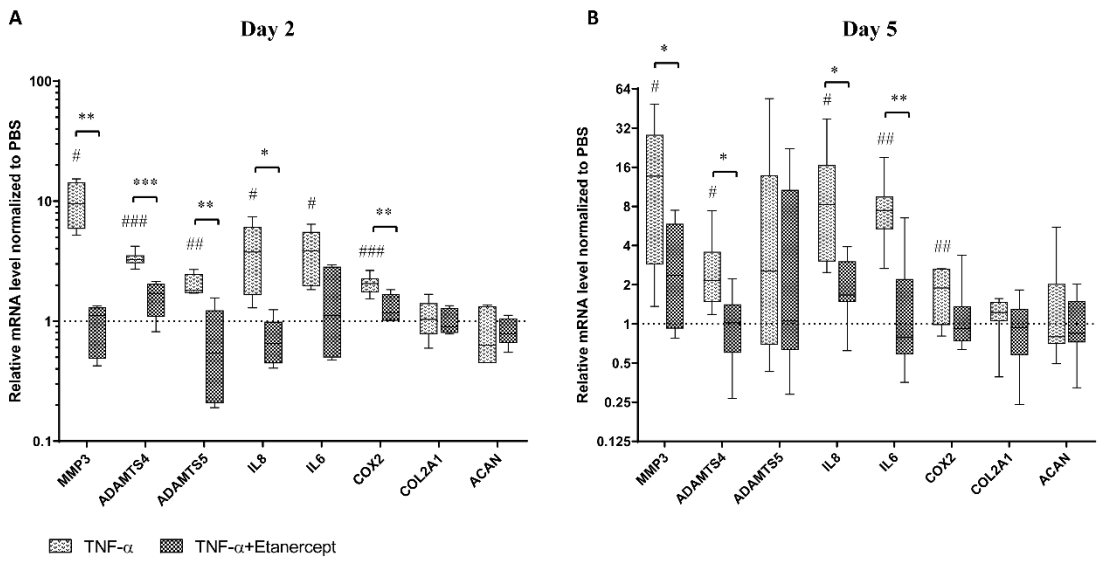

Figure 5. Relative mRNA expression level of NP tissue from IVDs.

*IVDs cultured with TNF-α injection (TNF-α), and TNF-α plus Etanercept injection (TNF-α + Etanercept), the gene expression level in NP tissue on day 2 (A) and day 5 (B), data were normalized to IVDs with PBS injection (PBS) as 1. Min to Max with median and interquartile range, samples on day 2, n = 5, samples on day 5, n = 8, #P < 0.05, ##P < 0.01, and ###P < 0.001 vs PBS group, *P < 0.05, **P < 0.01, and ***P < 0.001, TNF-α group vs TNF-α + Etanercept group.*

Consequently, intradiscal injection was performed with TNF-α at 100 ng/cm^3 disc volume after the first dynamic loading on day 1 to induce inflammation in the IVD organ culture model (TNF-α). Etanercept was injected after 30 minutes after TNF-α injection, at a ratio of Etanercept(w): TNF-α(w) = 100:1 as anti-inflammation positive control (TNF-α + Etanercept). Discs were injected with the same volume of PBS as negative control (PBS). Discs were cultured with daily physiological loading and culture media after overnight free swelling were collected daily for NO, IL-6, IL-8, and GAG measurement. NP tissue was collected at two time points, at 1 (Day 2) or 4 days (Day 5) after TNF-α injection. As shown in Figure 4 (Mean ± SD), starting from day 4, TNF-α injected discs released significantly higher NO (5.7 ± 5.0) and IL-8 (2.2 ± 0.8) compared with PBS (2.1 ± 0.9 NO, 1.6 ± 0.4 IL-8) and TNF-α+Etanercept (2.7 ±1.6 NO, 1.6 ± 0.8 IL-8). On day 5, TNF-α injected discs showed significantly higher amount of GAG (1.3 ± 0.5) and IL-6 (6.2 ± 1.5) release compared with PBS (0.7 ± 0.2 GAG, 4.4 ± 0.8 IL-6) and TNF-α+Etanercept (0.8 ± 0.2 GAG, 4.2 ± 1.2 IL-6). As shown in Figure 5 (median and interquartile range, day 2: TNF-α, TNF-α+Etanercept, day 5: TNF-α, TNF-α+Etanercept, respectively), the gene expression of *MMP3* (9.6 (5.9 to 14.2), 1.1 (0.5 to 1.3), 9.2 (1.2 to 19.9), 2.4 (0.9 to 5.9)), *ADAMTS4* (3.3 (3.1 to 3.5), 1.7 (1.1 to 2.0), 2.1 (1.5 to 3.6), 1.0 (0.6 to 1.4)), *IL-8* (3.8 (1.66 to 6.1), 0.7 (0.5 to 1.0), 5.2 (2.1 to 14.2), 1.7 (1.5 to 3.0)), IL-6 (3.9 (2.0 to 5.5), 1.1 (0.5 to 2.8), 7.4 (3.2 to 8.9), 0.8(0.6 to 2.2)), *COX2* (2.1 (1.7 to 2.3), 1.2 (1.0 to 1.7), 1.9 (1.0 to 2.6), 0.9 (0.7 to 1.4)) were significantly increased at day 2 and day 5 by TNF-α injection, and *ADAMTS5* (1.8(1.7 to 2.5), 0.5 (0.2 to 1.2), 2.5 (0.7 to 13.8), 1.1 (0.6 to 10.7)) was upregulated at day 2. All genes' upregulation can be eliminated by Etanercept. Nevertheless, *COL2A1* (1.0 (0.8 to 1.4), 0.9 (0.8 to 1.3), 1.2 (1.1 to 1.5), 0.9 (0.6 to 1.3)) and

ACAN (0.6 (0.5 to 1.3), 0.8 (0.7 to 1.1), 0.8 (0.7 to 2.0), 0.8 (0.7 to 1.5)) expression were not changed by TNF-α. After free swelling disc height increased by proximately 5% and disc volume increased by proximately 18%. After daily loading disc height decreased by approximately 10% and disc volume by approximately 5%, compared with day 0 when discs were isolated. However, the fold changes of disc height and volume did not show any difference among these 3 groups (Figure 6).

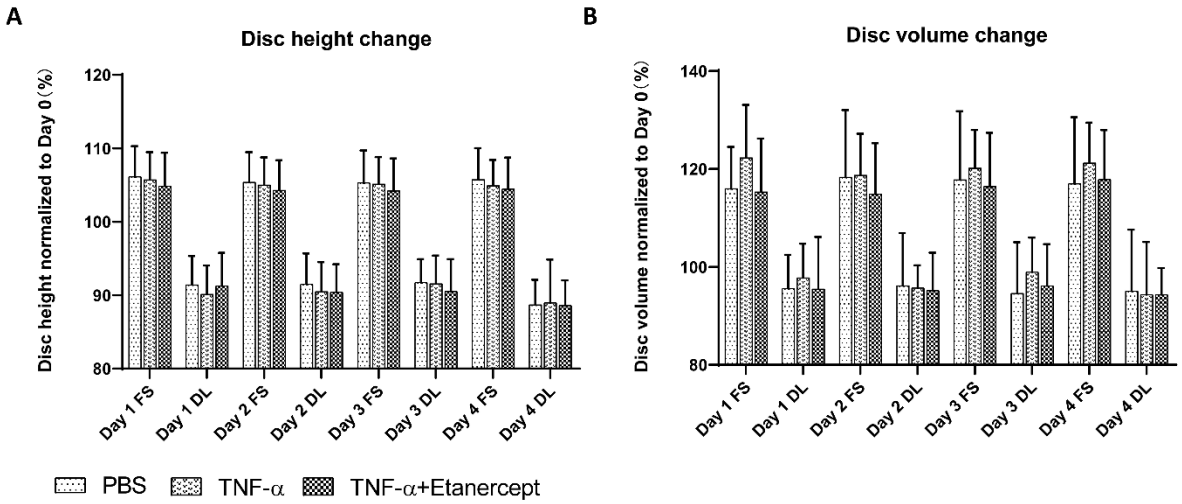

Figure 6. Disc height and volume change of cultured IVDs.

IVDs with PBS injection (PBS), TNF-α injection (TNF-α), and TNF-α plus Etanercept injection (TNF-α + Etanercept) at different time points: after free swelling culture overnight (FS) and after dynamic loading (DL) over 5 days of organ culture. Data were normalized to initial disc height (A) or volume (B) after dissection on Day 0 in percentage. Mean + SD, n = 9.

4. Discussion

Anti-inflammatory therapy has been considered as a promising approach to delay the IVD degeneration and relieve discogenic pain. TNF-α, as a pro-inflammatory factor, has been reported to be associated with IVD degeneration and discogenic pain [21, 61]. Anti-inflammatory therapies targeting TNF-α are widely reported, with preserved matrix production and restraint of matrix degradation [31, 37, 42]. Therefore, *in vitro* and *ex vivo* IVD inflammatory culture systems induced by TNF-α are clinically relevant models for drug development for treatment of disc degeneration. In the current study, several specific questions related to the inflammatory model were investigated. Firstly, due to the scarce access to human IVD tissue and especially to healthy samples, bovine IVD cells and bovine caudal whole IVDs have been widely used in spine research. While using TNF-α for inflammation induction of bovine disc cells or organs, one question which has not been well addressed is whether human and bovine recombinant TNF-α imply the same effect on bovine disc cells, or whether the TNF-α receptors on bovine disc cells can also transmit the signaling from human recombinant TNF-α. Present results showed both bovine and human recombinant TNF-α can equally induce inflammation in bovine NP cells *in vitro* (Figure 1). These results support most of the studies in the field, confirming that human recombinant TNF-α can be used for inflammation induction in bovine disc cells [38, 62].

Secondly, the required dose for an inflammatory IVD organ culture model based on intradiscal TNF-α injection is unclear. Takahashi et al. (1996) reported that the concentration of TNF-α in herniated disc tissue is a dozens of pgs per 100 mg tissue [32]. However, the dose of TNF-α used in all the artificial inflammatory models is much higher than the pathological dose, since such low dose of TNF-α may fail to induce significant inflammation response or need a very long time to reach significance *in vitro* and *ex vivo*. According to our previous study, TNF-α injection at a fixed dose of 100 ng per disc did not induce a consistent inflammatory response [7]. In contrast, TNF-α added into disc culture media at a dose 200 ng/mL induced significant inflammation in discs without cartilage endplates [38]. The current study showed that an injection dose normalized to the disc volume was necessary to induce a reproducible inflammatory effect in the IVD organ culture model. The injection dose was optimized to 100 ng TNF-α/cm^3 disc volume. This has effectively induced inflammation in bovine NP tissue, as shown by increased NO, GAG, IL-6, and IL-8 release in culture media, and upregulated *MMP3*, *ADAMTS4*, *IL-8*, *IL-6*, and *COX-2* expression in NP tissue on both day 2 and day 5. These results showed that TNF-α intradiscal injection at the adjusted dose increased expression of catabolic enzymes and inflammatory mediators in the whole IVD organ culture system, which is consistent with previous NP tissue and cell culture studies [34, 45]. This may be a realistic way to mimic the inflammatory and degenerative condition of IVD disease in preclinical models.

Our result showed that TNF-α downregulated gene expression of type II collagen in cell culture, but not in whole organ culture. In contrast, Seguin et al. (2005) showed that TNF-α decreased expression of type II collagen in NP tissue culture [34]. This suggests that the whole IVD organ culture system is beneficial for maintaining disc cell homeostasis, which may be due to the physiological osmolarity inside the intact organ that has been shown to maintain the NP tissue specific matrix composition [51].

Annular puncture may induce disc degeneration depending on the disc size and needle size [63]. A recent goat study revealed that 22G needle puncture did not result in degenerative changes in lumbar IVDs, nor was degeneration found in IVDs of Beagles injected using 25G needles [64, 65]. Also, in bovine caudal IVD we found that IVD puncture using a 30-gauge needle did not cause dysregulation on expression of anabolic, catabolic and inflammatory markers [7]. Therefore, injection using a 30-gauge needle is not expected to cause an effect on the state of IVD degeneration in the current experiments.

Analysis of the culture medium was undertaken to investigate whether the molecule release was related to the disc volume. This was performed with IVDs cultured under physiological loading and without TNF-α injection. The initial GAG release on day 1 from discs of different donors showed a high variation, which may result in an inundating difference between experimental groups. The day 2 GAG release was highly related with day 1, evaluated with linear regression (R^2 =0.935. Figure S2). The NO, IL6, and IL8 release data did not show such inter-donor variation (Figure S2). Therefore, the results of GAG release from the inflammatory model experiments (Figure 4D) were analyzed with normalized relative fold changes instead of using the original absolute content.

TNF-α induced a nonrecoverable catabolic shift of NP cells even when it was removed from the medium at 24 hours after supplementation, which is consistent with previous studies [38, 42]. More interestingly, our results showed that the time point of anti-inflammatory treatment with Etanercept is crucial for reversing the catabolic effect caused by TNF-α, where only Etanercept application at early time point could show a positive effect. This may explain the available clinical data where intradiscal Etanercept injection in patients with back pain showed controversy in pain relieving results. Etanercept epidural injection in patients with lumbosacral radicular pain of 6 to 26 weeks duration provided clinically significant reductions in mean daily worst leg pain and worst back pain [66]. However, Etanercept injection in patients with chronic LBP, more than 6 months' duration, was unable to resolve chronic discogenic pain [67]. Hence, anti-inflammatory treatment with Etanercept at early onset of disc inflammation may be beneficial to relieve discogenic pain by reversing the degenerative cascade. There seems to be a time-point dependent window of therapeutic applicability for anti-inflammation strategies. However, radicular pain indicates IVD herniation, which is a different entity from chronic LBP related to IVD degeneration and may therefore intrinsically respond differently to anti-inflammatory treatment. In clinics, patients are usually treated at a certain period after an acute inflammation or during chronic inflammation process. At this stage, targeting or removal of the inflammatory factor may not be sufficient. Also, treatment to prevent continuous degeneration needs to be included as well.

Limitations: This study solely focused on TNF-α induced acute inflammation within IVDs. Other proinflammatory factors such as IL-1β and lipopolysaccharide (LPS) may also be used for the same purpose, while the differences in the effects of various factors need to be further evaluated. Both *in vitro* and *ex vivo* experiments were only performed within one week. Therefore, further studies should be designed to investigate the effect of prolonged or repeated stimulation of TNF-α. The exogenous dose of TNF-α in the current study is much higher than *in vivo* pathological conditions, and a high dose of TNF-α can induce cell apoptosis and senescence, which play important roles in IVD degeneration [32, 38, 68]. In rat NP cells cultured with TNF-α at 50 ng/mL for 12 hours apoptosis was induced [68]. Also in IVD organs cultured with 200 ng/mL TNF-α for 21 days cell senescence was induced [38]. Further study is warranted to evaluate the effect of TNF-α on cell apoptosis and senescence in long-term within the current model in the future.

5. Conclusion

The present work sought to address several specific questions on the establishment of an IVD inflammatory model with TNF-α. Bovine and human recombinant TNF-α induced equal inflammatory effects in bovine NP cells. A bovine whole IVD inflammatory model was established by intradiscal injection of 100 ng TNF-α/cm^3 disc volume, as indicated by increased NO, GAG, IL-6, IL-8 release in culture media, and upregulated *MMP3*, *ADAMTS4*, *IL-8*, *IL-6*, and *COX-2* expression in NP tissue. The time points of anti-inflammatory treatment are crucial, and additional anti-catabolic treatment to prevent degeneration would be needed to completely maintain disc biology and function.

Acknowledgements:

This study was funded by AO Foundation, AOSpine International, and the European Union's Horizon2020 research and innovation programme under Marie Sklodowska-Curie Grant Agreement No 642414 (TargetCare) and No 801540 (RESCUE). Gernot Lang was supported by the Berta-Ottenstein-Programme for Advanced Clinician Scientists, Faculty of Medicine, University of Freiburg, Germany.

Author Contributions:

Jie Du: substantial contributions to study design, acquisition, analysis, interpretation of data, drafting the article, revising it critically, and final approval. Judith-J. Pfannkuche: substantial contributions to acquisition of data, analysis, interpretation of data, revising the article critically, and final approval. Gernot Lang, Sonja Häckel, Laura B. Creemers, Mauro Alini, and Sibylle Grad: substantial contributions to study design, revising the article critically, and final approval. Zhen Li: substantial contributions to study design, interpretation of data, drafting the article, revising it critically, final approval, and takes responsibility for the integrity of the work as a whole, from inception to finished article.

Conflict of Interest:

The authors have no conflict of interest.

Supplementary figures

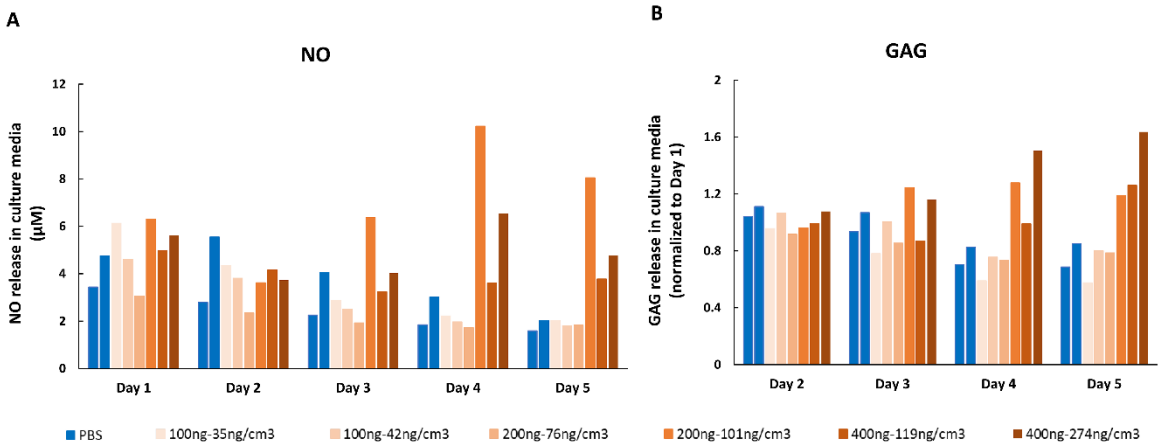

Supplementary figure 1. Preliminary experiments for optimization of the dose of intradiscal injection of TNF-α.

Eight discs obtained from 2 tails, 4 discs per tail. After day 1 loading, discs from each tail were randomly injected with PBS, 100 ng, 200 ng or 400 ng TNF-α respectively. The dose of TNF-α in each disc was calculated as a concentration in ng per cm3 disc volume. Discs were cultured with daily physiological loading over 5 days, GAG (A) and NO (B) release in culture media after overnight free swelling were measured.

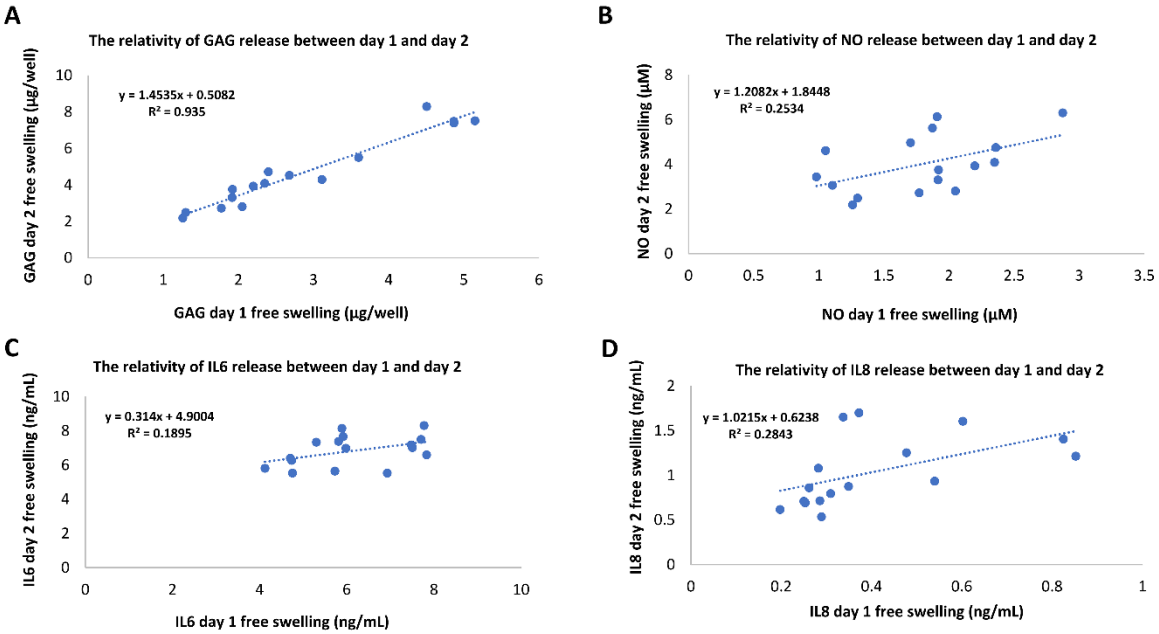

Supplementary figure 2. *Regression analysis of the GAG, NO, IL-6 and IL-8 release content in the conditioned media of bovine IVDs cultured during day 1 and day 2, under physiological culture condition without TNF-α injection.*

References

[1] S. Clark, R. Horton, Low back pain: a major global challenge, Lancet 391(10137) (2018) 2302.
[2] G.B. Andersson, Epidemiological features of chronic low-back pain, Lancet 354(9178) (1999) 581-5.
[3] A.J. Freemont, The cellular pathobiology of the degenerate intervertebral disc and discogenic back pain, Rheumatology (Oxford) 48(1) (2009) 5-10.
[4] T.S. Jensen, J. Karppinen, J.S. Sorensen, J. Niinimäki, C.J.E.S.J. Leboeuf-Yde, Vertebral endplate signal changes (Modic change): a systematic literature review of prevalence and association with non-specific low back pain, 17(11) (2008) 1407.
[5] M.A. Adams, P.J. Roughley, What is intervertebral disc degeneration, and what causes it?, Spine (Phila Pa 1976) 31(18) (2006) 2151-61.
[6] M.V. Risbud, I.M. Shapiro, Role of cytokines in intervertebral disc degeneration: pain and disc content, Nat Rev Rheumatol 10(1) (2014) 44-56.
[7] G. Lang, Y. Liu, J. Geries, Z. Zhou, D. Kubosch, N. Sudkamp, R.G. Richards, M. Alini, S. Grad, Z. Li, An intervertebral disc whole organ culture system to investigate proinflammatory and degenerative disc disease condition, J Tissue Eng Regen Med 12(4) (2018) e2051-e2061.
[8] J.P. Urban, S. Roberts, Degeneration of the intervertebral disc, Arthritis Res Ther 5(3) (2003) 120-30.
[9] P.P. Vergroesen, I. Kingma, K.S. Emanuel, R.J. Hoogendoorn, T.J. Welting, B.J. van Royen, J.H. van Dieen, T.H. Smit, Mechanics and biology in intervertebral disc degeneration: a vicious circle, Osteoarthritis Cartilage 23(7) (2015) 1057-70.
[10] V.K. Podichetty, The aging spine: the role of inflammatory mediators in intervertebral disc degeneration, Cell Mol Biol (Noisy-le-grand) 53(5) (2007) 4-18.
[11] L.I. Kerttula, W.S. Serlo, O.A. Tervonen, E.L. Paakko, H.V. Vanharanta, Post-traumatic findings of the spine after earlier vertebral fracture in young patients: clinical and MRI study, Spine (Phila Pa 1976) 25(9) (2000) 1104-8.
[12] M.A. Adams, B.J. Freeman, H.P. Morrison, I.W. Nelson, P. Dolan, Mechanical initiation of intervertebral disc degeneration, Spine (Phila Pa 1976) 25(13) (2000) 1625-36.
[13] N. Bergknut, J.P. Rutges, H.J. Kranenburg, L.A. Smolders, R. Hagman, H.J. Smidt, A.S. Lagerstedt, L.C. Penning, G. Voorhout, H.A. Hazewinkel, G.C. Grinwis, L.B. Creemers, B.P. Meij, W.J. Dhert, The dog as an animal model for intervertebral disc degeneration?, Spine (Phila Pa 1976) 37(5) (2012) 351-8.
[14] L. Kalichman, D.J. Hunter, The genetics of intervertebral disc degeneration. Familial predisposition and heritability estimation, Joint Bone Spine 75(4) (2008) 383-7.
[15] C.L. Le Maitre, J.A. Hoyland, A.J. Freemont, Catabolic cytokine expression in degenerate and herniated human intervertebral discs: IL-1beta and TNFalpha expression profile, Arthritis Res Ther 9(4) (2007) R77.
[16] M.F. Shamji, L.A. Setton, W. Jarvis, S. So, J. Chen, L. Jing, R. Bullock, R.E. Isaacs, C. Brown, W.J. Richardson, Proinflammatory cytokine expression profile in degenerated and herniated human intervertebral disc tissues, Arthritis Rheum 62(7) (2010) 1974-82.
[17] K. Jimbo, J.S. Park, K. Yokosuka, K. Sato, K. Nagata, Positive feedback loop of interleukin-1beta upregulating production of inflammatory mediators in human intervertebral disc cells in vitro, J Neurosurg Spine 2(5) (2005) 589-95.
[18] W.K. Kwon, H.J. Moon, T.H. Kwon, Y.K. Park, J.H. Kim, The Role of Hypoxia in Angiogenesis and Extracellular Matrix Regulation of Intervertebral Disc Cells During Inflammatory Reactions, Neurosurgery 81(5) (2017) 867-875.
[19] Z.I. Johnson, Z.R. Schoepflin, H. Choi, I.M. Shapiro, M.V. Risbud, Disc in flames: Roles of TNF-alpha and IL-1beta in intervertebral disc degeneration, Eur Cell Mater 30 (2015) 104-16; discussion 116-7.
[20] M.A. Gabr, L. Jing, A.R. Helbling, S.M. Sinclair, K.D. Allen, M.F. Shamji, W.J. Richardson, R.D. Fitch, L.A. Setton, J. Chen, Interleukin-17 synergizes with IFNgamma or TNFalpha to promote inflammatory mediator

release and intercellular adhesion molecule-1 (ICAM-1) expression in human intervertebral disc cells, J Orthop Res 29(1) (2011) 1-7.
[21] I. Altun, Cytokine profile in degenerated painful intervertebral disc: variability with respect to duration of symptoms and type of disease, Spine J 16(7) (2016) 857-61.
[22] J.S. Kim, M.B. Ellman, D. Yan, H.S. An, R. Kc, X. Li, D. Chen, G. Xiao, G. Cs-Szabo, D.W. Hoskin, D.D. Buechter, A.J. Van Wijnen, H.J. Im, Lactoferricin mediates anti-inflammatory and anti-catabolic effects via inhibition of IL-1 and LPS activity in the intervertebral disc, J Cell Physiol 228(9) (2013) 1884-96.
[23] K. Li, Y. Li, B. Xu, L. Mao, J. Zhao, Sesamin inhibits lipopolysaccharide-induced inflammation and extracellular matrix catabolism in rat intervertebral disc, Connect Tissue Res 57(5) (2016) 347-59.
[24] H. Makino, S. Seki, Y. Yahara, S. Shiozawa, Y. Aikawa, H. Motomura, M. Nogami, K. Watanabe, T. Sainoh, H. Ito, N. Tsumaki, Y. Kawaguchi, M. Yamazaki, T. Kimura, A selective inhibition of c-Fos/activator protein-1 as a potential therapeutic target for intervertebral disc degeneration and associated pain, Sci Rep 7(1) (2017) 16983.
[25] B. van Dijk, E. Potier, D.M. van, M. Langelaan, N. Papen-Botterhuis, K. Ito, Reduced tonicity stimulates an inflammatory response in nucleus pulposus tissue that can be limited by a COX-2-specific inhibitor, J Orthop Res 33(11) (2015) 1724-31.
[26] A.R. Tellegen, I. Rudnik-Jansen, M. Beukers, A. Miranda-Bedate, F.C. Bach, W. de Jong, N. Woike, G. Mihov, J.C. Thies, B.P. Meij, L.B. Creemers, M.A. Tryfonidou, Intradiscal delivery of celecoxib-loaded microspheres restores intervertebral disc integrity in a preclinical canine model, J Control Release 286 (2018) 439-450.
[27] W. Alimasi, Y. Sawaji, K. Endo, M. Yorifuji, H. Suzuki, T. Kosaka, T. Shishido, K. Yamamoto, Regulation of nerve growth factor by anti-inflammatory drugs, a steroid, and a selective cyclooxygenase 2 inhibitor in human intervertebral disc cells stimulated with interleukin-1, Spine (Phila Pa 1976) 38(17) (2013) 1466-72.
[28] S.M. Sinclair, M.F. Shamji, J. Chen, L. Jing, W.J. Richardson, C.R. Brown, R.D. Fitch, L.A. Setton, Attenuation of inflammatory events in human intervertebral disc cells with a tumor necrosis factor antagonist, Spine (Phila Pa 1976) 36(15) (2011) 1190-6.
[29] G.Q. Teixeira, C. Leite Pereira, F. Castro, J.R. Ferreira, M. Gomez-Lazaro, P. Aguiar, M.A. Barbosa, C. Neidlinger-Wilke, R.M. Goncalves, Anti-inflammatory Chitosan/Poly-gamma-glutamic acid nanoparticles control inflammation while remodeling extracellular matrix in degenerated intervertebral disc, Acta Biomater 42 (2016) 168-179.
[30] D. Sakai, J. Schol, Cell therapy for intervertebral disc repair: Clinical perspective, J Orthop Translat 9 (2017) 8-18.
[31] T. Sainoh, S. Orita, M. Miyagi, G. Inoue, H. Kamoda, T. Ishikawa, K. Yamauchi, M. Suzuki, Y. Sakuma, G. Kubota, Y. Oikawa, K. Inage, J. Sato, Y. Nakata, J. Nakamura, Y. Aoki, T. Toyone, K. Takahashi, S. Ohtori, Single Intradiscal Administration of the Tumor Necrosis Factor-Alpha Inhibitor, Etanercept, for Patients with Discogenic Low Back Pain, Pain Med 17(1) (2016) 40-5.
[32] H. Takahashi, T. Suguro, Y. Okazima, M. Motegi, Y. Okada, T. Kakiuchi, Inflammatory cytokines in the herniated disc of the lumbar spine, Spine (Phila Pa 1976) 21(2) (1996) 218-24.
[33] J. Wang, Y. Tian, K.L. Phillips, N. Chiverton, G. Haddock, R.A. Bunning, A.K. Cross, I.M. Shapiro, C.L. Le Maitre, M.V. Risbud, Tumor necrosis factor alpha- and interleukin-1beta-dependent induction of CCL3 expression by nucleus pulposus cells promotes macrophage migration through CCR1, Arthritis Rheum 65(3) (2013) 832-42.
[34] C.A. Seguin, R.M. Pilliar, P.J. Roughley, R.A. Kandel, Tumor necrosis factor-alpha modulates matrix production and catabolism in nucleus pulposus tissue, Spine (Phila Pa 1976) 30(17) (2005) 1940-8.
[35] T. Igarashi, S. Kikuchi, V. Shubayev, R.R. Myers, 2000 Volvo Award winner in basic science studies: Exogenous tumor necrosis factor-alpha mimics nucleus pulposus-induced neuropathology. Molecular, histologic, and behavioral comparisons in rats, Spine (Phila Pa 1976) 25(23) (2000) 2975-80.

[36] S. Hayashi, A. Taira, G. Inoue, T. Koshi, T. Ito, M. Yamashita, K. Yamauchi, M. Suzuki, K. Takahashi, S. Ohtori, TNF-alpha in nucleus pulposus induces sensory nerve growth: a study of the mechanism of discogenic low back pain using TNF-alpha-deficient mice, Spine (Phila Pa 1976) 33(14) (2008) 1542-6.
[37] H.J. Kim, J.S. Yeom, Y.G. Koh, J.E. Yeo, K.T. Kang, Y.M. Kang, B.S. Chang, C.K. Lee, Anti-inflammatory effect of platelet-rich plasma on nucleus pulposus cells with response of TNF-alpha and IL-1, J Orthop Res 32(4) (2014) 551-6.
[38] D. Purmessur, B.A. Walter, P.J. Roughley, D.M. Laudier, A.C. Hecht, J. Iatridis, A role for TNFalpha in intervertebral disc degeneration: a non-recoverable catabolic shift, Biochem Biophys Res Commun 433(1) (2013) 151-6.
[39] A. Lai, A. Moon, D. Purmessur, B. Skovrlj, D.M. Laudier, B.A. Winkelstein, S.K. Cho, A.C. Hecht, J.C. Iatridis, Annular puncture with tumor necrosis factor-alpha injection enhances painful behavior with disc degeneration in vivo, Spine J 16(3) (2016) 420-31.
[40] M. Doita, T. Kanatani, T. Ozaki, N. Matsui, M. Kurosaka, S. Yoshiya, Influence of macrophage infiltration of herniated disc tissue on the production of matrix metalloproteinases leading to disc resorption, Spine (Phila Pa 1976) 26(14) (2001) 1522-7.
[41] J. Wang, D. Markova, D.G. Anderson, Z. Zheng, I.M. Shapiro, M.V. Risbud, TNF-alpha and IL-1beta promote a disintegrin-like and metalloprotease with thrombospondin type I motif-5-mediated aggrecan degradation through syndecan-4 in intervertebral disc, J Biol Chem 286(46) (2011) 39738-49.
[42] B.A. Walter, D. Purmessur, M. Likhitpanichkul, A. Weinberg, S.K. Cho, S.A. Qureshi, A.C. Hecht, J.C. Iatridis, Inflammatory Kinetics and Efficacy of Anti-inflammatory Treatments on Human Nucleus Pulposus Cells, Spine (Phila Pa 1976) 40(13) (2015) 955-63.
[43] H. Liu, H. Pan, H. Yang, J. Wang, K. Zhang, X. Li, H. Wang, W. Ding, B. Li, Z. Zheng, LIM mineralization protein-1 suppresses TNF-alpha induced intervertebral disc degeneration by maintaining nucleus pulposus extracellular matrix production and inhibiting matrix metalloproteinases expression, J Orthop Res 33(3) (2015) 294-303.
[44] N. Fujita, S.S. Gogate, K. Chiba, Y. Toyama, I.M. Shapiro, M.V. Risbud, Prolyl hydroxylase 3 (PHD3) modulates catabolic effects of tumor necrosis factor-alpha (TNF-alpha) on cells of the nucleus pulposus through co-activation of nuclear factor kappaB (NF-kappaB)/p65 signaling, J Biol Chem 287(47) (2012) 39942-53.
[45] X. Wang, H. Wang, H. Yang, J. Li, Q. Cai, I.M. Shapiro, M.V. Risbud, Tumor necrosis factor-alpha- and interleukin-1beta-dependent matrix metalloproteinase-3 expression in nucleus pulposus cells requires cooperative signaling via syndecan 4 and mitogen-activated protein kinase-NF-kappaB axis: implications in inflammatory disc disease, Am J Pathol 184(9) (2014) 2560-72.
[46] R. Kang, H. Li, K. Rickers, S. Ringgaard, L. Xie, C. Bunger, Intervertebral disc degenerative changes after intradiscal injection of TNF-alpha in a porcine model, Eur Spine J 24(9) (2015) 2010-6.
[47] M. Alini, S.M. Eisenstein, K. Ito, C. Little, A.A. Kettler, K. Masuda, J. Melrose, J. Ralphs, I. Stokes, H.J. Wilke, Are animal models useful for studying human disc disorders/degeneration?, Eur Spine J 17(1) (2008) 2-19.
[48] C. Daly, P. Ghosh, G. Jenkin, D. Oehme, T. Goldschlager, A Review of Animal Models of Intervertebral Disc Degeneration: Pathophysiology, Regeneration, and Translation to the Clinic, Biomed Res Int 2016 (2016) 5952165.
[49] F.C. Bach, S.A. de Vries, F.M. Riemers, J. Boere, F.W. van Heel, M. van Doeselaar, S.S. Goerdaya, P.G. Nikkels, K. Benz, L.B. Creemers, A.F. Maarten Altelaar, B.P. Meij, K. Ito, M.A. Tryfonidou, Soluble and pelletable factors in porcine, canine and human notochordal cell-conditioned medium: implications for IVD regeneration, Eur Cell Mater 32 (2016) 163-80.
[50] M.C. Cornejo, S.K. Cho, C. Giannarelli, J.C. Iatridis, D. Purmessur, Soluble factors from the notochordal-rich intervertebral disc inhibit endothelial cell invasion and vessel formation in the presence and absence of pro-inflammatory cytokines, Osteoarthritis Cartilage 23(3) (2015) 487-96.

[51] B. van Dijk, E. Potier, K. Ito, Culturing bovine nucleus pulposus explants by balancing medium osmolarity, Tissue Eng Part C Methods 17(11) (2011) 1089-96.
[52] S. Illien-Junger, B. Gantenbein-Ritter, S. Grad, P. Lezuo, S.J. Ferguson, M. Alini, K. Ito, The combined effects of limited nutrition and high-frequency loading on intervertebral discs with endplates, Spine (Phila Pa 1976) 35(19) (2010) 1744-52.
[53] P.A. Sotiropoulou, S.A. Perez, M. Salagianni, C.N. Baxevanis, M. Papamichail, Characterization of the optimal culture conditions for clinical scale production of human mesenchymal stem cells, Stem Cells 24(2) (2006) 462-71.
[54] D. Sakai, Y. Nakamura, T. Nakai, T. Mishima, S. Kato, S. Grad, M. Alini, M.V. Risbud, D. Chan, K.S. Cheah, K. Yamamura, K. Masuda, H. Okano, K. Ando, J. Mochida, Exhaustion of nucleus pulposus progenitor cells with ageing and degeneration of the intervertebral disc, Nat Commun 3 (2012) 1264.
[55] Z. Li, G. Lang, L.S. Karfeld-Sulzer, K.T. Mader, R.G. Richards, F.E. Weber, C. Sammon, H. Sacks, A. Yayon, M. Alini, S. Grad, Heterodimeric BMP-2/7 for nucleus pulposus regeneration-In vitro and ex vivo studies, J Orthop Res 35(1) (2017) 51-60.
[56] T. Caliskan, D.Y. Sirin, N. Karaarslan, I. Yilmaz, H. Ozbek, Y. Akyuva, N. Kaplan, Y.E. Kaya, A.T. Simsek, A.Y. Guzelant, O. Ates, Effects of etanercept, a tumor necrosis factor receptor fusion protein, on primary cell cultures prepared from intact human intervertebral disc tissue, Exp Ther Med 18(1) (2019) 69-76.
[57] H. Mitoma, T. Horiuchi, H. Tsukamoto, Y. Tamimoto, Y. Kimoto, A. Uchino, K. To, S. Harashima, N. Hatta, M. Harada, Mechanisms for cytotoxic effects of anti-tumor necrosis factor agents on transmembrane tumor necrosis factor alpha-expressing cells: comparison among infliximab, etanercept, and adalimumab, Arthritis Rheum 58(5) (2008) 1248-57.
[58] Z. Li, P. Lezuo, G. Pattappa, E. Collin, M. Alini, S. Grad, M. Peroglio, Development of an ex vivo cavity model to study repair strategies in loaded intervertebral discs, Eur Spine J 25(9) (2016) 2898-908.
[59] S. Caprez, U. Menzel, Z. Li, S. Grad, M. Alini, M. Peroglio, Isolation of high-quality RNA from intervertebral disc tissue via pronase predigestion and tissue pulverization, JOR Spine 1(2) (2018) e1017.
[60] R.W. Farndale, D.J. Buttle, A.J. Barrett, Improved quantitation and discrimination of sulphated glycosaminoglycans by use of dimethylmethylene blue, Biochim Biophys Acta 883(2) (1986) 173-7.
[61] S. Ohtori, G. Inoue, Y. Eguchi, S. Orita, M. Takaso, N. Ochiai, S. Kishida, K. Kuniyoshi, Y. Aoki, J. Nakamura, T. Ishikawa, G. Arai, M. Miyagi, H. Kamoda, M. Suzuki, Y. Sakuma, Y. Oikawa, G. Kubota, K. Inage, T. Sainoh, T. Toyone, K. Yamauchi, T. Kotani, T. Akazawa, S. Minami, K. Takahashi, Tumor necrosis factor-alpha-immunoreactive cells in nucleus pulposus in adolescent patients with lumbar disc herniation, Spine (Phila Pa 1976) 38(6) (2013) 459-62.
[62] B.A. Walter, M. Likhitpanichkul, S. Illien-Junger, P.J. Roughley, A.C. Hecht, J.C. Iatridis, TNFalpha transport induced by dynamic loading alters biomechanics of intact intervertebral discs, PLoS One 10(3) (2015) e0118358.
[63] A.J. Michalek, M.R. Buckley, L.J. Bonassar, I. Cohen, J.C. Iatridis, The effects of needle puncture injury on microscale shear strain in the intervertebral disc annulus fibrosus, Spine J 10(12) (2010) 1098-105.
[64] S.E. Gullbrand, N.R. Malhotra, T.P. Schaer, Z. Zawacki, J.T. Martin, J.R. Bendigo, A.H. Milby, G.R. Dodge, E.J. Vresilovic, D.M. Elliott, R.L. Mauck, L.J. Smith, A large animal model that recapitulates the spectrum of human intervertebral disc degeneration, Osteoarthritis Cartilage 25(1) (2017) 146-156.
[65] N. Willems, G. Mihov, G.C. Grinwis, M. van Dijk, D. Schumann, C. Bos, G.J. Strijkers, W.J. Dhert, B.P. Meij, L.B. Creemers, M.A. Tryfonidou, Safety of intradiscal injection and biocompatibility of polyester amide microspheres in a canine model predisposed to intervertebral disc degeneration, J Biomed Mater Res B Appl Biomater 105(4) (2017) 707-714.
[66] B.J. Freeman, G.L. Ludbrook, S. Hall, M. Cousins, B. Mitchell, M. Jaros, M. Wyand, J.R. Gorman, Randomized, double-blind, placebo-controlled, trial of transforaminal epidural etanercept for the treatment of symptomatic lumbar disc herniation, Spine (Phila Pa 1976) 38(23) (2013) 1986-94.

[67] S.P. Cohen, D. Wenzell, R.W. Hurley, C. Kurihara, C.C. Buckenmaier, 3rd, S. Griffith, T.M. Larkin, E. Dahl, B.J. Morlando, A double-blind, placebo-controlled, dose-response pilot study evaluating intradiscal etanercept in patients with chronic discogenic low back pain or lumbosacral radiculopathy, Anesthesiology 107(1) (2007) 99-105.
[68] J. Wang, H. Chen, P. Cao, X. Wu, F. Zang, L. Shi, L. Liang, W. Yuan, Inflammatory cytokines induce caveolin-1/beta-catenin signalling in rat nucleus pulposus cell apoptosis through the p38 MAPK pathway, Cell Prolif 49(3) (2016) 362-72.

Chapter 3

Intradiscal Injection of Human Recombinant BMP-4 Does Not Reverse Intervertebral Disc Degeneration Induced by Nuclectomy in Sheep

Jie Du, João P. Garcia, Frances C. Bach, Anna R. Tellegen, Sibylle Grad, Zhen Li, René M Castelein, Björn P. Meij, Marianna A. Tryfonidou, Laura B. Creemers.

Published in Journal of Orthopaedic Translation
DOI: 10.1016/j.jot.2022.08.006

Jie Du contributed to the study design, acquisition, analysis, interpretation of data, drafting, and revising of the article, and final approval.

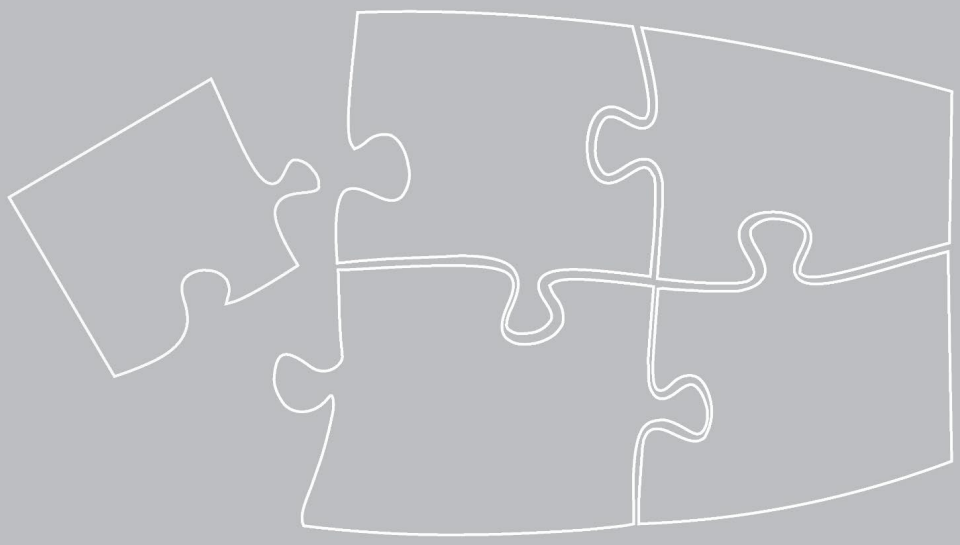

Abstract:

Background: Intervertebral disc (IVD) degeneration is suggested as a major cause of chronic low back pain (LBP). Intradiscal delivery of growth factors has been proposed as a promising strategy for IVD repair and regeneration. Previously, BMP-4 was shown to be more potent in promoting extracellular matrix (ECM) production than other BMPs and TGF-β in human nucleus pulposus (NP) cells, suggesting its applicability for disc regeneration.

Methods: The effects of BMP-4 on ECM deposition and cell proliferation were assessed in sheep NP and annulus fibrosus (AF) cells in a pellet culture model. Further, a nuclectomy induced sheep lumbar IVD degeneration model was used to evaluate the safety and effects of intradiscal BMP-4 injection on IVD regeneration. Outcomes were assessed by magnetic resonance imaging, micro-computed tomography, histological and biochemical measurements.

Results: *In vitro*, BMP-4 significantly increased the production of proteoglycan and deposition of collagen type II and proliferation of NP and AF cells. Collagen type I deposition was not affected in NP cells, while in AF cells it was high at low BMP-4 concentrations, and decreased with increasing concentration of BMP-4. Intradiscal injection of BMP-4 induced extradiscal new bone formation and Schmorl's node-like changes *in vivo*. No regeneration in the NP nor AF was observed.

Conclusion: Our study demonstrated that although BMP-4 showed promising regenerative effects in vitro, similar effects were not observed in a large IVD degeneration animal model.

The Translational Potential of This Article: The contradictory results of using BMP-4 on IVD regeneration between *in vitro* and *in vivo* demonstrate that direct BMP-4 injection for disc degeneration-associated human chronic low back pain should not be undertaken. In addition, our results may also shed light on the mechanisms behind pathological endplate changes in human patients as a possible target for therapy.

Keywords:

BMP-4, Intervertebral disc regeneration, Nucleus pulposus, Annulus fibrosus, Subchondral bone remodeling, Bone formation

1. Introduction

Low back pain (LBP) is one of the most common musculoskeletal disorders and a leading cause of disability worldwide [1]. LBP impairs patient quality of life, and particularly chronic LBP (CLBP) imposes a heavy burden on economy, healthcare and social systems. Intervertebral disc (IVD) degeneration (IVDD) is widely recognized as a major cause of CLBP [2-4]. IVDD progresses with age and is associated with mechanical stress, trauma, infection, genetic predisposition, and lifestyle [5]. Additionally, the spontaneous regeneration of the IVD is very limited, which is attributed to the low number of resident progenitor cells and the avascular nature of adult IVDs [6].

IVDD is characterized by abnormal extracellular matrix (ECM) metabolism, with decreasing anabolism and increasing catabolism. In degenerative IVDs, the proteoglycan content is reduced together with changes in collagen production, where collagen type II is being degraded and replaced by increasing amounts of collagen type I [7]. This is associated with enhanced activity of catabolic enzymes, such as matrix metalloproteinases (MMPs) and a disintegrin and metalloproteinase with thrombospondin motifs (ADAMTS) [8]. All these factors result in disorganization of ECM architecture, tears and clefts in IVD, and loss of water and IVD height [9]. Recently, the inflammatory environment and neoinnervation have been suggested as a source of the ensuing discogenic back pain [10]. Current therapies for CLBP mainly aim to relieve pain but do not restore the physiological composition and function of the degenerated IVDs. In this context, strategies for the repair and regeneration of IVD are promising alternatives. Approaches using growth factors to induce regeneration have been widely studied, because they effectively induce IVD cell proliferation and ECM production, and they can be potential minimally invasive [11].

Bone morphogenetic proteins (BMPs), a subfamily of the transforming growth factor-beta (TGF-β) superfamily, are widely known as potent inducers of bone formation [12]. Moreover, BMPs have also been studied for their role in chondrogenesis and the maintenance of ECM in both IVD and articular cartilage [13, 14]. Importantly, several studies showed that BMPs promote IVD regeneration both *in vitro* and *in vivo*. BMP-2 and BMP-7 and their heterodimers have been demonstrated to promote ECM anabolism in nucleus pulposus (NP) and/or annulus fibrosus (AF) cells in different species [15-17]. Intradiscal injection of BMP-7 increased disc height and proteoglycan content in both annular puncture and chondroitinase ABC-induced rabbit disc degeneration models [18, 19]. However, these results were not replicated in a canine model of mild IVDD [20]. Rabbit models in general show a higher spontaneous regenerative capacity in IVD than other species, possibly owing to the presence of notochordal cells in their NPs up to adulthood. Therefore, they may not be the optimal model for regenerative interventions of the IVD [21]. In this context, large animal models such as dog and sheep models of IVDD may be a better alternative for studying IVD regeneration, as their IVDs are similar to human in size and cell biology [22].

Previously, we compared BMP-2, BMP-4, BMP-6, BMP-7, and their combinations and heterodimers, for their regenerative effect on the pellet culture model of human NP cells or NP cells co-cultured with bone marrow mesenchymal stromal cells [23]. In this study, BMP-4 was identified as the most potent in inducing glycosaminoglycan (GAG) production and deposition,

suggesting a regenerative effect could be achieved upon direct intradiscal injection [23]. In order to investigate the applicability of BMP-4 for IVDD treatment, the effects of BMP-4 on IVDD were evaluated in the present study *in vitro* and in a large animal model of IVDD. *In vitro*, the effects of BMP-4 on ECM deposition and cell proliferation were assessed in both sheep NP and AF cells, because the AF cells could be affected by intradiscal injected BMP-4. *In vivo*, IVDD was induced by nuclectomy in a sheep model, and BMP-4 was intradiscally injected into the degenerative IVDs to evaluate the safety and effects on IVD regeneration. Outcomes were assessed by magnetic resonance imaging (MRI), micro-computed tomography (Micro-CT), histological and biochemical measurements.

2. Materials and methods

2.1. Ethics statement

All procedures involving animals were approved and conducted in accordance with the guidelines and described in the protocol number AVD108002015282 provided by the central national committee for animal experiments and overseen by the local welfare body, as required by Dutch regulation.

2.2. Isolation and culture of NP and AF cells

NP and AF cells were isolated from laboratory Swifter sheep's healthy IVDs. Swifter breed is known to include animals heterozygous and homozygous for the allele of the growth and differentiation factor-8 (GDF-8) gene at the 3' untranslated region *+6723*. As this may affect the regenerative response [24], animals for *in vitro* and *in vivo* experiments were genotyped and only animals homozygous for the *gg* allele were used; this phenotype excludes aberrant GDF-8 signaling. IVDs were obtained from remnants of other experiments, and identified by macroscopically scored according to Thompson grading, and grade I and II IVDs were included. NP tissue was carefully separated avoiding the transitional zone, and the AF was identified by its clear lamellar structure. Minced tissue was firstly digested with 0.004% DNase (D4138-80KU, Sigma-Aldrich), 0.2% Pronase (11459643001, Roche Diagnostics GmbH) for 1 hour at 37 °C, and subsequently digested with 0.004% DNAse and 0.05% collagenase type II (LS004176, Worthington Biochemical) for NP or 0.004% DNAse and 0.1% collagenase type II for AF overnight at 37 °C. All the digestion buffers were prepared in an antibiotic plus DMEM medium (DMEM (1×) + GlutaMAX™ (31966021, Gibco), 2% penicillin/streptomycin (P/S, 15140122, Gibco), 20 µg/mL amphotericin-B (15290026, Gibco) and 50 µg/mL gentamicin sulfate (BW17-518Z, Lonza™ BioWhittaker™ Antibiotics)). Single cells seeded with antibiotic plus DMEM medium supplemented with 10% fetal bovine serum (FBS, Biowest, Missouri, USA) at a density of 3000-4500 cells/cm^2 as passage 0. After passage one, cells were cultured in expansion medium, DMEM (1×) + GlutaMAX™ supplemented with 1% P/S, 10% FBS, and 1 ng/mL basic fibroblast growth factor (bFGF, PHP105, AbD Serotec). Both NP and AF cells were cryopreserved at passage 1.

2.3. Pellet culture and BMP-4 treatment

NP and AF cells were expanded until passage 2. They were pelleted at 2.5 × 10^5 cells in a round bottom ultra-low attachment 96-well plate (Costar, ME, USA) by centrifugation at 500*g* for 5 min. Pellets were cultured in 200 µL pellet culture medium (DMEM(1×) + GlutaMAX™ supplemented with), 2% bovine serum albumin (10735086001, Roche Diagnostics GmbH), 1% insulin-transferrin-selenium + premix (ITS+) (354352 Corning), 20 mg/mL proline (P5607, Sigma-Aldrich), 1% P/S, and 20 mM ascorbate-2-phosphate (Sigma-Aldrich)) with or without human recombinant BMP-4 (kind gift of dr Loredana Cecchetelli, Rome, Italy) at four different concentrations, 0.04 nM (1.36 ng/mL), 0.4 nM (13.6 ng/mL), 2 nM (68 ng/mL), and 4 nM (136 ng/mL), the concentration based on previous study [23]. Media were renewed twice a week. NP and AF pellets cultured for 28 days were used for biochemical analysis and histological and immunohistochemical staining. NP pellets cultured for 2 or 7 days were used for gene expression analysis.

2.4. Gene expression analysis

NP pellets cultured for 2 or 7 days were collected by adding 1 mL TRIzol™ reagent (Invitrogen) per 2 pellets for RNA isolation. Then pellets were minced by pipette tips. Before RNA isolation, samples were mixed with 70% ethanol 1 mL. Following RNA isolation was performed by using RNeasy Mini Kit (QIAGEN) according to the manufacturer's protocol. Reverse transcription was performed using High-Capacity cDNA Reverse Transcription Kit (4368814, Applied Biosystems). qRT-PCR was conducted on CFX96 Touch Real-Time PCR Detection System (BIO-RAD) with iTaq Universal SYBR Green Supermix (BIO-RAD). Primers: endogenous control, ribosomal protein L19 (*RPL19*), forward: 5`- AGCCTGTGACTGTCCATTCC-3`, reverse: 5`- ACGTTACCTTCTCGGGCATT-3` [25]; nuclear Ki-67 protein (*Ki-67*) forward: 5`- AAGATTCCAGTCCCCGTTCA-3`, reverse: 5`- TGAGGAACGAACACGACTGG-3`; SRY-box transcription factor-9 (*SOX-9*) forward: 5`- TTCGTGAAGATGACCGACGA-3`, reverse: 5`- AACTTGTCCTCCTCGCTCTC-3`. Data were analyzed using the $2^{-\Delta\Delta CT}$ method.

2.5. Animal experiment design

Four female Swifter sheep, 2 years old, were used in this study. All were confirmed by PCR to be *gg* wild type for the 3' untranslated region *+6723* of GDF-8. Multi-segment modeling was used in the current study and applied by various previous authors to address the 3Rs principle by reducing animal use. The adjacent healthy discs of degenerative positions did not show a degeneration in past studies using this approach in canines and goats [14, 20, 26]. And no evidence was found for effects of substances injection either [20, 26]. Degeneration of lumbar IVDs was induced by nuclectomy, and 6 weeks afterwards, degenerative IVDs were treated by intradiscal injection of BMP-4 (D-BMP4), or by a negative protein control consisting of a random ^{19}F peptide (sequence: CF_3CO-NH-Lys-(CO-CF_3)-DNRAHLHIDYHTDSD-COOH; D-sham) (This peptide injected IVDs were involved in a study to investigate the retention of peptide in IVD). As control for injection, also healthy IVDs were injected with this peptide (H-sham). Healthy discs without injection served as non-treated control (Healthy) (IVD levels and treatment layout as Supplementary Table 1). Three months after injection, sheep were euthanized, and samples were analyzed.

2.6. Sheep IVD nuclectomy

IVDD in the sheep was induced by surgical nuclectomy under anesthesia as previously reported [27]. Briefly, a longitudinal incision was made over the lumbar spine from the left side, and blunt dissection between the lumbar muscles was employed to facilitate visualization of the IVDs at L1-L2, L3 - L4, and L5 - L6 of each sheep and localization of the IVD segments was confirmed by fluoroscopy. Incision of the AF was performed with surgical blade no.11, whereafter NP tissue was partially removed with a round 1 mm ball-tipped probe. After nuclectomy, the muscle, fascial, subcutaneous and skin incisions were closed separately. Sheep received a single prophylactic antibiotic (amoxicilline & clavulanic acid, 10 mg/kg, intravenous, administration prior to surgery and Neopen (0.05 mL/kg containing 100 mg Neomycin and 200 mg Procaine benzylpenicilline per mL) for three days post-surgery. They also received analgesia by Buprenorfine (BuTrans pleister), 5 mg, release 5 µg/h for 7 days and intravenous and subcutaneous administration Meloxicam 0.5 mg/kg at day 0 and day 1-3 respectively after surgery. They were allowed ad libitum activity with free access to food and water.

2.7. Intradiscal injection

Sheep were anesthetized and lumbar IVDs were accessed by surgery as reported previously [27]. IVDs were exposed at the right side (opposite to nuclectomy). Twenty-four lumbar IVDs from 4 sheep, were divided into 4 groups (4 discs, Healthy; 8 discs, H-sham; 6 discs, D-sham; 6 discs, D-BMP4) (Supplementary Table 1). A 27 G syringe needle was inserted into the NP center, confirmed by fluoroscopy, and 200 µg of BMP-4, the injected dose based on a previous large animal study using BMP-7 [20], or a random peptide was injected into IVDs (dissolved in sterilized ultrapure water, 130 µL final volume for degenerative IVDs and 65 µL for healthy IVDs). Sheep received antibiotics and analgesia similar to the first operation.

2.8. Magnetic resonance imaging

Magnetic resonance imaging (MRI) of lumbar spine was performed under anesthesia prior to the surgery for intradiscal injection and immediately after euthanasia at three months after injection. MRI scans were obtained by using a Philips Ingenia 1.5 T scanner (Philips, Eindhoven, Netherlands). The sheep were positioned in dorsal recumbency with the pelvic limbs extending caudally. The MR protocol included a sagittal and transverse T2-weighted Turbo Spin Echo (time of repetition (TR) = 3000, time of echo (TE) = 110 ms, slice thickness = 2.5 mm) sequence, a T1-weighted Turbo Spin Echo (TR = 400 ms, TE = 8 ms, slice thickness = 2.5 mm). A sagittal multiple spin-echo T2w sequence for quantitative T2 mapping (using custom script in MeVisLab v3.1, MeVis Medical Solutions AG, Bremen, Germany) with a field of view (FOV) = 75 × 219 mm, acquisition matrix = 96 × 273, slice thickness = 3 mm, TR = 2000. Thirteen echoes were acquired with TE = 13 to 104 ms with 13 ms echo spacing. All images were assessed by a board-certified veterinary radiologist (Enterprise Imaging, version 8.1.2, Mortsel, Belgium). The lumbar discs were graded according to the Pfirrmann grading system on T2- weighted by two observers [28]. The disc height index (DHI) was measured on T2 weighted images obtained prior to injection and at 3 months after injection by using the method of Masuda *et al.* [29]. Three T2- weighted images (mid-sagittal and the parasagittal directly left and right of the mid-sagittal slice) of each IVD segment were used to measure the DHI, and results were averaged.

2.9. Sheep sample collection

Following euthanasia, the lumbar spine was harvested and used to perform micro-CT scans. Then single intact IVDs were obtained with partial vertebrae on both sides. The IVDs were cut into two equal half parts at the middle sagittal plane, and sagittal planes were imaged using a Canon 600D digital camera and EF-S 18-55 mm lens (Canon, Tokyo, Japan) at a fixed distance to evaluate the macroscopic degenerative level of each IVD according to the Thompson grading system [30]. The grading was performed in random order by two independent investigators blinded to treatment. One half of each IVD was fixed in 4% neutral phosphate buffered formaldehyde (w/v) for histology, and the other half was snap-frozen in liquid nitrogen and stored at −80 °C for biochemical analyses.

2.10. Micro-computed tomography

Each IVD was individually scanned with a micro-CT scanner (μCT, Quantum FX, Perkin Elmer, USA) at a voxel size of 143 μm^3 with 90 kV tube voltage and 200 μA tube current for 120 seconds. 3D reconstruction was carried out automatically after completion of each scan using the scanner's software (Quantum FX μCT software, Perkin Elmer, USA). Image analysis was performed using Fiji (software version 1.50, National Institutes of Health, Bethesda, USA). 3D images were used to evaluate new bone formation around IVDs; no osteophyte (0), osteophyte found (1). Sagittal 2D images were used to evaluate the presence of subchondral bone defects; no defect (0), defects found (1).

2.11. Biochemistry for glycosaminoglycan (GAG), DNA, and collagen content

GAG measurements were performed in pellet culture media, cell pellets, and IVD tissue. DNA and collagen content were measured in both pellets and IVD tissue. After culturing for 28 days, three pellets per condition per donor were separately digested in 300 μL papain buffer (250 μg/mL papain (P3125, Sigma-Aldrich) with 1.57 mg/mL cysteine HCl (C7880, Sigma-Aldrich)) overnight at 60 °C. These digested solutions were used to measure GAG, collagen, and DNA content.

Frozen IVDs were cut transversely at 30 μm thickness with a cryostat microtome (Thermo Fisher, USA). NP and AF tissue were collected separately. They were lysed in cOmplete lysis-M EDTA-free buffer (Roche Diagnostics GmbH, Mannheim, Germany), 1 mL for NP and 1.5 mL for AF, on a rotor at 4 °C overnight (Because the tissue lysate is needed to investigate ^{19}F labelled peptide retention in IVDs). Tissue lysates of NP and AF, 500 μl, were collected after centrifuging at 10,000 g at 4 °C for 20 min. The remaining NP and AF tissue were freeze-dried and weighed. The tissue lysates and freeze-dried tissue were digested in papain buffer (lysate: papain, v: v = 1: 10 for the lysate, 1 mg dry weight per 150 μL papain buffer for the freeze-dried tissue) at 60 °C overnight. Papain-digested samples were used to measure GAG, collagen, and DNA content in AF and NP tissue. The total content of GAG, collagen, and DNA was normalized to the weight of freeze-dried tissue of NP and AF separately.

The 1,9-dimethyl-methylene blue (DMMB, Sigma-Aldrich) assay was used to quantify GAG content using chondroitin sulfate (C4384, Sigma-Aldrich) as a standard, and the absorbance was read at 540/595 nm with a VersaMax microplate reader (Molecular Devices, San Jose, CA, USA). The hydroxyproline assay was used to measure total collagen content. Papain-digested samples were freeze-dried overnight, and hydrolyzed in 4 M NaOH at 108 °C overnight, then neutralized by 1.4 M citric acid (Fluka, Switzerland). Samples were incubated with Chloramine T reagent (Merck, Germany) for 20 minutes, then incubated with dimethylaminobenzaldehyde reagent (Merck, Germany) at 60 °C for 20 minutes. The absorbance was read at 570 nm by VersaMax microplate reader. The concentrations were calculated by using hydroxyproline (Merck, Germany) as a standard.

The Quant-iT™ PicoGreen™ dsDNA Assay Kit (Invitrogen, USA) was used to measure DNA content according to the manufacturer's protocol, using λDNA as standard. Fluorescence was read in a POLARstar Optima fluorescence microplate reader (Isogen Life Science, Utrecht, The Netherlands) at 485 nm excitation and 530 nm emission.

2.12. Histological and immunohistochemical staining

Two pellets per condition per donor were fixed overnight in 4% neutral phosphate buffered formaldehyde (w/v) and dehydrated and embedded in paraffin. Sections of 5 μm thickness were used for histological and immunohistochemical staining.

Fixed half IVDs were decalcified in 0.5 M EDTA dissolved in distilled water for 4 months, with two changes weekly and re-fixed for 2 days every 2 weeks. Full decalcification was verified by micro-CT. Decalcified IVDs were dehydrated and embedded in paraffin. Sagittal sections of 5 μm thickness were used for histological and immunohistochemical staining.

Hematoxylin and eosin (H&E) staining was performed with Mayer's hematoxylin solution (Merck, Germany) and then 2% eosin (Merck, Germany).

Safranin-O/Fast green (Saf-O FG) staining was performed by staining with Weigert's Hematoxylin (640500, Clin-Tech, UK), 0.125% Safranin-O (58884, Sigma-Aldrich), and finally 0.4% Fast Green (F7252, Sigma-Aldrich).

Alcian Blue/Picrosirius Red (AB/PR) staining was performed, by first staining with Weigert's hematoxylin (Clin-Tech, UK), followed by 1% Alcian Blue (05500, Fluka, Switzerland) at pH 2.5, and then 0.1% Picrosirius red (80115, Klinipath, Belgium). The IVD histological grading was performed in random order and by two independent investigators blinded for treatment under Olympus BX41 microscope based on H&E, AB/PR, and Saf-O FG staining and according to a previously described grading system [22]. Eight parameters were included, NP cell loss and cell death, NP cell clusters, NP matrix staining, AF morphology, AF cellular and matrix metaplasia/ distinction between AF and NP, tears and cleft formation in AF/NP, endplate (EP) morphology, and bone modeling at the external AF/ bone interface.

Tartrate-resistant acid phosphatase (TRAP) staining was performed to detect osteoclasts in the subchondral bone. Sections were pre-incubated with 0.2 M acetate buffer-tartaric acid for 20 min

at 37 °C. Subsequently, sections were incubated in 0.5 mg/mL naphthol AS-MX phosphate (Sigma-Aldrich) and 1.1 mg/mL Fast red TR salt (Sigma-Aldrich) for another 3 hours. Sections were counterstained with Mayer's hematoxylin. Osteoclasts were defined as multinucleated TRAP-positive cells and counted in the subchondral bone along whole two sides of IVD, in an area defined from the bottom edge (cartilaginous endplates) to the up edge (vertebrae) of view under a 20-times objective lens of Olympus BX41 microscope. The count was performed in a random order blinded for treatment.

Immunohistochemistry staining of collagen type I and II was performed after blocking endogenous peroxidase activity with 0.03% hydrogen peroxidase, antigen retrieval with 1 mg/mL Pronase followed by 1 mg/mL hyaluronidase (H3506, Sigma-Aldrich) and blocking with PBS + 5% bovine serum albumin (BSA, 10735078001, Roche Diagnostics GmbH). Primary antibodies for collagen type I (2 µg/mL, rabbit, EPR7785, Abcam, Cambridge, UK), type II collagen (0.4 µg/mL, mouse, DSHB II-II6B3, DSHB, IA, USA) or isotype control (DAKO, Glostrup, Denmark) (host species and concentrations matched with the primary antibody) were diluted in PBS + 5% BSA and incubated with sections overnight at 4 °C. Species-specific HRP-secondary antibodies (Immunologic a WellMed Company, Duiven, The Netherlands) were incubated with the sections for 1 hour at room temperature. Then staining was performed using the liquid DAB + Substrate Chromogen System (DAKO, Glostrup, Denmark). Sections were counterstained with Mayer's hematoxylin solution, dehydrated and mounted. Images were taken with an Olympus BX51 upright microscope with an Olympus SC50 camera (Olympus, Tokyo, Japan).

2.13. Statistical analyses

Statistical analyses were performed using the IBM SPSS statistics software, version 20. As the data were not normally distributed which was defined by Shapiro-wilk normality test. Mann-Whitney U test was used to determine differences between two groups; Kruskal Wallis with post-hoc test was used to determine differences among more than two groups. $P < 0.05$ was considered statistically significant.

3. Results

3.1. Effects of BMP-4 on sheep NP and AF cells *in vitro*

To verify that sheep IVD cells responded similarly to BMP-4 as human IVD cells [23], sheep NP and AF cells were cultured in pellets to allow for tissue formation.

3.1.1. BMP-4 promoted tissue formation, viability and cell content in NP and AF cell pellet culture

During culture, the diameter of the pellets decreased over time in pellets cultured without or with a low dose of BMP-4 (0.04 nM) in both NP and AF cells (Supplementary Figure 1), whereas pellets cultured with 0.4 nM BMP-4 maintained the same diameter throughout the culture period. At a concentration of 4 nM BMP-4 in NP cells ($P < 0.01$ at 28 days) and 2 and 4 nM in AF cells ($P < 0.001$ at 28 days), pellet size increased over time. As seen in figures 1A and 2A, the DNA content was significantly higher in BMP-4 treated pellets, at doses higher than 2 nM, compared to non-

treated controls in both NP ($P < 0.01$ at 2 nM, $P < 0.001$ at 4 nM) and AF ($P < 0.001$ at 2 nM and 4 nM) cells. At day 1, the LDH activity was not different between BMP-4-treated and non-treated cells for both NP and AF cells (Supplementary Figure 2). Normalized to DNA content in pellets at day 26, the relative LDH activity was decreased by BMP-4 at concentrations > 0.4 nM in NP cells ($P < 0.01$ at 0.4 nM, $P < 0.001$ at 2 nM and 4 nM) and at > 2 nM in AF cells ($P < 0.001$ at 2 nM and 4 nM) compared to the non-treated control.

3.1.2. BMP-4 increased ECM production in NP and AF pellet cultures

As shown in figures 1B and 2B, the GAG content was increased by BMP-4 supplementation at concentrations of 2 nM or higher in both NP ($P < 0.001$) and AF pellets ($P < 0.001$). GAG content per DNA followed the same trend as GAG content ($P < 0.01$ at 2 nM, $P < 0.001$ at 4 nM in NP; $P < 0.001$ at 2 and 4 nM in AF) (Figure 1E, 2E), as well as total GAG release in culture media ($P < 0.001$ in NP and AF) (Figure 1C, 2C). Additionally, Safranin-O/Fast Green staining showed that in both NP and AF pellets, more proteoglycans were deposited (red) when treated with 0.4 nM or higher doses of BMP-4 (Figure 1G, 2G).

Similar effects were observed regarding the total collagen deposition in NP and AF pellets. At doses of 2 nM or higher, the total collagen content, although not collagen per DNA, was significantly increased compared to non-treated controls ($P < 0.01$ at 2 nM, $P < 0.001$ at 4 nM in NP and AF) (Figure 1D, 2D, 1F, 2F). Collagen type II immunopositivity was enhanced in pellets treated with 0.4 nM or higher dose of BMP-4 compared to non-treated controls (Figure 1G, 2G). While collagen type I deposition was not altered in BMP-4-treated NP pellets, it appeared to be increased in AF pellets cultured with 0.4 and 2 nM BMP-4 (Figure 1G, 2G).

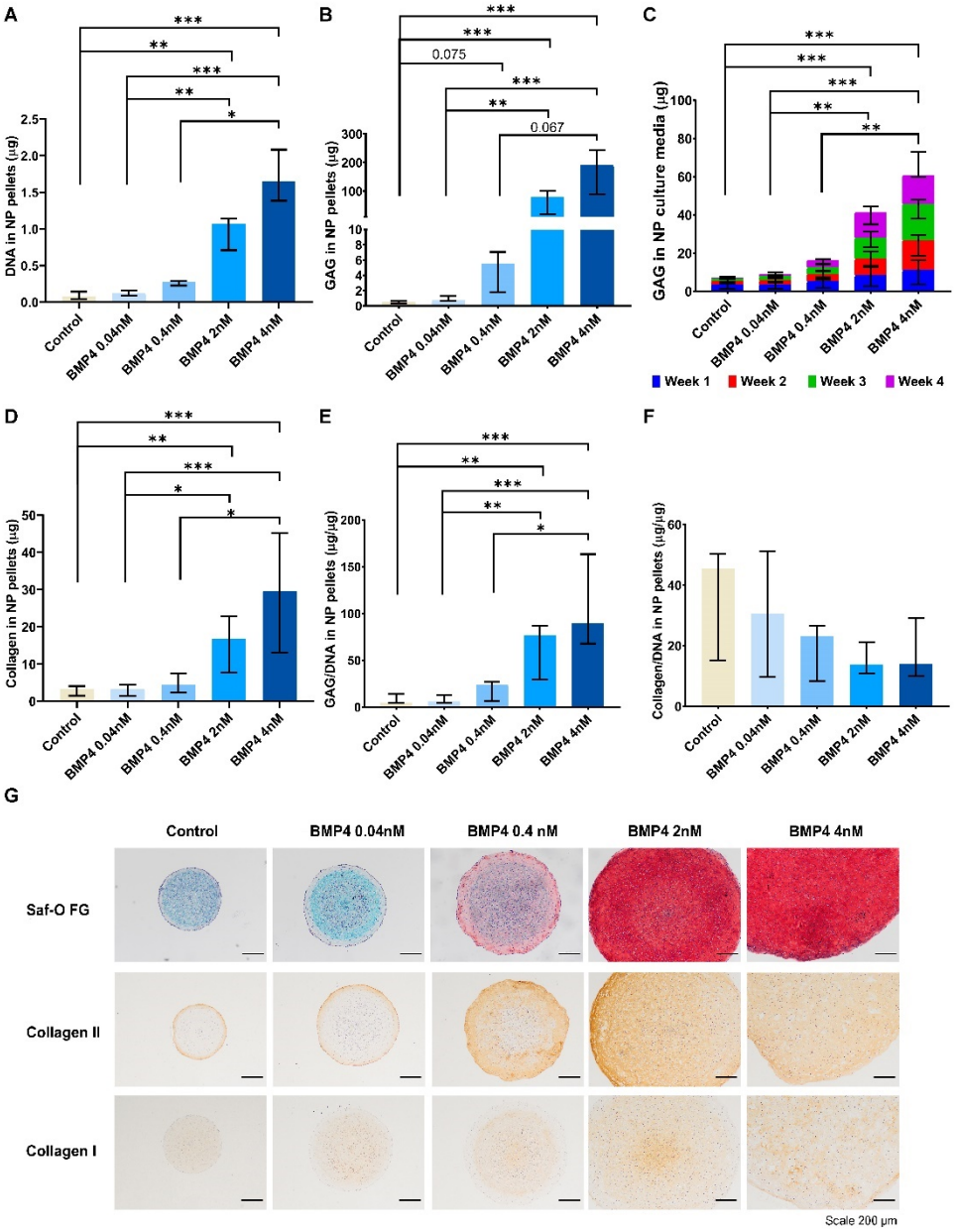

Figure 1. BMP-4 increased extracellular matrix production in NP cell pellet culture.

*Sheep nucleus pulposus (NP) cell pellets were cultured with (0.04 nM, 0.4 nM, 2 nM, 4 nM) or without bone morphogenetic protein-4 (BMP-4) at four different concentrations for 28 days. The DNA (A), glycosaminoglycan (GAG) (B), collagen (D) content in pellets, and GAG release (C) in culture media were measured. E, F, The GAG and collagen content in pellets were normalized to DNA. Additionally (G) the ECM deposition in pellets was evaluated by Safranin-O Fast Green (Saf-O FG) staining for proteoglycan (red) and total collagen (cyan), and by immunohistochemistry staining for collagen type II and I (brown). Kruskal Wallis with the post-hoc test was used to determine differences among more groups. Median with interquartile range, 3 donors in triplicates, n = 9, *P < 0.05, **P < 0.01, ***P < 0.001.*

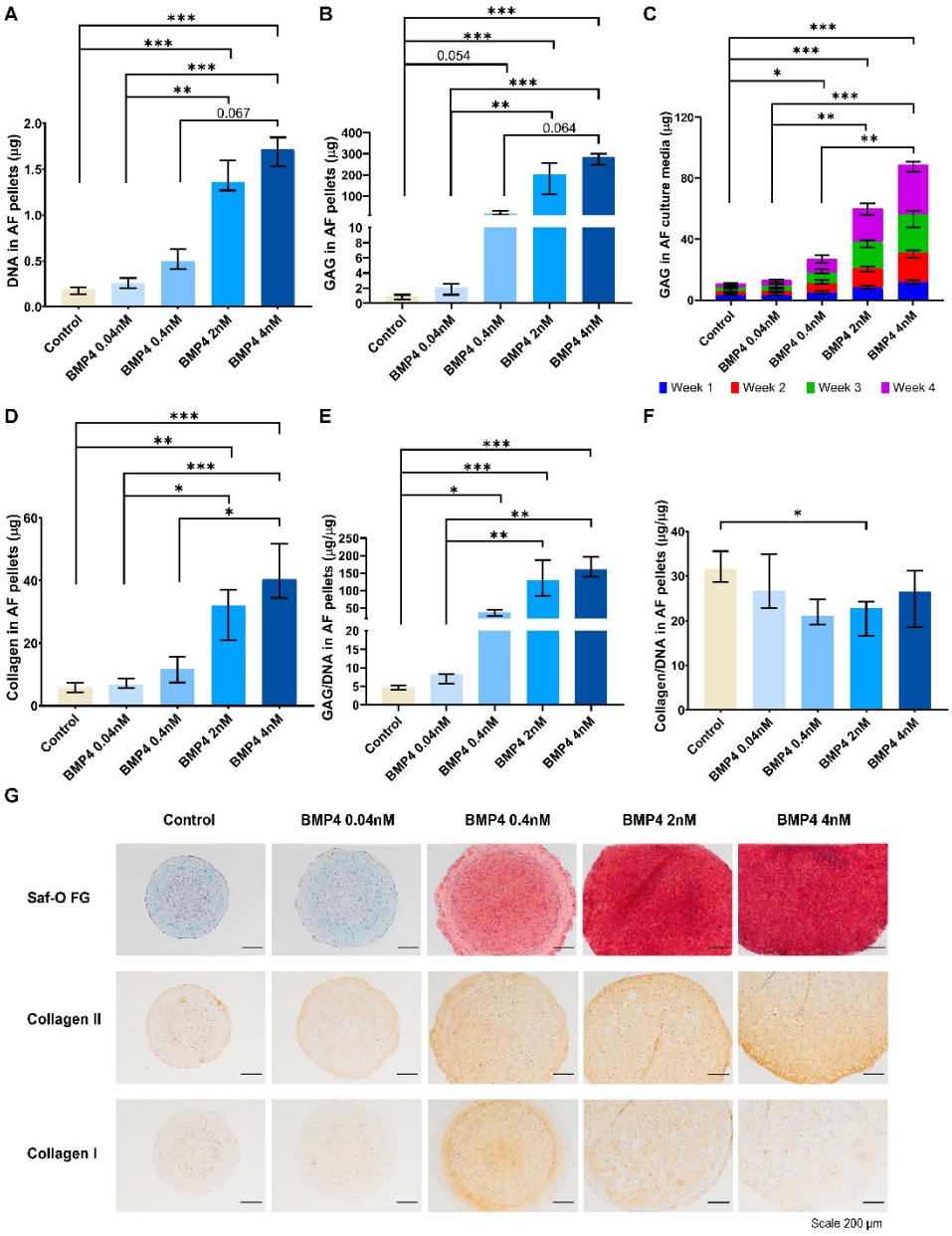

Figure 2. BMP-4 increased extracellular matrix production in AF cell pellet culture.

*Sheep annulus fibrosus (AF) cell pellets were cultured with (0.04 nM, 0.4 nM, 2 nM, 4 nM) or without bone morphogenetic protein-4 (BMP-4) at four different concentrations for 28 days. The DNA (A), glycosaminoglycan (GAG) (B), collagen (D) content in pellets, and GAG release (C) in culture media were measured. E, F, The GAG and collagen content in pellets were normalized to DNA. Additionally (G) the extracellular matrix deposition in pellets were evaluated by Safranin-O Fast Green (Saf-O FG) staining for proteoglycan (red) and total collagen (cyan), and by immunohistochemistry staining for collagen type II and I (brown). Kruskal Wallis with the post-hoc test was used to determine differences among groups. Median with interquartile range, 3 donors in triplicates, n = 9, *P < 0.05, **P < 0.01, ***P < 0.001.*

3.1.3. BMP-4 up-regulated the expression of cell proliferation marker, *Ki-67*, and ECM production-related gene, *SOX-9*

To further explore underlying molecular mechanism of BMP-4 induced cell proliferation and ECM production, BMP-4 treated pellets were collected to measure the expression of cell proliferation marker genes *Ki-67*, and ECM production related gene *SOX-9* at day 2 and day 7 (Figure 3). *Ki-67* was significantly upregulated by BMP-4 at 2 nM ($P < 0.01$) and 4 nM ($P < 0.001$) compared to 0.04 nM at day 2 (Figure 3A). However, it was downregulated at day 7 in which pellets treated by BMP-4 at 2 nM ($P < 0.001$ vs 0.04 nM, $P < 0.01$ vs control) and 4 nM ($P < 0.05$ vs 0.04 nM) compared to 0.04 nM and/or non-treated control (Figure 3C). *SOX-9* expression was significantly elevated by BMP-4 at 2 nM ($P < 0.05$ day 2; $P < 0.05$ vs control, $P < 0.01$ vs 0.04 nM at day 7) and 4 nM ($P < 0.01$ at day 2; $P < 0.05$ vs control, $P < 0.01$ vs 0.04 nM at day 7) compared to 0.04 nM and non-treated control at day 2 and day 7 (Figure 3B, 3D). In addition, *SOX-9* expression was elevated by BMP-4 at a lower concentration, 0.4 nM, at day 7 compared to non-treated control ($P < 0.05$) and 0.04 nM ($P < 0.01$) (Figure 3D). These results are consistent with above founding.

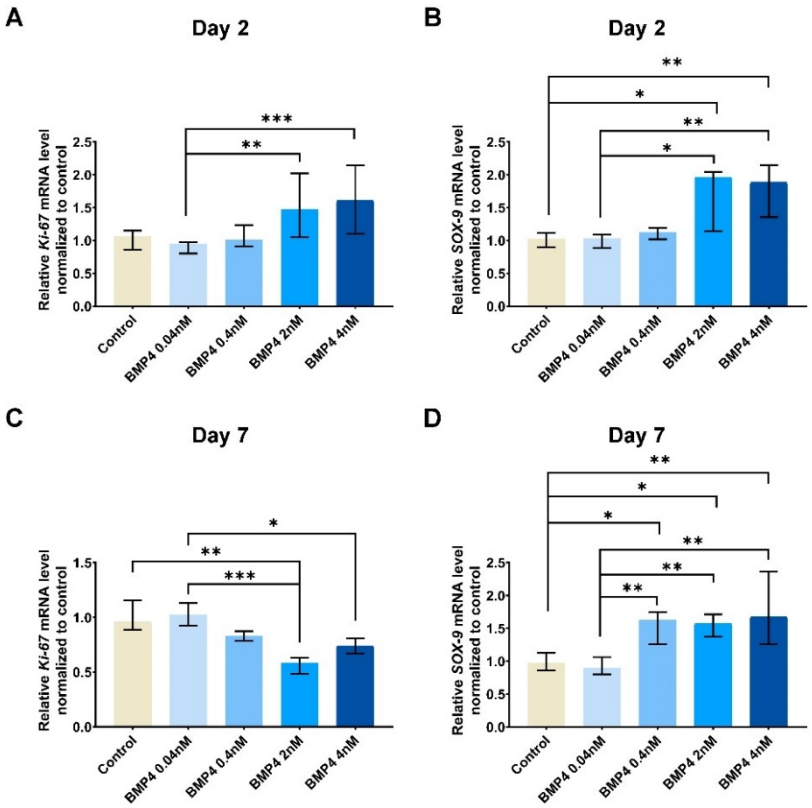

Figure 3. BMP-4 up-regulated the expression of cell proliferation marker, Ki-67, and ECM production related gene, SOX-9.

Sheep nucleus pulposus (NP) pellets were cultured with (0.04 nM, 0.4 nM, 2 nM, 4 nM) or without bone morphogenetic protein-4 (BMP-4) at four different concentrations for 2 and 7 days. The mRNA level of cell proliferation marker, nuclear Ki-67 protein (Ki- 67) (A, C), and ECM production-related gene, SRY-box transcription factor-9 (SOX-9) (B, D) was measured by quantitive PCR at day 2 and day 7 respectively.

*Results were normalized to the control group. Kruskal Wallis with the post-hoc test was used to determine differences among groups. Median with interquartile range, 3 donors in triplicates, n= 9, *P < 0.05, **P < 0.01, ***P < 0.001.*

3.2. Effects of BMP-4 on disc regeneration *in vivo*

In order to evaluate the effects of BMP-4 on IVD regeneration *in vivo*, IVDD was induced by nuclectomy in sheep, followed by intradiscal injection of BMP-4. Animals recovered well from surgery. No side effects of injection were noted, and no significant weight loss was observed in any of the 4 sheep (Supplementary Table 2). One BMP-4 injected IVD was excluded from the analysis because BMP-4 had been injected in the AF rather than the NP.

3.2.1. BMP-4 induced extradiscal bone formation, loss of subchondral bone, and cartilage ingrowth into the vertebral bone.

Before injection, IVDD was confirmed by a higher Pfirrmann grade in nuclectomy discs compared to control discs, although no difference in the DHI was noted (Supplementary Figure 3). Three months after injection, Pfirrmann grade was similar between healthy and healthy sham-injected discs, while it was increased in degenerated sham-injected ($P < 0.05$) and BMP-4-injected ($P < 0.05$) discs when compared to healthy sham-injected discs. Pfirrmann grade in the degenerated disc at 3 months follow up was not significantly different from that observed before injection (Figure 4B). As figure 4C shows, no difference in DHI was observed between the 4 conditions at 3 months after injection. DHI was significantly decreased 3 months after injection in sham-injected healthy ($P < 0.05$) and degenerated ($P < 0.05$) discs, but not in the healthy and BMP-4-injected degenerated discs. Upon macroscopic investigation, extradiscal bone formation and aberrant cartilage-like tissue ingrowth beyond the endplate (white tissue) were observed in BMP-4-injected discs (Figure 4 A20). The Thompson score was not different between healthy and healthy sham-injected IVDs. It was significantly higher in BMP-4-treated degenerated IVDs ($P < 0.01$), but not in untreated degenerated discs ($P = 0.06$), compared to healthy sham-injected IVDs (Figure 4D). Additionally, according to the results from micro-CT, extradiscal new bone formation (Figure 4 A6, A8) and subchondral bone loss (Figure 4 A12, A14) were only found in degenerated BMP-4-injected discs (5 out of 5 discs), and as such the frequency was significantly higher in BMP-4-injected than non-treated discs ($P < 0.01$) (Supplementary Table 3).

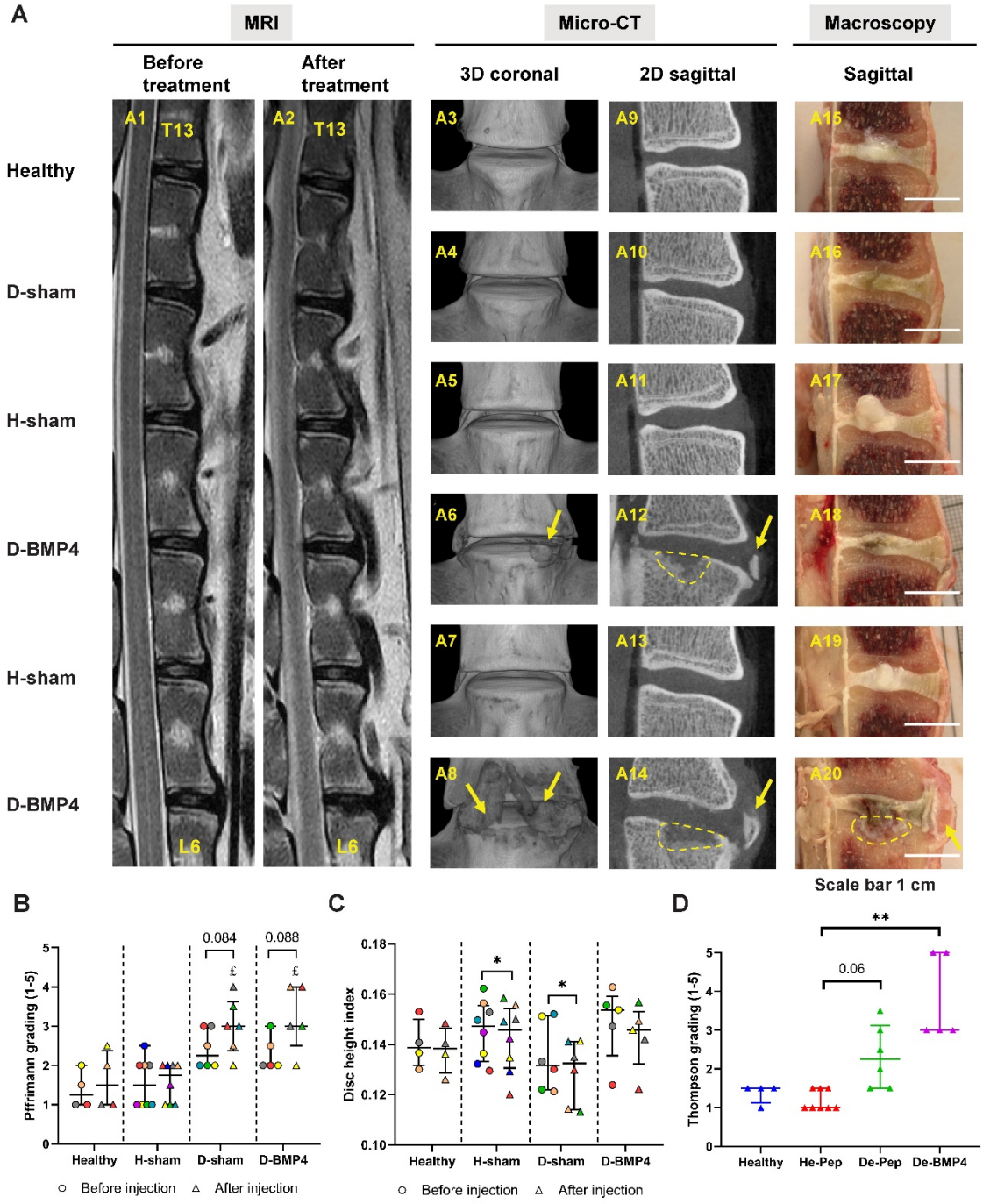

Figure 4. BMP-4 did not induce intervertebral disc regeneration but induced extradiscal new bone formation and subchondral bone remodeling.

(A) Sheep lumbar intervertebral discs were measured by magnetic resonance image (MRI) before and three months after treatment (healthy discs (Healthy), healthy disc with random peptide injection (H-sham), degenerated discs with random peptide (D-sham) and BMP-4 injection (D-BMP4)), sagittal T2-weighted images (A1, before treatment, A2, after treatment), then IVDs were scanned by micro-CT, three dimensional

*(3D) coronal images (A 3–8) and two dimensional (2D) sagittal images (A 9–14), and discs were cut into two parts at middle sagittal (A 15–20). Arrow: new bone formation, circle: subchondral bone rupture. T2-weighted images were used to evaluate Pffrimann grading (B) and disc height index (C) before (circle) and after (triangle) treatment (the same color indicates the same disc within groups). 2D sagittal macroscopic images were used to evaluate Thompson grading (D). Kruskal Wallis with the post-hoc test was used to determine differences among groups in Pffrimann grading and disc height index before or after treatment separately and Thompson grading, using paired t-test to define the difference between before and after treatment in Pffrimann grading and disc height index. Median with interquartile range, sample size as independent dots, £ $p < 0.05$, Paffrimann score of De-Pep and De-BMP4 vs He-Pep, *$P < 0.05$, **$P < 0.01$. Image A20 was reproduced from Lee N.N. et al. JOR Spine 4(2) (2021) e1162.*

3.2.2. In BMP-4-treated discs, regeneration was absent based on histological and biochemical analysis

To further confirm the aforementioned results, histological and biochemical analyses were performed. As seen in figure 5A, AB/PR staining showed an irregular thickening of the endplate in sham-injected degenerated IVDs, but not in healthy and healthy sham-injected IVDs. In BMP-4-injected degenerated IVDs, there was subchondral bone plate disruption with aberrant cartilaginous tissue. In the NP, heterogeneity, a decrease in alcian blue and an increase in picrosirius red staining were apparent in sham injected and BMP-4-injected degenerated IVDs, compared to healthy IVDs. In the AF, extradiscal bone formation and loss of lamellar structure were observed upon BMP-4 treatment. The degeneration score was performed based on AB/PR, H&E, and Saf-O fast green staining (H&E and Saf-O FG staining see Supplementary Figure 4). Accordingly, the degeneration score of the NP matrix staining was significantly higher in sham-injected degenerated IVDs ($P < 0.05$) compared to healthy sham-injected IVDs, but not in BMP4-treated degenerated IVDs (Figure 5B), while degenerative grading on endplate morphology ($P < 0.05$), AF morphology ($P < 0.01$), and bone modeling at the external AF/bone interface ($P < 0.05$) was significantly higher with BMP-4 treatment when compared to sham-injected healthy IVDs, but not sham-injected degenerated IVDs (Figure 5C-E). The total degeneration score was significantly higher in both sham-injected ($P < 0.05$) and BMP-4-injected degenerated IVDs ($P < 0.05$) compared to sham-injected healthy IVDs, but there was no difference between healthy and healthy sham-injected discs (Figure 5F), nor between degenerated controls and BMP4-injected IVDs were observed. In the remaining 4 parameters of the degeneration score, including NP cell clustering, NP cell loss, tears and clefts, and demarcation between AF and NP, no significant differences were observed between treatments (Supplementary Figure 5). Immunohistochemical staining of collagen type II and I is illustrated in Figure 5A. In the NP, heterogeneity and loss of collagen type II was found in sham-injected and BMP-4-injected degenerated discs compared to healthy discs, but no difference was observed between BMP-4 treated and non-treated degenerated discs. All AF tissues were slightly collagen type II positive. Collagen type I deposition was apparent in the NP in sham-injected degenerated IVDs and also in BMP-4-injected degenerated IVDs. No difference was found regarding collagen type I staining in AF among treatments. Interestingly, when looking into the area of subchondral bone disruption in BMP-4 treated IVD (Figure 6), subchondral bone was replaced with cartilage-like tissue, which was alcian blue- and collagen II-positive, but negative for collagen type I. In these particular areas a high cell density and many chondrocyte-like cell clusters were observed. In the area of extradiscal bone

formation, chondrocyte-like cells were surrounded by positive alcian blue and slight collagen type II and I staining in the interface between AF and extradiscal bone.

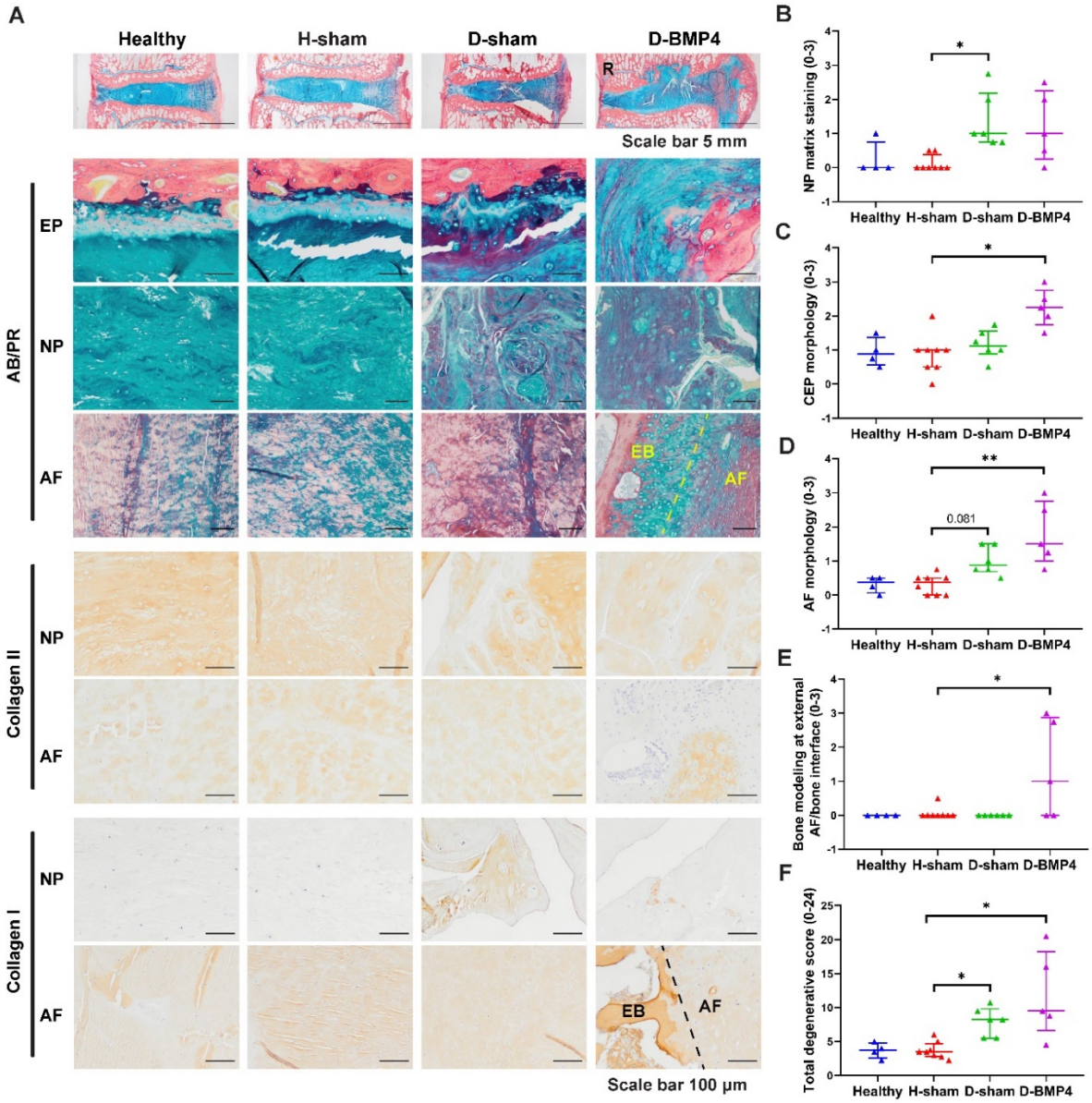

Figure 5. BMP-4 did not promote disc regeneration evaluated by histological degenerative grading.

(A) Sheep IVDs were collected and performed histological staining including alcian blue and picrosirius red staining (AB/PR, proteoglycan (blue), collagen (red)) and immunohistochemical staining for collagen type I and II (healthy discs (Healthy), healthy disc with random peptide injection (H-sham), degenerated discs with random peptide (D-sham) and BMP-4 injection (D- BMP4)). Histological grading of disc degeneration was performed based on AB/PR, hematoxylin and eosin (H&E) and Safranin-O Fast Green (Saf O/FG) staining (H&E and Saf O/FG see Supplementary Figure 4). Endplate (EP), Annulus Fibrosus

*(AF), Nucleus Pulposus (NP), Extradiscal Bone (EB). Histological grading for NP matrix staining (B), cartilage endplate (CEP) morphology (C), AF morphology (D), bone modeling at the external AF/bone interface (E), and the total score of histological grading (F). The rest of grading parameters are in supplementary data 5. Kruskal Wallis with the post-hoc test was used to determine differences among groups. Median with interquartile range, sample size as independent dots, *p < 0.05, **p < 0.01. R: image of D-BMP-4 AB/ PR staining macroscopy was reproduced from Lee N.N. et al. JOR Spine 4(2) (2021) e1162.*

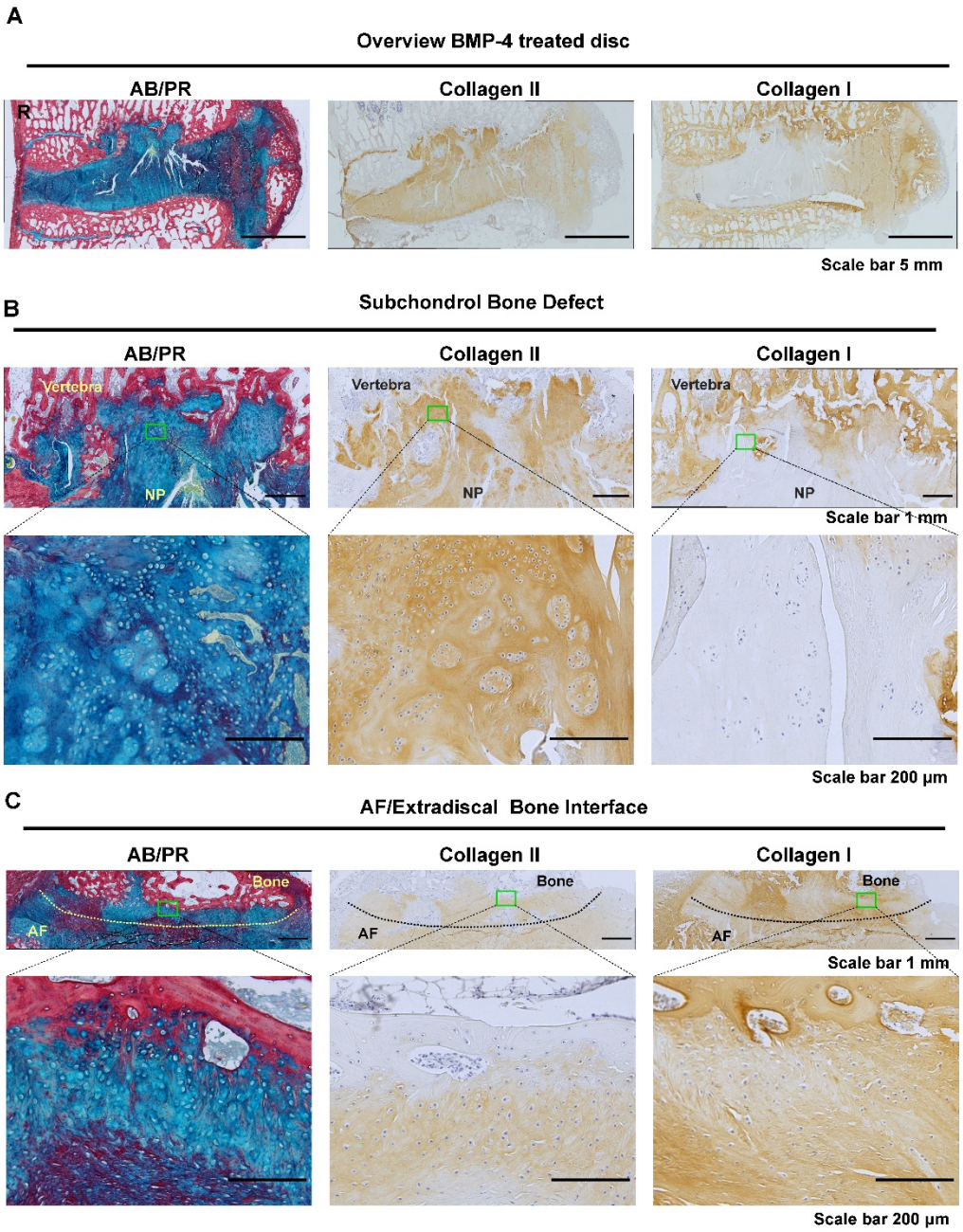

Figure 6. The overview and the area of subchondral bone defect and extradiscal bone in BMP-4 treated IVD.

The overview (A) and the area of subchondral bone defect (B) and extradiscal bone (C) in BMP-4 treated IVD. Section stained by Alcian blue and picrosirius red staining (AB/PR, proteoglycan (blue), collagen (red)) and immunohistochemical staining for collagen type II and I (brown). R: image of D-BMP-4 AB/PR staining was reproduced from Lee N.N. et al. JOR Spine 4(2) (2021) e1162.

As seen in figure 7A and 7D, the GAG content was reduced in sham-injected and BMP-4-injected degenerated IVDs compared to healthy sham-injected IVDs in both NP and AF ($P < 0.05$), and no difference was observed between healthy and healthy sham-injected IVDs. No difference was observed in collagen and DNA content in NP and AF (Figure 7B, C, E, F).

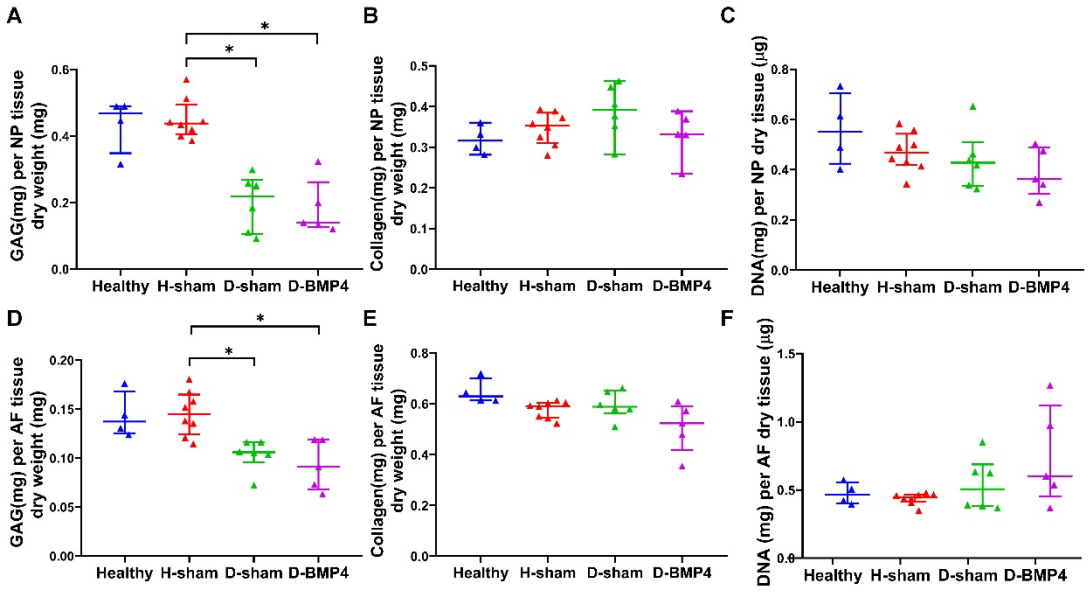

Figure 7. BMP-4 did not show positive effects on disc regeneration evaluated by biochemical analysis.

*Half part of the IVDs was collected for biochemical analysis. The glycosaminoglycan (GAG) (A, D), total collagen (B, E), and DNA (C, F) content were measured in both nucleus pulposus (NP) (A, B, C) and annulus fibrosus (AF) (D, E, F) tissue. GAG and total collagen content were normalized to tissue dry weight, and DNA content showed by μg per mg of tissue dry weight. Kruskal Wallis with the post-hoc test was used to determine differences among groups. Median with interquartile range, sample size as independent dots, *$p < 0.05$.*

3.3 Osteoclast numbers in the subchondral bone.

To check whether the subchondral bone loss in the BMP-4 treated IVDs was related to osteoclast activity, TRAP staining was used to detect osteoclasts. As figure 8A shows, osteoclasts were found in IVDs treated by BMP-4, especially in the area around subchondral bone loss. The number of $TRAP^+$ multinucleated cells was significantly higher in the IVDs treated with BMP-4 ($P < 0.05$), but not sham-injected degenerated IVDs when compared to sham-injected healthy IVDs (Figure 8B).

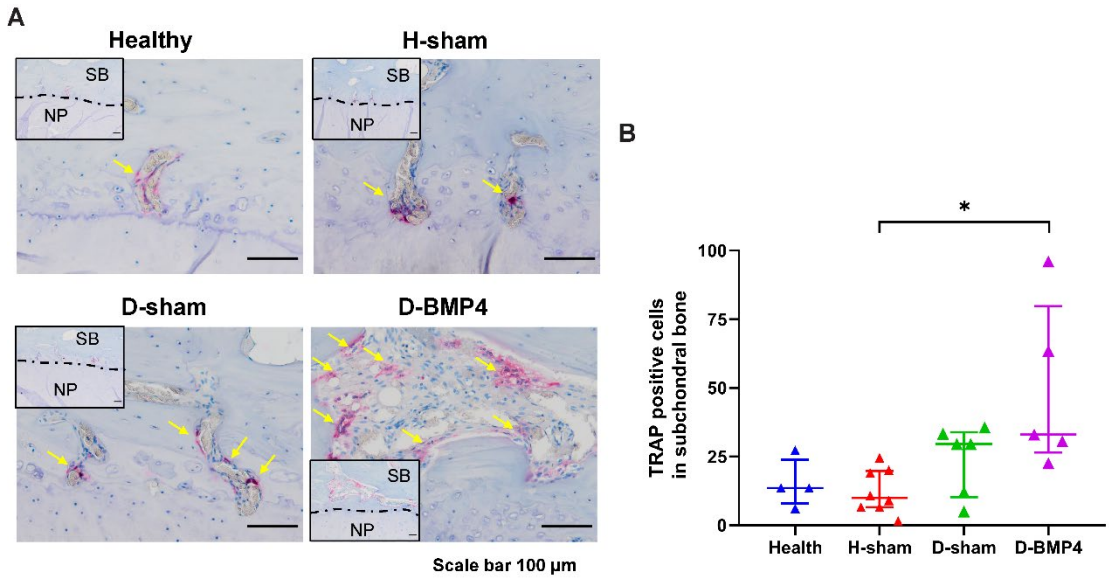

Figure 8. Osteoclast numbers were increased in subchondral bone of discs that were treated with BMP-4 and had subchondral bone rupture.

*(A) Tartrate-resistant acid phosphatase (TRAP) staining was performed to detect osteoclast in subchondral bone of IVDs (healthy discs (Healthy), healthy disc with random peptide injection (H -sham), degenerated discs with random peptide (D-sham) and BMP-4 injection (D-BMP4)). TRAP positive cells (yellow arrow) were counted in both sides of subchondral bone (B). Corner images at low magnification show the position was located at the subchondral bone, SB: subchondral bone, NP: nucleus pulposus. Kruskal Wallis with the post-hoc test was used to determine differences among groups. Median with interquartile range, sample size as independent dots, *p < 0.05.*

4. Discussion

IVD regeneration has been proposed as a promising strategy to treat discogenic CLBP. Inducing regeneration by growth factors has been widely investigated. In this study, we report that although BMP-4 showed powerful regenerative effects *in vitro* by promoting cell proliferation and ECM anabolism in sheep NP and AF cells, extradiscal bone formation and aberrant cartilage tissue overgrowth associated with subchondral bone loss were found when BMP-4 was applied intradiscally *in vivo*.

In NP pellet culture, cell proliferation and deposition of proteoglycan and collagen type II, but not collagen type I, was dose-dependently increased by BMP-4. These findings are consistent with previous studies, where BMP-4 was used to treat human NP cells or overexpressed in bovine NP cells using adenoviruses [23, 31]. In addition, in the current study, the effect of BMP-4 in promoting cell proliferation was confirmed by increasing *Ki-67* expression by the high concentration of BMP-4 on day 2, while decreasing *Ki-67* expression on day 7 may be due to inverse feedback. Moreover, BMP-4 up-regulated *SOX-9*, indicating that BMP-4 enhanced ECM deposition may be via *SOX-9*. In the current study, AF cells treated with BMP-4 showed similar effects as NP cells,

including enhanced production of proteoglycans and collagen II and increased proliferation. However, in contrast to NP cells, the production of collagen I appeared to be increased in AF at low concentrations BMP-4, then declined with further increasing BMP-4 concentration. The underlying mechanism may warrant further study to tune stimulation of ECM production by BMP-4 in AF cells. In AF tissue, the proteoglycan and collagen II content gradually decreases from the inner to outer AF, while collagen I increases [9]. Proteoglycan content in the inner AF may provide functional compensation when the proteoglycan declines in NP with disc degeneration [32]. Although the majority of studies on IVDD focused on NP tissue, pathological changes in AF tissue are commonly associated with pain and disability and therefore AF repair merits attention [33, 34]. In contrast to our *in vitro* data, intradiscal injection of BMP-4 did not promote disc regeneration *in vivo*.

Severe side effects were found in BMP-4-treated discs, including ectopic bone formation, subchondral and vertebral bone loss, and aberrant growth of cartilage-like tissue through the EP to the vertebral bone. The extradiscal bone formation could be induced by BMP-4 leakage and diffusion from the IVD. In the current study, the volumes injected were limited, as was needle size. A recent study showed that this risk of leakage could be minimized to zero by using small injection volume, small needle diameters [35]. Hence direct leakage through the injection tract is less likely, and extradiscal bone formation is probably due to diffusion. BMPs are known as potent inducers of bone formation. Overexpression of BMP-4 in rat adipose-derived stromal cells, NIH/3T3 and C2C12 cells induced osteogenic and/or endochondral bone formation after implanting these cells into immunodeficient mice [36, 37]. Similarly, extradiscal bone formation also occurred in a previous study after intradiscal injection of BMP-7 at a similar dose in a canine spontaneous IVDD model, although no effects the endplate nor subchondral bone were observed [20].

Besides extradiscal bone formation, BMP-4 also induced subchondral and vertebral bone loss and aberrant cartilage-like tissue through the EP to the vertebral bone. This change is highly similar to a Schmorl's node, in which the soft disc tissue bulges out into the adjacent vertebrae through an EP defect [38]. The pathogenesis of Schmorl's nodes is still uncertain. In our case, it may be associated with weakened vertebral bone and/or cartilage EP. One explanation could be that the loss of vertebral bone initiated this Schmorl's node-like change. In the current study, although the osteoclast number along subchondral bone was not different between BMP-4-treated and non-treated degenerated discs, the osteoclast number was significantly higher in the area around the subchondral bone loss in IVDs treated with BMP-4, indicating BMP-4 may induce osteoclast proliferation or activation which causes bone resorption. Despite the increasing osteoclast numbers, it could be a consequence of EP rupture. Our hypothesis could be confirmed by a previous study that showed overexpression of BMP-4 in bone induced severe osteopenia with increasing osteoclast number and phosphorylated Smads 1/5/8 BMP signaling in mice [39]. This suggests that BMP-4 may be associated with both bone formation and bone resorption. These contradictory effects on bone metabolism were also reported for BMP-2 when it was used for transforaminal lumbar interbody fusion showing evidence of transient vertebral endplate osteoclastic activity in radiographs [40]. Studies suggested the BMP-2-induced osteolysis may be related to an increase of inflammation [40, 41]. A recent study showed circulating BMP-4 levels were elevated during thoracic surgery and positively correlated with pro-inflammatory cytokines, including IL-1β and TNF-α, and suggested that BMP-4 may exert pro-inflammatory properties via

cyclooxygenase-II signaling pathways [42]. Whether the BMP-4-related bone resorption in the current study is associated with inflammation remains unclear, and warrants further study. Another potential explanation should be that the deteriorated EP initiated Schmorl's node-like change. The effect of BMP-4 on EP has, however, rarely been studied. A previous study showed that injection of 100 μg BMP-2 in a rabbit IVDD model caused EP hypertrophy [43]. A better understanding of the effects and underlying mechanism of BMP-4 in bone and cartilage-like tissue will facilitate further evaluation of BMP-4 for IVD regeneration or bone regeneration for spine fusion.

Overall, given the complete absence of any regenerative effect of the injected BMP-4 on NP or AF tissue in the current large animal model, achieving intradiscal regeneration in IVDs with established degeneration may provide a challenge. Possibly more factors like injection dose and method, limited nutrient, and inflammation should be taken into account when using growth factors for IVD regeneration.

5. Conclusion

In conclusion, BMP-4 promoted chondrogenic ECM production and cell proliferation of NP and AF cells *in vitro*. Intradiscal injection of a single dose of BMP-4 failed to halt disc degeneration or induce disc regeneration. Instead, extradiscal bone formation, endplate hypertrophy and Schmorl’s node-like changes were induced. Therefore, a similar dose of soluble BMP-4 should not be considered for directly intradiscal injection as a strategy for IVD regeneration.

Funding:

This project has received funding from the European Union's Horizon 2020 research and innovation programme under Marie Sklodowska-Curie CoFund, grant agreement 801540, under grant agreement no 825925 and the Dutch Arthritis Society (LLP12 and LLP22).

Author contributions:

Jie Du: Methodology, Investigation, Formal analysis, Writing - Original Draft, Writing - Review & Editing. João P. Garcia: Methodology, Investigation, Formal analysis, Writing - Review & Editing. Frances C. Bach: Formal analysis, Writing - Review & Editing. Anna R. Tellegen: Formal analysis, Writing - Review & Editing. Sibylle Grad: Methodology, Writing - Review & Editing. Zhen Li: Methodology, Writing - Review & Editing. René M Castelein: Methodology, Writing - Review & Editing. Björn P. Meij: Methodology, Investigation, Writing - Review & Editing. Marianna A. Tryfonidou: Conceptualization, Methodology, Writing - Review & Editing. Laura B. Creemers: Conceptualization, Methodology, Writing - Review & Editing, Funding acquisition.

Acknowledgments

Frank M. Riemers is gratefully acknowledged for the genetic screening of the sheep.

Conflicts of interest statement

The authors have no conflicts of interest relevant to this article.

Supplementary figures and tables

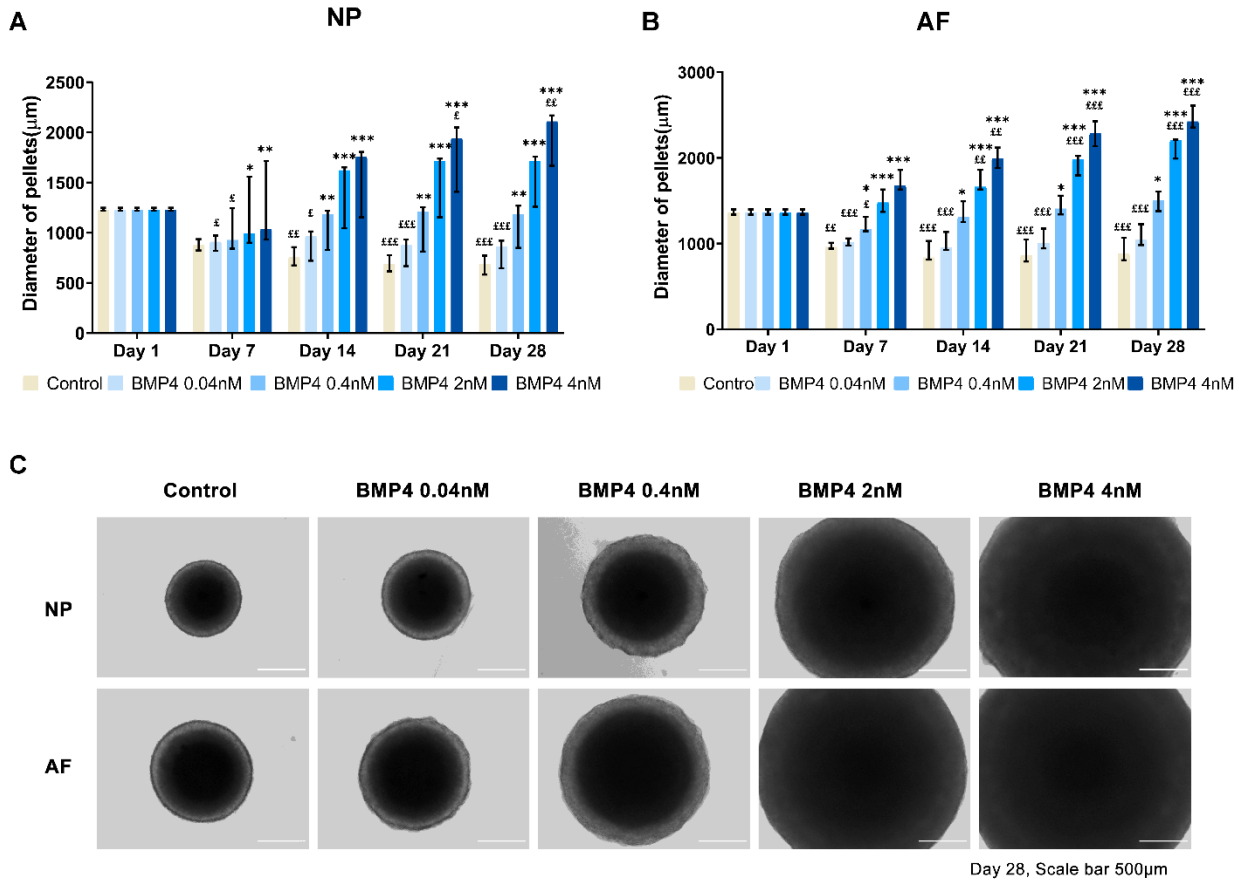

Supplementary figure 1. BMP-4 increased pellet size over time and with increasing of dose.

*Sheep nucleus pulposus (NP) and annulus fibrosus (AF) cell pellets were cultured with (0.04 nM, 0.4 nM, 2 nM, 4 nM,) or without BMP-4 at four different concentrations for 4 weeks. The diameter of pellets of NP (**A**) and AF (**B**) was measured at day 1 and every week. **C,** The Pellet's size of NP and AF after 4 weeks culture. Kruskal Wallis with the post-hoc test was used to determine differences among more groups. Median with interquartile range, 3 donors in triplicates, n=9, £ p< 0.05, ££ p< 0.01, £££ p< 0.001 vs day 1 within each condition by time points, * p< 0.05, ** p< 0.01, *** p< 0.001 vs control within each time point by conditions.*

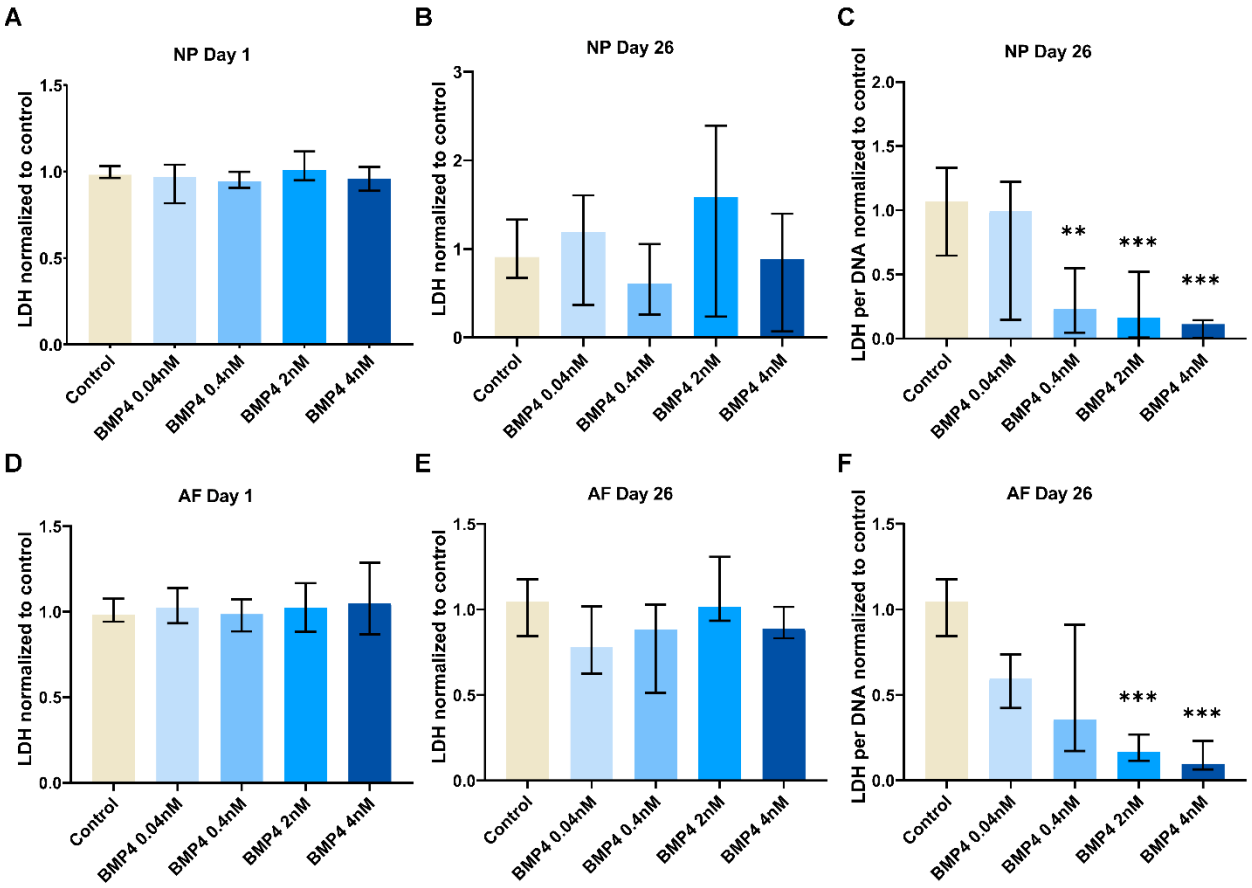

Supplementary figure 2. No cytotoxicity was found after treatment by BMP-4 in sheep NP and AF pellets.

Sheep nucleus pulposus (NP) ***(A, B, C)*** *and annulus fibrosus (AF)* ***(D, E, F)*** *cell pellets were cultured with (0.04 nM, 0. 4 nM, 2 nM, 4 nM,) or without BMP-4 at four different concentrations for 4 weeks. Cytotoxicity was measured by detection of lactate dehydrogenase (LDH) activity in culture media at day 1 (**A, D**) and day 26 (**B, E**) for 1 day incubation with BMP-4, and results were normalized to non-treated control.* ***(C, F)*** *LDH activity per DNA at day 26 were calculated and normalized to non-treated control. Cytotoxicity was measured using the Cytotoxicity Detection Kit (4744926001, Roche Diagnostics GmbH, Mannheim, Germany) according to the manufacturer's protocol. Kruskal Wallis with the post-hoc test was used to determine differences among more groups. Median with interquartile range, 3 donors in triplicates, n=9, ** p< 0.01, *** p< 0.001 vs control.*

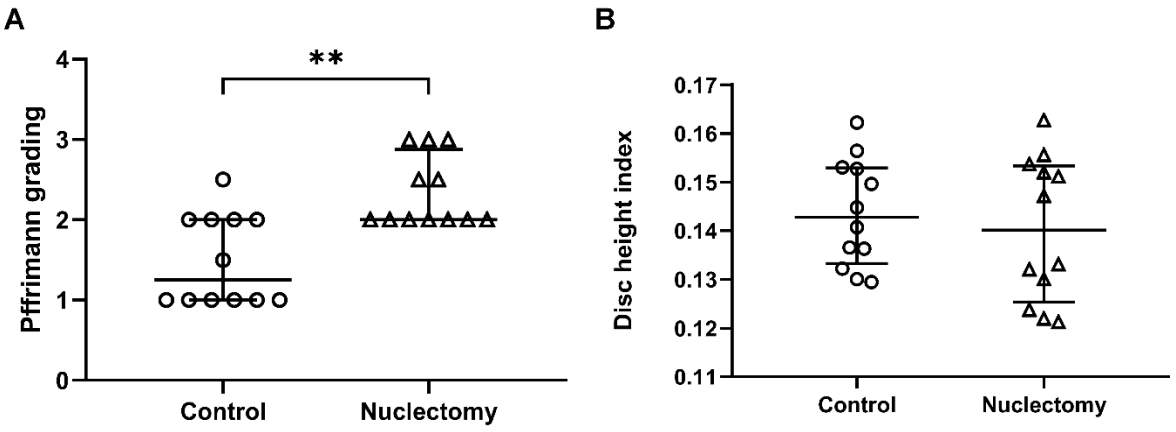

Supplementary figure 3. IVD degeneration induced by nucleotomy.

*Three months after nucleotomy conduction, magnetic resonance image (MRI) was used to evaluate degeneration of disc, then Pffrimann grading (**A**) and disc height index (**B**) were performed. Statistical analysis performed using Mann-Whitney U test. Median with interquartile range, sample size as independent dots, ** p< 0.01.*

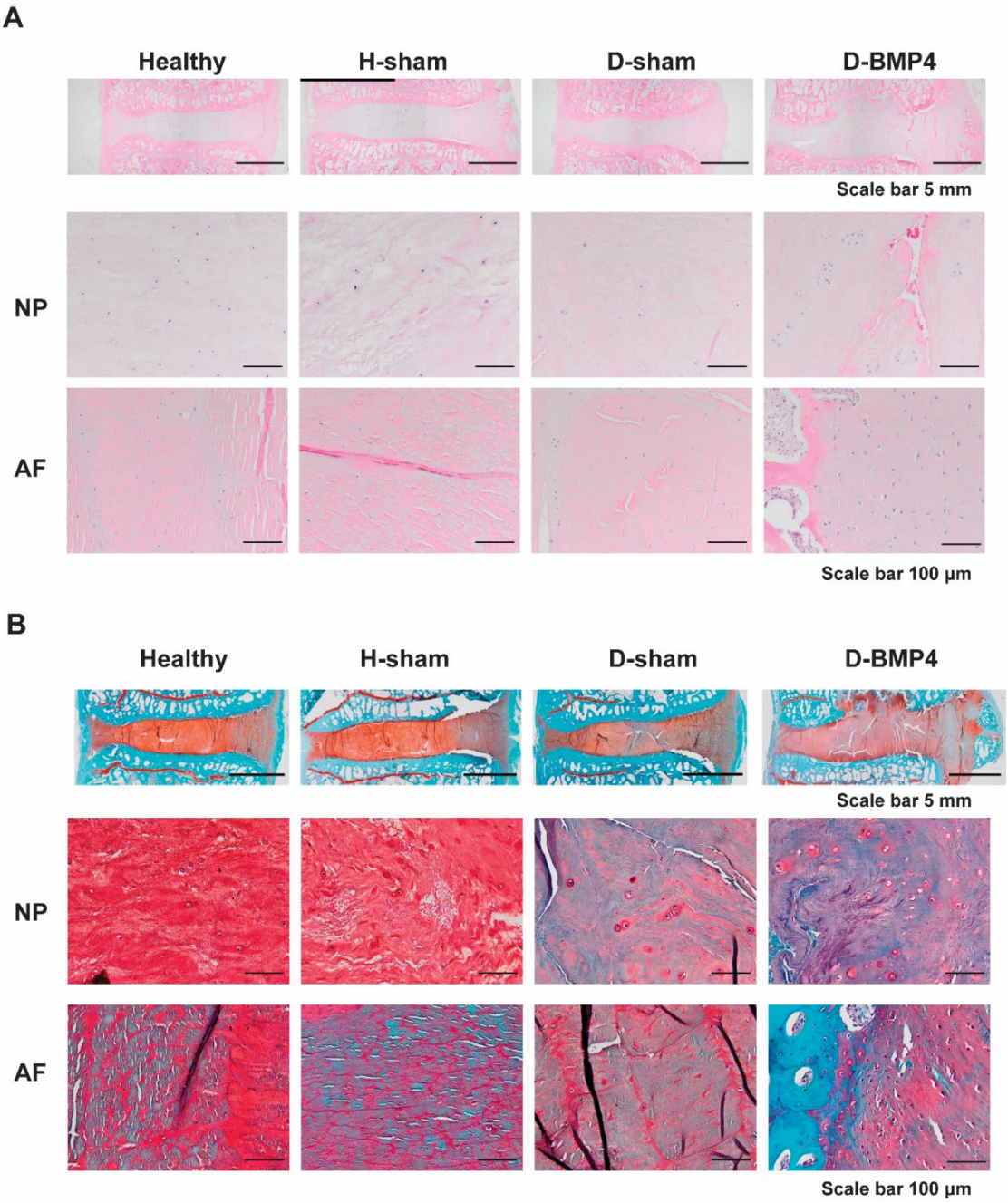

Supplementary figure 4. BMP-4 did not show positive effects on disc regeneration evaluated by histological analysis.

*(**A**) hematoxylin and eosin (H&E) and (**B**) Safranin-O Fast Green (Saf O/FG) staining for the discs (healthy discs (Healthy), healthy disc with random peptide injection (H-sham), degenerated discs with random peptide (D-sham) and BMP-4 injection (D-BMP4)). Nucleus Pulposus (NP), Annulus Fibrosus (AF).*

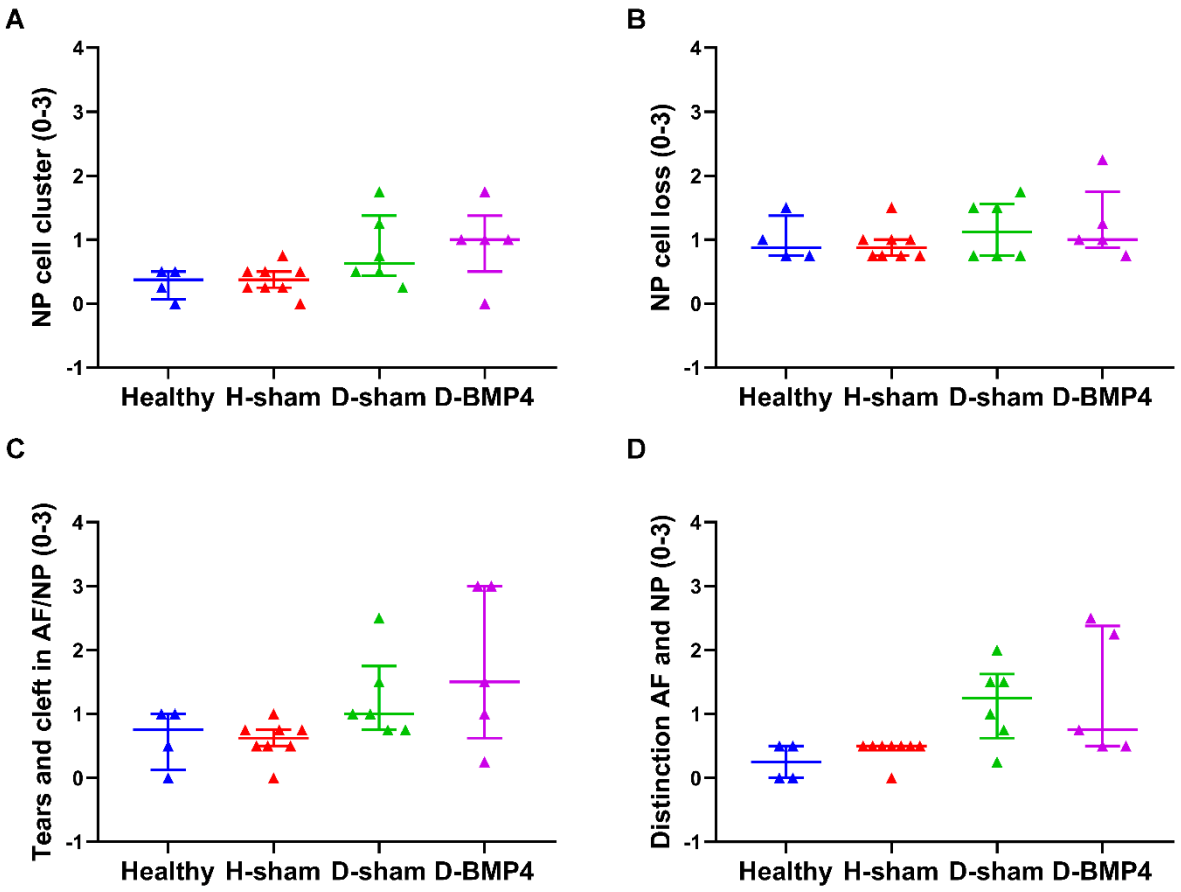

Supplementary figure 5. BMP-4 did not show positive effects on disc regeneration evaluated by histological grading (parameters show no difference among groups).

*Histological grading of disc degeneration was performed based on alcian blue and picrosirius red (AB/PR), hematoxylin and eosin (H&E) and Safranin-O Fast Green (Saf O/FG). Histological grading for NP cell cluster **(A)**, NP cells loss (**B**), tears and cleft in AF/NP (**C**), distinction AF and NP (**D**). Kruskal Wallis with the post-hoc test was used to determine differences among groups. Median with interquartile range, sample size as independent dots.*

Supplementary Table 1. Sheep discs and treatment.

		Treatment			
		Sheep 1	**Sheep 2**	**Sheep 3**	**Sheep 4**
IVDs	**T13-L1**	Healthy	Healthy	Healthy	Healthy
	L1-2	D-sham	D-BMP4	D-BMP4	D-sham
	L2-3	H-sham	H-sham	H-sham	H-sham
	L3-4	D-BMP4	D-sham	D-sham	D-BMP4*
	L4-5	H-sham	H-sham	H-sham	H-sham
	L5-6	D-BMP4	D-sham	D-BMP4	D-sham

** This disc was excluded from results. Because BMP-4 was injected to AF.*

Supplementary Table 2. Sheep's weight before and 3 months after treatment.

		Weight (kg)	
		Before treatment	**Three months after treatment**
Animals	**Sheep 1**	97	95
	Sheep 2	86	85
	Sheep 3	78	81
	Sheep 4	75	77.5

Supplementary Table 3. Extradiscal new bone formation and subchondral bone rupture after treatment.

		Extradiscal new bone formation		***Subchondral bone rupture***	
Treatment		**No**	**Yes**	**No**	**Yes**
	Healthy (n=4)	4	0	4	0
	H-sham (n=8)	8	0	6	2
	D-sham (n=6)	6	0	6	0
	D-BMP4 (n=5)	0	5*	0	5*

* Frequency is significant different (*P*< 0.01) than De-Pep, tested by Fisher's Exact Test.

References

[1] G.B.D. Disease, I. Injury, C. Prevalence, Global, regional, and national incidence, prevalence, and years lived with disability for 328 diseases and injuries for 195 countries, 1990-2016: a systematic analysis for the Global Burden of Disease Study 2016, Lancet 390(10100) (2017) 1211-1259.
[2] B. Arnbak, T.S. Jensen, N. Egund, A. Zejden, K. Horslev-Petersen, C. Manniche, A.G. Jurik, Prevalence of degenerative and spondyloarthritis-related magnetic resonance imaging findings in the spine and sacroiliac joints in patients with persistent low back pain, Eur Radiol 26(4) (2016) 1191-203.
[3] S.E. Navone, G. Marfia, A. Giannoni, M. Beretta, L. Guarnaccia, R. Gualtierotti, D. Nicoli, P. Rampini, R. Campanella, Inflammatory mediators and signalling pathways controlling intervertebral disc degeneration, Histol Histopathol 32(6) (2017) 523-542.
[4] E. Krock, D.H. Rosenzweig, A.J. Chabot-Dore, P. Jarzem, M.H. Weber, J.A. Ouellet, L.S. Stone, L. Haglund, Painful, degenerating intervertebral discs up-regulate neurite sprouting and CGRP through nociceptive factors, J Cell Mol Med 18(6) (2014) 1213-25.
[5] T. Oichi, Y. Taniguchi, Y. Oshima, S. Tanaka, T. Saito, Pathomechanism of intervertebral disc degeneration, JOR Spine 3(1) (2020) e1076.
[6] R. Rodrigues-Pinto, S.M. Richardson, J.A. Hoyland, An understanding of intervertebral disc development, maturation and cell phenotype provides clues to direct cell-based tissue regeneration therapies for disc degeneration, Eur Spine J 23(9) (2014) 1803-14.
[7] F. Yang, V.Y. Leung, K.D. Luk, D. Chan, K.M. Cheung, Injury-induced sequential transformation of notochordal nucleus pulposus to chondrogenic and fibrocartilaginous phenotype in the mouse, J Pathol 218(1) (2009) 113-21.
[8] Z. Zhou, S. Cui, J. Du, R.G. Richards, M. Alini, S. Grad, Z. Li, One strike loading organ culture model to investigate the post-traumatic disc degenerative condition, J Orthop Translat 26 (2021) 141-150.
[9] C.L. Le Maitre, A. Pockert, D.J. Buttle, A.J. Freemont, J.A. Hoyland, Matrix synthesis and degradation in human intervertebral disc degeneration, Biochem Soc Trans 35(Pt 4) (2007) 652-5.
[10] S. Lee, M. Millecamps, D.Z. Foster, L.S. Stone, Long-term histological analysis of innervation and macrophage infiltration in a mouse model of intervertebral disc injury-induced low back pain, J Orthop Res 38(6) (2020) 1238-1247.
[11] T. Hodgkinson, B. Shen, A. Diwan, J.A. Hoyland, S.M. Richardson, Therapeutic potential of growth differentiation factors in the treatment of degenerative disc diseases, JOR Spine 2(1) (2019) e1045.
[12] X. Cao, D. Chen, The BMP signaling and in vivo bone formation, Gene 357(1) (2005) 1-8.
[13] Z. Zhang, W. Yang, Y. Cao, Y. Shi, C. Lei, B. Du, X. Li, Q. Zhang, The Functions of BMP3 in Rabbit Articular Cartilage Repair, Int J Mol Sci 16(11) (2015) 25934-46.
[14] M. Peeters, S.E. Detiger, L.S. Karfeld-Sulzer, T.H. Smit, A. Yayon, F.E. Weber, M.N. Helder, BMP-2 and BMP-2/7 Heterodimers Conjugated to a Fibrin/Hyaluronic Acid Hydrogel in a Large Animal Model of Mild Intervertebral Disc Degeneration, Biores Open Access 4(1) (2015) 398-406.
[15] Z. Li, G. Lang, L.S. Karfeld-Sulzer, K.T. Mader, R.G. Richards, F.E. Weber, C. Sammon, H. Sacks, A. Yayon, M. Alini, S. Grad, Heterodimeric BMP-2/7 for nucleus pulposus regeneration-In vitro and ex vivo studies, J Orthop Res 35(1) (2017) 51-60.
[16] K. Takegami, H.S. An, F. Kumano, K. Chiba, E.J. Thonar, K. Singh, K. Masuda, Osteogenic protein-1 is most effective in stimulating nucleus pulposus and annulus fibrosus cells to repair their matrix after chondroitinase ABC-induced in vitro chemonucleolysis, Spine J 5(3) (2005) 231-8.
[17] M. Okada, J.H. Kim, S.T. Yoon, W.C. Hutton, Pulsed Electromagnetic Field (PEMF) plus BMP-2 upregulates intervertebral disc-cell matrix synthesis more than either BMP-2 alone or PEMF alone, J Spinal Disord Tech 26(6) (2013) E221-6.

[18] K. Masuda, Y. Imai, M. Okuma, C. Muehleman, K. Nakagawa, K. Akeda, E. Thonar, G. Andersson, H.S. An, Osteogenic protein-1 injection into a degenerated disc induces the restoration of disc height and structural changes in the rabbit anular puncture model, Spine (Phila Pa 1976) 31(7) (2006) 742-54.
[19] Y. Imai, M. Okuma, H.S. An, K. Nakagawa, M. Yamada, C. Muehleman, E. Thonar, K. Masuda, Restoration of disc height loss by recombinant human osteogenic protein-1 injection into intervertebral discs undergoing degeneration induced by an intradiscal injection of chondroitinase ABC, Spine (Phila Pa 1976) 32(11) (2007) 1197-205.
[20] N. Willems, F.C. Bach, S.G. Plomp, M.H. van Rijen, J. Wolfswinkel, G.C. Grinwis, C. Bos, G.J. Strijkers, W.J. Dhert, B.P. Meij, L.B. Creemers, M.A. Tryfonidou, Intradiscal application of rhBMP-7 does not induce regeneration in a canine model of spontaneous intervertebral disc degeneration, Arthritis Res Ther 17 (2015) 137.
[21] C. Daly, P. Ghosh, G. Jenkin, D. Oehme, T. Goldschlager, A Review of Animal Models of Intervertebral Disc Degeneration: Pathophysiology, Regeneration, and Translation to the Clinic, Biomed Res Int 2016 (2016) 5952165.
[22] N.N. Lee, E. Salzer, F.C. Bach, A.F. Bonilla, J.L. Cook, Z. Gazit, S. Grad, K. Ito, L.J. Smith, A. Vernengo, H.J. Wilke, J.B. Engiles, M.A. Tryfonidou, A comprehensive tool box for large animal studies of intervertebral disc degeneration, JOR Spine 4(2) (2021) e1162.
[23] A. Krouwels, J.D. Iljas, A.H.M. Kragten, W.J.A. Dhert, F.C. Oner, M.A. Tryfonidou, L.B. Creemers, Bone Morphogenetic Proteins for Nucleus Pulposus Regeneration, Int J Mol Sci 21(8) (2020).
[24] F. Bach, Mimicking developmental biology to regenerate the intervertebral disc (PhD thesis), Faculty of Veterinary Medicine, Utrecht University, Utrecht, The Netherlands, 2018, pp. 328-329.
[25] W.R. Vorachek, Hugejiletu, G. Bobe, J.A. Hall, Reference gene selection for quantitative PCR studies in sheep neutrophils, Int J Mol Sci 14(6) (2013) 11484-95.
[26] A.R. Tellegen, I. Rudnik-Jansen, M. Beukers, A. Miranda-Bedate, F.C. Bach, W. de Jong, N. Woike, G. Mihov, J.C. Thies, B.P. Meij, L.B. Creemers, M.A. Tryfonidou, Intradiscal delivery of celecoxib-loaded microspheres restores intervertebral disc integrity in a preclinical canine model, J Control Release 286 (2018) 439-450.
[27] F.C. Bach, A.R. Tellegen, M. Beukers, A. Miranda-Bedate, M. Teunissen, W.A.M. de Jong, S.A.H. de Vries, L.B. Creemers, K. Benz, B.P. Meij, K. Ito, M.A. Tryfonidou, Biologic canine and human intervertebral disc repair by notochordal cell-derived matrix: from bench towards bedside, Oncotarget 9(41) (2018) 26507-26526.
[28] C.W. Pfirrmann, A. Metzdorf, M. Zanetti, J. Hodler, N. Boos, Magnetic resonance classification of lumbar intervertebral disc degeneration, Spine (Phila Pa 1976) 26(17) (2001) 1873-8.
[29] K. Masuda, Y. Aota, C. Muehleman, Y. Imai, M. Okuma, E.J. Thonar, G.B. Andersson, H.S. An, A novel rabbit model of mild, reproducible disc degeneration by an anulus needle puncture: correlation between the degree of disc injury and radiological and histological appearances of disc degeneration, Spine (Phila Pa 1976) 30(1) (2005) 5-14.
[30] J.P. Thompson, R.H. Pearce, M.T. Schechter, M.E. Adams, I.K. Tsang, P.B. Bishop, Preliminary evaluation of a scheme for grading the gross morphology of the human intervertebral disc, Spine (Phila Pa 1976) 15(5) (1990) 411-5.
[31] Y. Zhang, H.S. An, E.J. Thonar, S. Chubinskaya, T.C. He, F.M. Phillips, Comparative effects of bone morphogenetic proteins and sox9 overexpression on extracellular matrix metabolism of bovine nucleus pulposus cells, Spine (Phila Pa 1976) 31(19) (2006) 2173-9.
[32] K. Singh, K. Masuda, E.J. Thonar, H.S. An, G. Cs-Szabo, Age-related changes in the extracellular matrix of nucleus pulposus and anulus fibrosus of human intervertebral disc, Spine (Phila Pa 1976) 34(1) (2009) 10-6.

[33] H.J. Moon, J.H. Kim, H.S. Lee, S. Chotai, J.D. Kang, J.K. Suh, Y.K. Park, Annulus fibrosus cells interact with neuron-like cells to modulate production of growth factors and cytokines in symptomatic disc degeneration, Spine (Phila Pa 1976) 37(1) (2012) 2-9.
[34] A.M.R. Groh, D.E. Fournier, M.C. Battie, C.A. Seguin, Innervation of the Human Intervertebral Disc: A Scoping Review, Pain Med 22(6) (2021) 1281-1304.
[35] L.J. Varden, E.J. Turner, A.T. Coon, A.J. Michalek, Establishing a through-puncture model for assessing post-injection leakage in the intervertebral disc, Eur Spine J 31(4) (2022) 865-873.
[36] L. Lin, X. Fu, X. Zhang, L.X. Chen, J.Y. Zhang, C.L. Yu, K.T. Ma, C.Y. Zhou, Rat adipose-derived stromal cells expressing BMP4 induce ectopic bone formation in vitro and in vivo, Acta Pharmacol Sin 27(12) (2006) 1608-15.
[37] G. Li, H. Peng, K. Corsi, A. Usas, A. Olshanski, J. Huard, Differential effect of BMP4 on NIH/3T3 and C2C12 cells: implications for endochondral bone formation, J Bone Miner Res 20(9) (2005) 1611-23.
[38] G. Schmorl, Über die an den Wirbelbandscheiben vorkommenden Ausdehnungs-und Zerreissungsvorgänge und die dadurch an ihnen und der Wirbelspongiosa hervorgerufenen Veränderungen, Verhandlungen Dtsch Ges Für Pathol 22 (1927) 250-62.
[39] M. Okamoto, J. Murai, H. Yoshikawa, N. Tsumaki, Bone morphogenetic proteins in bone stimulate osteoclasts and osteoblasts during bone development, J Bone Miner Res 21(7) (2006) 1022-33.
[40] J.D. Stensby, R.W. Kaliney, B. Alford, F.H. Shen, J.T. Patrie, M.G. Fox, Radiographic Appearance of Transforaminal Lumbar Interbody Fusion Performed With and Without Recombinant Human Morphogenetic Protein-2, AJR Am J Roentgenol 206(3) (2016) 588-94.
[41] G. Mbalaviele, D.V. Novack, G. Schett, S.L. Teitelbaum, Inflammatory osteolysis: a conspiracy against bone, J Clin Invest 127(6) (2017) 2030-2039.
[42] X. Zhao, J. Zhang, W. Zhang, R. Dai, J. Xu, Z. Li, L. Yang, The Relationship Between Circulating Bone Morphogenetic Protein-4 and Inflammation Cytokines in Patients Undergoing Thoracic Surgery: A Prospective Randomized Study, J Inflamm Res 14 (2021) 4069-4077.
[43] K.Y. Huang, J.J. Yan, C.C. Hsieh, M.S. Chang, R.M. Lin, The in vivo biological effects of intradiscal recombinant human bone morphogenetic protein-2 on the injured intervertebral disc: an animal experiment, Spine (Phila Pa 1976) 32(11) (2007) 1174-80.

Chapter 4

Functional Cell Phenotype Induction with TGF-β1 and Collagen-polyurethane Scaffold for Annulus Fibrosus Rupture Repair

Jie Du, Rose G. Long, Tomoko Nakai, Daisuke Sakai, Lorin M. Benneker, Guangqian Zhou, Bin Li, David Eglin, James C. Iatridis, Mauro Alini, Sibylle Grad, Zhen Li

Published in European Cells and Materials
DOI: 10.22203/eCM.v039a01

Jie Du contributed to the study design, acquisition, analysis, interpretation of data, drafting, and revising of the article, and final approval.

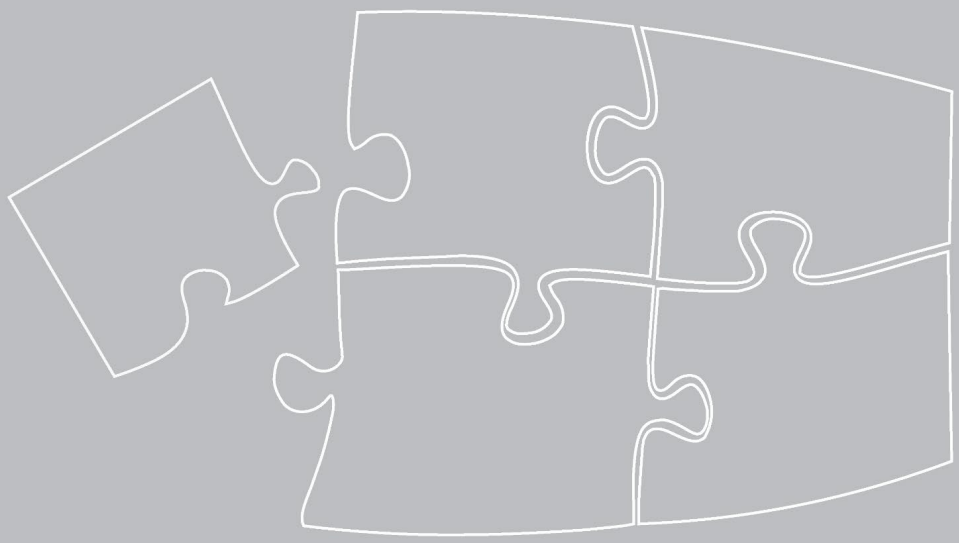

Abstract:

Appropriate cell sources, bioactive factors and biomaterials for generation of functional and integrated annulus fibrosus (AF) tissue analogues are still an unmet need. In the present study, the AF cell markers, collagen type I, cluster of differentiation 146 (CD146), mohawk (MKX), and smooth muscle protein 22α (SM22α) were found to be suitable indicators of functional AF cell induction. *In vitro* 2D culture of human AF cells showed that transforming growth factor β1 (TGF-β1) upregulated the expression of the functional AF markers and increased cell contractility, indicating that TGF-β1-pre-treated AF cells were an appropriate cell source for AF tissue regeneration. Furthermore, a tissue engineered construct, composed of polyurethane (PU) scaffold with a TGF-β1 supplemented collagen type I hydrogel and human AF cells, was evaluated with *in vitro* 3D culture and *ex vivo* preclinical bioreactor-loaded organ culture models. The collagen type I hydrogel helped maintaining the AF functional phenotype. TGF-β1 supplement within the collagen I hydrogel further promoted cell proliferation and matrix production of AF cells within *in vitro* 3D culture. In the *ex vivo* IVD organ culture model with physiologically relevant mechanical loading, TGF-β1 supplement in the transplanted constructs induced the functional AF cell phenotype and enhanced collagen matrix synthesis. In conclusion, TGF-β1-containing collagen-PU constructs could induce the functional cell phenotype of human AF cells *in vitro* and *in situ*. This combined cellular, biomaterial and bioactive agent therapy has a great potential for AF tissue regeneration and rupture repair.

Key words:

Annulus fibrosus, Annular rupture repair, Tissue engineering, Transforming growth factor β1, Polyurethane scaffold, Collagen type I hydrogel

1. Introduction

Low back pain (LBP) has become one of most common chronic health problems. Approximately 80% of the population has been affected by LBP at least once in their life, representing a high economic and social burdens [1-3]. Intervertebral disc (IVD) degeneration and disc herniation are well-known as the leading causes of specific LBP [4]. In IVD herniation the nucleus pulposus (NP) protrudes out of the defective annulus fibrosus (AF) and irritates and compresses the spinal nerves, resulting in pain and dysfunction. Furthermore, the integrity of the IVD is destroyed, which leads to mechanical property loss (consequently, reduced disc height), inflammation and further disc degeneration [5, 6]. Microdiscectomy/sequestrectomy is the standard surgical treatment for patients with severe dysfunction or without satisfactory outcomes after conservative therapy. The acute symptoms are relieved by removing herniated tissue. However, AF defects remain unrepaired, which leads to a 10-30% of re-herniation rate resulting in recurrent pain and continuing disc degeneration [7-9]. Aggressive discectomy with removal of all NP material reduces the risk of re-herniation but will lead to a post-discectomy syndrome with rapid disc degeneration and pain in nearly one third of the patients [10].

Several attempts have been made at AF repair after discectomy, such as direct suture and conglutination with glue; however, outcomes have been unsatisfactory [11-14]. The self-healing capacity of the AF tissue is confined due to its avascular nature. Additionally, with the IVD as a load-bearing tissue, the repair of the AF should not only restore its mechanical properties but also reproduce its biological integrity [15]. Tissue engineering has been demonstrated to be a prospective approach for AF repair in the last few decades [16-20]. However, appropriate cell sources, growth factors and biomaterials for generation of functional and integrated AF tissue analogues are still an unmet need.

Mesenchymal stem cells (MSCs) have been proposed as a suitable cell source for IVD regenerative therapies [21]. In an ovine lumbar disc degeneration model, injection of bone marrow derived MSCs into previously incised AF resulted in a significant improvement in histological, biochemical and MRI analyses [22]. Nevertheless, the fate of the implanted cells and their potential to differentiate into AF-like cells remain uncertain. In our previous study, MSCs were transplanted into AF defects of bovine caudal IVDs and cultured in an organ culture model under dynamic load for 14 days, to investigate the phenotype of MSCs after transplantation and their paracrine effect on native disc cells [19]. MSCs showed the ability to positively affect the phenotype of the host disc cells, as indicated by the up-regulation of anabolic genes and down-regulation of catabolic genes. However, no effect was detected on new matrix formation at the AF defect site. This finding demonstrated that non-primed MSCs have limited capacity to differentiate into AF cells *in situ*. An effective cell population with repair ability is required to reconstruct an AF tissue with normal functions. AF cells possess the innate capacity to rebuild the biological properties of tissue engineered AF analogues [23, 24]. However, phenotypic markers of functional AF cells as a guideline for seed cell selection are still missing, except for collagen type I, which is the prominent extracellular matrix (ECM) component in the AF. Recently, Nakai et al. (2016) have demonstrated that $CD146^+$ murine AF cells deposit more collagen type I-rich ECM as compared with $CD146^-$ cells, indicating that CD146 may be a marker of functional AF cells. The present

study unravelled further molecular markers of healthy AF cells as compared with NP cells. Then, these markers were used as indicators of functional AF cell induction.

Several studies have shown that TGF-β1 enhanced ECM production and cell proliferation of human AF cells in both 2D and 3D cultures *in vitro* cultures [25, 26]. TGF-β1 increases myofibroblast contractility in wound healing, which plays a pivotal role in physiological tissue remodeling [27]. TGF-β1 can also prevent degenerative processes and inhibit inflammatory responses in the dorsal root ganglion and prevent pain development in a rat IVD degeneration model [28].Therefore, the effect of TGF-β1 on the expression of the functional markers in human AF cells was investigated. In addition to 2D and 3D *in vitro* culture systems, TGF-β1 treated AF cells were also tested in a preclinical IVD organ culture model to reveal their repair effect *in situ*.

In addition to cell source and growth factor, a biomaterial with appropriate biological and biomechanical compatibility is crucial for successful regeneration of AF tissue *in situ*. Polyurethane (PU) scaffold have been reported to have excellent biocompatibility, mechanical property and stability for AF tissue engineering [16, 29]. Whatley et al. (2011) developed a PU scaffold to mimic the native shape and structure of the IVD that exhibited elastic behavior during compressive and shear testing and supported cell growth [30]. Lee et al. (2005) and Li et al. (2009) have performed research on PU scaffolds with an interconnected pore structure for cartilage tissue engineering. Results showed that the PU scaffolds have sufficient elasticity, resiliency and stiffness to endure *in vitro* mechanical loading [31, 32]. Hydrogels such as collagen, agarose, fibrin, and alginate are widely used to encapsulate and deliver cells into scaffolds, preventing cell loss from scaffold and enhancing the retention of matrix molecules [33]. Collagen type I, the main component of AF ECM, has been coated on to plastic, promoting AF cell proliferation and matrix production *in vitro* [34]. A crosslinked collagen I hydrogel was injected to repair AF rupture in a punctured rat-tail model. Results showed that collagen gel can preserve the integrity of the AF and NP after needle puncture, while delaying the degeneration of the IVD [35]. Bowles et al. (2010) found that a collagen I hydrogel seeded with ovine AF cells display a capacity for self-assembly of aligned tissue-engineered AF through collagen gel contraction [36]. Those studies indicated a good potential of collagen I hydrogel for AF cells proliferation and AF matrix synthesis. However, the specific phenotypes of the AF cells within these various biomaterials have not yet been reported.

The current study aimed to define the functional markers of healthy AF cells and assess the *in vitro* and *ex vivo* effect of a bioactive agent-biomaterial approach for functional AF cells priming and AF rupture repair. First, the markers of functional AF cells were defined; then, potential cell sources (AF cells) with growth factor (TGF-β1) for functional phenotype induction were assessed; finally, those were combined with biomaterials. PU scaffolds with/ without collagen I hydrogel were assessed for their capacity to support and maintain the functional phenotype of AF cells in an *in vitro* 3D culture model and an *ex vivo* preclinical organ culture model. Cell proliferation, matrix production and gene expression were evaluated *in vitro*. *Ex vivo* tests were performed on bovine caudal IVDs with an organ culture system including a mechanical loading bioreactor. The morphology of regenerated tissue and the phenotype of implanted and native disc cells were analyzed to assess the repair effect of constructs in an AF defect *in situ*.

2. Materials and methods

2.1. Fabrication of PU scaffold and PU membrane

Polyurethane (PU) was synthesized using a one-step solution polycondensation as described previously [37]. Briefly, the monomers and macromers used for the synthesis were 1,6-hexamethylene diisocyanate (HMDI) (Sigma-Aldrich), a hydroxyl-terminated poly(ε-caprolactone) (PCL) (Sigma-Aldrich) with an average molecular weight of 530 g/mol and a functionality of 2 and 1,4,3,6-Dianhydro-D-sorbitol (ISO) (Sigma-Aldrich). The reactants underwent a one-step polycondensation in solution in the presence of a catalyst. The HMDI: PCL:ISO molar ratio used was kept at 1:0.32:0.64. The PU obtained had intrinsic viscosity, weight average molecular weight and a polydispersity of 1.3 dL/g, 500,000 g/mol and 2.00, respectively.

Membranes were produced by casting the *N,N*-dimethylformamide solution of the synthesized PU into a flat-bottom glass Petri-dish and allowing the solvent to evaporate under a chemical hood. The measured ultimate strength of the PU membrane was 53.0 ± 2.0 MPa, the yield strength 4.9 ± 1.4 MPa and the elongation at break 593.8 ± 57.7 %. The surface of the PU membrane did not present large porosity and was mostly smooth on the top and bottom [19].

Porous PU sponges with interconnected pore size diameter of 150-300 µm were produced using a salt leaching-phase inverse fabrication extensively reported elsewhere [31, 38]. Water jet cutting was used to produce cylindrical scaffolds of 3 mm diameter, 4 mm thickness and scaffolds were sterilized by cold ethylene oxide and degassed for 5 days before use. The unconfined compressive stiffness of the prepared scaffolds was approximately 20 kPa [39].

2.2. Isolation and expansion of human AF cells

Human IVD tissue was harvested with ethical approval (Cantonal Ethics Commission Bern 2016) and the written patient consent from traumatic injured IVDs (30-55 years old, 6 male donors), which were classified as mildly degenerated (Pfirrmann grade 2-3). To ensure purity of AF samples, AF tissue was collected after removing all the adjacent NP tissue and cartilage endplate. The collected AF tissue was incubated with red blood cell lysis buffer (155 mM NH_4Cl, 10 M $KHCO_3$ and 0.1 mM EDTA in Milli-Q water) for 5 min on a shaker at room temperature, and then washed with phosphate buffered saline (PBS). Then, the chopped tissue was enzymatically digested for 1 hour with 0.2% w/v Pronase (Roche) in alpha Minimum Essential Medium (αMEM, Gibco, followed by 12-14 hours at 37 °C in 130 U/mL collagenase type II (Worthington) in αMEM / 10% fetal bovine serum (FBS, PAN Biotech, Germany). Single-cell suspension was obtained by filtering through a 100 µm cell strainer. Next, cells were seeded at a concentration of 10,000 cells/cm^2 and expanded with αMEM supplemented with 10% FCS, 100 U/mL penicillin and 100 mg/mL streptomycin (1% P/S, Gibco). Incubation conditions were set to 5% CO_2 at 37 °C at a hypoxic condition of 2% O_2. Culture medium was changed twice a week and cells were detached at ~ 80% confluence using a dissociation buffer composed of 0.05% Trypsin/EDTA (Gibco) and 0.01% Collagenase P (Roche) for 5 min at 37 °C. Cells were sub-cultured at a cell density of 3,000 cells/cm^2 for expansion in the same medium as above. Passage 2 AF cells were used in the present study.

2.3. AF cells, 2D and 3D culture in vitro

2D culture in vitro: Passage 2 human AF cells were treated with either basal medium: αMEM, 5% FBS, 1% ITS+ (BD Biosciences), 1% P/S; or TGFβ medium: the basal medium with 5 ng/mL recombinant human TGF-β1 (Fitzgerald, Acton, MA, USA) for 4 days. Then, cells were then dissociated for gene expression analysis, contractility study or flow cytometry analysis. AF cells pre-treated with TGFβ medium for 4 days were used for the *in vitro* 3D culture experiments and *ex vivo* organ culture experiments.

3D culture in vitro: PU scaffolds were pre-wetted for 1 hour in αMEM with 10% FBS under vacuum conditions. Medium was completely aspirated from the scaffolds, which were placed into 0.5 mL protein-low-binding Eppendorf tubes. Tubes were pre-coated for 1 hour at 37 °C with 1% BSA (Gibco). TGF-β1-treated AF cells were harvested and resuspended with medium or Corning® Collagen I, rat tail solution at a cell density of 2×10^5 cells per 30 µL. The final concentration of the collagen I hydrogel was 1.81 mg/mL. For the TGF-β1 containing group, 5 ng TGF-β1 was added within the AF-cells-collagen I solution suspension. Cell suspension in medium or collagen I solution was dropped onto the scaffold (30 µL per scaffold). Scaffolds were compressed mildly with forceps to allow cell suspension infiltration into the scaffold, then incubated for 1 hour at 37 °C to allow cell adhesion and collagen-hydrogel gelation. Next, constructs were transferred into a 24-well plate and cultured at 37 °C, 5% CO_2, 2% O_2 in high-glucose DMEM supplemented with 1% P/S, 2% FBS, 50 mg/mL L-ascorbic acid 2-phosphate (Sigma-Aldrich), 1% ITS+ and 1% NEAA (Gibco). The medium volume was 1 mL per scaffold and it was replaced twice a week. After 7 days of culture, scaffolds were collected for gene expression analysis, DNA and GAG quantification and toluidine blue staining. For the *ex vivo* organ culture study, constructs were immediately implanted into the AF defect after gelation of the collagen type I hydrogel.

2.4. Bovine caudal intervertebral disc dissection

Caudal IVDs were harvested from 6-12-month-old calves obtained from local abattoir after fresh sacrifice. Disc dissection was performed as described previously [40]. IVDs with cartilage EPs were isolated using a band saw, then scraped using scalpel to remove the vertebral bone and growth plate and ensure two parallel planes of disc. EP surfaces were cleaned with Ringer's balanced salt solution using a Pulsavac Wound Debridement Irrigation System (Zimmer, Minneapolis, USA) to remove cutting debris and blood clots. IVDs were prewashed in PBS with 10% P/S (Gibco) at room temperature for 20 min, then cultured at 37 °C, 5% CO_2 in 6-well plates with 7.5 mL IVD culture medium: high glucose DMEM supplemented with 1% P/S and 50 mg/mL Primocin (Invitrogen), 2% FBS, 50 mg/mL ascorbate-2phosphate, 1% ITS+, 1% NEAA. Culture media were replaced every day.

Different parts of healthy IVD tissue, including NP tissue (gel-like inner core of 6-8 mm in diameter), outer AF tissue (oAF, distinguishable lamellar AF tissue, ring at thickness of ~4 mm) and inner AF tissue (iAF, located between NP and oAF) from 6 bovine tails (age 6-12 months) were collected for gene expression analysis on day 0, to measure the expression level of potential AF markers (Table 1).

2.5. Annulotomy model for preclinical testing of AF repair therapy in whole organ IVD culture

Twenty-four caudal IVDs were dissected from 4 bovine tails (age 6-12 months). Day 0 control group comprised 4 IVDs. The AF defect repair groups comprised 6 IVDs per group and were consisted of 1) an acellular PU scaffold-collagen hydrogel (PU-Col), 2) PU-Col with TGF-β1 pre-treated AF cells (PU-Col-AFCs) and 3) PU-Col with TGF-β1 pre-treated AF cells and 5 ng TGF-β1 (PU-Col-AFCs-TGFβ). Within the 6 replicates in each group, 4 IVDs were used for gene expression analysis of human AF cells in scaffold and native IVD tissue, 2 IVDs were used for safranin-O/fast green staining. Two IVDs served as non-repair negative control on day 15 and were used for safranin-O/fast green staining.

The IVD AF defect was created with a biopsy punch (diameter 3 mm, length 7 mm). Full thickness of AF tissue and some NP tissue were removed. Then, the defect was refilled with different groups of scaffolds as described above. A PU membrane (12 mm x 7 mm) was affixed to the IVD with 2 µL of EPIGLU® (Meyer-Haake GmbH, Ober-Mörlen, Germany) surrounding the defect area, to maintain the scaffold within the defect. IVDs were cultured in IVD culture media, and loaded with physiological compressive loading for 1 hour at 0.02 - 0.2 MPa, 0.2 Hz daily within a bioreactor [40]. The disc height was measured using a caliper at 2 positions to calculate percentage change normalised to day 0 after dissection. After 14 days of culture, the IVDs were collected for evaluations.

2.6. Flow cytometry analysis

TGF-β1-treated and -non-treated AF cells were harvested by trypsinization. Single-cell suspension was prepared at a cell density of 1×10^5 cells per 100 µL staining buffer (PBS with 0.2% BSA and 1 mM EDTA). Cell suspensions were incubated at 4 °C in the dark for 30 min with 10 µL fluorescence-conjugated mouse monoclonal anti-human CD146 antibody (CD146-APC, human, Miltenyi Biotec) or 10 µL mouse IgG1-APC (isotype control, Miltenyi Biotech). After incubation and washing, DAPI at a final concentration of 0.1 µg/mL was added for live/dead staining. Flow cytometric analysis was performed on a FACS AriaIII (BD Biosciences) and at least 30,000 events per sample were recorded. Data analysis was performed using BD FACSDiva software. A gating strategy was used to exclude dead cells and cell doublets.

2.7. Gene expression analysis

RNA isolation from 2D-cultured AF cell samples was performed using TRI reagent (Molecular Research Centre Inc., Cincinnati, OH, USA) according to the manufacturer's protocol. AF cells in PU scaffold-collagen type I hydrogel constructs were placed into 1 mL TRI reagent with 5 µL polyacryl carrier (Molecular Research Centre Inc. USA), and homogenized by a tissue-lyser (Retsch GmbH & Co., Haan, Germany). After centrifugation at 12000 × *g* for 15 min, the supernatant was collected in a fresh EP tube and the RNA isolation was performed according to the manufacturer's protocol. Native IVD tissues, including NP tissue and AF tissue in intact disc, as well as AF tissue adjacent and opposite to the repair constructs, were collected on day 0 and day 14. Tissues of 150-200 mg/sample were cut into small pieces and snap-frozen by liquid

nitrogen and hammering [41]. Then, tissue was transferred into 3 mL TRI reagent with 15 µL polyacryl carrier. Samples were homogenized using a tissue-lyser. After centrifugation, the supernatant was extracted with phase separation by adding 100 µL bromochloropropane per 1 mL of TRI reagent. The aqueous phase after centrifugation was transferred to a fresh tube and mixed with the same volume of 70 % ethanol. Then, RNA isolation was then performed using the QIAGEN RNeasy MINI kit according to the manufacturer's protocol. Reverse transcription was performed using SuperScript® VILO™ cDNA Synthesis Kit (Invitrogen).

The quantitative real-time polymerase chain reaction (qRT-PCR) was conducted on QuantStudio6 System (Applied Biosystems). Sequences of the primers and probes used in qRT-PCR of bovine and human cells/tissue are listed in Table 1. *RPLP0* ribosomal RNA was used as endogenous control. Data were analyzed using $2^{-\Delta\Delta CT}$ method.

Table 1. Oligonucleotide primers and probes (bovine and human) used for qRT-PCR.

Gene	Primer/probe type	Sequence
bCOL1A2	Primer fw (5′–3′)	TGC AGT AAC TTC GTG CCT AGC A
	Primer rev (5′–3′)	CGC GTG GTC CTC TAT CTC CA
	Probe (5′FAM/3′TAMRA)	CAT GCC AAT CCT TAC AAG AGG CAA CTG C
bCOL2A1	Primer fw (5′–3′)	AAG AAA CAC ATC TGG TTT GGA GAA A
	Primer rev (5′–3′)	TGG GAG CCA GGT TGT CAT C
	Probe (5′FAM/3′TAMRA)	CAA CGG TGG CTT CCA CTT CAG CTA TGG
bACAN	Primer fw (5′–3′)	CCA ACG AAA CCT ATG ACG TGT ACT
	Primer rev (5′–3′)	GCA CTC GTT GGC TGC CTC
	Probe (5′FAM/3′TAMRA)	ATG TTG CAT AGA AGA CCT CGC CCT CCA T
bMMP3	Primer fw (5′–3′)	GGC TGC AAG GGA CAA GGA A
	Primer rev (5′–3′)	CAA ACT GTT TCG TAT CCT TTG CAA
	Probe (5′FAM/3′TAMRA)	CAC CAT GGA GCT TGT TCA GCA ATA TCT AGA AAA C
bADAMTS5	Primer fw (5′–3′)	GAT GGT CAC GGT AAC TGT TTG CT
	Primer rev (5′–3′)	GCC GGG ACA CAC CGA GTA C
	Probe (5′FAM/3′TAMRA)	AGG CCA GAC CTA CGA TGC CAG CC
bCD146		Bt03258894_m1
bSM22α		Bt03234600_m1
bSCX		Hs03054634_g1
bMKX		Bt04292311_m1
bELN		Bt03216594_m1
bVCAN		Bt03217632_m1
bRPLP0		Bt03218086_m1
hCOL1A1	Primer fw (5′–3′)	CCC TGG AAA GAA TGG AGA TGA T
	Primer rev (5′–3′)	ACT GAA ACC TCT GTG TCC CTT CA
	Probe (5′FAM/3′TAMRA)	CGG GCA ATC CTC GAG CAC CCT
hCOL2A1	Primer fw (5′–3′)	GGC AAT AGC AGG TTC ACG TAC A
	Primer rev (5′–3′)	GAT AAC AGT CTT GCC CCA CTT ACC
	Probe (5′FAM/3′TAMRA)	CCT GAA GGA TGG CTG CAC GAA ACA TAC
hACAN	Primer fw (5′–3′)	AGT CCT CAA GCC TCC TGT ACT CA
	Primer rev (5′–3′)	CGG GAA GTG GCG GTA ACA
	Probe (5′FAM/3′TAMRA)	CCG GAA TGG AAA CGT GAA TCA GAA TCA ACT

hMMP3		Hs00968305_m1
hADAMTS5		Hs01095518_m1
hCD146		Hs00174838_m1
hSM22α		Hs00162558_m1
hSCX		Hs03054634_g1
hMKX		Hs00543190_m1
hELN		Hs00355783_m1
hVCAN		Hs00171642_m1
hRPLP0	Primer fw (5′–3′)	TGG GCA AGA ACA CCA TGA TG
	Primer rev (5′–3′)	CGG ATA TGA GGC AGC AGT TTC
	Probe (5′FAM/3′TAMRA)	AGG GCA CCT GGA AAA CAA CCC AGC

Note: Primers and probes with the sequence shown were custom-designed; primers and probes with the catalog number were from Applied Biosystems. Abbreviations: COL1A2: collagen, type I, alpha 2; COL1A1: collagen, type I, alpha 1; COL2A1: collagen, type II, alpha 1; ACAN: Aggrecan; CD146: Cluster of Differentiation 146; SM22α: Smooth Muscle Protein 22-alpha; SCX: Scleraxis; MKX: Mohawk Homeobox; ELN: Elastin; VCAN: Versican; MMP3: Matrix Metalloproteinase-3; ADAMTS5: A Disintegrin and Metalloproteinase with Thrombospondin Motifs 5; RPLP0: Ribosomal Protein Lateral Stalk Subunit P0. fw: Forward; rev: Reverse; FAM: Carboxyfluorescein; TAMRA: Tetramethylrhodamine. Gene prefix 'b' bovine, prefix 'h' human.

2.8. Cell contraction functionality assay

Contractility of TGF-β1-treated and -non-treated cells was evaluated by a cell contraction assay in collagen I hydrogel. A 24-well plate was coated with 1 % BSA and incubated at 37 °C for at least 1 hour. Cells from 3 donors were encapsulated in 1.81 mg/mL type I collagen with 4 technical replicates at a seeding density of 1.5×10^5 cells/mL. Cells were cultured at 37 °C, 2 % O_2 in αMEM with 10% FBS. After 24 hours, gels were photographed (Canon PowerShot SX50 HS) and well and gel diameters were measured using NIS-Elements D 3.2 (NIKON Japan). Two gel diameters were averaged to calculate the gel area. The gel area after 24 hours was divided by the well area, calculated with the well diameter.

2.9. Toluidine blue staining

Cell distribution and ECM deposition within PU scaffold with or without hydrogel were evaluated by toluidine blue staining. Samples at day 1 and day 7 were snap-frozen in cryo-compound (Leica). Vertical sections of scaffold were made at a thickness of 12 µm. Slides were fixed in 70% methanol for 10 min, 100% methanol for 10 min, dried overnight, stained with 0.1% toluidine blue for 2 min and rinsed with deionized water (4-5 times).

2.10. Safranin-O / fast green staining

IVD samples after 14 days of culture were snap-frozen in cryo-compound after removal of the cartilage endplate from one side. IVD transverse cryo-sections were made at a thickness of 12 µm. Slices was fixed as above, stained with 0.1% safranin-O and 0.02% fast green to reveal proteoglycan and collagen deposition respectively, and counterstained with Weigert's haematoxylin to reveal cells distribution [40].

Cell density in the implanted constructs was calculated using the safranin-O / fast green stained images. High-magnification images (676 × 535.6 μm) were taken at 6 random positions of each slide, with 2 slides per IVD, and 2 IVDs per group. In total, cells from 24 images of each group were counted by Image J 1.52a (National Institutes of Health, USA).

2.11. GAG and DNA content measurement

Cell-scaffold constructs after 7 days of culture were digested overnight at 56 °C with 0.5 mg/mL proteinase K (Roche, Mannheim, Germany) solution. DNA content was measured using the PicoGreen kit (Invitrogen) according to the manufacturer's instruction. GAG content was determined by dimethylmethylene blue assay (1.9-DMMB; Sigma-Aldrich).

2.12. Statistical analysis

Statistical analyses were performed using GraphPad Prism 7 software (GraphPad Software, Inc., La Jolla, CA, USA). D'Agostino-Pearson omnibus normality test was used to define whether the data were normally distributed. For data that were normally distributed, unpaired t test was used to determine differences between two groups; One-way ANOVA was used to determine differences between three or more groups. For data that were not normally distributed, Mann–Whitney U test was used to determine differences between two groups; Kruskal Wallis test was used to determine differences between three or more groups. A difference with $p < 0.05$ was considered statistically significant.

3. Results

3.1. Phenotype markers of AF cells

Phenotype markers of AF cells were defined by comparison of the gene expression levels in Different parts of bovine IVD tissue. Compared with NP tissue and iAF, oAF expressed higher levels of *COL1A2* ($p < 0.05$), *CD146* ($p < 0.05$), *SM22α* ($p < 0.05$) and *MKX* ($p < 0.05$) (Figure 1), which were, therefore, defined as phenotype markers of healthy and functional AF cells. Furthermore, oAF tissue expressed lower levels of *COL2A1* ($p < 0.001$), *ACAN* ($p < 0.001$) and *SCX* ($p < 0.001$) as compared with NP tissue. Interestingly, the transient zone iAF tissue showed a comparable gene expression pattern to NP tissue, except for lower levels of *CD146* ($p < 0.001$).

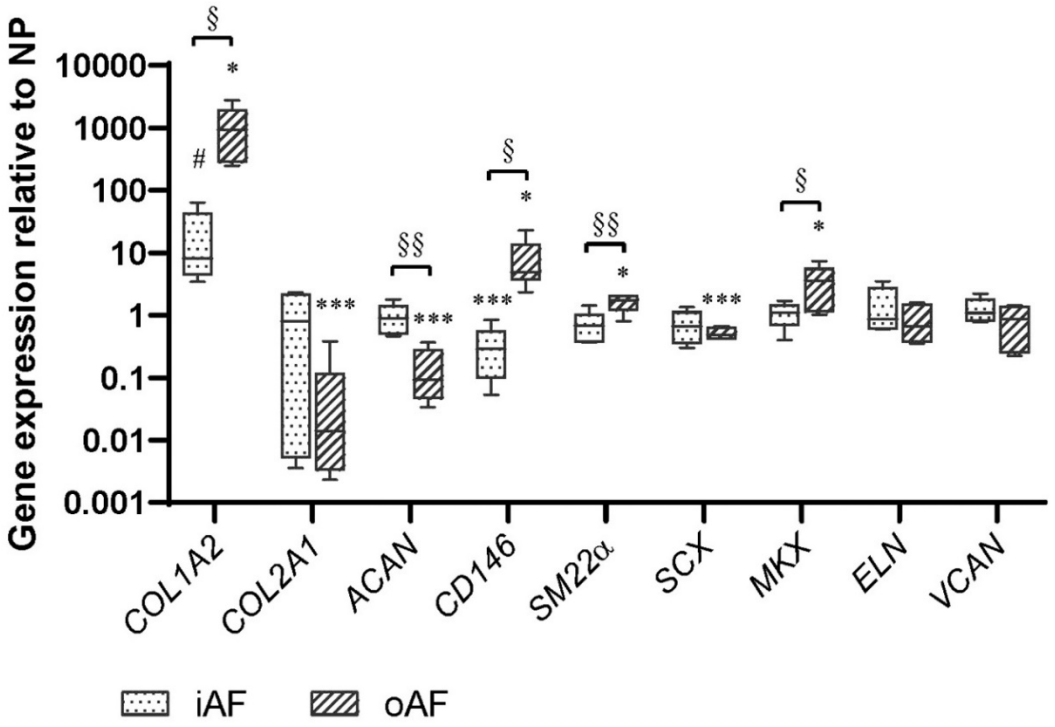

Figure 1. Relative mRNA expression in NP, iAF and oAF from healthy bovine IVDs.

*Data were normalized to the expression level of NP tissue. n = 6, # p < 0.1, * p < 0.05, *** p < 0.001 vs. gene expression level in NP, § p < 0.05, §§ p < 0.01 comparing iAF and oAF.*

3.2. Induction of the functional human AF cell phenotype for AF repair - *in vitro* 2D culture

To evaluate the functional phenotype of human AF cells induced by TGF-β1, gene expression levels of the AF markers were measured in human AF cells cultured with or without 5 ng/mL TGF-β1 for 4 days, since cells reached 70–80% confluency after 4 days of culture, which is the optimal time point for cell trypsinization and seeding on to the scaffold (Figure 2a). mRNA levels of *CD146* ($p < 0.05$), *SM22a* ($p < 0.01$), *SCX* ($p < 0.01$), *MKX* ($p < 0.01$) and *COL2A1* ($p < 0.01$) were significantly upregulated by TGF-β1 treatment. CD146 upregulation at the protein level was confirmed by flow cytometry (Figure 2b, c). The percentage of $CD146^+$ cells in 4 donors was 30.50 ± 14.55 % in basal medium, which increased to 72.25 ± 22.02 % in TGFβ medium. In contrast, ECM degrading enzymes, *MMP3* ($p < 0.001$) and *ADAMTS5* ($p < 0.001$), were downregulated by TGF-β1 treatment (Figure 2a). Cell contractility was determined in collagen I hydrogel by measuring the surface area of the collagen gel after 24 h of incubation, as a functionality test. TGFβ medium induced a larger reduction of the gel area (22.8 ± 8.1 %) as compared with basal medium (38.3 ± 5.9 %) (Figure 2d, e), which indicated a higher cell contractility after TGF-β1 treatment.

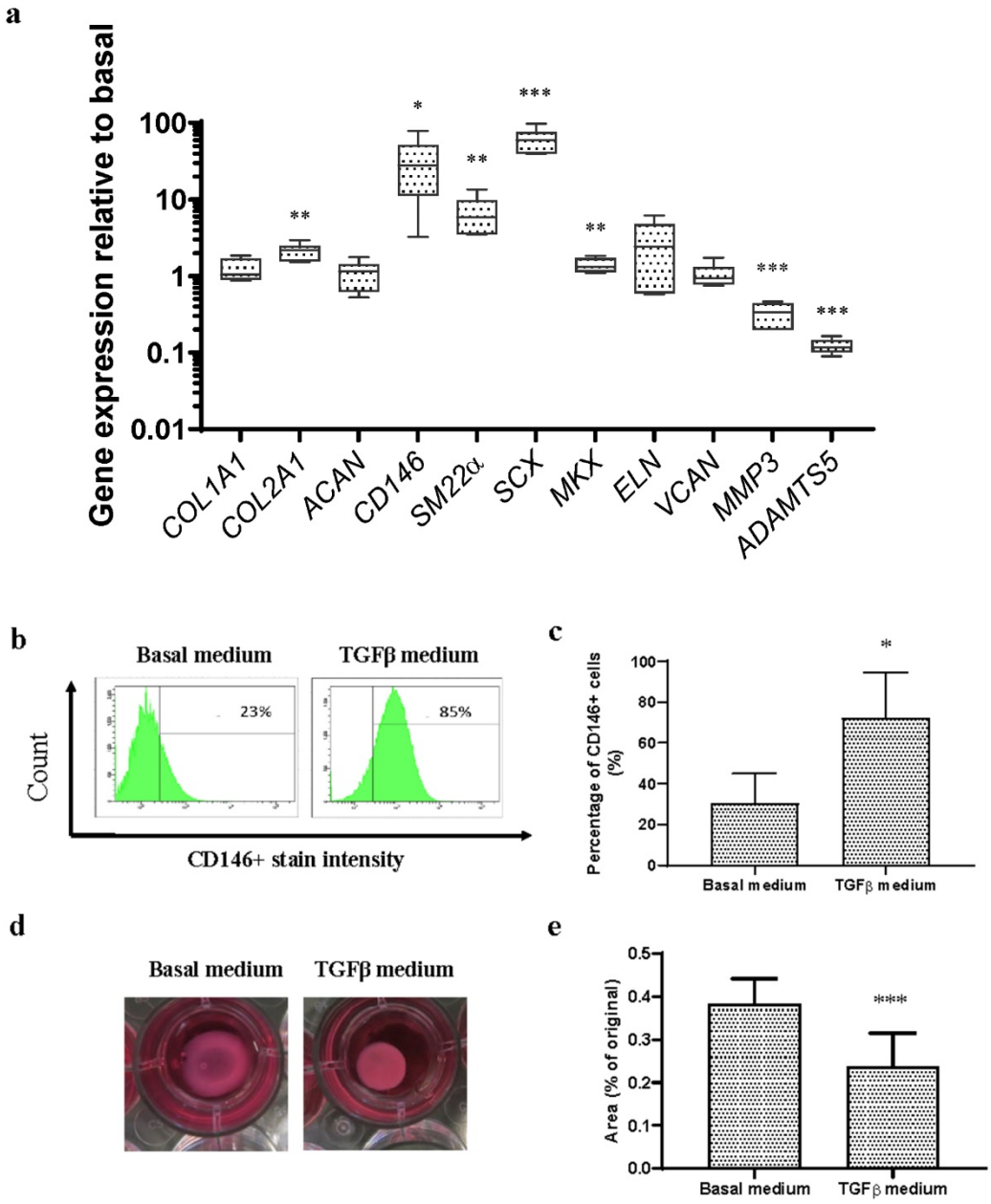

Figure 2. Phenotype of human AF cells after treatment with TGF-β1 for 4 days.

*(**a**) Relative mRNA expression, data were normalized to basal medium. (**b**) Representative and (**c**) average percentage of CD146$^+$ cells detected by flow cytometry. (**d**,**e**) Cell contractibility of AF cells cultured with basal or TGFβ medium. Mean + SD; n = 4, * $p < 0.05$, ** $p < 0.01$, *** $p < 0.001$ vs. cells treated with basal medium.*

3.3. Preservation of the functional human AF cells phenotype for AF repair – *in vitro* 3D culture

To assess cell phenotype and tissue construction capabilities of induced functional human AF cells in an *in vitro* 3D model, human AF cells pre-treated with TGF-β1 for 4 days were seeded on to PU scaffold only (PU-AFCs) or PU scaffold-collagen I hydrogel constructs with (PU-Col-AFCs-TGFβ) or without (PU-Col-AFCs) 5 ng TGF-β1 supplement. Gene expression was measured at day 7, cell proliferation and matrix production both at day 1 and 7 after cell seeding, to investigate the effect of the cell carrier on functional AF cell phenotype maintenance and AF tissue regeneration.

AF cells were evenly distributed in the PU scaffold both with or without collagen I hydrogel at day 1 after seeding (Figure 3a–c). After 7 days of culture, higher cell density and more intense ECM staining were observed in PU-Col-AFCs-TGFβ (Figure 3f) as compared to the other two groups (Figure 3d, e), especially around the outer surface of the PU scaffold. Furthermore, DNA and GAG content and GAG/DNA ratio were significantly higher in the PU-Col-AFCs-TGFβ scaffold when compared with PU-Col-AFCs (Figure 3g–i). When comparing day 7 with day 1, DNA and GAG content and GAG/DNA ratio increased only in the PU-Col-AFCs-TGFβ group.

Gene expression levels were evaluated in PU-AFCs, PU-Col-AFCs and PU-Col-AFCs-TGFβ after 7 days of culture and data were normalized to PU-AFCs. AF cells in PU-Col-AFCs and PU-Col-AFCs-TGFβ expressed higher levels of *COL2A1*, *CD146*, *SM22a*, *SCX* and *MKX* and lower levels of *MMP3* and *ADAMTS5* when compared with PU-AFCs (Figure 4). TGF-β1 supplementation into the PU scaffold-collagen I hydrogel did not further affect the gene expression profile of AF cells as compared with the PU-Col-AFCs group.

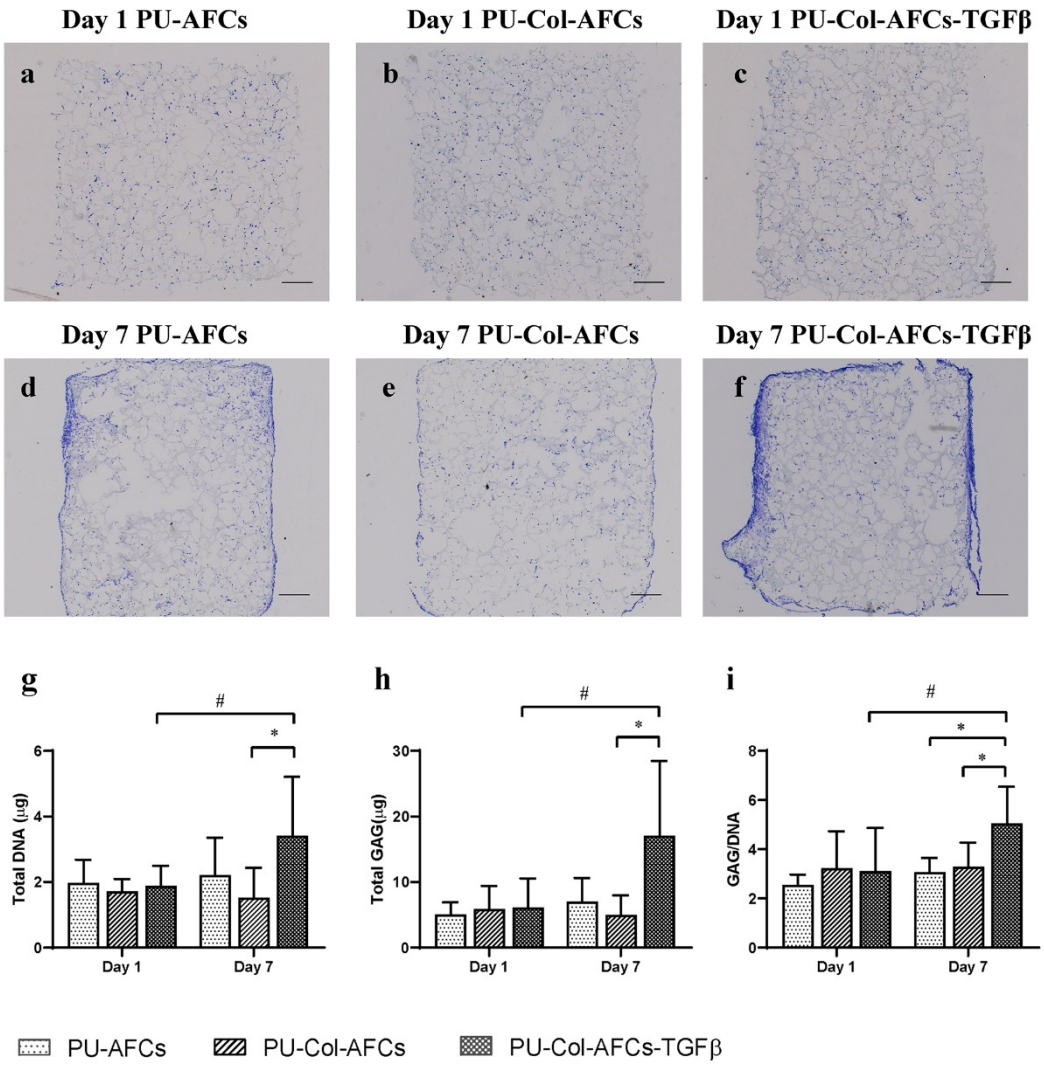

Figure 3. 3D culture of human AF cells in vitro.

*(**a-f**) Representative toluidine-blue-stained sections of scaffolds. TGF-β1-pre-treated human AF cells seeded on to (**a**,**d**) scaffolds PU-AFCs, (**b**,**e**) PU-Col-AFCs and (**c**,**f**) PU-Col-AFCs-TGFβ after 1 and 7 days. Scale bar: 500 µm. (**g**) DNA content, (**h**) GAG content and (**i**) GAG/DNA ratio in scaffolds after 1 and 7 days of culture. Mean + SD, n = 6, # $p < 0.1$, * $p < 0.05$.*

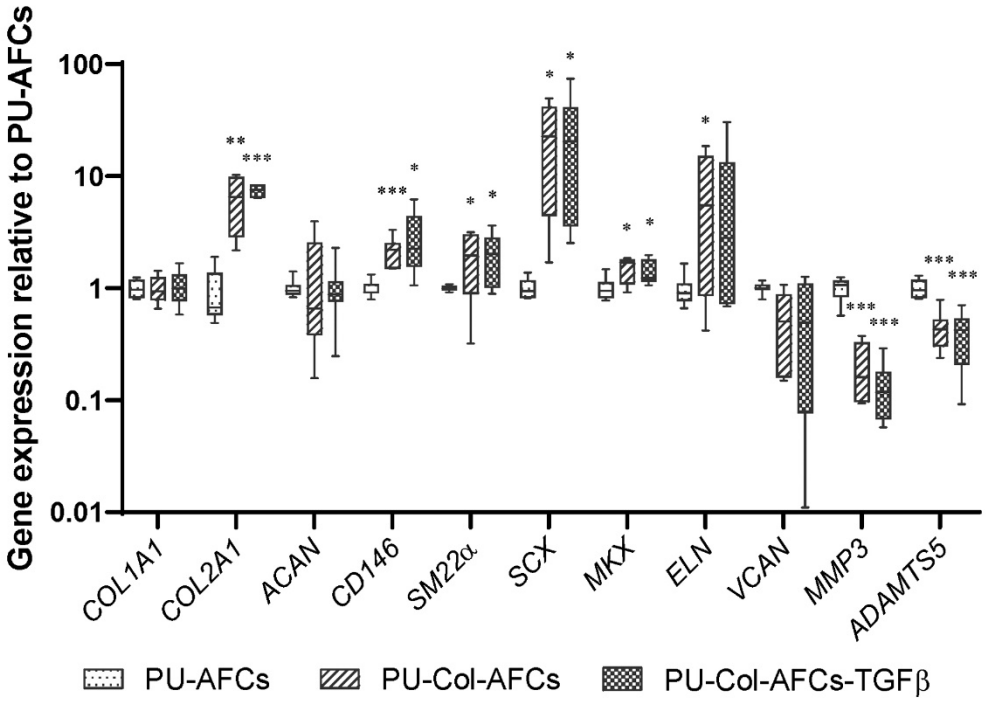

Figure 4. Gene expression of human AF cells 3D-cultured in vitro.

*Relative mRNA expression of TGF-β1-pre-treated human AF cells seeded on to PU scaffold only (PU-AFCs), PU scaffold-collagen I hydrogel construct (PU-Col-AFCs) and PU-Col scaffold supplemented with 5 ng TGF-β1 (PU-Col-AFCs-TGFβ) after 7 days of culture. Data were normalized to expression level of PU-AFCs. n = 6, * p < 0.05, ** p < 0.01, *** p < 0.001 vs. gene expression levels of PU-AFCs.*

3.4. AF rupture repair – preclinical testing in *ex vivo* IVD organ culture system

To test the property of the constructs in a preclinical organ culture model, anatomized IVDs were repaired with PU scaffold-collagen hydrogel (PU-Col), or PU-Col with AF cells with (PU-Col-AFCs-TGFβ) or without (PU-Col-AFCs) supplement of 5 ng TGF-β1. Then, IVDs were then cultured under physiological loading condition for 2 weeks, mimicking the *in situ* microenvironment for testing of AF rupture repair. The disc height change was measured during the whole culture period (Figure 5). At day 2, disc height slightly increased for all groups after overnight free swelling (FS) compared with day 0. Dynamic loading for 1 hour caused a physiological disc height loss in all the groups repaired with implants: PU-Col 8.6% ± 2.9%, PU-Col-AFCs 8.6% ± 1.0%, PU-Col-AFCs-TGFβ 6.8% ± 1.4%. After 14 days of repetitive dynamic loading, the IVDs showed about 2% of further disc height loss: PU-Col 10.8% ± 1.9%, PU-Col-AFCs 10.2 % ± 1.5 %, PU-Col-AFCs-TGFβ 8.4% ± 2.2%. However, all the IVDs recovered after free swelling. After 15 days culture with daily dynamic loading, no significant disc height loss was observed. Cell implantation and TGF-β1 supplementation did not show any effect on disc height change under dynamic loading.

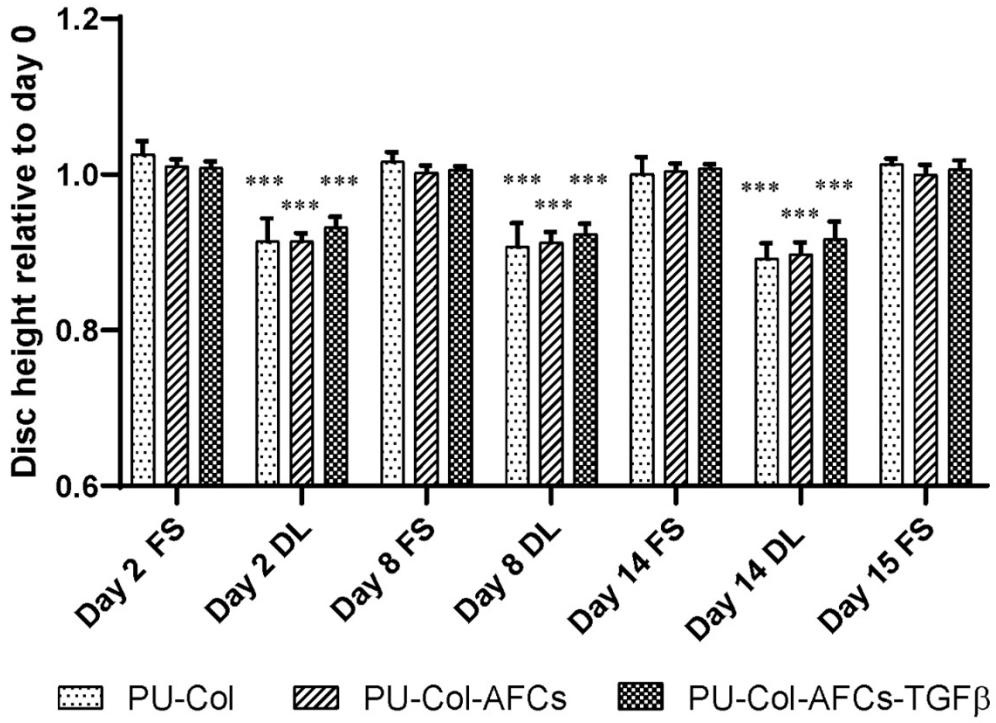

Figure 5. Disc height change during 15 days organ culture.

*Disc height change relative to initial dimension after dissection (day 0) at Different time points: after free swelling culture overnight and after dynamic loading over 15 days of organ culture. PU-Col: annulotomized IVDs implanted with PU-Col scaffold; PU-Col-AFCs: PU-Col scaffold seeded with AF cells; PU-Col-AFCs-TGFβ: PU-Col-AFCs supplemented with TGF-β1. Mean + SD, n = 6. *** $p < 0.001$ vs. disc height on day 0.*

Safranin O / fast green staining of transverse IVD sections after 15 days of culture is shown in Figure 6. Part of the NP tissue protruded into the AF defect region in the injury control group without repair (Figure 6a). In all the IVDs repaired with PU scaffold-collagen hydrogel (PU-Col cells free, PU-Col-AFCs, and PU-Col-AFCs-TGFβ), the NP tissue was maintained in its native position (Figure 6b, c, d). When the AF defect was repaired with PU-Col scaffold without AF cells (Figure 6b, e), after 15 days of culture, no fast-green staining could be detected at the defect site. When the defect was repaired with PU-Col scaffold with AF cells (Figure 6c, f), AF cells were found in the scaffold after 15 days of culture. Collagen staining with fast green was also detected at the defect site. Furthermore, when TGF-β1 was supplemented in the collagen hydrogel (Figure 6d, g), a higher cell density and stronger collagen staining intensity was observed at the defect site. The average cell number in high magnification visual fields was significantly higher in PU-Col-AFCs-TGFβ as compared with PU-Col-AFCs ($p<0.001$) (Figure 6h).

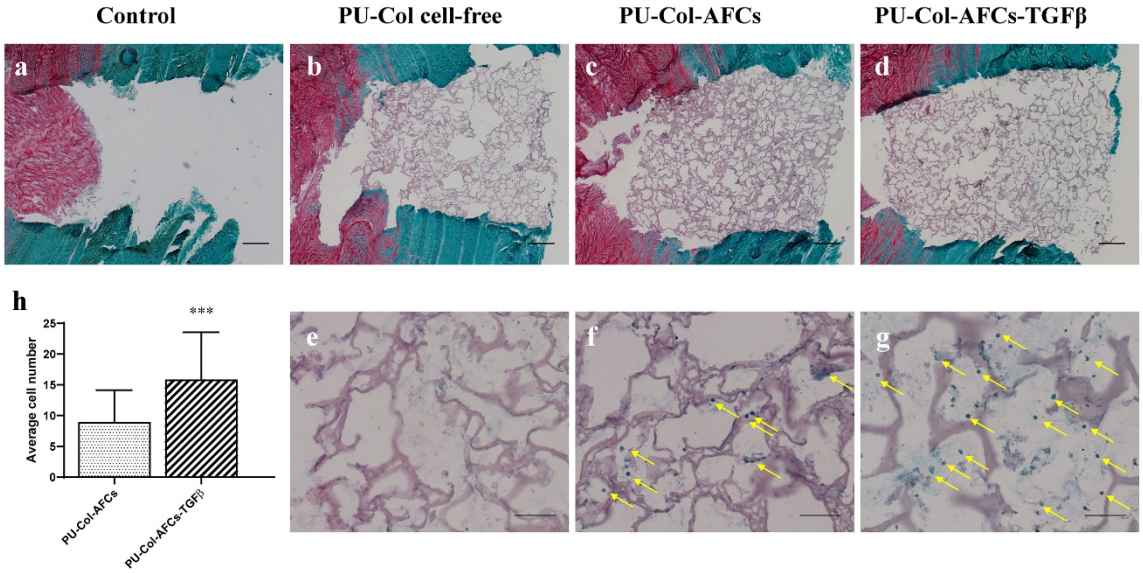

Figure 6. Representative safranin O/fast green-stained sections of IVDs after 15 days organ culture.

*(**a**) Annulotomized discs and annulotomized discs repaired with (**b**,**e**) PU-Col cell-free, (**c**,**f**) PU-Col scaffold seeded with TGF-β1-pre-treated AF cells (PU-Col-AFCs) and (**d**,**g**) PU-Col-AFCs supplemented with TGF-β1 (PU-Col-AFCs TGFβ), cultured for 15 days under dynamic load. (**h**) Cell numbers counted from the high magnification images in safranin O/ fast green-stained sections. Mean + SD, n = 24, *** p < 0.001 vs. PU-Col-AFCs. Scale bar: (**a-d**) 500 µm, (**e-g**) 100 µm. Yellow arrows indicate cells.*

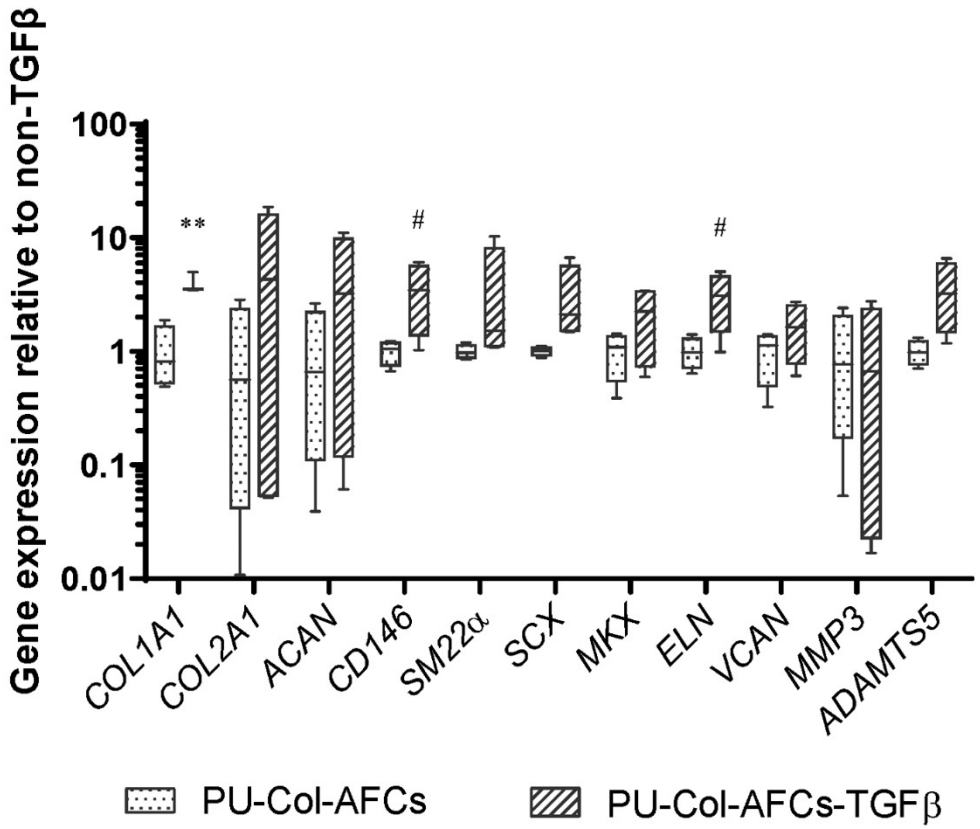

Figure 7. Relative mRNA expression of human AF cells which were encapsulated in implants after 15 days organ culture.

*AF cells were encapsulated in PU-Col scaffold (PU-Col-AFCs) or PU-Col scaffold supplemented with TGF-β1 (PU-Col-AFCs-TGFβ) and implanted into AF defect, cultured for 15 days in situ with dynamic loading. Data were normalized to expression level of PU-Col-AFCs. n = 4, # $p < 0.1$, ** $p < 0.01$ vs. gene expression levels of PU-Col-AFCs.*

Gene expression levels of implanted AF cells after 15 days of organ culture was analyzed (Figure 7). Results showed that *COL1A1* ($p < 0.01$) expression was significantly higher in PU-Col-AFCs-TGFβ as compared with PU-Col-AFCs, which correlated with the fast green staining results. There was also a trend for increased *CD146* ($p < 0.1$) and *ELN* ($p < 0.1$) expression by TGF-β1 supplementation in the collagen gel. Gene expression levels in the native IVD tissues, including AF close to PU scaffold, NP tissue and AF opposite PU scaffold, were also measured after 15 days of organ culture. No significant difference was found among the 3 repaired groups (Figure 8).

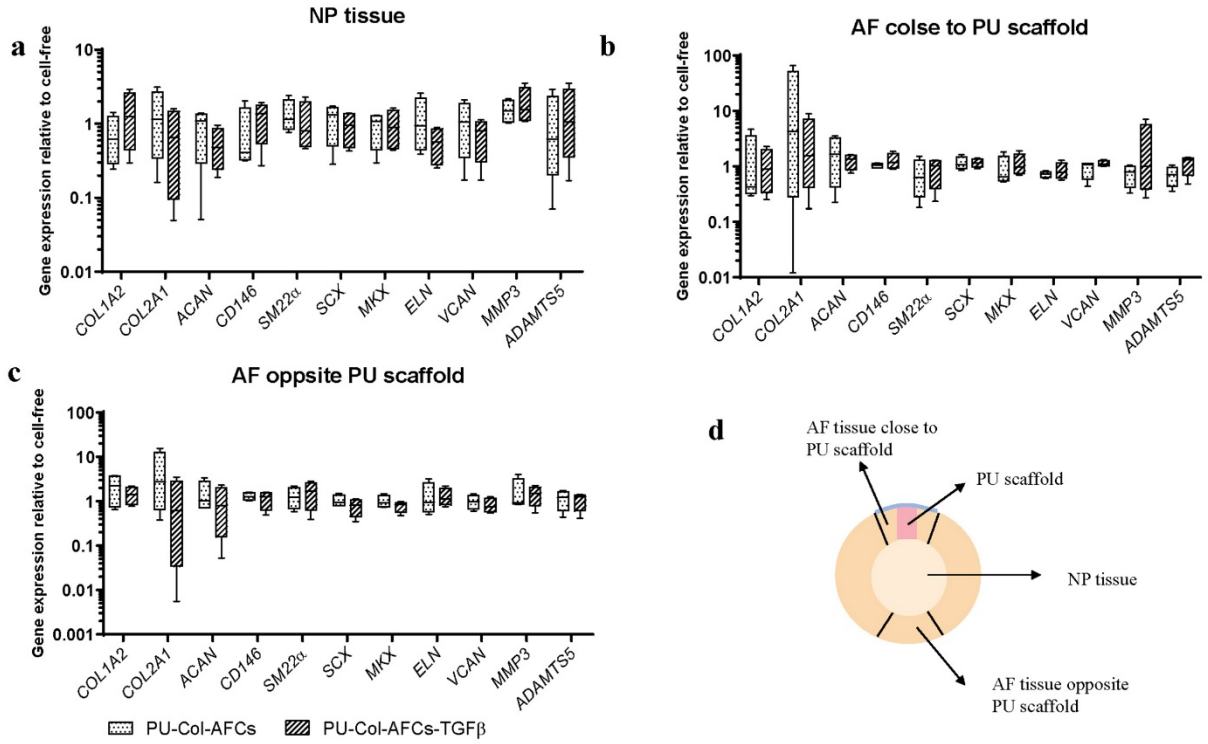

Figure 8. Relative mRNA expression of host disc tissue after 15 days of organ culture.

*Relative mRNA expression in (**a**) NP, (**b**) adjacent AF and (**c**) distal AF tissue of discs repaired with PU-Col cell-free (PU-Col), PU-Col scaffold seeded with TGF-β1-pre-treated AF cells (PU-Col-AFCs) and PU-Col-AFCs supplemented with TGF-β1 (PU-Col-AFCs-TGFβ) after 15 days of organ culture with dynamic loading. Data were normalized to the expression level of PU-Col. n = 4. (**d**) Transverse schematic view of discs implanted with scaffolds and disc tissue collected for gene expression analysis.*

4. Discussion

There is an unmet clinical need for AF rupture repair, especially for large AF defects. Tissue engineering AF for large AF rupture is considered to be a promising approach to prevent disc re-herniation and associated discogenic pain and to reconstitute the disc biological and mechanical function [15, 42, 43].

A clear understanding of markers related to the healthy and functional AF cell phenotype is fundamental to define proper cell sources for AF tissue regeneration. However, there is surprisingly limited research on AF cell phenotype so far [44, 45]. In the current study, the expression profile of several potential phenotypic markers of functional AF cells was measured in healthy oAF tissue as compared with iAF and NP tissue. It was clearly observed that *COL1A2*, *CD146*, *SM22α* and *MKX* were most highly expressed in the oAF (Figure 1). Thus, they were defined as markers of functional AF cells [46-49]. Each of these markers had previously been shown to be related to AF tissue function. Collagen type I expression at both gene and protein level is a well-known marker of AF cells in all species related with the tissue ECM property, since

the proportion of collagen type I increases from the NP towards the outer AF [46]. MKX expression at both gene and protein level has recently been identified as a transcription factor for AF cell differentiation, where MKX knock-out mice showed a smaller collagen fibril diameter and a more rapid IVD degeneration as compared with the wild type mice [47]. Nakai et al. (2016) found that CD146 and SM22α are co-expressed in the mouse oAF tissue [50], which may be correlated with the maximum shear strain in the oAF tissue under lateral bending of IVD [48, 49]. Interestingly, the expression level of CD146 in iAF was significantly lower than in NP. The exact reason is unclear, since few studies have been reported CD146 in NP and iAF tissue. Milinos et al. (2015) found that 22.3% of bovine primary NP cells are positive for CD146 FACS staining [51], while in human primary NP cells, CD146 expression is not detected on the cell surface [52]. Based on the results from the current study, CD146 may serve as a candidate marker to distinguish NP and iAF. However, further studies are needed with a larger sample size and the protein expression should be confirmed. The current study, for the first time, systematically measured and identified these molecules as a marker pool for functional AF cells. These markers were defined in healthy bovine tissue due to very limited access to healthy human IVD tissue with good zonal structures. Some of the markers have been reported to be relevant to AF function in human and other species, as discussed above. Therefore, they were expected to be similar between bovine and human species and were used as a guideline for cell induction with human AF cells.

In previous studies, TGF-β1 was shown to increase collagen type I and II as well as GAG production in a rat fetal AF cell micromass model; additionally, it tended to promote cell proliferation [53]. Blanquer et al. (2017) [54] reported that TGF-β3 is essential to support AF differentiation of human adipose stem cells. However, the effects of TGF-β on the functional properties of AF cells and cell fate of MSCs were not clear, as markers of the functional AF cells were not tested in those studies. The present results corroborated the hypothesis that TGF-β1 induced a functional AF cell phenotype in human mildly degenerated AF cells, as indicated by upregulated expression of phenotypic markers (*CD146*, *SM22α* and *MKX*) and increased cell contractility. These results indicate that TGF-β1 induced AF cells from mildly degenerated disc tissue may be used as a cell source for AF rupture repair. It would be meaningful to further investigate the effect of TGF-β1 on AF phenotype differentiation of MSCs under an appropriate microenvironment. Which may expand the cell source options with an easily accessible endogenous cell type.

Interestingly, results showed that TGF-β1 induced *COL2A1* expression in human AF cells under *in vitro* 2D culture condition (Figure 2a). However, in the *ex vivo* organ culture study, addition of TGF-β1 within the hydrogel induced *COL1A1* gene expression in human AF cells (Figure 7), highlighting the context-specific behaviors of TGF-β1. These results indicated that the native AF tissue microenvironment *in situ* may orient the effect of TGF-β1 towards the native cell phenotype. ELN expression was also upregulated in implanted AF cells by TGF-β1 supplementation (Figure 7), which plays an important role in maintenance of collagen organization and recovery of the disc size and shape after deformation [55]. Nakai et al. (2016) showed that *ELN* upregulation in $CD146^{+}$ AF cells may contribute to the development of a contractile phenotype in these AF cells [50]. SCX, a basic helix-loop-helix transcription factor that marks the tendon/ligament cell lineage and is present in the AF cells [56, 57], was highly upregulated in both 2D and 3D cultures treated with TGF-β1 (Figure 2a, 4). Interestingly, it had lower expression in oAF vs NP in bovine IVD

(Figure 1). However, it has been shown that the SCX^+ AF cells function in healing of AF rupture in neonatal mice [58], which may explain the low expression level in mature bovine AF tissue. IVD cells fail to maintain the balance of anabolism and catabolism during aging and degeneration, with decreased ECM synthesis and increased ECM degrading enzymes, such as MMP and ADAMTS family. The upregulation of MMP3 and ADAMTS5 has been reported in degenerated IVDs [59]. Present results showed, that TGF-β1 not only upregulated ECM production, but also downregulated the expression of ECM catabolic enzymes MMP3 and ADAMTS 5 (Figure 2a, 4). This indicates that TGF-β1 treated AF cells may possess an anti-catabolic effect in AF rupture repair for prevention of further tissue degeneration. When AF cells were cultured in collagen I hydrogel both *in vitro* and *ex vivo,* higher cell density was found in TGF-β1 supplemented scaffolds (Figure 3, 6). which indicated that TGF-β1 promoted cell proliferation and/or cell survival of human AF cells. This is essential for rebuilding of the biological function when cells are implanted into the avascular disc milieu. In summary, results showed that TGF-β1 is an effective agent for biological functional recovery of AF.

PU materials are promising biomaterials for AF regeneration, as they are biodegradable, biocompatible, mechanically robust and elastic [16, 29]. In the present study, AF cells were evenly distributed within the porous PU scaffold, with or without collagen gel as a cell carrier (Figure 3a, b, c). Furthermore, the scaffold size can be easily tuned for custom-designed patient need in further application. Type I collagen is a component of AF matrix and was used to deliver the functional AF cells in PU scaffold and create a biomimetic environment of AF. Collagen type I has been reported to promote AF cells proliferation and matrix production *in vitro* [34]. Present results showed that collagen I hydrogel maintained AF cell survival after 7 days of 3D culture *in vitro* but did not further enhance the cell proliferation. Importantly, collagen I hydrogel as a cell carrier could preserve the functional phenotype of TGF-β1 induced human AF cells, as indicated by higher expression level of *CD146*, *SM22α* and *MKX* as compared with PU scaffold only (Figure 4). These results demonstrated the potential capacity of collagen I hydrogel for cell delivery and functional phenotype maintenance in AF rupture repair.

In the *ex vivo* preclinical study, AF defects were repaired with PU-Col constructs and PU membrane sealing. After 14 days of organ culture under daily dynamic loading, PU-Col constructs could still completely fill the AF defect and no herniation of NP tissue was found. While in injury control discs, part of the NP tissue protruded into the AF defect area (Figure 6). Implantation of AF cells into the AF defect was carried out by delivering them in PU-Col constructs. After 14 days of *in situ* culture with daily dynamic load, the implanted AF cells remained in the PU-Col constructs and started matrix production. Interestingly, cell density and matrix production were more pronounced when TGF-β1 had been added in the constructs. On the other hand, cells expressed significantly higher *COL1A1* and showed a trend for higher levels of *CD146* and *ELN* in TGF-β1 supplied constructs. These results indicated that TGF-β1 administration within the selected biomaterial could better facilitate the enhancement of functional AF cell phenotype and neo-tissue formation *in situ*. Pirvu et al. (2015) showed that implantation of MSCs positively modulates cell phenotype of host disc tissue by up-regulating anabolic mechanisms and down-regulating catabolic mechanisms by paracrine effect [19]. However, there was no evidence showing the same effect on native disc tissue with AF cells implantation (Figure 8); while new matrix production was only observed with the functional AF cells implantation. These findings suggested that MSCs

and AF cells had different mechanisms of action. MSCs, which can be derived from a wide range of sources, can positively modulate the cells of the host disc tissue, but may have limited potential for AF matrix production. In contrast, AF cells are suitable for neo-tissue formation, but do not influence the phenotype of adjacent host cells. To further improve the homeostasis in AF tissue repair and prevent further IVD degeneration, combination of functional AF cells and the effective paracrine factors from MSCs may bring further valued outcomes.

The limitations of the current study remain in the following aspects: the random porous architecture of the PU scaffold likely did not promote matrix deposition in an angle-plied lamellar microstructure similar to that of native AF fibers, despite its good cell seeding capacity. Implementation of additive manufacturing for production of PU scaffolds may further promote maintenance/induction of the functional AF cell phenotype and formation of a native-mimicking ECM structure. Both *in vitro* and *ex vivo* studies were performed with 2 weeks follow-up. Further longer follow-up study may be needed to evaluate the long-term culture property such as cell survival, ECM production and degradation of PU scaffold. Additional studies with high force, fatigue and complex loading to evaluate herniation risk of the construct are needed. Ultimately, *in vivo,* a higher load is expected in the disc. A press-fit and biocompatible material filler is needed to close the defect and restore the mechanical function of the IVD with high adhesion strength and adequate compressive, shear and tensile moduli [60], to provide structural support for the biological repair.

5. Conclusions

The current study explored a novel AF repair strategy aiming at functional cell phenotype induction. A set of AF cell phenotype markers were defined in healthy AF tissue as compared with NP, including *COL1A2*, *CD146*, *SM22α* and *MKX*. TGF-β1 upregulated gene and protein expression of the AF cell markers in human mildly degenerated AF cells and increased the cell contractility, indicating that TGF-β1 pre-treated AF cells may be an appropriate cell source for AF tissue engineering or rupture repair. Collagen type I hydrogel as a cell carrier in the PU scaffold maintained the phenotype of human AF cells. TGF-β1 treatment within the collagen hydrogel further promoted cell proliferation and matrix production of AF cells both *in vitro* and *ex vivo*. TGF-β1 and collagen type I hydrogel-PU scaffold hybrid system retained the AF phenotype of implanted cells. These constructs have potential for generating tissue engineered AF and warrant further investigation for their use in repairing AF defects after discectomy.

Acknowledgements:

The study was supported by the AO Foundation, AO Spine International, the National Natural Science Foundation of China (81772333, 51873069) and National Institutes of Health (R01AR064157). Jie Du was supported by the European Union's Horizon 2020 research and innovation programme under Marie Sklodowska-Curie fellowship (642414). Rose Long was supported by the Whitaker Foundation.

Author contributions:

Jie Du: contributions to study design, acquisition, analysis, interpretation of data, drafting the article, revising it critically, and final approval. Rose G. Long: substantial contributions to acquisition of data, analysis, interpretation of data, revising the article, and final approval. Tomoko Nakai, Daisuke Sakai, Lorin M. Benneker, Guangqian Zhou, Bin Li, David Eglin, James C. Iatridis, Mauro Alini: contribution to study design, revising the article, and final approval. Sibylle Grad, Zhen Li: contribution to study design, interpretation of data, revising it critically, final approval, and takes responsibility for the integrity of the work as a whole, from inception to finished article.

References

[1] C.E. Dionne, K.M. Dunn, P.R. Croft, Does back pain prevalence really decrease with increasing age? A systematic review, Age Ageing 35(3) (2006) 229-34.
[2] D. Hoy, C. Bain, G. Williams, L. March, P. Brooks, F. Blyth, A. Woolf, T. Vos, R. Buchbinder, A systematic review of the global prevalence of low back pain, Arthritis Rheum 64(6) (2012) 2028-37.
[3] D. Hoy, L. March, P. Brooks, A. Woolf, F. Blyth, T. Vos, R. Buchbinder, Measuring the global burden of low back pain, Best Pract Res Clin Rheumatol 24(2) (2010) 155-65.
[4] S. Roberts, H. Evans, J. Trivedi, J. Menage, Histology and pathology of the human intervertebral disc, J Bone Joint Surg Am 88 Suppl 2 (2006) 10-4.
[5] P. Goupille, M.I. Jayson, J.P. Valat, A.J. Freemont, The role of inflammation in disk herniation-associated radiculopathy, Semin Arthritis Rheum 28(1) (1998) 60-71.
[6] S.C. Humphreys, J.C. Eck, Clinical evaluation and treatment options for herniated lumbar disc, Am Fam Physician 59(3) (1999) 575-82, 587-8.
[7] E.J. Carragee, M.Y. Han, P.W. Suen, D. Kim, Clinical outcomes after lumbar discectomy for sciatica: the effects of fragment type and anular competence, J Bone Joint Surg Am 85-A(1) (2003) 102-8.
[8] J.S. Smith, A.T. Ogden, S. Shafizadeh, R.G. Fessler, Clinical outcomes after microendoscopic discectomy for recurrent lumbar disc herniation, J Spinal Disord Tech 23(1) (2010) 30-4.
[9] G.L. Ambrossi, M.J. McGirt, D.M. Sciubba, T.F. Witham, J.P. Wolinsky, Z.L. Gokaslan, D.M. Long, Recurrent lumbar disc herniation after single-level lumbar discectomy: incidence and health care cost analysis, Neurosurgery 65(3) (2009) 574-8; discussion 578.
[10] W.C. Watters, 3rd, M.J. McGirt, An evidence-based review of the literature on the consequences of conservative versus aggressive discectomy for the treatment of primary disc herniation with radiculopathy, Spine J 9(3) (2009) 240-57.
[11] B.D. Ahlgren, W. Lui, H.N. Herkowitz, M.M. Panjabi, J.P. Guiboux, Effect of anular repair on the healing strength of the intervertebral disc: a sheep model, Spine (Phila Pa 1976) 25(17) (2000) 2165-70.
[12] A. Bailey, A. Araghi, S. Blumenthal, G.V. Huffmon, G. Anular Repair Clinical Study, Prospective, multicenter, randomized, controlled study of anular repair in lumbar discectomy: two-year follow-up, Spine (Phila Pa 1976) 38(14) (2013) 1161-9.
[13] C.C. Guterl, O.M. Torre, D. Purmessur, K. Dave, M. Likhitpanichkul, A.C. Hecht, S.B. Nicoll, J.C. Iatridis, Characterization of mechanics and cytocompatibility of fibrin-genipin annulus fibrosus sealant with the addition of cell adhesion molecules, Tissue Eng Part A 20(17-18) (2014) 2536-45.
[14] F. Heuer, S. Ulrich, L. Claes, H.J. Wilke, Biomechanical evaluation of conventional anulus fibrosus closure methods required for nucleus replacement. Laboratory investigation, J Neurosurg Spine 9(3) (2008) 307-13.
[15] G. Chu, C. Shi, J. Lin, S. Wang, H. Wang, T. Liu, H. Yang, B. Li, Biomechanics in Annulus Fibrosus Degeneration and Regeneration, Adv Exp Med Biol 1078 (2018) 409-420.
[16] L.D. Agnol, F.T. Gonzalez Dias, N.F. Nicoletti, A. Falavigna, O. Bianchi, Polyurethane as a strategy for annulus fibrosus repair and regeneration: a systematic review, Regen Med 13(5) (2018) 611-626.
[17] R. Borem, A. Madeline, J. Walters, H. Mayo, S. Gill, J. Mercuri, Angle-ply biomaterial scaffold for annulus fibrosus repair replicates native tissue mechanical properties, restores spinal kinematics, and supports cell viability, Acta Biomater 58 (2017) 254-268.
[18] I. Hussain, S.R. Sloan, Jr., C. Wipplinger, R. Navarro-Ramirez, M. Zubkov, E. Kim, S. Kirnaz, L.J. Bonassar, R. Hartl, Mesenchymal Stem Cell-Seeded High-Density Collagen Gel for Annular Repair: 6-Week Results From In Vivo Sheep Models, Neurosurgery (2018).

[19] T. Pirvu, S.B. Blanquer, L.M. Benneker, D.W. Grijpma, R.G. Richards, M. Alini, D. Eglin, S. Grad, Z. Li, A combined biomaterial and cellular approach for annulus fibrosus rupture repair, Biomaterials 42 (2015) 11-9.
[20] D.A. Frauchiger, R.D. May, E. Bakirci, A. Tekari, S.C.W. Chan, M. Woltje, L.M. Benneker, B. Gantenbein, Genipin-Enhanced Fibrin Hydrogel and Novel Silk for Intervertebral Disc Repair in a Loaded Bovine Organ Culture Model, J Funct Biomater 9(3) (2018).
[21] D. Sakai, S. Grad, Advancing the cellular and molecular therapy for intervertebral disc disease, Adv Drug Deliv Rev 84 (2015) 159-71.
[22] B.J. Freeman, J.S. Kuliwaba, C.F. Jones, C.C. Shu, C.J. Colloca, M.R. Zarrinkalam, A. Mulaibrahimovic, S. Gronthos, A.C. Zannettino, S. Howell, Allogeneic Mesenchymal Precursor Cells Promote Healing in Postero-lateral Annular Lesions and Improve Indices of Lumbar Intervertebral Disc Degeneration in an Ovine Model, Spine (Phila Pa 1976) 41(17) (2016) 1331-9.
[23] J. Iu, E. Massicotte, S.Q. Li, M.B. Hurtig, E. Toyserkani, J.P. Santerre, R.A. Kandel, (*) In Vitro Generated Intervertebral Discs: Toward Engineering Tissue Integration, Tissue Eng Part A 23(17-18) (2017) 1001-1010.
[24] L. Yang, R.A. Kandel, G. Chang, J.P. Santerre, Polar surface chemistry of nanofibrous polyurethane scaffold affects annulus fibrosus cell attachment and early matrix accumulation, J Biomed Mater Res A 91(4) (2009) 1089-99.
[25] P.H. Chou, S.T. Wang, H.L. Ma, C.L. Liu, M.C. Chang, O.K. Lee, Development of a two-step protocol for culture expansion of human annulus fibrosus cells with TGF-beta1 and FGF-2, Stem Cell Res Ther 7(1) (2016) 89.
[26] H.E. Gruber, K. Leslie, J. Ingram, G. Hoelscher, H.J. Norton, E.N. Hanley, Jr., Colony formation and matrix production by human anulus cells: modulation in three-dimensional culture, Spine (Phila Pa 1976) 29(13) (2004) E267-74.
[27] J.J. Tomasek, G. Gabbiani, B. Hinz, C. Chaponnier, R.A. Brown, Myofibroblasts and mechano-regulation of connective tissue remodelling, Nat Rev Mol Cell Biol 3(5) (2002) 349-63.
[28] J. Zhang, Z. Li, F. Chen, H. Liu, H. Wang, X. Li, X. Liu, J. Wang, Z. Zheng, TGF-beta1 suppresses CCL3/4 expression through the ERK signaling pathway and inhibits intervertebral disc degeneration and inflammation-related pain in a rat model, Exp Mol Med 49(9) (2017) e379.
[29] M. Yeganegi, R.A. Kandel, J.P. Santerre, Characterization of a biodegradable electrospun polyurethane nanofiber scaffold: Mechanical properties and cytotoxicity, Acta Biomater 6(10) (2010) 3847-55.
[30] B.R. Whatley, J. Kuo, C. Shuai, B.J. Damon, X. Wen, Fabrication of a biomimetic elastic intervertebral disk scaffold using additive manufacturing, Biofabrication 3(1) (2011) 015004.
[31] C.R. Lee, S. Grad, K. Gorna, S. Gogolewski, A. Goessl, M. Alini, Fibrin-polyurethane composites for articular cartilage tissue engineering: a preliminary analysis, Tissue Eng 11(9-10) (2005) 1562-73.
[32] Z. Li, L. Kupcsik, S.J. Yao, M. Alini, M.J. Stoddart, Chondrogenesis of human bone marrow mesenchymal stem cells in fibrin-polyurethane composites, Tissue Eng Part A 15(7) (2009) 1729-37.
[33] M. Alini, W. Li, P. Markovic, M. Aebi, R.C. Spiro, P.J. Roughley, The potential and limitations of a cell-seeded collagen/hyaluronan scaffold to engineer an intervertebral disc-like matrix, Spine (Phila Pa 1976) 28(5) (2003) 446-54; discussion 453.
[34] L. Xiao, M. Ding, O. Saadoon, E. Vess, A. Fernandez, P. Zhao, L. Jin, X. Li, A novel culture platform for fast proliferation of human annulus fibrosus cells, Cell Tissue Res 367(2) (2017) 339-350.
[35] Y. Wang, X. Wang, J. Shang, H. Liu, Y. Yuan, Y. Guo, B. Huang, Y. Zhou, Repairing the ruptured annular fibrosus by using type I collagen combined with citric acid, EDC and NHS: an in vivo study, Eur Spine J 26(3) (2017) 884-893.
[36] R.D. Bowles, R.M. Williams, W.R. Zipfel, L.J. Bonassar, Self-assembly of aligned tissue-engineered annulus fibrosus and intervertebral disc composite via collagen gel contraction, Tissue Eng Part A 16(4) (2010) 1339-48.

[37] K. Gorna, S. Gogolewski, Biodegradable porous polyurethane scaffolds for tissue repair and regeneration, J Biomed Mater Res A 79(1) (2006) 128-38.
[38] C.I. Boissard, P.E. Bourban, A.E. Tami, M. Alini, D. Eglin, Nanohydroxyapatite/poly(ester urethane) scaffold for bone tissue engineering, Acta Biomater 5(9) (2009) 3316-27.
[39] S. Grad, L. Kupcsik, K. Gorna, S. Gogolewski, M. Alini, The use of biodegradable polyurethane scaffolds for cartilage tissue engineering: potential and limitations, Biomaterials 24(28) (2003) 5163-71.
[40] G. Lang, Y. Liu, J. Geries, Z. Zhou, D. Kubosch, N. Sudkamp, R.G. Richards, M. Alini, S. Grad, Z. Li, An intervertebral disc whole organ culture system to investigate proinflammatory and degenerative disc disease condition, J Tissue Eng Regen Med 12(4) (2018) e2051-e2061.
[41] M.U. Caprez Stephanie, Li Zhen, Grad Sibylle, Alini Mauro, Peroglio Marianna, Isolation of High-Quality RNA from Intervertebral Disc Tissue via Pronase Pre-Digestion and Tissue Pulverization, JOR spine (2018).
[42] S.R. Sloan, Jr., M. Lintz, I. Hussain, R. Hartl, L.J. Bonassar, Biologic Annulus Fibrosus Repair: A Review of Preclinical In Vivo Investigations, Tissue Eng Part B Rev 24(3) (2018) 179-190.
[43] J.C. Iatridis, S.B. Nicoll, A.J. Michalek, B.A. Walter, M.S. Gupta, Role of biomechanics in intervertebral disc degeneration and regenerative therapies: what needs repairing in the disc and what are promising biomaterials for its repair?, Spine J 13(3) (2013) 243-62.
[44] G. Pattappa, Z. Li, M. Peroglio, N. Wismer, M. Alini, S. Grad, Diversity of intervertebral disc cells: phenotype and function, J Anat 221(6) (2012) 480-96.
[45] O.M. Torre, V. Mroz, M.K. Bartelstein, A.H. Huang, J.C. Iatridis, Annulus fibrosus cell phenotypes in homeostasis and injury: implications for regenerative strategies, Ann N Y Acad Sci 1442(1) (2019) 61-78.
[46] J.L. Bron, M.N. Helder, H.J. Meisel, B.J. Van Royen, T.H. Smit, Repair, regenerative and supportive therapies of the annulus fibrosus: achievements and challenges, Eur Spine J 18(3) (2009) 301-13.
[47] R. Nakamichi, Y. Ito, M. Inui, N. Onizuka, T. Kayama, K. Kataoka, H. Suzuki, M. Mori, M. Inagawa, S. Ichinose, M.K. Lotz, D. Sakai, K. Masuda, T. Ozaki, H. Asahara, Mohawk promotes the maintenance and regeneration of the outer annulus fibrosus of intervertebral discs, Nat Commun 7 (2016) 12503.
[48] H. Schmidt, A. Kettler, F. Heuer, U. Simon, L. Claes, H.J. Wilke, Intradiscal pressure, shear strain, and fiber strain in the intervertebral disc under combined loading, Spine (Phila Pa 1976) 32(7) (2007) 748-55.
[49] J.J. Costi, I.A. Stokes, M. Gardner-Morse, J.P. Laible, H.M. Scoffone, J.C. Iatridis, Direct measurement of intervertebral disc maximum shear strain in six degrees of freedom: motions that place disc tissue at risk of injury, J Biomech 40(11) (2007) 2457-66.
[50] T. Nakai, D. Sakai, Y. Nakamura, T. Nukaga, S. Grad, Z. Li, M. Alini, D. Chan, K. Masuda, K. Ando, J. Mochida, M. Watanabe, CD146 defines commitment of cultured annulus fibrosus cells to express a contractile phenotype, J Orthop Res 34(8) (2016) 1361-72.
[51] M. Molinos, C.R. Almeida, R.M. Goncalves, M.A. Barbosa, Improvement of Bovine Nucleus Pulposus Cells Isolation Leads to Identification of Three Phenotypically Distinct Cell Subpopulations, Tissue Eng Part A 21(15-16) (2015) 2216-27.
[52] D. Sakai, Y. Nakamura, T. Nakai, T. Mishima, S. Kato, S. Grad, M. Alini, M.V. Risbud, D. Chan, K.S. Cheah, K. Yamamura, K. Masuda, H. Okano, K. Ando, J. Mochida, Exhaustion of nucleus pulposus progenitor cells with ageing and degeneration of the intervertebral disc, Nat Commun 3 (2012) 1264.
[53] A.J. Hayes, J.R. Ralphs, The response of foetal annulus fibrosus cells to growth factors: modulation of matrix synthesis by TGF-beta1 and IGF-1, Histochem Cell Biol 136(2) (2011) 163-75.
[54] S.B.G. Blanquer, A.W.H. Gebraad, S. Miettinen, A.A. Poot, D.W. Grijpma, S.P. Haimi, Differentiation of adipose stem cells seeded towards annulus fibrosus cells on a designed poly(trimethylene carbonate) scaffold prepared by stereolithography, J Tissue Eng Regen Med 11(10) (2017) 2752-2762.
[55] J. Yu, P.C. Winlove, S. Roberts, J.P. Urban, Elastic fibre organization in the intervertebral discs of the bovine tail, J Anat 201(6) (2002) 465-75.

[56] Y. Yoshimoto, A. Takimoto, H. Watanabe, Y. Hiraki, G. Kondoh, C. Shukunami, Scleraxis is required for maturation of tissue domains for proper integration of the musculoskeletal system, Sci Rep 7 (2017) 45010.
[57] B.A. Pryce, A.E. Brent, N.D. Murchison, C.J. Tabin, R. Schweitzer, Generation of transgenic tendon reporters, ScxGFP and ScxAP, using regulatory elements of the scleraxis gene, Dev Dyn 236(6) (2007) 1677-82.
[58] O.M. Torre, R. Das, R.E. Berenblum, A.H. Huang, J.C. Iatridis, Neonatal mouse intervertebral discs heal with restored function following herniation injury, FASEB J 32(9) (2018) 4753-4762.
[59] N.V. Vo, R.A. Hartman, T. Yurube, L.J. Jacobs, G.A. Sowa, J.D. Kang, Expression and regulation of metalloproteinases and their inhibitors in intervertebral disc aging and degeneration, Spine J 13(3) (2013) 331-41.
[60] R.G. Long, O.M. Torre, W.W. Hom, D.J. Assael, J.C. Iatridis, Design Requirements for Annulus Fibrosus Repair: Review of Forces, Displacements, and Material Properties of the Intervertebral Disk and a Summary of Candidate Hydrogels for Repair, J Biomech Eng 138(2) (2016) 021007.

Chapter 5

The Function of CD146 in Human Annulus Fibrosus Cells and Mechanism of the Regulation by TGF-β

Jie Du, Wei Guo, Sonja Häckel, Sven Hoppe, João P. Garcia, Mauro Alini, Marianna A. Tryfonidou, Laura B. Creemers, Sibylle Grad, Zhen Li

Published in Journal of Orthopaedic Research
DOI: 10.1002/jor.25190

Jie Du contributed to the study design, acquisition, analysis, interpretation of data, drafting, and revising of the article, and final approval.

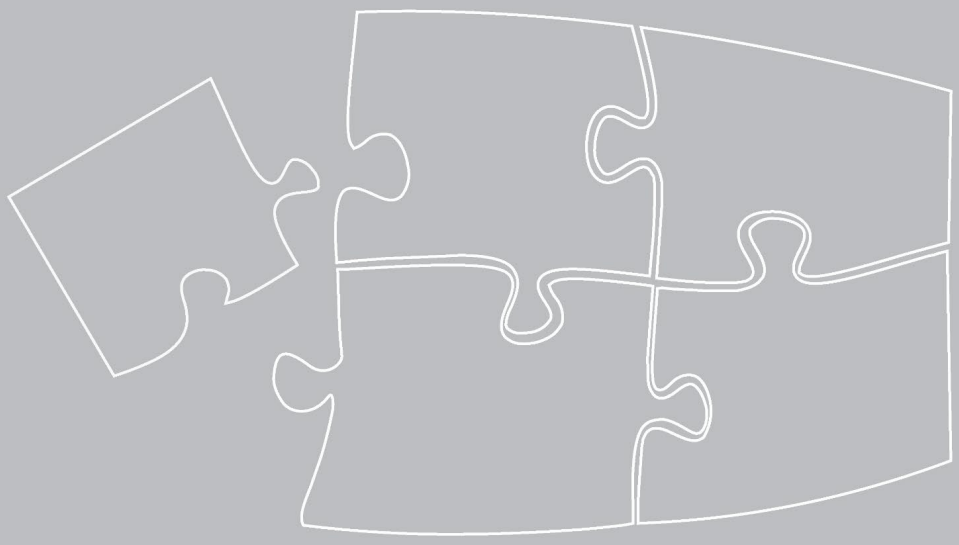

Abstract:

The mouse outer annulus fibrosus (AF) was previously shown to contain $CD146^+$ AF cells, while *in vitro* culture and exposure to transforming growth factor-beta (TGF-β) further increased the expression of CD146. However, neither the specific function of CD146 nor the underlying mechanism of TGF-β upregulation of $CD146^+$AF cells have been elucidated yet. In the current study, CD146 expression and its role in cultured human AF cells was investigated studying the cells' capacity for matrix contraction and gene expression of functional AF markers. In addition, TGF-β pathways were blocked by several pathway inhibitors and short hairpin RNAs (shRNAs) targeting SMAD and non-SMAD pathways to investigate their involvement in TGF-β-induced CD146 upregulation. Results showed that knockdown of CD146 led to reduction in AF cell-mediated collagen gel contraction, downregulation of versican and smooth muscle protein 22α (*SM22α*), and upregulation of scleraxis. TGF-β-induced CD146 upregulation was significantly blocked by inhibition of TGF-β receptor ALK5, and partially inhibited by shRNA against SMAD2 and SMAD4 and by a protein kinase (AKT) inhibitor. Interestingly, the inhibition of extracellular signal-regulated kinase (ERK) pathway induced CD146 upregulation. In conclusion, CD146 was shown to be crucial to maintain the cell contractility of human AF cells *in vitro*. Furthermore, TGF-β upregulated CD146 via ALK5 signaling cascade, partially through SMAD2, SMAD4 and AKT pathway, whereas, ERK was shown to be a potential negative modulator. Our findings suggest that CD146 can potentially be used as a functional marker in AF repair strategies.

Keywords:

AKT, ALK5, Annulus fibrosus, CD146 regulation, Cell contractility, SMADs, TGF-β.

1. Introduction

The intervertebral disc (IVD) consists of a gel-like central structure, the nucleus pulposus (NP), a connective tissue-like outer layer, the annulus fibrosus (AF), and the cartilaginous endplates. Pathologies of the IVD, including herniation and degeneration, are known triggers of chronic low back pain, one of the world leading causes of disability [1]. The AF plays important roles in linking adjacent vertebrae and withstanding mechanical forces, allowing bending, flexion and torsion of the spine. Acute and chronic injuries of the AF can lead to IVD degeneration and herniation [2, 3]. While discectomy is a common surgical treatment method, unrepaired AF defects after discectomy can lead to re-herniation in 10% – 30% of cases, which results in recurrent pain and progressive disc degeneration [4-6]. AF repair is a challenge due to its complex structure, high mechanical loading environment, and poor self-healing capability as a virtually avascular tissue [7]. AF cell-based tissue engineering appears to be a promising strategy. Different approaches were taken to repair the AF by using cells alone or in combination with drugs and biomaterials, showing AF cells can orient themselves on biomaterials, proliferate and deposit matrix [8, 9]. However, there is a fundamental barrier for clinical translation, which is the limited knowledge about AF cell biology. A better understanding of the populations and phenotypes of AF cells will facilitate the establishment of reparative regeneration strategies to improve AF rupture healing.

Recently, AF cells at the outermost annulus layer of the mouse IVD were found to be cluster of differentiation 146 (CD146) positive, and *in vitro* positive subpopulations were identified in both human and mouse AF cells [10]. Furthermore, studies confirmed that CD146 has higher expression levels in AF than NP in the human IVD [11, 12]. CD146 was identified as a cell adhesion molecule (CAM) in the plasma membrane of human melanoma cells and was thus also named as melanoma cell adhesion molecule (MCAM) [13]. CAMs are proteins located on the cell surface that are involved in the process of cell adhesion by binding with other cells or extracellular matrix (ECM) [14]. They are highly associated with cell behavior such as cell growth, survival, migration, and differentiation, which are essential for embryonic development and maintaining the integrity of tissue architecture in adults [15, 16]. In healthy cells, CD146 is strongly expressed on blood endothelium, smooth muscle, and active T cells, and is defined as a marker of mesenchymal stromal cells (MSCs) [17-21]. In the vasculature, CD146 plays crucial roles in vessel structure, angiogenesis, and inflammation [22]. In a variety of carcinomas, accumulating evidence demonstrated that CD146 overexpression may be linked to either the initial development of the primary lesion or progression to metastases [13, 23-25]. A high expression of CD146 molecule in bone marrow derived MSCs is associated with a commitment to a vascular smooth muscle cell lineage characterized by a strong upregulation of muscle protein 22 alpha (SM22α) and an ability to contract collagen matrix [20]. In line with this, also $CD146^+$ AF cells expressed SM22α and demonstrated significantly enhanced contractile properties, although the exact role of CD146 in this enhanced contractility was not investigated [10].

Expression of CD146 by AF cells was promoted by transforming growth factor-beta (TGF-β), in addition to enhancing ECM synthesis by TGF-β-pretreated AF cells in a bovine whole IVD organ culture model [26]. In fact, induction of CD146 expression by TGF-β has been widely reported in different cell types [10, 26-28]. TGF-β increases CD146 expression in progenitor cells originated from human umbilical cord blood and induces their differentiation into vascular smooth muscle

cells [27]. In mouse embryonic fibroblasts, TGF-β upregulated CD146 during epithelial mesenchymal transition and activated the extracellular signal-regulated kinase ERK pathway and silencing CD146 blocked TGF-β induced ERK activation [28]. These results indicate that TGF-β induced activation of ERK is CD146-dependent, although inhibition of ERK increased CD146 expression, suggesting a feedback mechanism. Upregulation of CD146 by endothelin-3 is protein kinase (AKT) and PI3K-dependent in human melanocytes [29]. CD166 has also been shown to positively regulate CD146 via inhibition of ubiquitin E3 ligases Smurf1 and βTrCP through PI3K/AKT and c-Raf/MEK/ERK signaling in Bel-7402 hepatocellular carcinoma cells [30]. However, which pathway plays the most important role in TGF-β-induced CD146 upregulation in AF cells is still unknown.

The current study aims to investigate the function of CD146 and the TGF-β signaling pathway underlying the upregulation of CD146 in human AF cells. The multiple functions of CD146 were investigated by short hairpin RNA (shRNA) knockdown of CD146 in human AF cells. Cell contractility and gene expression of various functional phenotype markers of AF cells were evaluated. Furthermore, we interfered with the SMAD and non-SMAD TGF-β signaling pathways in order to elucidate the mechanism behind TGF-β-induced CD146 expression.

2. Materials and methods

2.1. Human AF cells isolation and expansion

Human AF tissue was obtained with written consent from waste tissue of traumatic IVDs (6 donors, Inselspital Bern, Switzerland). The Swiss Human Research Act does not apply to research which involves anonymized biological material and/or anonymously collected or anonymized health-related data. Therefore, this project does not need to be approved by the ethics committee. General Consent which also covers anonymization of health-related data and biological material was obtained. Intact IVDs (2 donors, University Medical Center Utrecht, Netherlands) were obtained as part of the standard postmortem procedure as approved by the medical ethics committee of the University Medical Center Utrecht (METC No. 12-364). Donor's age was from 19 to 61, mean age 35, and disc degeneration level was classified on magnetic resonance imaging (MRI) or naked eyes (Pfirrmann grade II (4 donors), I (2 donors), no information (2 donors)) (Supplementary Table 1). The isolation and expansion methods of human AF cells have been described previously [26]. Briefly, after removing adjacent NP and cartilaginous endplate, the purified AF tissue was incubated with 20 mL red blood cell lysis buffer (155 mM NH_4Cl, 10 M $KHCO_3$ and 0.1 mM EDTA in ultrapure water) for 5min at room temperature. Then, minced tissue was first digested for 1 hour with 0.2% w/v Pronase (Roche) in αMEM (Gibco), followed by 12–14 hours at 37 °C in 130 U/mL collagenase type II (Worthington) in αMEM with 10% fetal bovine serum (FBS, PAN Biotech, Germany). Single cells were washed once with expansion culture medium (αMEM supplemented with 10% FBS, 100 U/mL penicillin and 100 mg/mL streptomycin (1% P/S, Gibco)), then seeded at a concentration of 10,000 cells/cm^2 and expanded. AF cells were cultured at a hypoxic condition at 2% O_2, 5% CO_2, at 37 °C. Culture medium was changed twice a week. Cells were passaged at a ~ 80% confluency, detached by 0.05% trypsin/EDTA (Gibco) with 0.01% collagenase P (Roche) for 5 min at 37 °C. Cells were frozen at passage 1 for further use.

2.2. AF cells treatment with TGF-β1 and pathway inhibitors

AF cells at passage 1 were thawed, seeded in T150 flasks at 0.5×10^6 cells per flask and expanded in expansion culture medium until passage 2. At ~ 80% confluence, cells were sub-cultured to passage 3 at a ratio of 1:4 to T75 flasks. When cells were ~ 60% confluent, they were treated with or without inhibitors in either basal medium (αMEM supplemented with 5% FBS, 1% P/S, 1% ITS+ (BD Biosciences)) or TGF-β medium (basal medium supplemented with 5 ng/mL of TGF-β1 (Fitzgerald)) for 2 days. After treatment, cells were detached. Half of the cells were used for flow cytometry analysis, and the remaining cells were used for RNA isolation and gene expression analysis. The inhibitors used in current study are listed in Table 1.

Table 1. List of TGF-β pathway inhibitors

Inhibitor	Source	Target	Solvent	Used Concentration
MK-2206 2HCl	Selleckchem	AKT	DMSO	1 μM [31]
SB525334	Selleckchem	ALK5	DMSO	1 μM [32]
BIRB 796	Selleckchem	P38	DMSO	1 μM [33]
SCH 772984	Selleckchem	ERK1/2	DMSO	1 μM [34]
SP 600125	Selleckchem	JNK	DMSO	10 μM [35]
SIS3 HCl	Selleckchem	SMAD3	DMSO	3 μM [36]
Y-27632	Sigma	ROCK	DMSO	1 μM [37]

2.3. Cell treatment with shRNA-lentivirus

AF cells were transfected with shRNA-lentivirus at passage 3. Briefly, single cell and virus suspensions were prepared at a concentration of 0.5×10^5 cells/mL and 2×10^6 TU/mL respectively within transfection medium (αMEM supplemented with 10% FBS, 1% P/S, 5 μg/mL polybrene (VectorBuilder)). Transfection was performed by mixing single cell and virus suspension at a ratio v: v = 1:2. Cells and virus mixture were then seeded and incubated for 24 hours at hypoxic condition. All the shRNA-lentiviruses were bought from VectorBuilder, US. shCD146 was labeled with EGFP, sequence 5′- TTCCTGGAGCTGGTCAATTTA-3′; shSMAD4 was labeled with EGFP, sequence 5′- GCCAGCTACTTACCATCATAA -3′; shSMAD2 was labeled with mCherry, sequence 5′- CAAGTACTCCTTG CTGGATTG-3′; shScrambled was labeled with EGFP. For flow cytometry and gene expression analysis, cells and virus mixture was seeded in 6 well-plate at 1.5 mL per well. After a 24 hours transfection, cells were treated with basal medium or TGF-β medium for another 2 days. For the cell contractility assay, transfection was performed in 100 mm culture dish with 9 mL mixture. After 24 hours incubation, transfection medium was refreshed with culture medium for another 24 hours, where after cells were detached and seeded into collagen I gel (from rat tail, Corning). Transfection efficiency was estimated under fluorescence microscope (supplementary figure 1).

2.4. Flow cytometry analysis

Treated cells were detached and suspended in 100 μL staining buffer: phosphase buffered saline (PBS) with 0.2% bovine serum albumin (BSA) and 1 mM EDTA. Cell suspensions were incubated

with 5 µL fluorescence-conjugated mouse monoclonal anti-human CD146 antibody (CD146-APC, Miltenyi Biotec) at final concentration 5 µg/mL or the same amount of IgG1-APC (isotype control, Miltenyi Biotech) in the dark for 30 min at 4°C. After incubation and washing, 4′,6- diamidino-2-phenylindole (DAPI) or Propidium Iodide was used for dead cell staining at a final concentration of 0.1 µg/mL (AKT inhibitor, MK-2206 2HCl, has autofluorescence and interferes with DAPI channel; thus Propidium Iodide was used to label dead cells for cells treated with AKT inhibitor). Flow cytometric analysis was performed on a FACS AriaIII (BD Biosciences) and at least 30,000 events per sample were recorded. Data analysis was performed using BD FACSDiva software. A gating strategy was used to exclude dead cells and cell doublets. In lentivirus-transfected cells, the percentage of $CD146^+$ cells was calculated in the transfection positive cell fraction, identified by labeling of fluorescent protein EGFP and mCherry.

2.5. Cell contractility assay

The cell contractility assay was performed with shCD146 and scramble transfected AF cells from three donors. Cells were encapsulated in 1.81 mg/mL type I collagen at a seeding density of 1×10^5 cells/mL. The collagen gel was seeded in 24-well pre-coated 1% BSA plates at 0.5 mL per well with 4 technical replicates and incubated at 37 °C for at least 1 hour. After gelling, gels were cultured expansion culture medium with or without TGF-β1 5 ng/mL at hypoxia condition. Gels were photographed on day 1, 4 ,7 after seeding. The diameter of the gels was measured by ImageJ 1.53c. Gel diameters were averaged to calculate diameter change with the formula $Dwell - Dgel/Dwell$ (Dwell: diameter of well, Dgel: diameter of gel), and the diameter change was normalized to day 1 scramble by donor, whereby greater change equaled with higher contractility. This method was modified from a previous study [10].

2.6. RNA isolation and quantitative real-time PCR

RNA isolation was performed using TRI reagent (Molecular Research Centre Inc., Cincinnati, OH, USA) with polyacryl carrier (Molecular Research Centre Inc.) at a ratio v: v= 200: 1 according to the manufacturer's protocol. Phase separation was performed by adding 100 µL bromo-chloropropane per 1 mL of TRI reagent. The aqueous phase after centrifugation was transferred to a fresh tube and mixed with 250 µL of isopropanol followed by 250 µL of high salt precipitation solution (MRC) per 1 mL of TRI reagent. After precipitation and washing, RNA was dissolved in DEPC treated water and quantified by NanoDrop 1000 (Thermo Scientific, USA). Reverse transcription was performed using SuperScript® VILO™ cDNA Synthesis Kit (Invitrogen) with 500 ng total RNA. Quantitative real-time PCR was conducted on QuantStudio6 System (Applied Biosystems). Sequences of the primers and probes used in qRT-PCR are listed in Table 2. RPLP0 ribosomal RNA was used as endogenous control. Data were analyzed using the $2^{-\Delta\Delta CT}$ method.

Table 2. List of oligonucleotide primers and probes used for quantitative real-time PCR.

Gene	Primer/probe type	Sequence
COL1A1	Primer fw (5′–3′)	CCC TGG AAA GAA TGG AGA TGA T
	Primer rev (5′–3′)	ACT GAA ACC TCT GTG TCC CTT CA

	Probe (5′FAM/3′TAMRA)	CGG GCA ATC CTC GAG CAC CCT
COL2A1	Primer fw (5′–3′)	GGC AAT AGC AGG TTC ACG TAC A
	Primer rev (5′–3′)	GAT AAC AGT CTT GCC CCA CTT ACC
	Probe (5′FAM/3′TAMRA)	CCT GAA GGA TGG CTG CAC GAA ACA TAC
ACAN	Primer fw (5′–3′)	AGT CCT CAA GCC TCC TGT ACT CA
	Primer rev (5′–3′)	CGG GAA GTG GCG GTA ACA
	Probe (5′FAM/3′TAMRA)	CCG GAA TGG AAA CGT GAA TCA GAA TCA ACT
MMP3		Hs00968305_m1
ADAMTS5		Hs01095518_m1
CD146		Hs00174838_m1
SM22α		Hs00162558_m1
SCX		Hs03054634_g1
MKX		Hs00543190_m1
ELN		Hs00355783_m1
VCAN		Hs00171642_m1
RPLP0	Primer fw (5′–3′)	TGG GCA AGA ACA CCA TGA TG
	Primer rev (5′–3′)	CGG ATA TGA GGC AGC AGT TTC
	Probe (5′FAM/3′TAMRA)	AGG GCA CCT GGA AAA CAA CCC AGC

Note: Primers and probes with the sequence shown were custom-designed; primers and probes with the catalog number were from Applied Biosystems. Abbreviations: fw: Forward; rev: Reverse; FAM: Carboxyfluorescein; TAMRA: Tetramethylrhodamine. COL1A1: Type I Collagen; COL2A1: Type II Collagen; ACAN: Aggrecan; CD146: Cluster of Differentiation 146; SM22α: Smooth Muscle Protein 22-alpha; SCX: Scleraxis; MKX: Mohawk Homeobox; ELN: Elastin; VCAN: Versican; MMP3: Matrix Metalloproteinase-3; ADAMTS5: A Disintegrin and Metalloproteinase with Thrombospondin Motifs 5; RPLP0: Ribosomal Protein Lateral Stalk Subunit P0.

2.7. Western blot

Cells transfected with shSMAD2, shSMAD4 or both were cultured in 100 mm dish and scramble was transfected as control. At 80% confluency, cells were treated with basal medium or TGF-β medium for 1 hour. Cell lysis was carried out by RIPA buffer (Sigma-Aldrich, R0278) with protease inhibitor cocktail (Sigma, P8340) and phosphatase inhibitors, PhosSTOP™ (Sigma-Aldrich). Protein concentration was determined using the Bicinchoninic Acid (BCA) protein assay method, with BCA Solution (Sigma), Copper (II) Sulfate Solution (Sigma-Aldrich), Serum Albumin Standard (Bio-Rad), then mixed with a 5× sample buffer (GeneScript). The samples were loaded at 10 μg total protein, separated by electrophoresis in 8% Sodium dodecyl-sulfate polyacrylamide gel electrophoresis (SDS-PAGE), transferred to nitrocellulose membranes (0.45 μm), hybridized with corresponding antibodies, detected using the SuperSignal™ West Dura Extend Duration Substrate (Thermo Scientific, 34075), and photographed by ChemiDoc® Touch

Imaging system (BIO-RAD). Primary antibodies included rabbit anti-human SMAD2/3 (Cell Signaling, #8685), rabbit anti-human SMAD2 (Cell Signaling, # 5339) and rabbit anti-human Phospho-SMAD2 (Ser465/467) (Cell Signaling, #3108), were diluted in 5% BSA in PBS (PBS-BSA) at v: v = 1:1000; endogenous control, mouse anti-human GAPDH (Abcam, ab9484) and mouse anti-human γ-tubulin (Sigma, T6557) diluted in PBS-BSA at v: v = 1:3000. Secondary antibodies polyclonal rabbit anti-mouse-HRP (Dako, P0260) and polyclonal swine anti-mouse-HRP (Dako, P0217) were diluted in 5% non-fat milk in PBS at v: v = 1:2000.

2.8. Statistical analysis

Statistical analyses were performed using the IBM SPSS statistics software, version 20. One-sample Wilcoxon test versus '1' was used to determine the difference of CD146 expression upon treatment with shSMADs and inhibitors. One-way analysis of variance (ANOVA) was used to determine the differences between two groups with Bonferroni (homogeneity variance) or Dunnett T3 (non-homogeneity variance) post-hoc testing. $p < 0.05$ was considered statistically significant.

3. Results

3.1. CD146 knockdown impairs the contractility of human AF cells

To evaluate the role of CD146 in cell contractility, shCD146 lentivirus was used to silence *CD146* in human AF cells cultured with basal and TGF-β media. Transfection efficiency was estimated to be more than 50% using fluorescence microscope (Supporting Information Data 1). Cell viability, evaluated by Alamar Blue Assay, was decreased after transfection with lentivirus, but no differences were observed between scramble and shCD146 (Supporting Information Data 2).

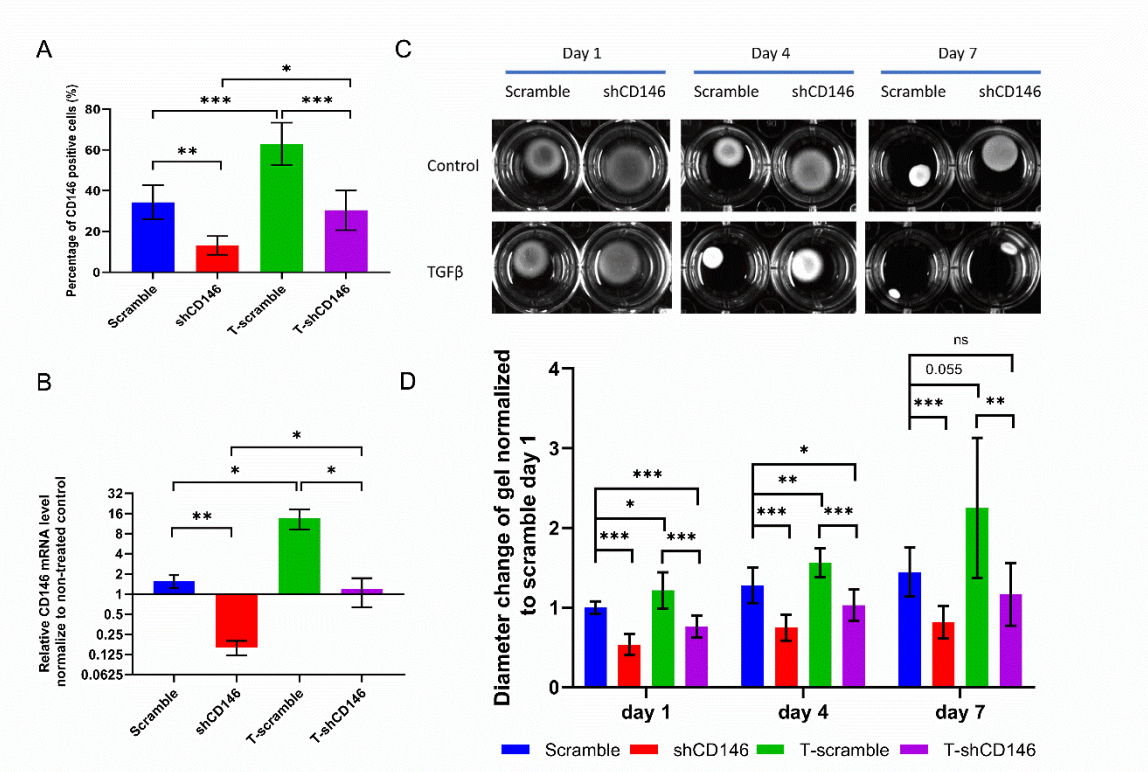

Figure 1. Cell contractility assay performed in CD146 knockdown AF cells.

*CD146 was knocked down by shCD146 transfection, scramble served as control, and cultured with basal medium (Scramble, shCD146) or TGF-β medium (T-scramble, T-shCD146). (A) Percentage of CD146+ cells and (B) mRNA expression level normalized to cells which were non-transfected and cultured with basal medium (Scramble, shCD146) or TGF-β medium (T-scramble, T-shCD146). Mean ± SD, n = 5. (C, D) Cell contractility assay performed in collagen Type I gels in three donors with four replicates after CD146 knockdown. (C) Macroscopic images of gels, (D) quantified diameter change of gels normalized to Day 1 Scramble (Mean ± SD, n = 12). Statistical analysis performed using one-way ANOVA with Bonferroni (homogeneity variance) or Dunnett T3 (non-homogeneity variance) post-hoc testing. AF, annulus fibrosus; ANOVA, analysis of variance; TGF-β, transforming growth factor-beta. *p < 0.05, **p < 0.01, ***p < 0.001.*

As shown in Figure 1A, the percentage of CD146⁺ cells was upregulated by TGF-β ($p < 0.001$), and it was significantly decreased by shCD146 when cultured with ($p < 0.001$) and without TGF-β ($p < 0.01$) compared with scramble. Likewise, the relative *CD146* mRNA expression levels in shCD146-treated cells was significantly downregulated when compared with scramble in basal ($p < 0.01$) and TGF-β ($p < 0.05$) media (Figure 1B). Altogether, these results confirm shCD146-mediated knockdown of CD146 at the gene and protein level in both baseline expression and TGF-β- induced upregulation.

Cell contractility assay was performed in three donors and measured at different timepoints. As shown in Figure 1C, D, the gels contracted with time, and this contraction was enhanced by TGF-β (Day 1 $p < 0.05$, Day 4 $p < 0.01$, Day 7 $p = 0.055$). Interestingly, this contraction was inhibited

by shCD146 independently of time. The diameter change was significantly smaller in shCD146 compared with scrambled shRNA with (Day 1 $p < 0.001$, Day 4 $p < 0.001$, Day 7 $p < 0.01$) or without (Day 1, Day 4, and Day 7, $p < 0.001$) TGF-β at each time point.

3.2. CD146 is associated with the expression of AF marker genes

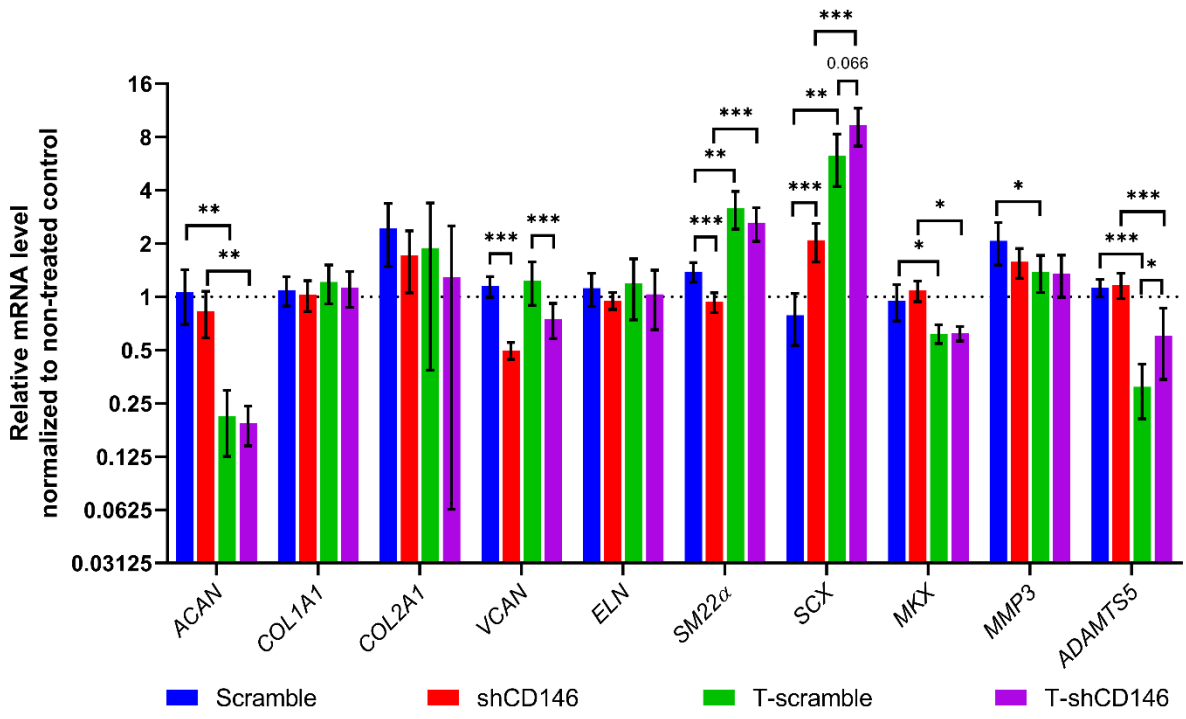

Figure 2. Gene expression of AF cells after CD146 silencing.

*Relative mRNA expression of AF cells transfected with shCD146, scrambled shRNA as control, and cultured with basal medium (Scramble, shCD146) or medium containing TGF-β (T-scramble, T-shCD146) in three donors. Data were normalized to expression level of cells which were non-transfected and cultured with basal medium. Statistical analysis performed using one-way ANOVA with Bonferroni (homogeneity variance) or Dunnett T3 (non-homogeneity variance) post hoc testing. Mean ± SD, n = 8. AF, annulus fibrosus; ANOVA, analysis of variance; TGF-β, transforming growth factor-beta. *p < 0.05, **p < 0.01, ***p < 0.001.*

Several genes that are associated with AF function and phenotype were evaluated after *CD146* silencing, including ECM genes (*ACAN*, *COL1A1*, *COL2A1*, *VCAN*, *ELN*), catabolic genes of ECM (*MMP3*, *ADAMTS5)*, and tendon/ligaments-related genes (*SM22α*, *SCX* and *MKX)* (Figure 2). In AF cells treated with TGF-β and scramble shRNA, *SM22α* ($p < 0.01$) and *SCX* ($p < 0.01$) were significantly upregulated, and *ACAN* ($p < 0.01$), *MKX* ($p < 0.05$), *MMP3* ($p < 0.05$) and *ADAMTS5* ($p < 0.001$) were significantly downregulated compared to non-treated controls. The expression level of *VCAN* was significantly decreased by shCD146 in absence ($p < 0.001$) and presence ($p < 0.001$) of TGF-β compared with scramble. *SM22α* was downregulated by shCD146 in absence ($p < 0.001$), but not in the presence of TGF-β. However, the expression of *SCX* was significantly

upregulated by shCD146 in absence ($p < 0.001$) of TGF-β, but not significant in presence ($p = 0.066$) of TGF-β. *ADAMTS5* was upregulated by shCD146 compared with scramble in the presence of TGF-β ($p < 0.05$).

3.3. Investigation on signaling pathways of TGF-β induced CD146 upregulation

The above-mentioned results show that TGF-β treatment induced CD146 upregulation in human AF cells. However, the underlying mechanism is not known yet. TGF-β signaling pathways generally include SMAD pathways and non-SMAD pathways, also known as canonical and non-canonical pathways. In this study, we studied the TGF-β-induced signaling cascade employing the inhibitor targeting TGF-β receptor type I, activin receptor-like kinases 5 (ALK5). Furthermore, inhibition of SMAD pathways was performed using SMAD3 inhibitor and shRNA targeting *SMAD1*, *SMAD2* and *SMAD4*. Inhibitors targeting AKT, ERT, P38, JNK, and ROCK were also utilized to block non-SMAD pathways.

3.3.1. TGF-β upregulates CD146 via TGF-β receptor type I, ALK5

When treated with iALK5 the percentage of $CD146^+$ AF cells was significantly decreased in basal medium ($p < 0.05$) and TGF-β medium ($p < 0.05$) compared with non-treated control (Figure 3A, 3B). The mRNA level of *CD146* was significantly reduced by iALK5 in TGF-β medium ($p < 0.05$), but not in basal medium ($p = 0.075$) compared to non-treated control (Figure 3B). These results indicate that TGF-β induced CD146 upregulation is ALK5 dependent.

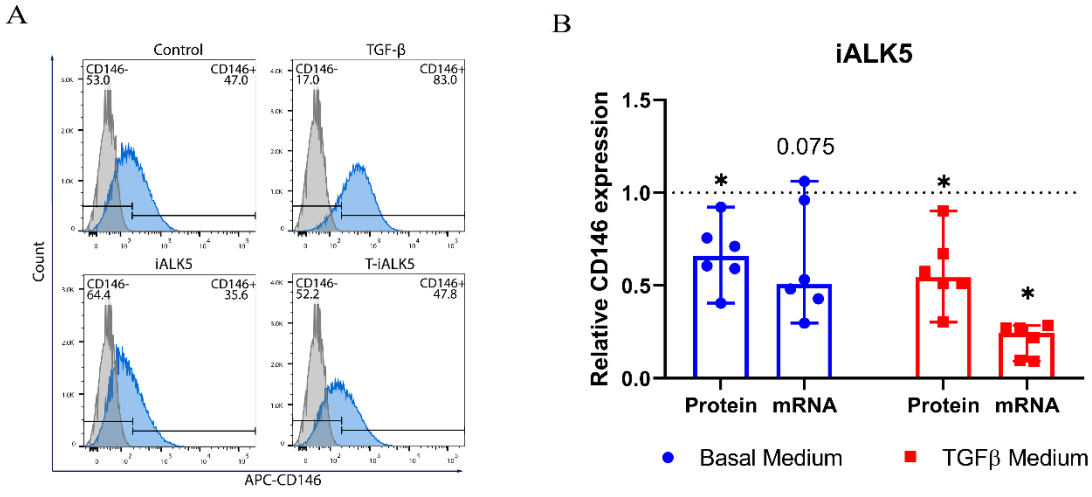

Figure 3. Expression of CD146 after treatment with TGF-β receptor type I (ALK5) inhibitor.

*ALK5 was blocked using a specific inhibitor and cultured with basal medium (Control, iALK5) or TGF-β medium (TGF-β, T-iALK5). (A) The percentage of $CD146^+$ cells (protein) was measured by flow cytometry. (B) CD146 mRNA level was analyzed by qRT-PCR. Results were normalized to nontreated control in basal and TGF-β medium separately. Statistical analysis performed by using one-sample Wilcoxon versus "1". Median with 95% CI, n = 6, *p < 0.05. qRT-PCR, quantitative real-time polymerase chain reaction; TGF-β, transforming growth factor-beta.*

3.3.2. TGF-β upregulates CD146 partially via SMAD4- SMAD2 pathways

AF cells were transfected with shSMAD2 and shSMAD4, whereby the transfection efficiency was more than 50% (Supplementary figure 1). Cell viability was decreased by transfection, but less affected by shSMAD4 compared with scramble (Supplementary figure 2). SMAD2 and SMAD4 were significantly down-regulated by shSMAD2 and shSMAD4, respectively, at both the protein (Figure 4A) and mRNA level ($p < 0.001$) (Figure 4B). The phosphorylation of SMAD2 was also down-regulated by shSMAD2 in medium with or without TGF-β (Figure 4A). Knockdown of *SMAD2* reduced *CD146* expression, as indicated by lower percentage of $CD146^+$ cells and *CD146* mRNA level in basal and TGF-β media compared to scramble ($p < 0.05$) (Figure 4C, 4D). Knockdown of *SMAD4* led to lower percentage of $CD146^+$ cells, decreased *CD146* expression in basal condition compared to scramble ($p < 0.05$), lower percentage of $CD146^+$ cells ($P< 0.05$), but not change of mRNA level in TGF-β condition compared to scramble. Simultaneous knockdown of *SMAD2* and *SMAD4* was performed in two independent donors. However, there was no further reduction in expression of *CD146* compared with individual knockdown (Supplementary figure 3). Cells were also treated with SMAD3 inhibitor or transfected with shSMAD1, which did not show any inhibition of TGF-β-induced *CD146* upregulation (Supplementary figure 4). Taken together, TGF-β highly upregulated *CD146*, as indicated by increased percentage of $CD146^+$ cells and *CD146* gene expression in human AF cells. This upregulation was partly neutralized by blocking SMAD4-SMAD2 pathways. However, there was no effect when blocking SMAD3 or SMAD1. These results indicate that TGF-β, if at all, only partially upregulates CD146 via SMAD4-SMAD2 pathways.

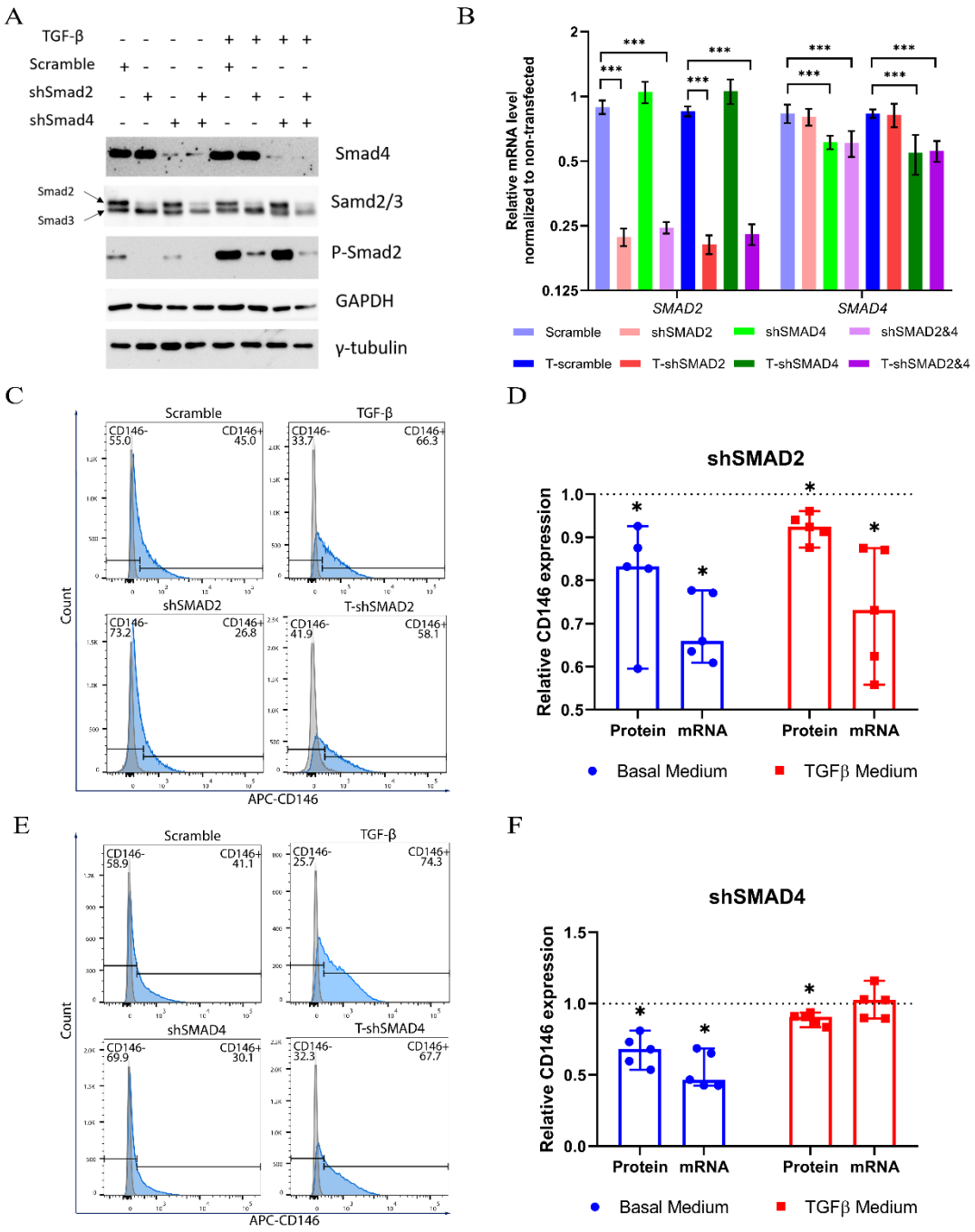

Figure 4. Expression of CD146 after blocking SMAD4-SMAD2 pathway.

SMAD2 and SMAD4 were knocked down by shSMAD2 or/and shSMAD4 transfection, scramble as control, and cultured with basal (Scramble, shSMAD2, shSMAD4, shSMAD2&4) or TGF-β medium (T-Scramble, T-shSMAD2, T-shSMAD4, T shSMAD2&4). (A) The protein level of SMAD4, SMAD2/3, and P-SMAD2 (phosphorylation of SMAD2) examined by Western Blot. (B) The mRNA expression of SMAD2 and SMAD4 measured by qRT-PCR (mRNA was normalized to expression level of cells which were non-transfected control), statistical analysis performed by using one-way ANOVA with Bonferroni (homogeneity variance)

*or Dunnett T3 (non-homogeneity variance) post hoc testing. Mean ± SD, n = 6, ***p < 0.001. (C, E) The percentage of CD146^{+} cells (protein) measured by flow cytometry after knockdown SMAD2 and SMAD4. (D, F) CD146 mRNA level analyzed by qRT-PCR after knockdown SMAD2 and SMAD4. Results were normalized to scramble in basal and TGF-β media separately. Statistical analysis performed by using one-sample Wilcoxon test versus "1". Median with 95% CI, n = 5, *p < 0.05. ANOVA, analysis of variance; qRT-PCR, quantitative real-time polymerase chain reaction; TGF-β, transforming growth factor-beta.*

3.3.3. The AKT and ERK pathways play roles in regulation of CD146 expression

AF cells were treated with non-SMAD signaling pathway inhibitors in media supplemented with or without TGF-β. Inhibitors targeting ROCK, p38 and JNK did not show any regulatory effect on the TGF-β-induced upregulation of *CD146* (Supplementary figure 4). When treated with AKT inhibitor, the percentage of CD146^{+} cells and *CD146* mRNA showed a decrease in basal medium and TGF-β medium compared to non-treated control ($p < 0.05$) (Figure 5A, 5B). Interestingly, the percentage of CD146^{+} cells significantly increased when cells were treated with ERK inhibitor in basal medium ($p < 0.05$), and the same trend was observed in TGF-β medium ($p < 0.05$) (Figure 5C, 5D). The *CD146* mRNA level was comparable between iERK-treated and non-treated groups cultured with both media (Figure 5D). These results indicate that AKT and ERK signaling pathways may play a role in the regulation of *CD146* expression in baseline and TGF-β-induced upregulation, whereby AKT may be a positive modulator, while ERK may be a negative modulator.

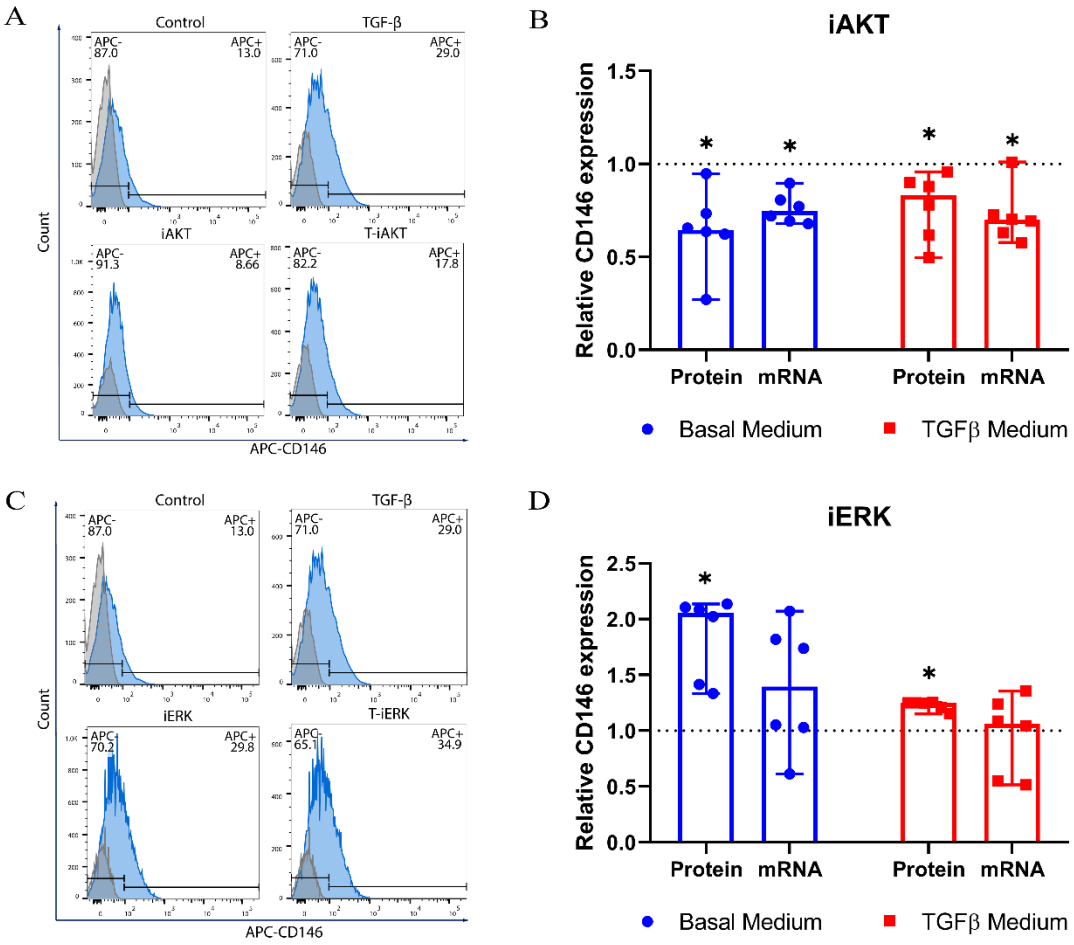

Figure 5. Expression of CD146 after blocking AKT and ERK pathways.

*The percentage of CD146$^+$ cells and the CD146 mRNA level of AF cells treated with (A, B) AKT and (C, D) ERK inhibitors and cultured with basal medium (Control, iAKT, iERK) or TGF-β medium (TGF-β, T-iAKT, T-iERK). (A,C) The percentage of CD146 + cells (protein) was measured by flow cytometry. (B, D) CD146 mRNA level was analyzed by qRT-PCR. Results were normalized to nontreated control in basal and TGF-β medium separately. Statistical analysis performed by using one-sample Wilcoxon versus "1". Median with 95% CI, n = 6, *p < 0.05. TGF-β, transforming growth factor-beta.*

4. Discussion

In the current study, we evaluated the role of CD146 in human AF cells, and partly elucidated the mechanisms underlying TGF-β mediated upregulation of CD146. Our results showed that CD146 was required for contractility of human AF cells. Knockdown of CD146 impaired cell contractility in collagen I hydrogel, which is the major component of AF ECM. These results indicated that CD146 may be a modulator of cell-matrix interaction in AF and a potential marker for AF tissue engineering; self-assembly of aligned tissue-engineered annulus fibrosus composite via collagen gel contraction could be used to create a mechanically functional tissue-engineered IVD [38]. Also in vascular smooth muscle cells, enhanced contractility and mobility mediated by SM22a, was

crucial for maintaining their differentiated phenotype [39]. In a previous study, $CD146^+$ AF cells showed better contractility and higher expression of SM22α and elastin in mouse [10]. In line with these results, we showed that CD146 knockdown caused downregulation of *SM22α*, albeit not of elastin, in human AF cells. This suggests that CD146 contributes to the development of a contractile phenotype by upregulating *SM22α*, but not elastin in human AF cells.

CD146 can also be implicated in ECM remodeling. VCAN, a large proteoglycan presents in ECM and expressed in both NP and AF, has been shown to be elevated at early stages of degeneration and to decrease in severely degenerated tissues [40]. The mRNA expression of *VCAN* was decreased by *CD146* silencing which indicates that *CD146* may be a positive modulator of *VCAN*. Interestingly, when *CD146* was upregulated by TGF-β, *VCAN* was not. These results indicate that the expression of *VCAN* may not be only CD146-dependent. Furthermore, TGF-β led to a reduction of *ADAMTS5* expression, and this effect was partly neutralized by *CD146* knockdown. These findings indicate a potential role of CD146 in ECM turnover and AF contractility, although the contribution of proteoglycans to the ECM in the hydrogel was likely limited.

Blocking *CD146* expression increased the TGF-β-dependent and independent expression of *SCX*, pointing toward an interaction between *CD146* and *SCX*. SCX is a marker of tendon and ligaments cells and deletion of SCX leads to severely hypoplastic long-range tendons, and causes defective maturation of tendons, ligaments, and the outer AF [41-43]. In tendon, SCX plays important roles in progenitor cell proliferation, tenogenic differentiation, and maturation [44, 45], while CD146 is a maker of progenitor cells with powerful capability for tendon regeneration [44, 46]. A recent study showed that the loss of regeneration potential of AF cells in adult mice is accompanied with lower SCX expression compared with neonatal mice [47]. $CD146^+$ AF cells showed comparable multiple differentiation potential and weaker cell proliferation capacity than $CD146^-$ AF cells [10]. Altogether, in tendon progenitor cells, the expression of *SCX* and *CD146* indicates a potential for tendon regeneration; while in AF cells, the expression of *SCX* may suggest a stem cell probability, and the expression of *CD146* may indicate a mature AF cells phenotype. The phenotype induced by TGF-β with upregulation of *SCX* and *CD146* tend to be a mature differentiated cell type in cultured AF cells, namely, TGF-β maintains differentiation of AF cells during *in vitro* expansion. Hereby, we report for the first time *SCX* expression is regulated by *CD146*. Whether this regulation is related to differentiation and regeneration of tendon and AF needs further investigation.

Altogether these findings indicate that CD146 may be involved in AF function. The expression of CD146 is known to be regulated by several factors, including proinflammatory factors and growth factors, such as tumor necrosis factor alpha (TNF-α) [48], interleukin -13 (IL-13) [49], TGF-β1, or bone morphogenetic protein 4 (BMP-4) [28]. Our results showed the upregulation of CD146 by TGF-signaling in human AF cells was partially mediated by ALK5. ALK5 is one of the TGF-β type I receptors which propagates the extracellular signals with TGF-β type II receptor via phosphorylation of mediators, and activation of SMAD and non-SMAD signaling pathways [50, 51]. ALK5 can mediate TGF-β signaling by activating Smad2/3 in most cell types, while in endothelial cells ALK1 activates Smad1/5/8 for TGF-β signaling [52, 53]. In the current study, CD146 expression by AF cells in baseline and TGF-β-induced upregulation was modulated via ALK5- SMAD2/4 cascade, but SMAD3 and SMAD1 seem not to be involved.

Besides the SMAD pathways, non-SMAD pathways play an important role in TGF-β signaling. Here we showed that TGF-β may upregulate CD146 via AKT, rather than the JNK, p38 or ROCK pathways. Previous studies showed endothelin-3 promoted CD146 expression via PI3K/AKT in melanocytes [29], and PI3K/AKT and c-Raf/MEK/ERK positively regulated CD146 via inhibition of its ubiquitination and degradation in hepatoma cell [30]. Interestingly, in the present study, inhibition of the ERK pathway upregulated CD146 in human AF cells. Further investigation is needed to clarify the dual function of ERK in the regulation of CD146.

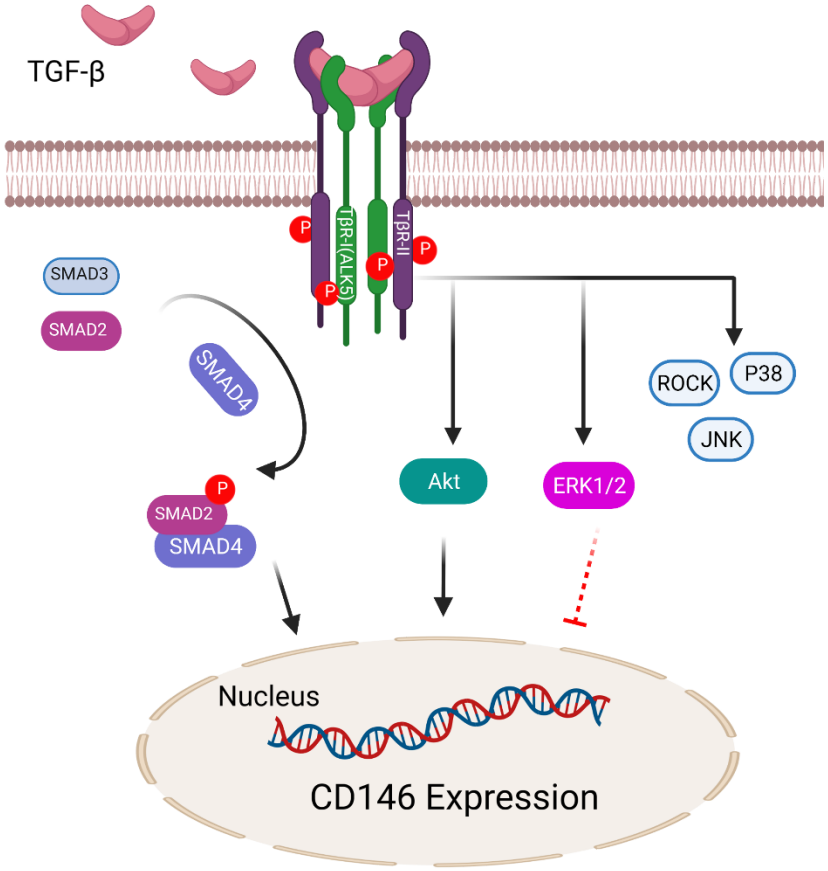

Figure 6. Conceptual model of signaling pathways of TGF-β-induced CD146 upregulation.

TGF-β upregulate CD146 via TGF type I receptor, ALK5, and cascade canonical pathway SMAD2 and SMAD4, not SMAD3, and noncanonical pathway AKT, but not ROCK, JNK, and P38. ERK1/2 is a negative modulator of CD146 expression in protein level but not mRNA level. Created with BioRender. com. TGF-β, transforming growth factor-beta.

The limitations of the current study remain in the following aspects: This study investigated the effect of CD146 only on cell contractility and AF functional gene expression. Therefore, the roles of CD146 in other biological functions, such as cell migration, proliferation, differentiation, inflammation, and 3D ECM production warrant further investigation. The roles of SMADs and non-SMAD pathways in modulation of CD146 expression were only investigated by using shRNAs or

inhibitors to eliminate the function of candidate pathways. It may be necessary to confirm our finding by overexpression of those key factors. So far, all studies of $CD146^+$ cells for AF tissue engineering were performed *in vitro,* hence further *in vivo* studies are needed.

In conclusion, CD146 expression in AF cells was significantly upregulated by TGF-β1 *in vitro*, a growth factor known to support the reparative capacity of AF cells. CD146 is crucial to maintain the AF cell phenotype, by regulating several AF markers and cell contractility. Additionally, the present study demonstrated that the TGF-β induced CD146 expression in human AF cells, involves ALK5, SMAD2/4 and AKT signaling, and that ERK may be a negative modulator (Figure 6). Altogether, the findings from this study indicate that CD146 is a biomarker of functional AF cells and its regulation by TGF-β involves several pathways.

Acknowledgments:

This research was funded by AO Foundation, AOSpine International, and European Union's Horizon2020 research and innovation programme under Marie Sklodowska-Curie Grant Agreement No 801540 (RESCUE). L.B.C. and M.A.T. are supported by funding from the Dutch Arthritis Society (LLP12 and LLP22, respectively).

Author contributions:

Mauro Alini, Sibylle Grad, Laura B. Creemers, and Zhen Li contributed to the study design, Jie Du performed the experiments and wrote the manuscript, Wei Guo, Sonja Häckel, and Sven Hoppe helped with the experimental work. Marianna A. Tryfonidou, João P. Garcia, Laura B. Creemers, Sibylle Grad, Zhen Li, Wei Guo, and Sonja Häckel contributed to manuscript revision. All authors read and approved the final manuscript.

Supplementary figures and tables

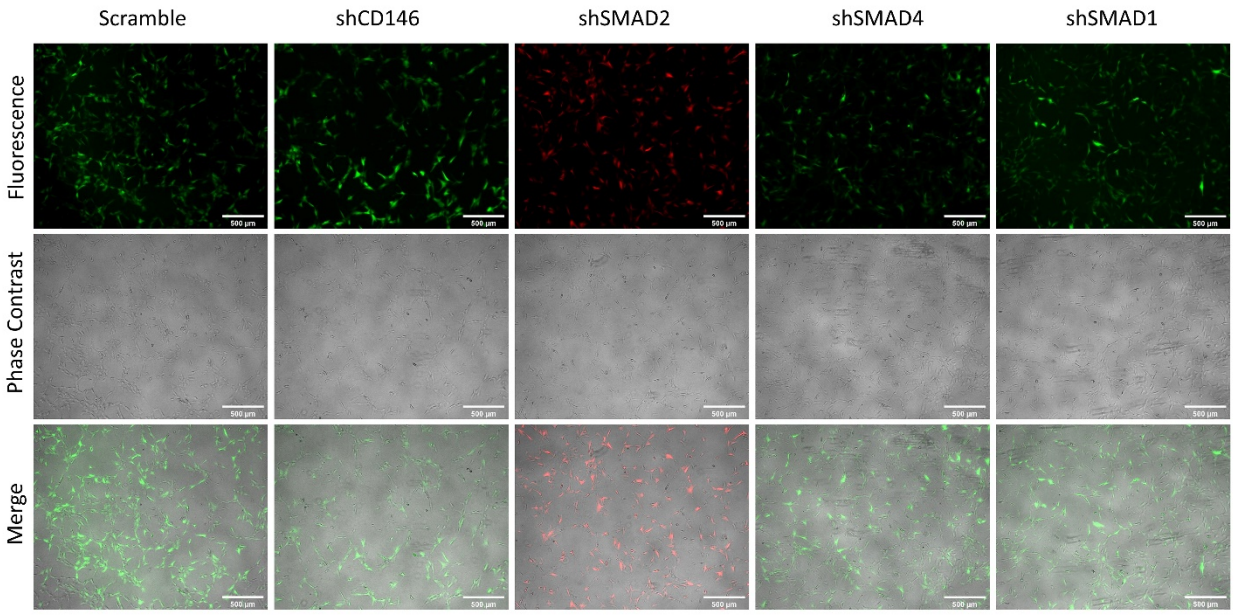

Supplementary figure 1. Transfection efficiency of shRNA lentiviruses at 72 hours after transfection of AF cells.

AF cells transfection with shRNA lentiviruses were performed in 6-well-plate, after a 24 hours transfection with shRNA viruses, cells were culture with basal medium for another 2 days, as described in methods. Images were captured on the EVOS FL Auto 2 Microscope (Thermo Scientific™ Invitrogen™). The transfection efficiency of each shRNA was more than 50%.

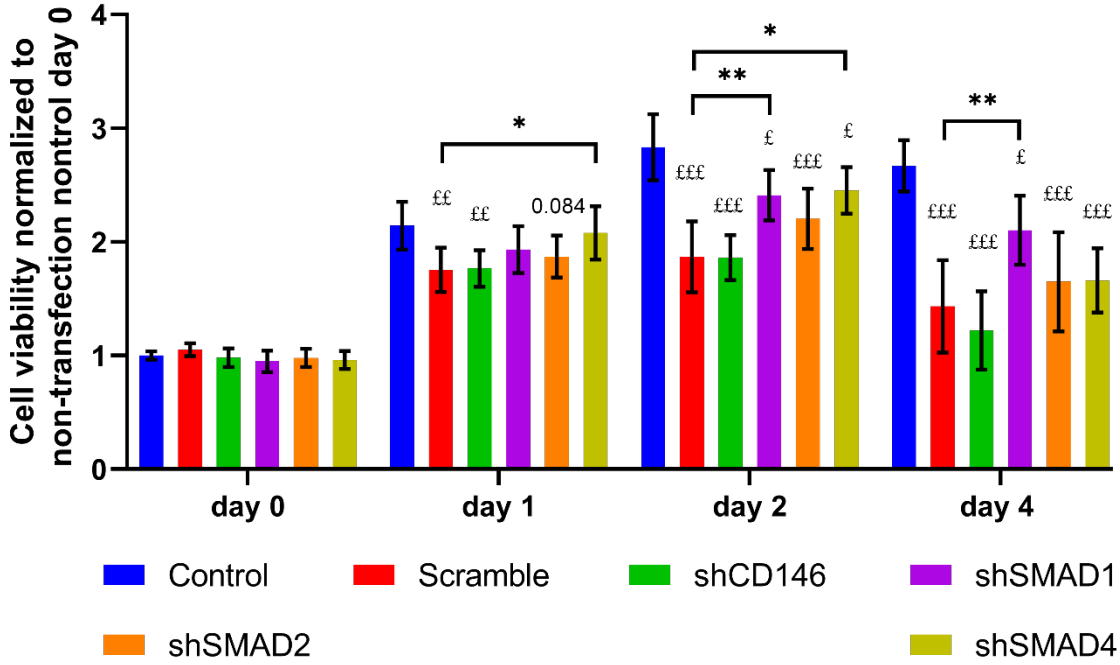

Supplementary figure 2. Cell viability after transfecting with shRNA lentivirus.

*Cell viability was measured by Alamar Blue Assay. Transfection was performed in 96-well plate, single cell and virus suspensions were prepared at a concentration of 1 × 10^5 cells/mL and 4 × 10^6 TU/mL respectively within transfection medium. Transfection was performed by mixing 50 µl single cell suspension and 50 µl virus suspension per well and incubated for 24 hours at hypoxia condition. Then transfection media were refreshed with culture medium. Cell viability was measured at day 0, day 1, day 2 and day 4 after transfection by adding 10 µl of resazurin sodium salt (Alfa Aesar, Germany) solution, 440 mM in PBS, then plate was incubated for 4 hours and fluorescence was measured at 544 nm excitation and 620 nm emission in Fluoroskan (Labsystems, Finland). Cell viability was normalized to non-transfected control. Statistical analysis performed using one-way ANOVA with Bonferroni post-hoc testing. Mean± SD, £ p< 0.05, ££ p< 0.01, £££ p< 0.001 vs non-transfected control; * p< 0.05, ** p< 0.01 vs Scramble.*

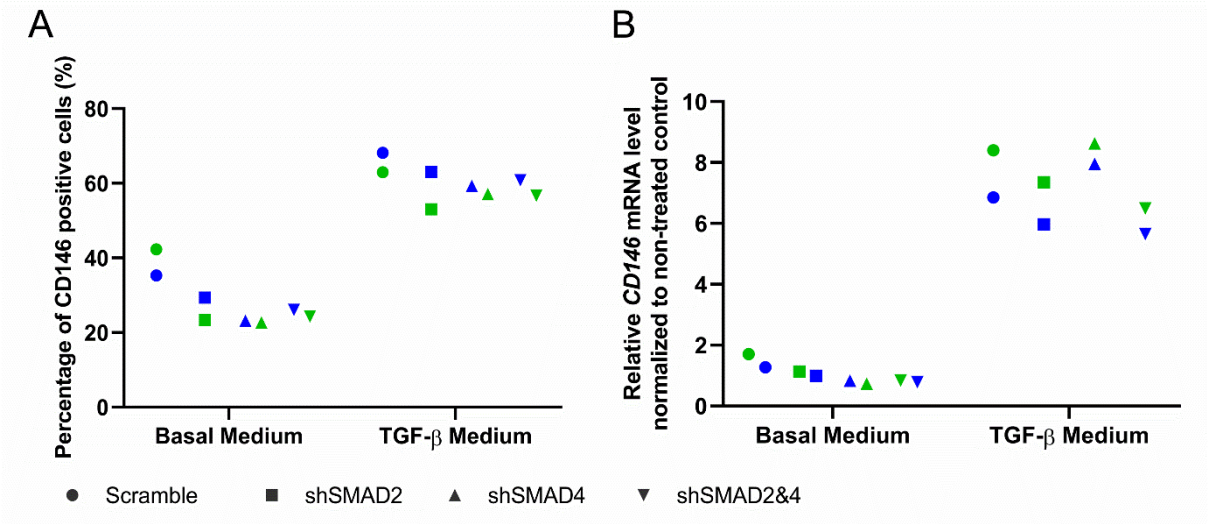

Supplementary figure 3. Expression of CD146 after blocking Smad2 and -4 together.

Smad2 and Smad4 were knocked down together in 2 independent donors cultured with basal or TGF-β medium. Scramble and knockdown separately served as control. ***A,*** *the percentage of CD146$^+$ cells was measured by flow cytometry and* ***B,*** *the CD146 mRNA level was analyzed by Q-PCR (mRNA was normalized to expression level of cells which were non-transfected and cultured with basal medium.). Two colors represented two donors.*

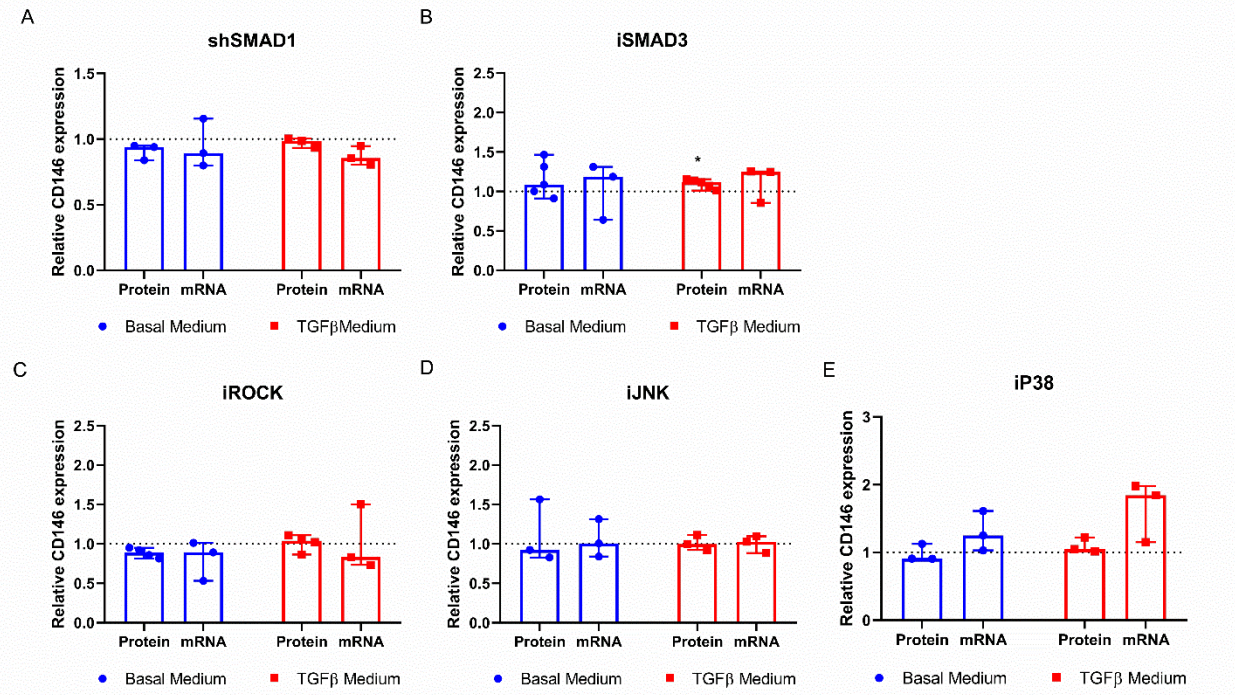

Supplementary figure 4. Expression of CD146 after blocking SMAD1, SMAD3, ROCK, JNK and p38.

A, *SMAD1 was knocked down by shSMAD1 transfection (shSMAD1),* ***B, C, D, E,*** *SMAD3, ROCK, JNK and p38 were blocked with specific inhibitors (iSAMD3, iROCK, iJNK, ip38) separately and cultured with basal medium or TGF-β medium. The percentage of CD146^{+} cells (protein) was measured by flow cytometry and CD146 mRNA level was analyzed by Q-PCR, results were normalized to scramble for shSMAD1 and non-treated for inhibitor treatment in basal medium and TGF-β medium separately. Statistical analysis performed using one-sample Wilcoxon vs '1'. Median with 95% CI, * P < 0.05.*

Supplementary table 1, AF cells donor information.

Tissue Resource	Age	Gender	Degeneration Level	IVD Position
Trauma patient	49	M	Pfirrmann Grade II	T12/L1
Trauma patient	34	M	Pfirrmann Grade II	T12/L1
Trauma patient	37	M	Pfirrmann Grade II	L3/4
Trauma patient	30	M		
Trauma patient	33	M	Pfirrmann Grade II	T12/L1
Trauma patient	21	M	Pfirrmann Grade I	L1/L2
Organ donor	61	F		
Organ donor	19	M	Pfirrmann Grade I	

References

[1] G.B.D. Disease, I. Injury, C. Prevalence, Global, regional, and national incidence, prevalence, and years lived with disability for 328 diseases and injuries for 195 countries, 1990-2016: a systematic analysis for the Global Burden of Disease Study 2016, Lancet 390(10100) (2017) 1211-1259.
[2] J.C. Iatridis, A.J. Michalek, D. Purmessur, C.L. Korecki, Localized Intervertebral Disc Injury Leads to Organ Level Changes in Structure, Cellularity, and Biosynthesis, Cell Mol Bioeng 2(3) (2009) 437-447.
[3] D. Alexeev, S. Cui, S. Grad, Z. Li, S.J. Ferguson, Mechanical and biological characterization of a composite annulus fibrosus repair strategy in an endplate delamination model, JOR spine n/a(n/a) (2020) e1107.
[4] E.J. Carragee, M.Y. Han, P.W. Suen, D. Kim, Clinical outcomes after lumbar discectomy for sciatica: the effects of fragment type and anular competence, J Bone Joint Surg Am 85-A(1) (2003) 102-8.
[5] G.L. Ambrossi, M.J. McGirt, D.M. Sciubba, T.F. Witham, J.P. Wolinsky, Z.L. Gokaslan, D.M. Long, Recurrent lumbar disc herniation after single-level lumbar discectomy: incidence and health care cost analysis, Neurosurgery 65(3) (2009) 574-8; discussion 578.
[6] J.S. Smith, A.T. Ogden, S. Shafizadeh, R.G. Fessler, Clinical outcomes after microendoscopic discectomy for recurrent lumbar disc herniation, J Spinal Disord Tech 23(1) (2010) 30-4.
[7] C.C. Guterl, E.Y. See, S.B. Blanquer, A. Pandit, S.J. Ferguson, L.M. Benneker, D.W. Grijpma, D. Sakai, D. Eglin, M. Alini, J.C. Iatridis, S. Grad, Challenges and strategies in the repair of ruptured annulus fibrosus, Eur Cell Mater 25 (2013) 1-21.
[8] N.L. Nerurkar, D.M. Elliott, R.L. Mauck, Mechanics of oriented electrospun nanofibrous scaffolds for annulus fibrosus tissue engineering, J Orthop Res 25(8) (2007) 1018-28.
[9] T.R. Christiani, E. Baroncini, J. Stanzione, A.J. Vernengo, In vitro evaluation of 3D printed polycaprolactone scaffolds with angle-ply architecture for annulus fibrosus tissue engineering, Regen Biomater 6(3) (2019) 175-184.
[10] T. Nakai, D. Sakai, Y. Nakamura, T. Nukaga, S. Grad, Z. Li, M. Alini, D. Chan, K. Masuda, K. Ando, J. Mochida, M. Watanabe, CD146 defines commitment of cultured annulus fibrosus cells to express a contractile phenotype, J Orthop Res 34(8) (2016) 1361-72.
[11] Y. Takeoka, T. Yurube, K. Morimoto, S. Kunii, Y. Kanda, R. Tsujimoto, Y. Kawakami, N. Fukase, T. Takemori, K. Omae, Y. Kakiuchi, S. Miyazaki, K. Kakutani, T. Takada, K. Nishida, M. Fukushima, R. Kuroda, Reduced nucleotomy-induced intervertebral disc disruption through spontaneous spheroid formation by the Low Adhesive Scaffold Collagen (LASCol), Biomaterials 235 (2020) 119781.
[12] A.K. Schubert, J.J. Smink, M. Arp, J. Ringe, A.A. Hegewald, M. Sittinger, Quality Assessment of Surgical Disc Samples Discriminates Human Annulus Fibrosus and Nucleus Pulposus on Tissue and Molecular Level, Int J Mol Sci 19(6) (2018).
[13] J.M. Lehmann, B. Holzmann, E.W. Breitbart, P. Schmiegelow, G. Riethmuller, J.P. Johnson, Discrimination between benign and malignant cells of melanocytic lineage by two novel antigens, a glycoprotein with a molecular weight of 113,000 and a protein with a molecular weight of 76,000, Cancer Res 47(3) (1987) 841-5.
[14] M. Trzpis, P.M. McLaughlin, L.M. de Leij, M.C. Harmsen, Epithelial cell adhesion molecule: more than a carcinoma marker and adhesion molecule, Am J Pathol 171(2) (2007) 386-95.
[15] A.E. Aplin, A.K. Howe, R.L. Juliano, Cell adhesion molecules, signal transduction and cell growth, Curr Opin Cell Biol 11(6) (1999) 737-44.
[16] Z. Wang, Q. Xu, N. Zhang, X. Du, G. Xu, X. Yan, CD146, from a melanoma cell adhesion molecule to a signaling receptor, Signal Transduct Target Ther 5(1) (2020) 148.
[17] N. Bardin, F. George, M. Mutin, C. Brisson, N. Horschowski, V. Frances, G. Lesaule, J. Sampol, S-Endo 1, a pan-endothelial monoclonal antibody recognizing a novel human endothelial antigen, Tissue Antigens 48(5) (1996) 531-9.

[18] N. Bardin, F. Anfosso, J.M. Masse, E. Cramer, F. Sabatier, A. Le Bivic, J. Sampol, F. Dignat-George, Identification of CD146 as a component of the endothelial junction involved in the control of cell-cell cohesion, Blood 98(13) (2001) 3677-84.
[19] W.F. Pickl, O. Majdic, G.F. Fischer, P. Petzelbauer, I. Fae, M. Waclavicek, J. Stockl, C. Scheinecker, T. Vidicki, H. Aschauer, J.P. Johnson, W. Knapp, MUC18/MCAM (CD146), an activation antigen of human T lymphocytes, J Immunol 158(5) (1997) 2107-15.
[20] N. Espagnolle, F. Guilloton, F. Deschaseaux, M. Gadelorge, L. Sensebe, P. Bourin, CD146 expression on mesenchymal stem cells is associated with their vascular smooth muscle commitment, J Cell Mol Med 18(1) (2014) 104-14.
[21] L. Harkness, W. Zaher, N. Ditzel, A. Isa, M. Kassem, CD146/MCAM defines functionality of human bone marrow stromal stem cell populations, Stem Cell Res Ther 7 (2016) 4.
[22] A.S. Leroyer, M.G. Blin, R. Bachelier, N. Bardin, M. Blot-Chabaud, F. Dignat-George, CD146 (Cluster of Differentiation 146), Arterioscler Thromb Vasc Biol 39(6) (2019) 1026-1033.
[23] G. Zabouo, A.M. Imbert, J. Jacquemier, P. Finetti, T. Moreau, B. Esterni, D. Birnbaum, F. Bertucci, C. Chabannon, CD146 expression is associated with a poor prognosis in human breast tumors and with enhanced motility in breast cancer cell lines, Breast Cancer Res 11(1) (2009) R1.
[24] X. Zhang, Z. Wang, Y. Kang, X. Li, X. Ma, L. Ma, MCAM expression is associated with poor prognosis in non-small cell lung cancer, Clin Transl Oncol 16(2) (2014) 178-83.
[25] A. Onisim, C. Vlad, I. Simon, C. Dina, P. Achimas Cadariu, The role of CD146 in serous ovarian carcinoma, J BUON 24(3) (2019) 1009-1019.
[26] J. Du, R.G. Long, T. Nakai, D. Sakai, L.M. Benneker, G. Zhou, B. Li, D. Eglin, J.C. Iatridis, M. Alini, S. Grad, Z. Li, Functional cell phenotype induction with TGF-beta1 and collagen-polyurethane scaffold for annulus fibrosus rupture repair, Eur Cell Mater 39 (2020) 1-17.
[27] H. Yang, L. Zhang, S.M. Weakley, P.H. Lin, Q. Yao, C. Chen, Transforming growth factor-beta increases the expression of vascular smooth muscle cell markers in human multi-lineage progenitor cells, Med Sci Monit 17(3) (2011) BR55-61.
[28] Y. Ma, H. Zhang, C. Xiong, Z. Liu, Q. Xu, J. Feng, J. Zhang, Z. Wang, X. Yan, CD146 mediates an E-cadherin-to-N-cadherin switch during TGF-beta signaling-induced epithelial-mesenchymal transition, Cancer Lett 430 (2018) 201-214.
[29] B. Williams, R.J. Schneider, S. Jamal, Akt and PI3K-dependent but CREB-independent upregulation of MCAM by endothelin-3 in human melanocytes, Melanoma Res 24(4) (2014) 404-7.
[30] X. Tang, X. Chen, Y. Xu, Y. Qiao, X. Zhang, Y. Wang, Y. Guan, F. Sun, J. Wang, CD166 positively regulates MCAM via inhibition to ubiquitin E3 ligases Smurf1 and betaTrCP through PI3K/AKT and c-Raf/MEK/ERK signaling in Bel-7402 hepatocellular carcinoma cells, Cell Signal 27(9) (2015) 1694-702.
[31] D. Ercan, C. Xu, M. Yanagita, C.S. Monast, C.A. Pratilas, J. Montero, M. Butaney, T. Shimamura, L. Sholl, E.V. Ivanova, M. Tadi, A. Rogers, C. Repellin, M. Capelletti, O. Maertens, E.M. Goetz, A. Letai, L.A. Garraway, M.J. Lazzara, N. Rosen, N.S. Gray, K.K. Wong, P.A. Janne, Reactivation of ERK signaling causes resistance to EGFR kinase inhibitors, Cancer Discov 2(10) (2012) 934-47.
[32] E.M. Alzayadneh, M.C. Chappell, Angiotensin-(1-7) abolishes AGE-induced cellular hypertrophy and myofibroblast transformation via inhibition of ERK1/2, Cell Signal 26(12) (2014) 3027-35.
[33] Y. Kuma, G. Sabio, J. Bain, N. Shpiro, R. Marquez, A. Cuenda, BIRB796 inhibits all p38 MAPK isoforms in vitro and in vivo, J Biol Chem 280(20) (2005) 19472-9.
[34] N. Chen, W. Fang, J. Zhan, S. Hong, Y. Tang, S. Kang, Y. Zhang, X. He, T. Zhou, T. Qin, Y. Huang, X. Yi, L. Zhang, Upregulation of PD-L1 by EGFR Activation Mediates the Immune Escape in EGFR-Driven NSCLC: Implication for Optional Immune Targeted Therapy for NSCLC Patients with EGFR Mutation, J Thorac Oncol 10(6) (2015) 910-23.

[35] J.M. Balko, L.J. Schwarz, N.E. Bhola, R. Kurupi, P. Owens, T.W. Miller, H. Gomez, R.S. Cook, C.L. Arteaga, Activation of MAPK pathways due to DUSP4 loss promotes cancer stem cell-like phenotypes in basal-like breast cancer, Cancer Res 73(20) (2013) 6346-58.
[36] M. Jinnin, H. Ihn, K. Tamaki, Characterization of SIS3, a novel specific inhibitor of Smad3, and its effect on transforming growth factor-beta1-induced extracellular matrix expression, Mol Pharmacol 69(2) (2006) 597-607.
[37] T. Nakahara, H. Moriuchi, M. Yunoki, K. Sakamato, K. Ishii, Y-27632 potentiates relaxant effects of beta 2-adrenoceptor agonists in bovine tracheal smooth muscle, Eur J Pharmacol 389(1) (2000) 103-6.
[38] R.D. Bowles, R.M. Williams, W.R. Zipfel, L.J. Bonassar, Self-assembly of aligned tissue-engineered annulus fibrosus and intervertebral disc composite via collagen gel contraction, Tissue Eng Part A 16(4) (2010) 1339-48.
[39] M. Han, L.H. Dong, B. Zheng, J.H. Shi, J.K. Wen, Y. Cheng, Smooth muscle 22 alpha maintains the differentiated phenotype of vascular smooth muscle cells by inducing filamentous actin bundling, Life Sci 84(13-14) (2009) 394-401.
[40] G. Cs-Szabo, D. Ragasa-San Juan, V. Turumella, K. Masuda, E.J. Thonar, H.S. An, Changes in mRNA and protein levels of proteoglycans of the anulus fibrosus and nucleus pulposus during intervertebral disc degeneration, Spine (Phila Pa 1976) 27(20) (2002) 2212-9.
[41] R. Schweitzer, J.H. Chyung, L.C. Murtaugh, A.E. Brent, V. Rosen, E.N. Olson, A. Lassar, C.J. Tabin, Analysis of the tendon cell fate using Scleraxis, a specific marker for tendons and ligaments, Development 128(19) (2001) 3855-66.
[42] N.D. Murchison, B.A. Price, D.A. Conner, D.R. Keene, E.N. Olson, C.J. Tabin, R. Schweitzer, Regulation of tendon differentiation by scleraxis distinguishes force-transmitting tendons from muscle-anchoring tendons, Development 134(14) (2007) 2697-708.
[43] Y. Yoshimoto, A. Takimoto, H. Watanabe, Y. Hiraki, G. Kondoh, C. Shukunami, Scleraxis is required for maturation of tissue domains for proper integration of the musculoskeletal system, Sci Rep 7 (2017) 45010.
[44] C.F. Hsieh, Z. Yan, R.G. Schumann, S. Milz, C.G. Pfeifer, M. Schieker, D. Docheva, In Vitro Comparison of 2D-Cell Culture and 3D-Cell Sheets of Scleraxis-Programmed Bone Marrow Derived Mesenchymal Stem Cells to Primary Tendon Stem/Progenitor Cells for Tendon Repair, Int J Mol Sci 19(8) (2018).
[45] J.P. Gumucio, M.M. Schonk, Y.A. Kharaz, E. Comerford, C.L. Mendias, Scleraxis is required for the growth of adult tendons in response to mechanical loading, JCI Insight 5(13) (2020).
[46] C.H. Lee, F.Y. Lee, S. Tarafder, K. Kao, Y. Jun, G. Yang, J.J. Mao, Harnessing endogenous stem/progenitor cells for tendon regeneration, J Clin Invest 125(7) (2015) 2690-701.
[47] O.M. Torre, V. Mroz, A.R.M. Benitez, A.H. Huang, J.C. Iatridis, Neonatal annulus fibrosus regeneration occurs via recruitment and proliferation of Scleraxis-lineage cells, NPJ Regen Med 4 (2019) 23.
[48] D.G. Belair, J.A. Whisler, J. Valdez, J. Velazquez, J.A. Molenda, V. Vickerman, R. Lewis, C. Daigh, T.D. Hansen, D.A. Mann, J.A. Thomson, L.G. Griffith, R.D. Kamm, M.P. Schwartz, W.L. Murphy, Human vascular tissue models formed from human induced pluripotent stem cell derived endothelial cells, Stem Cell Rev Rep 11(3) (2015) 511-25.
[49] G.C. Simon, R.J. Martin, S. Smith, J. Thaikoottathil, R.P. Bowler, S.J. Barenkamp, H.W. Chu, Up-regulation of MUC18 in airway epithelial cells by IL-13: implications in bacterial adherence, Am J Respir Cell Mol Biol 44(5) (2011) 606-13.
[50] C.S. Hill, Transcriptional Control by the SMADs, Cold Spring Harb Perspect Biol 8(10) (2016).
[51] Y.E. Zhang, Non-Smad Signaling Pathways of the TGF-beta Family, Cold Spring Harb Perspect Biol 9(2) (2017).
[52] F. Lebrin, M.J. Goumans, L. Jonker, R.L. Carvalho, G. Valdimarsdottir, M. Thorikay, C. Mummery, H.M. Arthur, P. ten Dijke, Endoglin promotes endothelial cell proliferation and TGF-beta/ALK1 signal transduction, EMBO J 23(20) (2004) 4018-28.

[53] X.H. Feng, R. Derynck, Specificity and versatility in tgf-beta signaling through Smads, Annu Rev Cell Dev Biol 21 (2005) 659-93.

Chapter 6

Drug Retention after Intradiscal Administration

Imke Rudnik-Jansen*, Jie Du*, Nina Woike, Anna R. Tellegen, Wadhwani, Parvesh, Daniele Zuncheddu, Björn P. Meij, Jens Thies, Pieter Emans, Fetullah C. Öner, George Mihov, Joao Pedro Garcia, Anne Ulrich, Sibylle Grad, Marianna A. Tryfonidou, Hugo van Ingen, Laura B. Creemers

Manuscript in preparation

Jie Du contributed to the study design, acquisition, analysis, interpretation of data, drafting, and revising of the manuscript.

* Imke Rudnik-Jansen and Jie Du contributed equally to this manuscript.

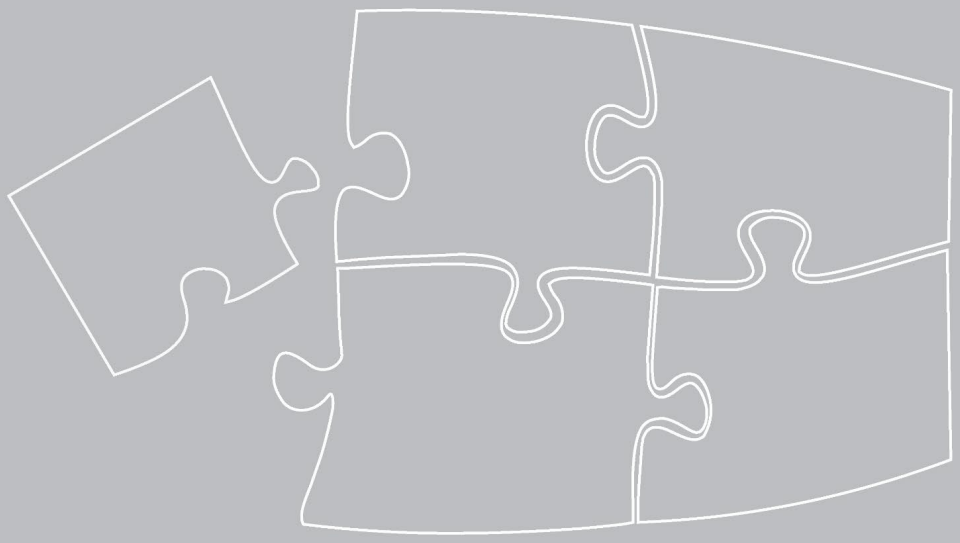

Abstract:

Intradiscal drug delivery is a promising strategy for treating intervertebral disc degeneration (IVDD). Local degenerative processes in the IVD, as well as the intrinsic low fluid exchange, are likely to influence drug retention, and understanding their connection will enable the optimization of IVDD therapeutics.

In the current study, local drug retention in the IVD was investigated using small molecular drug models involving the ^{19}fluorine (^{19}F) labeled peptide (^{19}F-P) and the near-infrared fluorescent dye IR-780 using *ex vivo* and *in vivo* models of IVDD. ^{19}F-P was injected into bovine caudal IVDs cultured in a dynamic loading bioreactor. For 7 days, ^{19}F-P release and retention were evaluated by measuring ^{19}F signal in culture media and IVD tissue extracts using nuclear magnetic resonance spectroscopy (NMRS). In addition, ^{19}F-P was intradiscally injected into healthy and degenerative sheep lumbar IVDs to assess the presence of ^{19}F-P three months after intradiscal injection. Noninvasive near-infrared imaging was used to visualize IR-780 retention upon injection in healthy and degenerative caudal IVDs in a rat model of disc degeneration. Furthermore, IR-780-loaded degradable polyester amide (PEA) microspheres were injected in healthy and degenerative caudal rat IVDs, subcutaneously, and knee joints with and without surgically-induced osteoarthritis.

The majority of ^{19}F-P was released from the IVD into the culture medium after 7 days. Also, *in vivo*, ^{19}F-P signal was lost three months after intradiscal injection from both degenerated and healthy IVDs. IR-780 signal intensity declined over a 14-week period after bolus injection, with no apparent difference between healthy and degenerative discs. IR-780 delivery by PEA microspheres enhanced disc retention over a 16-week period. Moreover, in degenerated IVDs the IR-780 signal was even higher than in healthy IVDs. In contrast, IR-780 signal declined faster in the subcutaneous area and knee joints compared to the IVDs, and no difference between OA and healthy joints was noted.

We conclude that the clearance of peptides and hydrophilic small drug molecules from the IVD is relatively fast when delivered without drug delivery system. The retention of hydrophilic small drug molecules within drug delivery microspheres is dependent on tissue location, most likely related to local clearance rates. Only in the IVD the disease state of the tissue affected the retention, suggesting an interaction between clearance and biomaterial degradation rate of microspheres or degeneration-induced changes in tissue diffusivity.

Keywords:

Drug retention, Peptide, Small molecule, Polyester amide microspheres, ^{19}Fluorine- nuclear magnetic resonance, Near-infrared fluorescence, Intervertebral disc, Knee joint, Degeneration

1. Introduction

Chronic low back pain (CLBP) is one of the leading causes of disability [1]. This painful disability causes functional limitations leading to decreased productivity accompanied by enormous health care costs and a high socio-economic burden [2, 3]. Degeneration of the intervertebral disc (IVD) has been indicated to be the underlying factor for CLBP in approximately 40% of the cases [4]. During the process of IVD degeneration, loss and remodeling of extracellular matrix (ECM) proteins from the macromolecular framework of collagens and proteoglycans will lead to a decrease in water content in the disc [5, 6]. The disorganized and dehydrated IVD in turn will fail to provide the compressive strength that is needed to absorb shocks and to allow movements of the spine [7]. Inflammation plays a considerable role in the acceleration of these degenerative processes [8]. In addition, the degenerative environment stimulates an increase in local neurotrophic factors leading to the ingrowth of peripheral nociceptive sensory neurons into the IVD, resulting in pain sensitization [9, 10]. Anti-inflammatory and analgesic medication is commonly used to relieve pain, such as non-steroidal anti-inflammatory drugs (NSAIDs) and opioids [11], but long-term use is associated with severe adverse effects such as gastro-intestinal and cardiovascular complications or addiction [12, 13]. More importantly, systemic drug administration used to treat CLBP remains inefficient, most likely due to the fact that the IVD is the biggest avascular tissue in the human body, and systemically taken drugs hardly reach the tissue [14, 15]. A promising strategy for CLBP treatment could, therefore, be intradiscal delivery of therapeutic molecules. Compared to systemic administration, intradiscal injections may in addition increase local drug concentration and diminish side effects.

Drugs such as peptides have gained interest as pharmaceutical therapeutics because of their selectivity and low toxicity [16], exemplified in an *in vivo* study showing attenuated IVD degeneration (IVDD) after intradiscal delivery of an NF-κB essential modulator binding domain peptide [17]. Another peptide termed Link N peptide consisting of an N-terminal region of link protein stabilizing proteoglycan aggregates, has been shown *in vitro* and *in vivo* to increase disc ECM production necessary to induce tissue regeneration [18-20]. The systemic half-life of peptides is typically short, but local peptide degradation and clearance rates from the IVD have not been reported. The use of drug delivery systems (DDS) could be exploited to extend the local exposure of bioactive agents prolonging discogenic CLBP treatment and/or to reverse IVD degeneration [21]. Polyesteramides (PEAs) are biodegradable polymers that can be used as a DDS, consisting of natural α-amino acids [22, 23]. PEA is broken down into non-toxic waste products by proteolytic enzymes [24] and shows good biocompatibility in knee joints [22] and IVD [25]. Intradiscal delivery of the anti-inflammatory drug celecoxib-loaded PEA microspheres protected IVD integrity in a puncture-induced disc degeneration canine model and reduced owner-reported pain symptoms in a small cohort of canine CLBP patients at 6 and 12 weeks follow-up [23, 26]. However, in order to develop optimal formulations for the local delivery of bio-actives, insight into local clearance kinetics is required.

Drug distribution and retention in tissue after local administration can be investigated by invasive methods such as mass spectrometry and enzyme-linked immunosorbent assay (ELISA) [27, 28] and non-invasive methods, including imaging based on fluorophore-labeled methods [29]. Non-

invasive methods can longitudinally track drugs when labeled with a tracer such as a fluorescent dye. Weak tissue penetration of these tracers usually limits their use in deep tissues like the lumbar IVD. In contrast, invasive methods are normally performed *post-mortem,* but are highly sensitive and often do not require specific drug labeling.

The present study used invasive and non-invasive tracking methods to investigate drug retention after intradiscal injection (figure 1). ^{19}Fluorine nuclear magnetic resonance (^{19}F NMR) spectroscopy, an invasive method, is a highly specific tool for detecting, identifying, and quantifying fluorine-containing drugs and their metabolites in bio-fluids without interference by endogenous components [30]. To this end, ^{19}F NMR spectroscopy was here used for the first time to investigate peptide release and retention after intradiscal injection into whole bovine caudal IVDs cultured with dynamical loading and *in vivo* in healthy and degenerative lumbar sheep IVDs. Additionally, non-invasive near-infrared (NIR) imaging was used to evaluate intradiscal retention, including the effect of degeneration. The NIR dye, IR-780 iodide, served as a model for small molecule drugs and was locally injected in healthy and degenerative caudal rat IVDs. Furthermore, IR-780 was loaded into PEA microspheres to determine drug retention after injection in healthy and degenerated IVDs, and release was in addition compared to body locations with higher vascularization, like the skin or knee joints.

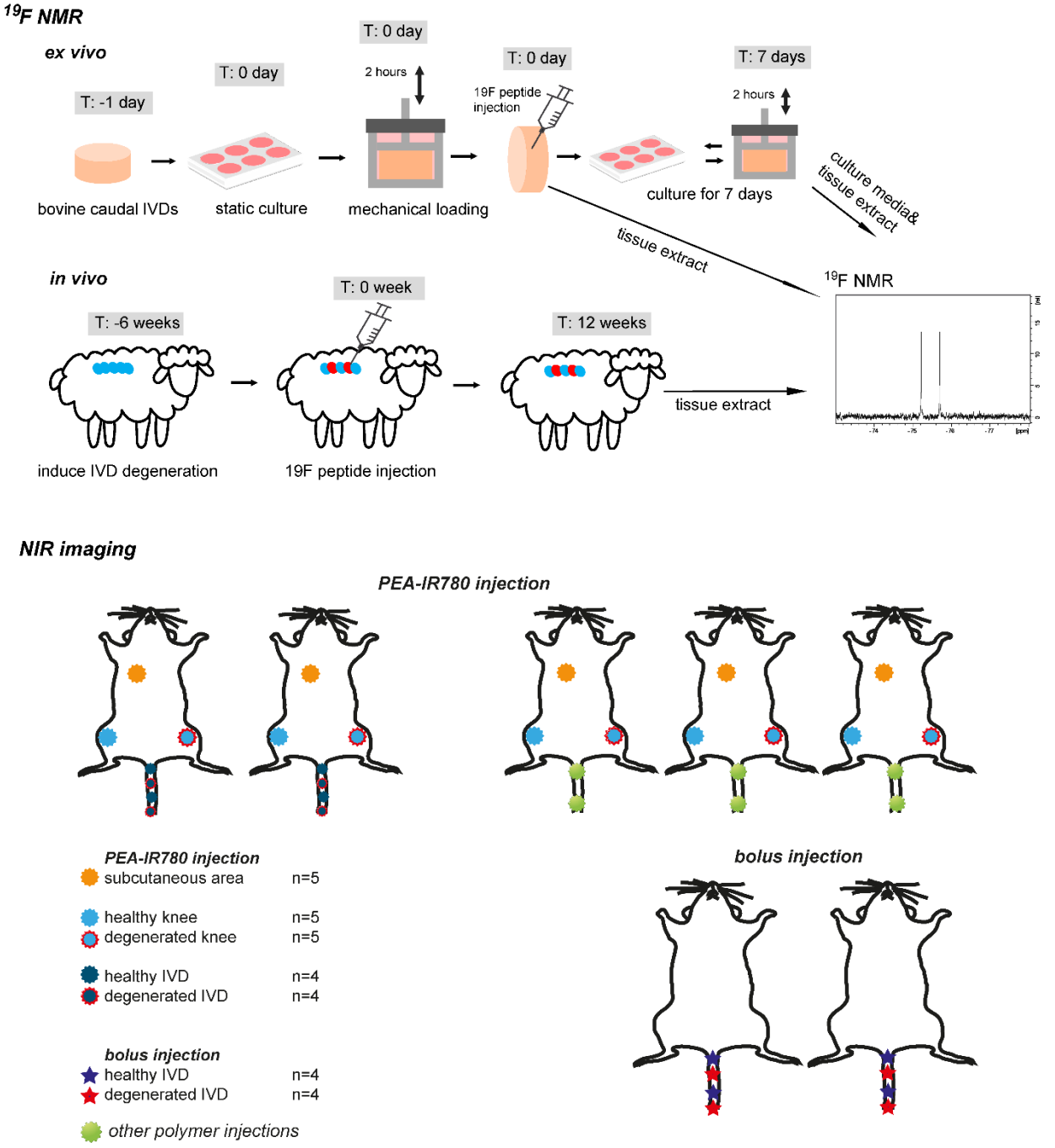

Figure 1. Schematic overview of the study designs including ex vivo bovine IVD explants, in vivo sheep IVD and in vivo rat study. *IVD = intervertebral disc, PEA = polyesteramide.*

2. Materials and methods

2.1. Peptide and microsphere preparation

^{19}Fluorine labeled 16 amino acid residues random peptide (sequence: CF3CO–NH-Lys–(CO–CF3)-DNRAHLHIDYHTDSD-COOH) was purchased from CanPeptide (Canada). PEA was

synthesized in accordance to procedures reported previously [31, 32]. For the preparation of loaded microspheres, PEA was dissolved in dichloromethane (DCM, Merck Millipore, Darmstadt, Germany) and 2 wt% IR-780 iodide (425311, Sigma-Aldrich, Darmstadt, Germany) was added to the solution and homogenized by ultrasound. The homogenized suspension was added to 20 mL of an aqueous solution containing surfactants for stabilization (1 wt% of poly(vinyl alcohol and 2.5 wt% NaCl, Sigma Aldrich) and emulsified under high shear, using an Ultra-Turrax. Thereafter, the particles were allowed to harden overnight in 100 mL water. The excess water and surfactant were removed by rinsing and centrifugation. Before freeze-drying to remove residuals, particles were resuspended in 0.04% Tween 80. Once dried, closed vials were sterilized with ɣ-radiation on dry ice. The size distribution of PEA particles was measured by static light scattering using a Malvern Mastersizer 2000S and ranged from 8 to 50 µm.

2.2. ^{19}F peptide retention in bovine IVD *ex vivo* culture

Bovine caudal IVDs were collected from fresh sacrificed 6- to 12-month-old calves from a local slaughterhouse. Whole IVDs with cartilaginous endplates were isolated according to a previously published protocol [33]. In short, the surrounding muscle and soft tissue were removed, then whole IVDs with cartilaginous endplates were isolated, and redundant vertebral bone and growth plates were carefully cut off. After cleaning and washing, IVDs were cultured at the free swelling condition in a 6-well plate containing 7 mL culture medium per well and subjected to daily dynamic uniaxial loading in chambers containing 5 mL culture medium at 37 °C, 5% CO_2. The culture medium consisted of DMEM supplemented with 100 U/mL penicillin and 100 mg/mL streptomycin (1% P/S, Gibco, Paisley, UK), 50 mg/mL Primocin (Invitrogen, San Diego, California), 2% fetal bovine serum (PAN Biotech, Aidenbach, Germany), 50 µg/mL ascorbate 2-phosphate, 1% ITS+ (BD Biosciences), 1% nonessential amino acid (NEAA, Gibco, Paisley, UK)) [34]. IVDs were cultured at the free swelling condition before and after the loading cycle. Dynamic loading was performed at 0.02 to 0.2 MPa amplitude, 0.2 Hz for 2 hours daily. After the first loading cycle, 6 IVDs were immediately injected with 1 mg ^{19}F peptide dissolved in 50 µL PBS into the center NP. Then, 3 IVDs were kept in an empty culture plate for 3 hours and harvested as fresh injection control, and another 3 IVDs were cultured under daily mechanical loading for 7 days. Culture media from free swelling and loading were collected separately every day. After 7 days of culture, the endplate of one side of the IVDs was carefully removed, and the IVD was snap-frozen in liquid nitrogen and stored at -20 °C.

2.3. *In vivo* retention

2.3.1. Ethics statement

The *in vivo* study designs were approved by the National Commission of animal experiments (AVD108002015282), and the working protocol was supervised by the local Animal Welfare Body (WP#105078-2) and (WP#282-5-02) and met the guidelines for animal research in the Netherlands.

2.3.2. *In vivo* ^{19}F retention in sheep IVDD

Four female Swifter sheep, 2 years old, were used in this and another non-related study [35]. Surgery and intradiscal injection were performed as previously described [35]. Briefly,

degeneration of lumbar IVDs at L1- L2, L3 - L4, and L5 - L6 of each sheep was induced by nuclectomy, and 6 weeks afterward, magnetic resonance imaging (MRI) was used to confirm degeneration. ^{19}F-P, 200 µg per disc, was injected into 8 healthy and 6 degenerative lumbar IVDs. Another 6 degenerative lumbar IVDs were intradiscal injected with BMP-4, 200 µg per disc. Three months after injection, sheep were euthanized, and IVDs were collected. The ^{19}F-P injected IVDs were cut mid-sagittal into two parts. One-half of the IVDs were processed for NMR measurement to determine retention of the ^{19}F-P.

2.3.3. Experimental set-up of *in vivo* IR-780 retention in rat IVDD and OA

In this study, 8 female 10 weeks old Sprague-Dawley rats (Charles River Laboratories International, the Netherlands) were used and housed in groups (4 rats, randomized) in polycarbonate cages with wire tops, wood chip bedding, and access to *ad libitum* food and tap water. Rats were allowed to acclimatize for 7 days before the start of the experiment. One rat died at t=0 directly after IR-780 injection (cause of death; not recovered from anesthesia) and could not be included in the study. The experimental unit in this study was a single injection site for every tissue (PEA-IR780 skin *n=5*, PEA-IR780 healthy knee *n=5*, PEA-IR780 degenerated knee *n=5*, PEA-IR780 healthy IVD *n=4*, PEA-IR780 degenerated IVD *n=4*, free IR-780 healthy IVD *n=4*, free IR-780 degenerated IVD *n=4*). Primary experimental outcomes included IR-780 retention (free or released from PEA microspheres) during the complete follow-up and disc height changes after 16 weeks complemented by histopathology to confirm disc degeneration. Complying with the 3R principles, 4 rat tails (*n=8* degenerated IVDs and *n=8* healthy IVDs) were used to study the IR-780 retention delivered by PEA microspheres, the other 3 for a similar study with a different version of the polymer (unpublished data), which does not influence the present study.

2.3.4. Rat model of induced IVD and knee degeneration

All rats received pre- and post-operatively 0.03 mg/kg buprenorphine (buprecare®) and 4 mg/kg carporal® (AST farma B.V., Oudewater) subcutaneous as prophylactic analgesia. IVD degeneration induction was executed under general anesthesia consisting of isoflurane gas (4-5% induction, 1-2 % for maintenance), delivered in a 1:1 oxygen:air mixture. A pre-puncture radiograph (t-4) was taken and used as the baseline for IVD height measurements. Tail IVDs were located by palpation on the coccygeal (Co) vertebrae and confirmed by radiograph. In each animal, IVD degeneration was induced in levels Co4-Co5 and Co6-Co7. Adjacent levels (Co5-Co6 and Co7-Co8) were included as healthy IVD controls. Tail skin was sterilized, and a sterile 20-gauge needle was inserted perpendicular to the skin, at 5 mm depth through the AF into the NP, rotated 360°, and held for 30 seconds, as previously reported by Han *et al.*(2008) [36]. Correct needle placement was confirmed by intra-operative fluoroscopy. After IVD degeneration induction, the anterior cruciate ligament was transected, and a part of the medial meniscus was removed from the left joint under isoflurane anesthesia (4-5% induction, 1-2% for maintenance). After IVD puncture and knee OA induction, the animals were put back into their cages to recover from surgery. All animals received 0.03 mg/kg buprenorphine subcutaneously as post-operative analgesia for the following three days.

2.3.5. IR-780 injection

IR-780 intradiscal injections (bolus or loaded in PEA microspheres) were performed 4 weeks after degeneration induction. All rats received pre-operative analgesia by subcutaneous injection of

carprofen (4 mg/kg) and buprenorphine (0.03 mg/kg). All IR-injections were carried out under general anesthesia consisting of isoflurane gas (4-5% induction, 1-2 % for maintenance), delivered in a 1:1 oxygen:air mixture. Before intradiscal injection, radiographs (t0) were taken to determine changes in IVD height. Then, IR-780 iodide dye alone or IR-780 loaded PEA microparticles were intradiscally injected under fluoroscopic guidance to confirm the correct needle position in the center of the IVD at 625 µg/mL IR-780 in a total volume of 2 µl. Gastight Hamilton syringes (25 µL) connected to 29G needles (Hamilton Company USA, Reno, Nevada) were used for the intradiscal injections. In the same animals, subcutaneous and intra-articular PEA-IR-780 injections were done using 1 mL 29G insulin needles (Becton Dickson, Franklin Lakes, USA) at a concentration of 625 µg/mL IR-780 in a total volume of 25 µL.

2.4. NMR spectroscopy

2.4.1. Sample preparation

Frozen ^{19}F-P-injected bovine and transversely cut sheep IVDs were sectioned using a cryostat microtome (Thermo Fisher, USA) at 30 µm thickness. Almost all the NP and AF tissue were sectioned and separately collected. Tissue was lysed in cOmplete lysis-M EDTA-free buffer (Roche Diagnostics GmbH, Mannheim, Germany) on a rotor at 4 °C overnight, 3 mL per bovine NP, 6 mL per bovine AF, 1 mL per sheep NP and 1.5 mL per sheep AF. Tissue extracts were collected after centrifuging at 10,000 g at 4 °C for 20 min, then were stored at −80 °C until NMR measurements. Additionally, fresh bovine and sheep IVDs were used to prepare tissue extracts for diluting a ^{19}F-P standard for NMR.

Bovine caudal IVD culture media collected daily at days 1-7 were lyophilized, then reconstituted in ultrapure water to concentrate media, 5 times for free swelling media and 4 times for dynamic loading media. Before NMR measurement, 500 µL of each concentrated culture medium and IVD extract was mixed with 50 µL D_2O and transferred into a 5 mm NMR tube. The standard curve was prepared by dissolving ^{19}F-P at 100 µg/mL, 10 µg/mL, 1 µg/mL in the same type of concentrated medium and IVD extract.

2.4.2. NMR Measurements

All ^{19}F NMR spectra on bovine IVDs were recorded on a Bruker Avance III 600 MHz spectrometer equipped with a Prodigy QCI HFCN quadruple resonance cryo-probe (Billerica, MA). All spectra on sheep IVD extracts were recorded on a Bruker Avance 500 MHz spectrometer equipped with a room temperature HCN probehead that is tuneable to ^{19}F. One-dimensional (1D) ^{19}F spectra were acquired at 298 K using an acquisition time of 2.89 s, recycle delay of 4.5 s, and recording 32k complex points with a spectral width of 100 ppm centered at -75 ppm. The total recovery delay (7.39 s) was more than 5x the estimated T_1 relaxation time, based on analysis of an inversion recovery experiment of ^{19}F-P standard sample (T_1 ~0.7 s). Spectra on media and IVD tissue samples were recorded using 600 (total acquisition time ~1 h), while for some IVD samples with weak or no signal, 7200 scans and 10240 scans (total acquisition time ~12 h and 17h) were used for bovine IVDs and sheep IVDs, respectively. All spectra were recorded without ^{1}H decoupling as the ^{19}F signal in the COCF3 groups is not affected by ^{19}F-^{1}H couplings. Raw data were zero-filled to 64 k complex points, and a 2 Hz line broadening window function was applied before Fourier transformation and subsequent automated phase correction and baseline

correction using Bruker Topspin 4.1. Chemical shifts of ^{19}F were referenced with respect to $CFCl_3$ at 0 ppm.

2.4.3. NMR-based quantitation

Standard curves were obtained by integrating the signal from -75.0 to -75.8 ppm in tissue samples or -74.9 to -75.7 ppm in media samples, then regressing based on the linear fit as shown in supplementary data 1. The amount of ^{19}F-P in IVDs was calculated by $W_{IVD} = C_{NP} \times V_{NP} + C_{AF} \times V_{AF}$, W_{IVD}: the total amount of ^{19}F-P in IVD, $C_{NP/AF}$: measured ^{19}F-P concentration in NP/AF, $V_{NP/AF}$ volume of lysis buffer added. Accumulated ^{19}F-P release from IVD was calculated by summing the amount of ^{19}F-P in the culture media of each day, which was calculated by $W_M = C_F / 5 \times V_F + C_D / 4 \times V_D$, W_M: the total amount of ^{19}F-P in culture medium each day, $C_{F/D}$ measured ^{19}F-P concentration in free swelling/ dynamic loading medium, $V_{F/D}$ volume of free swelling/ dynamic loading medium added.

2.5. Near-infrared imaging

Injection sites (skin, knee joints and tail IVDs) were scanned every other week for *in vivo* IR-780 detection, starting at week 2 after injection. Rats were first sedated by intraperitoneal injection of ketamine (75 mg/kg) and dexmedetomidine (0.25 mg/kg). Images were acquired with the Pearl Impulse Small Animal Imager (LI-COR, Westburg B.V., Leusden, the Netherlands) with 785-nm excitation light to detect IR-780 signal. The Pearl camera automatically optimizes exposure times. Imaging data were acquired with a thermoelectrically cooled CCD sensor. Fluorescence intensity was quantified using Image Studio Lite software (LI-COR, Westburg B.V., Leusden, the Netherlands). Regions of interest were selected using an equal-sized circle, and a mean value was calculated with localized background subtraction analysis. The IR-780 intensity of each time point was normalized to the value of week 2 after injection (100%). Unloaded PEA microparticles showed no fluorescence spectra. NIR Imaging was also performed on *post-mortem* IVDs after the skin was removed and paraffin-embedded sections.

2.6. Disc height analysis

Caudal disc radiographs were taken before induction of IVD degeneration (t-4) and directly after IR-780 injection (t0). The rats were placed in the prone position with their tails straight during radiography. IVD height was measured using the digital radiographs in Adobe Photoshop software (Adobe Systems Incorporated, version 13.0.1, San Jose, California, USA) using the ruler tool. IVD height was expressed as the disc height index (DHI) by averaging the measurements obtained from the dorsal, middle, and caudal portions of the IVD and dividing that by the average of adjacent vertebral body heights described by Masuda *et al.* (2005) [37].

2.7. Histopathology

Rats were terminated by CO_2 suffocation 16 weeks after degeneration induction on t-4. Tails and knee joints were harvested. Tails were skinned and imaged again before fixation. Tails and knees were fixed in 4% formaldehyde solution (Klinipath B.V., Duiven, the Netherlands) for 1 week. Thereafter, they were decalcified in 0.5 M EDTA (VWR international B.V., Amsterdam, the

Netherlands) solution for a total of 6 and 8 weeks, respectively, re-fixating for 3 days in 4% formaldehyde solution every 2 weeks. The IVDs were embedded in paraffin as spinal units containing the adjacent vertebral bodies. Five µm sections were used to take NIR images and stain with Picrosirius red / Alcian blue staining protocols [38]. The cellularity and morphology of all IVDs were examined in a random blinded fashion. Five µm thick transversal knee joint sections were cut and stained either with Safranin-O/Fast green or hematoxylin/eosin to evaluate cartilage degeneration using the Mankin score [39] or synovitis using the Krenn score [40], respectively.

2.8. Statistical analysis

All data were analyzed using IBM® SPSS® Statistics software (version 21). One-Sample t-tests were used to analyze the significance of differences in DHI between healthy and degenerated IVDs and cartilage degeneration and synovitis between healthy and degenerated knee joints. All IR-780 fluorescence intensity data were evaluated for equality of data variances by Q-Q plots and homoscedasticity of residuals by scatterplots. In all cases, the assumptions were not met, and Kruskal–Wallis tests were used to analyze nonparametric data with post-hoc pairwise comparisons using the Dunn-Bonferroni approach. All data were expressed as the mean ± standard error of the mean. Statistically significant differences were considered at values $p<0.05$. Statistical analysis of peptide measurements was limited to descriptive statistics.

3. Results and Discussion

Intradiscal delivery of drugs is gaining acceptance as a promising approach to treating CLBP or regenerating IVD as an alternative to systemic administration. In the current study, we investigated the relation between drug retention and the local environment and disease state of the injected tissue by using ^{19}F-P and IR-780 as a model of peptide and small molecule, respectively.

3.1. ^{19}F-peptide clearance from the intervertebral disc

In this study, for the first time, a ^{19}F-labelled peptide was used as an inert model peptide to investigate drug release and retention in the IVD. This was done in an *ex vivo* bovine IVD culture model and *in vivo* sheep model of IVDD by using ^{19}F NMR. The main signals were located at -75.2 and -75.7 ppm, and a small peak was found between the two main peaks that may indicate free trifluoroacetic anhydride (TFA). A chemical shift was found when ^{19}F-P was dissolved in the IVD culture medium and concentrated culture medium compared to lysis buffer and tissue extracts. In the IVD culture model, three hours after injection of 1 mg of ^{19}F-P in bovine IVDs (Figure 2A), most ^{19}F-P was found in the NP tissue, which was ~29% of the total dose injected, while only ~4% was detected in AF tissue extracts (Figure 2B). Almost 70% could not be recovered from tissue extracts. During culture, ~22% of the injected ^{19}F-P was released to the culture medium in the first 4 days. The cumulative release was 24% after 7 days of culture (figure 2C). After 7 days of culture, only less than 1%, ^{19}F-P was retrieved from the NP, but not the AF. In the sheep model, 3 months after intradiscal injection, no ^{19}F-P signal was detected after even 10240 scans in both AF and NP of healthy and degenerative IVDs, as in figure 2E, 2F.

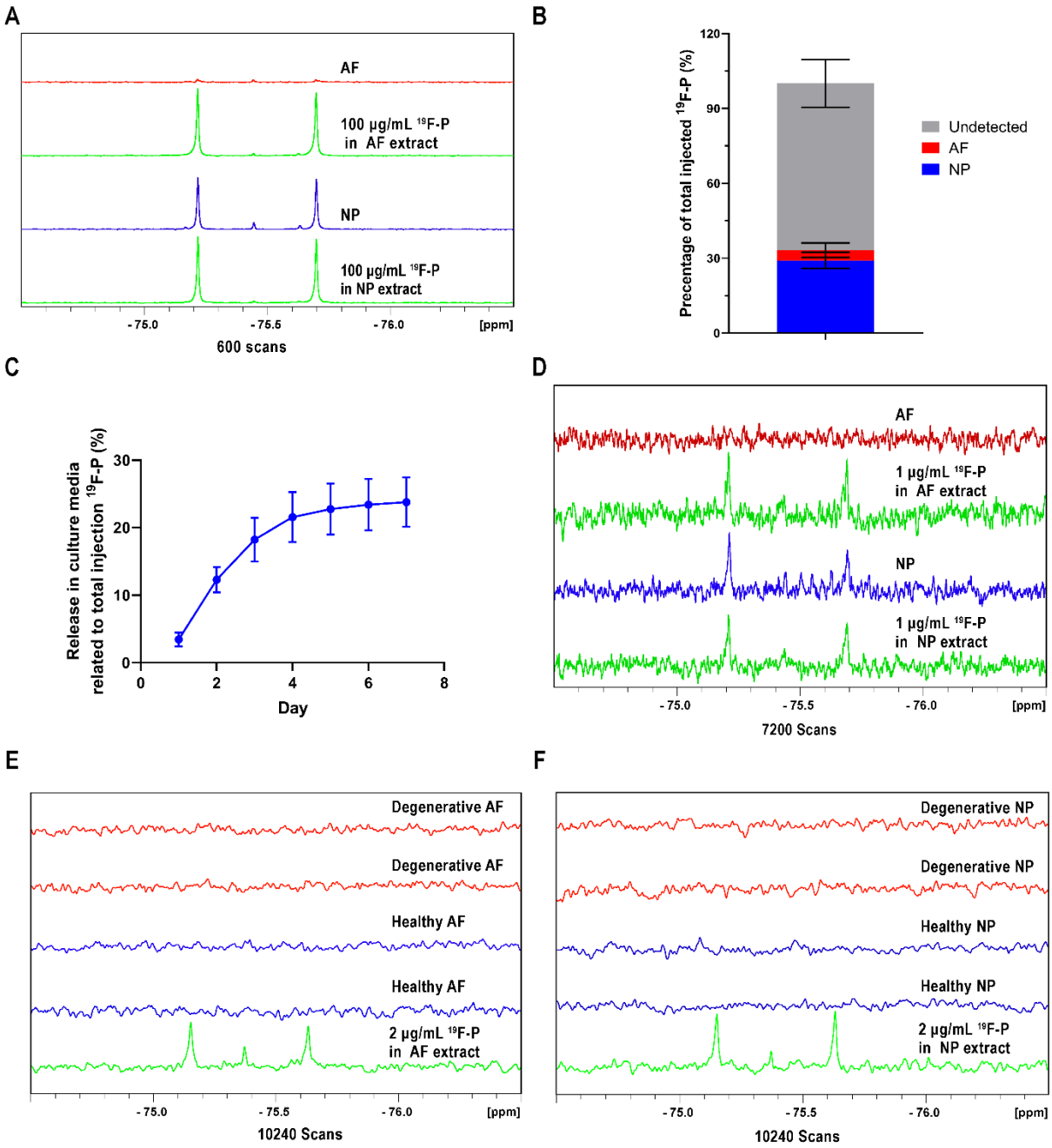

Figure 2. ^{19}F-P release and retention in cultured bovine caudal IVD and sheep IVD in vivo after intradiscal injection evaluated by NMR.

***A)** Evaluation and **B)** quantification of ^{19}F-P in bovine AF and NP tissue extracts in a static culture, 3 hours after intradiscal injection. **C)** The release profile and **D)** retention of ^{19}F-P in bovine caudal IVDs cultured with daily dynamic loading for 7 days after intradiscal injection. Only in NP tissue, the peptide was retrieved. No ^{19}F-P was detected in AF **E)** and NP **F)** tissue of healthy and degenerative sheep IVDs, 3 months after intradiscal injection.*

In general, peptide drugs have a relatively short serum half-life and hence low bioavailability due to rapid clearance by the liver or kidney [41]. Intradiscal peptide application has been performed in order to increase local drug concentrations and prolong drug retention in rat and rabbit IVDD models [17, 20]. Actual peptide retention over time, however, was not investigated yet. Present results showed that the majority of ^{19}F-P may be cleared from IVD after one week in an *ex vivo* model. No ^{19}F-P was found in sheep IVD after 3 months.

^{19}F NMR used to quantify fluoropyrimidine, and its metabolites from plasma in rat and dog showed comparable sensitivity to liquid chromatography with tandem mass spectrometry [42]. In the present study, ^{19}F-P can be detected in IVD extracts at µg level. However, only one-third of ^{19}F-P was recovered from freshly injected IVDs. Fractions of the ^{19}F-P might have been lost during sample processing or may have diffused to the cartilaginous endplates, which were not analyzed in the current study. Moreover, when calculating the total volume of tissue lysate, the volume of NP/AF tissue was not included. The amount of ^{19}F-P was calculated by multiplying the concentration and total volume of the lysis buffer added. Therefore, the real recovered ^{19}F-P could have been underestimated. In cultured IVDs, the majority of ^{19}F-P recovered from the cumulative release in culture medium was released in the first 4 days and was below detection after 7 days (supplementary data 3). Our results are in line with a previous study, in which the soluble fluorescent dye, isothiocyanate isomer 1 (FITC), was injected in the NP explant cultured with a cartilage ring and static weight compression that showed 90% FITC signal decrease after 4 days culture [43]. An alternative explanation could be that ^{19}F-P binds to the ECM of the IVD, and hence did not dissolve in the tissue extracts that were used to measure ^{19}F-P. To confirm this, other methods should be used to destroy peptide-ECM interaction and enable release of the ^{19}F-P into the tissue extract.

Based on our findings in the *ex vivo* IVD model, the absence of ^{19}F-P in sheep IVDs 3 months post-injection was expected. Compared to the tissue culture model, ^{19}F-P was injected at a lower dose per disc, and only half of the tissue was used for ^{19}F-NMR. Additional limitations encompass the cutting process possibly leading to ^{19}F-P loss and a lower sensitive scanner used in the sheep samples.

^{19}F NMR can also be used for the detection of peptide metabolites based on chemical shifts [42]. In the present study, a considerable chemical shift was not found in the NP extract after 7 days of culture. This may suggest ^{19}F-P was not degraded. Alternatively, the limited chemical shift detected may be due to the limited sensitivity of the scanner used or that the ^{19}F was only labeled on one amino acid residue on the N-terminal. The latter implies that the chemical shift would not be detected when degradation happens at other positions.

The invasive ^{19}F NMR method is only able to measure endpoint read-outs. Non-invasive ^{19}F nuclear magnetic resonance imaging (^{19}F MRI) could offer *in vivo* detection and tracking of injected substances [44, 45]. ^{19}F MRI has high specificity due to the lack of endogenous ^{19}F but is challenged by the low sensitivity of ^{19}F detection. Usually, it requires a local ^{19}F concentration over 80 mM to generate high-quality images, however, *in vivo* drug concentrations are usually in the sub-mM range [46]. Recently, a labeling strategy for *in vivo* ^{19}F-MRI based on highly fluorinated, short hydrophilic peptide probes or drug carriers has been developed [46, 47].

Intradiscal delivery of such systems could increase local concentrations enabling real-time detection of drug retention over time, including peptides.

3.2. IR-780 retention from the intervertebral disc

In small animal models, real-time monitoring of drug presence can be done via noninvasive imaging techniques, such as NIR fluorescence imaging [48, 49]. Another advantage of using NIR imaging to assess local drug release over time is the minimal tissue autofluorescence in the NIR wavelength region [50]. Percutaneous needle puncture of rat tail IVDs resulted in significant disc space narrowing after 4 weeks, measured prior to intradiscal IR-780 delivery, in comparison with adjacent control discs (Figure 3A). *Post-mortem* histological images confirmed the healthy disc status of the latter, showing normal IVD tissue compositions containing organized collagen lamellae of the AF surrounding a round and notochordal cell-rich NP, which in rodents is the predominant cell type in the healthy NP (Figure 3B). The presence of degeneration processes 16 weeks after needle puncture was indicated by disorganized collagen content transitioning into the irregularly shaped NP with disrupted endplates (Figure 3B). The retention of free IR-780 after intradiscal delivery gradually declined at a pace that appeared to be independent of the IVD health status (Figure 3C&D, n.s). The IR-780 signal was below detection 10 weeks after injection in degenerated IVDs, while the detection limit was reached after 14 weeks in healthy IVDs.

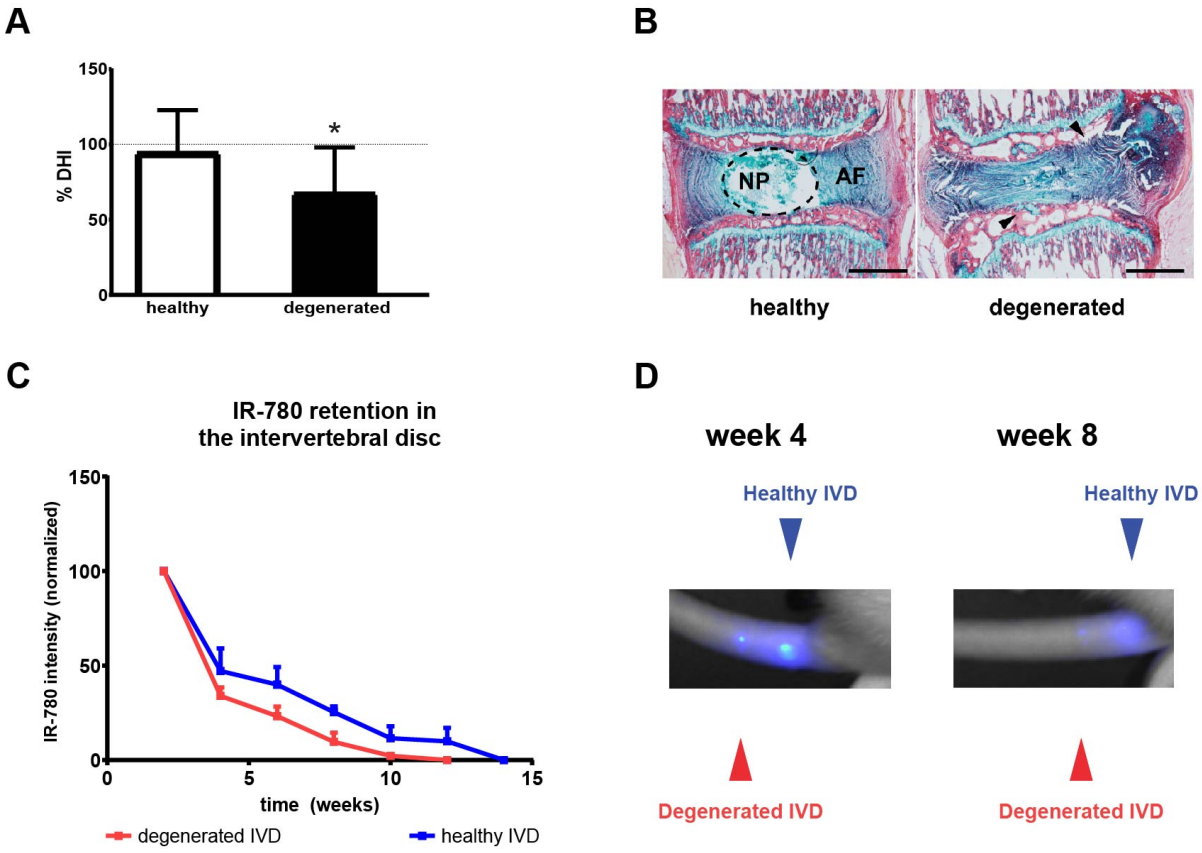

Figure 3. Retention of free IR-780 after intradiscal injection in healthy or degenerated IVDs.

*A) Decreased disc height index, 4 weeks after degeneration induction by NP needle puncture. *p<0.05. B) Histologic overview of a healthy and degenerated IVD, stained with picrosirius red / alcian blue. The dotted circle indicates a distinct NP (left), and black arrows indicate disrupted endplates (right). Scale bar = 500 µm. C) Quantification of IR-780 intensity signal after IR-780 injection in healthy (n=4) or degenerated (n=4) rat IVDs. The IR-780 intensity was normalized to 2 weeks after injection. Data represent mean ± SEM. D) IR-780 signal after 4 and 8 weeks in tail IVDs, detected by fluorescence optical imaging. AF = annulus fibrosus, IVD = intervertebral disc, NP = nucleus pulposus.*

3.3. IR-780 delivery and retention using a PEA-based drug delivery platform

PEA microspheres were used as a model of the controlled release platform for local injection. For this purpose, IR-780-loaded PEA microspheres were injected into the vascularized skin and the healthy knee joint, both locations with a high fluid exchange, as well as in the healthy avascular IVD. IR-780 retention gradually decreased in the skin and knee joint and was not detected 16 weeks after injection. In contrast, the IR-780 signal increased in the first 6 weeks after intradiscal injection, and thereafter a slow, gradual decrease was observed (Figure 4A). IR-780 signal remained visible after the 16 weeks follow-up period, and the relative IR-780 intensity was significantly higher in the IVD compared to the skin and knee joint (Figure 4A&B, p<0.05).

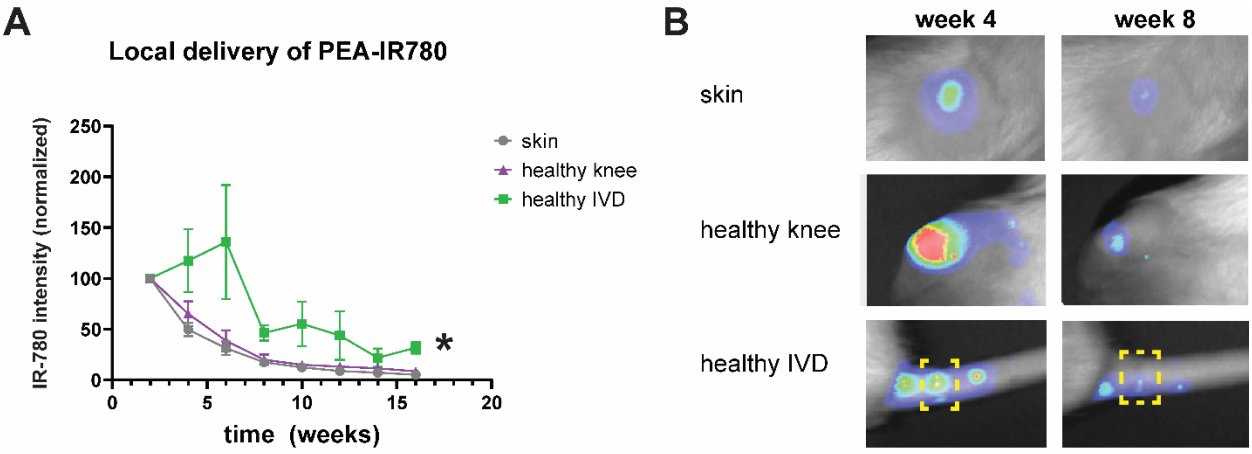

Figure 4. Tissue-dependent retention of IR-780 over 16 weeks, released from PEA microspheres.

*A) Quantification of IR-780 intensity signal after IR-780 injection in healthy skin (n=5), knee joint (n=5), and IVD (n=4). The IR-780 intensity was normalized to 2 weeks after injection. Data represent mean ± SEM. A significant increase in IR-780 intensity was found in IVD compared to skin and knee joints, indicated by *p<0.05. B) Fluorescence optical images 4 and 8 weeks after IR-780 loaded PEA microsphere injections in rats. The yellow dotted box indicates healthy IVD. IVD = intervertebral disc, PEA = polyesteramide.*

The retention and inherent release rate of the drug loaded on a DDS depend on the biomaterial-based DDS properties such as porosity, properties of the drug such as size and charge, and on clearance from the injected tissue. In addition, release from the PEA polymer is also enzyme-

responsive, being sensitive to serine protease-dependent degradation. Various serine proteinases have been described to play a role in (osteo)arthritis pathology [51]. In particular, plasmin and HtrA1 have been detected in degenerated IVDs, at higher levels compared to healthy IVD tissue [52-54]. The differences in serine proteases present in the healthy knee joint and IVD might explain the observed differences in IR-780 signal intensity over time. In a synovial joint, the elimination of intra-articularly injected drugs occurs through the synovial membrane [55], while fluid transport in and out of the IVD is regulated by a combination of diffusive and convective transport [56, 57]. The observed differences in IR-780 as model drug presence over time could, therefore, partially be explained by the properties of the injected tissues. Tissues rich in lymphatic vessels are the skin and knee [58, 59], in contrast to the tightly enclosed IVD [60]. In these tissues with an intrinsically higher fluid clearance, IR-780 retention was indeed lower.

3.4. IR780-PEA retention from healthy and degenerated IVD and knee joint

In degenerated IVDs, the IR-780 intensity pattern was similar compared to healthy IVDs over time. Interestingly, the relative IR-780 intensity increased higher in degenerated IVDs than in healthy IVDs. Even 16 weeks after injection, the IR-780 intensity did not significantly decrease compared to 2 weeks in degenerative IVDs. This IR-780 intensity pattern was not observed in knee joints, regardless of health status, that showed a gradual decrease over the 16 weeks period (Figure 5C, n.s. 5D).

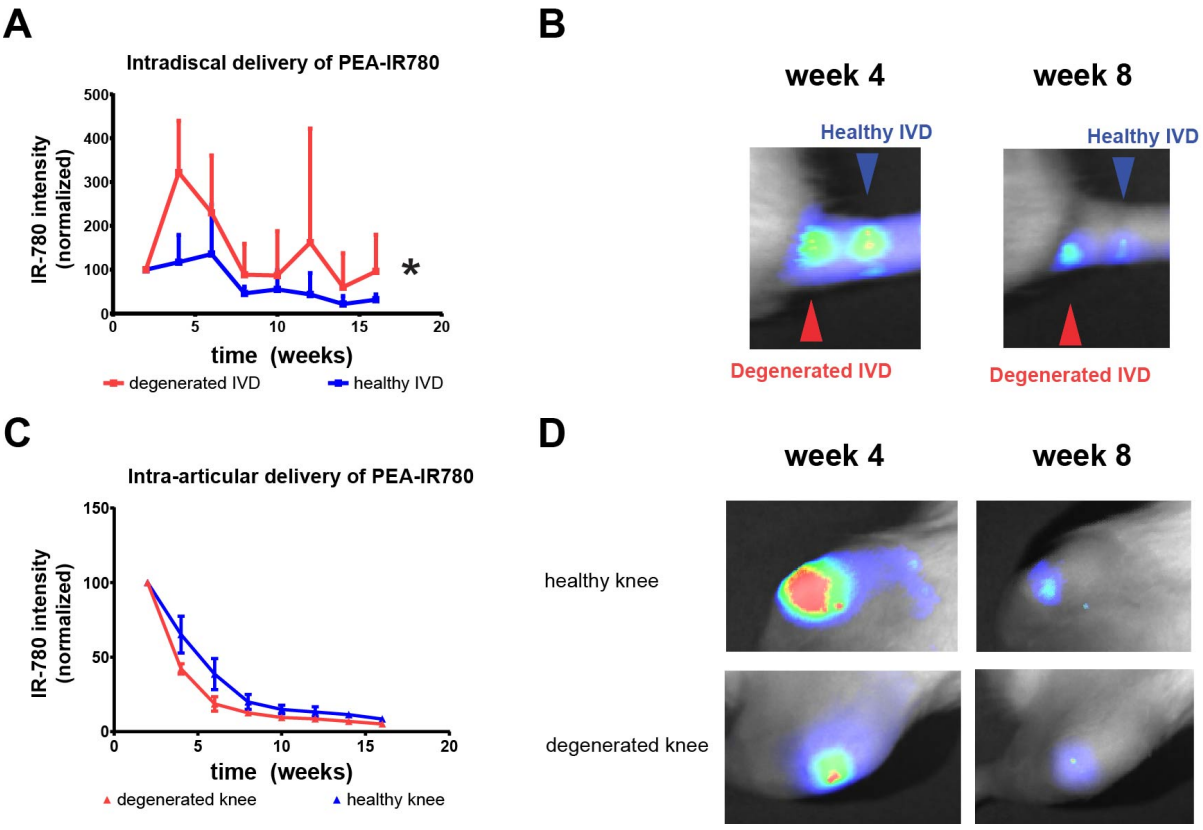

Figure 5. Disease-dependent joint retention of IR-780 over 16 weeks, released from PEA microspheres.

*A) Quantification of IR-780 intensity signal after IR-780 loaded PEA microsphere (PEA-IR780) injection in healthy IVDs (n=4) versus degenerated IVDs (n=4). The IR-780 intensity was normalized to 2 weeks after injection. Data represent mean ± SEM. A significant increase of IR-780 intensity released from PEA microspheres was found in degenerated IVDs compared to healthy IVDs at *p<0.05. B) Fluorescence optical images 4 and 8 weeks after PEA-IR780 injections in healthy and degenerated tail IVDs in rats. The blue arrows indicate healthy IVD, the red arrows indicate degenerated IVD. C) Quantification of IR-780 intensity signal after PEA-IR780 injection in healthy knee joints (n=5) versus degenerated knee joints (n=5). The IR-780 intensity was normalized to 2 weeks after injection. Data represent mean ± SEM, and no significant differences were found. D) Fluorescence optical images 4 and 8 weeks after PEA-IR780 injections in healthy and degenerated knee joints in rats. IVDs = intervertebral discs, PEA = polyesteramide.*

Post-mortem, in IR780-PEA injected IVDs, IR-780 signal was still detected after 16 weeks follow-up in degenerated discs, although no statistically significant differences were found in IR-780 signal between degenerated and healthy IVDs (supplementary figure 5A). After tissue processing for histological analysis, local IR-780 signals could still be detected in IVD tissue sections (supplementary figure 5B).

Unexpectedly, no difference in IR-780 retention was observed between healthy and degenerated knee joints upon delivery by PEA microspheres, while enhanced clearance of glucocorticoids [61] or large molecules such as hyaluronic acid [62] in inflamed joints has been explained by the increased vascular permeability due to synovitis [63]. Considering that the current model displays an OA state in which an increase in lymphatic vasculature has been described 12 weeks after induction of degeneration [59], differences in IR-780 retention in this time window were expected. In addition, PEA degradation and release of the incorporated small molecule drug celecoxib has previously been shown to be enhanced in OA joints, possibly due to the increase in serine protease activity [22]. Although a trend was observed towards a faster clearance during the first 12 weeks after OA induction in knee joints, the current study may have been underpowered to detect statistically significant differences. For IVD tissues, we did detect statistically significant differences in IR-780 retention between healthy and degenerated IVDs. In contrast to the knee joints and the skin, the IR-780 signal in IVDs increased the first weeks after intradiscal injection. Moreover, this increase was more pronounced in degenerated IVDs compared to the healthy tissues, where IR-780 signal intensity showed a more gradual increase. The extent of fluid exchange plays an important role in determining local IR-780 retention, as was shown in an elegant finite element model predicting that degenerative changes of the IVD (such as blood supply, endplate permeability, disc geometry or matrix and cellular properties) can impair effects on the concentration gradients of nutrients and metabolites throughout the disc [64] which might also apply for drug retention in the disc. IVD degeneration accompanied by disc deformation results in lower fluid exchange rates, which might lead to a lower clearance and hence may explain higher retention in degenerated IVDs, compared to healthy IVDs [65].

The increase in IR-780 signal upon release in the IVDs can be explained by the phenomenon that high IR-780 dye molar content in drug delivery systems can induce quenching inside the microparticles, leading to a relative increase upon release into the tissue [66]. Due to the relatively fast clearance in the knee joint and skin, in combination with the relatively larger tissue volume

compared to the IVD, IR-780 quenching will probably not lead to a signal increase in this tissue. The IR-780 peak signal was higher in degenerated IVDs compared to healthy IVDs, most likely due to increased levels of serine proteases in degenerated IVDs [54], which can enhance PEA microsphere degradation [22]. Also, IR-780 signal *post-mortem* could still be detected in most degenerated IVDs.

The increase in IR-780 signal observed in the first 4 weeks indicates that care must be taken to load IR-780 at non-quenching quantities. Of course, even then it will remain unclear what part of the total IR-780 signal is detected from the IR-780 molecules inside the microspheres and what emerges from the already released IR-780 molecules after microsphere degradation. In this study, the first time point of IR-780 signal intensity measurement was at two weeks post-injection to exclude signal from remnants of free IR-780 outside the microspheres after encapsulation [67]. As a consequence, other phenomena, including a sharp decrease in NIR signal due to quenching inside the microparticles, may have been missed. Although the use of NIR dyes can provide a general insight into local delivery and retention, their release kinetics cannot be directly translated to every other small molecules (e.g. small molecule drugs). IR-780 is a hydrophobic cyanine dye with a comparable order of molecular weight to hydrophobic small molecule drugs such as triamcinolone acetonide. Labeling the drug of interest with a fluorescence marker might improve the approach, although the ensuing size and charge changes might alter the release properties of the drug in question.

The degenerative processes in an arthritic joint and the IVD are quite similar [68], but here we show that drug retention is most likely not comparable. Therefore, the many drug delivery formulations that are being developed to improve therapies for various musculoskeletal conditions should be tailored to the specific needs per disease. Modifications that might improve drug delivery for a specific condition can influence the degradation properties of the polymer. For example, cleavage sites of specific serine proteases might be incorporated into the polymer to increase the sensitivity of the predominant degenerative processes in the target tissue. Musculoskeletal conditions with acute inflammation as a driver might need a different drug exposure time than conditions in which chronic inflammation determines disease progression.

4. Conclusions

Direct injection of small molecules, such as peptides or IR780 iodide, in the IVD increased their systemic half-life and appeared dependent on IVD health status. Using a drug delivery platform to sustain drug release, small molecule retention was prolonged in the IVD compared to other anatomical locations. In addition, retention appeared to be disease-dependent, which was not the case for the knee joint. Therefore, extrapolation of drug retention patterns from one type of tissue to another type of tissue is not recommended. Drug delivery targeting an avascular IVD with a confined space might benefit from PEA microspheres containing polymers with a more accelerated degradation pace than a knee joint with a relatively higher fluid exchange.

Acknowledgments:

This work was financially supported by a research grant from Life Sciences Health (LSH) Impulse, (ArIADNE; project #40-43100-98-022), and funding from the European Union's Horizon 2020 research and innovation program under Marie Sklodowska-Curie grant agreement No. 642414 and the Research and Innovation Program iPSpine under Grant agreement #825925 (www.ipspine.eu). Also, the financial contribution of the Dutch Arthritis Society is gratefully acknowledged (LLP22 and LLP12) and the uNMR-NL Grid: a distributed, state-of-the-art magnetic resonance facility for the Netherlands (NWO grant 184.035.002). The authors would like to thank Nico Attevelt, Alessia Longoni, and Sabrina Oliveira for their technical assistance.

Authors contributions:

Imke Rudnik-Jansen, Jie Du: contribution to study design, acquisition, analysis, interpretation of data, drafting and revising the manuscript. Nina Woike, Anna R. Tellegen, Wadhwani, Parvesh, Daniele Zuncheddu: contribution to study design, acquisition of data and revising the manuscript. Björn P. Meij, Jens Thies, Pieter Emans, Fetullah C. Öner, George Mihov, Joao Pedro Garcia, Anne Ulrich, Sibylle Grad, Marianna A. Tryfonidou: contribution to study design, revising the manuscript. Hugo van Ingen: contributions to study design, acquisition, interpretation of data, revising the manuscript. Laura B. Creemers: contributions to study design, interpretation of data, drafting and revising the manuscript, and takes responsibility for the integrity of the work as a whole, from inception to finished manuscript.

Supplementary figures

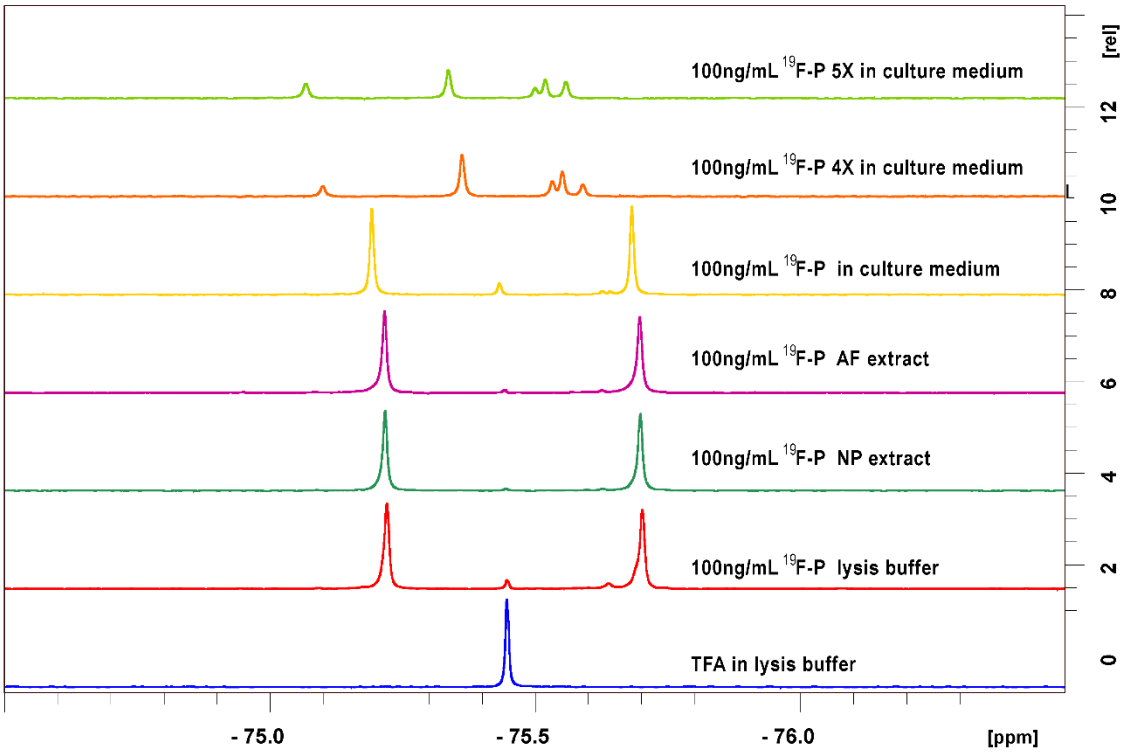

Supplementary figure 1. ^{19}F signal of ^{19}F-P dissolved in different solutions.

^{19}F-P was dissolved at 100 µg/mL in different buffers, including lysis buffer, NP lysate, AF lysate, IVD culture medium, 4/5 times concentrated IVD culture medium, and trifluoroacetic anhydride (TFA) was dissolved in lysis buffer at 1: 500,000 (v:v). All the samples were measured by ^{19}F NMR for 600 scans.

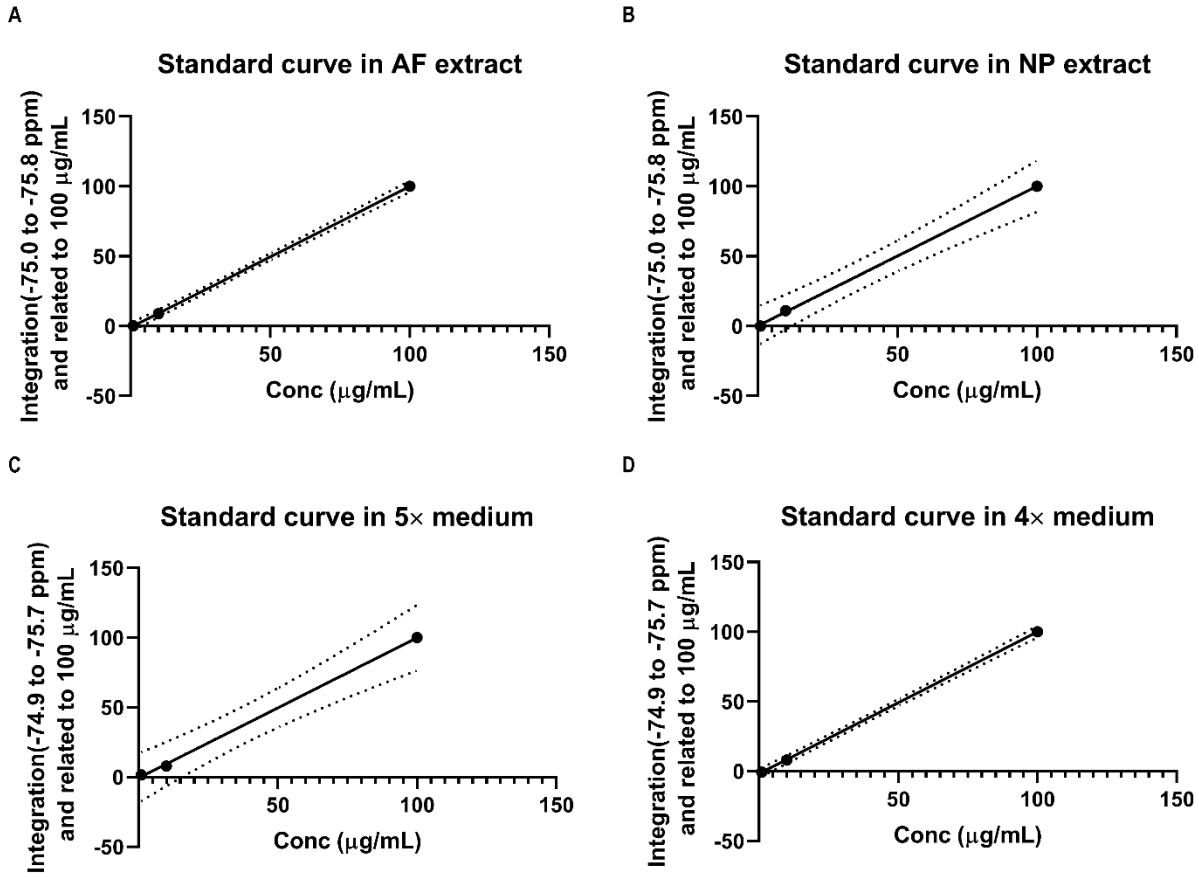

Supplementary figure 2. The ^{19}F-P standard curve in different solutions.

Three different concentrations of ^{19}F-P, 100 μg/mL, 10 μg/mL, 1 μg/mL, were prepared in different solutions according to the experiment samples, ***A)*** *AF lysate,* ***B)*** *NP lysate,* ***C)*** *5 times concentrated IVD culture medium,* ***D)*** *4 times concentrated IVD culture medium. The integral signal was highly related to ^{19}P-F concentration in all types of solution.*

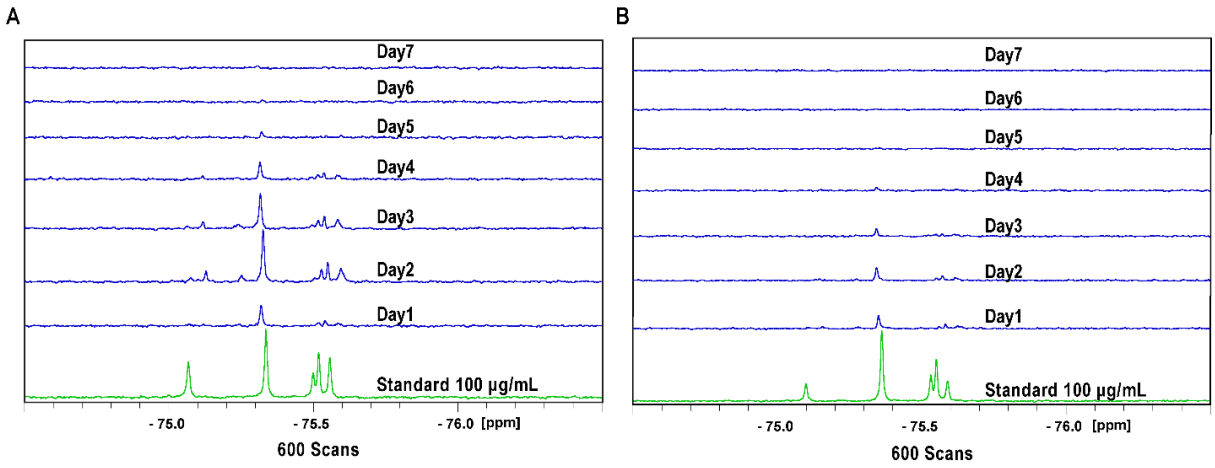

Supplementary figure 3. ^{19}F-P signal in IVD culture medium.

*IVD culture media were collected after static-free swelling **A)** and dynamic loading **B)** every day for 7 days. Media were lyophilized and reconstituted to concentrate 5 and 4 times, respectively. ^{19}F NMR has performed 600 scans at around 1 h for all the culture media and standard samples.*

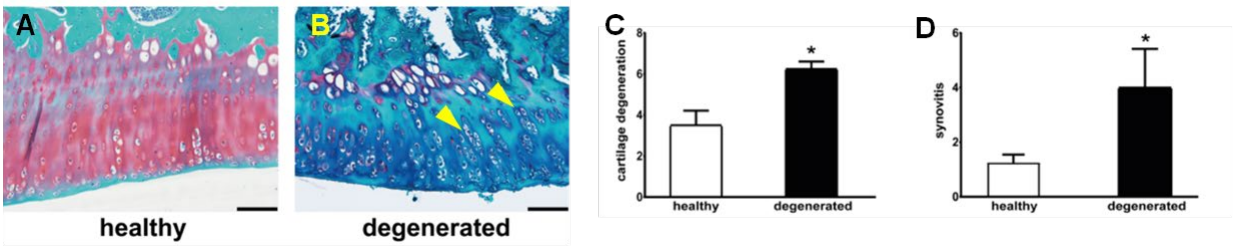

Supplementary figure 4. Confirmed degeneration of knee joints.

Degeneration of the knee joints, measured 4 weeks after induction using Mankin (C) and Krenn score (D) for cartilage degeneration and synovitis, respectively. Histologic image of a healthy non-operated knee joint (A) and degenerated knee joint (B) displaying loss of proteoglycans and chondrocyte cloning, indicated by yellow arrows. Scale bars = 50 µm.

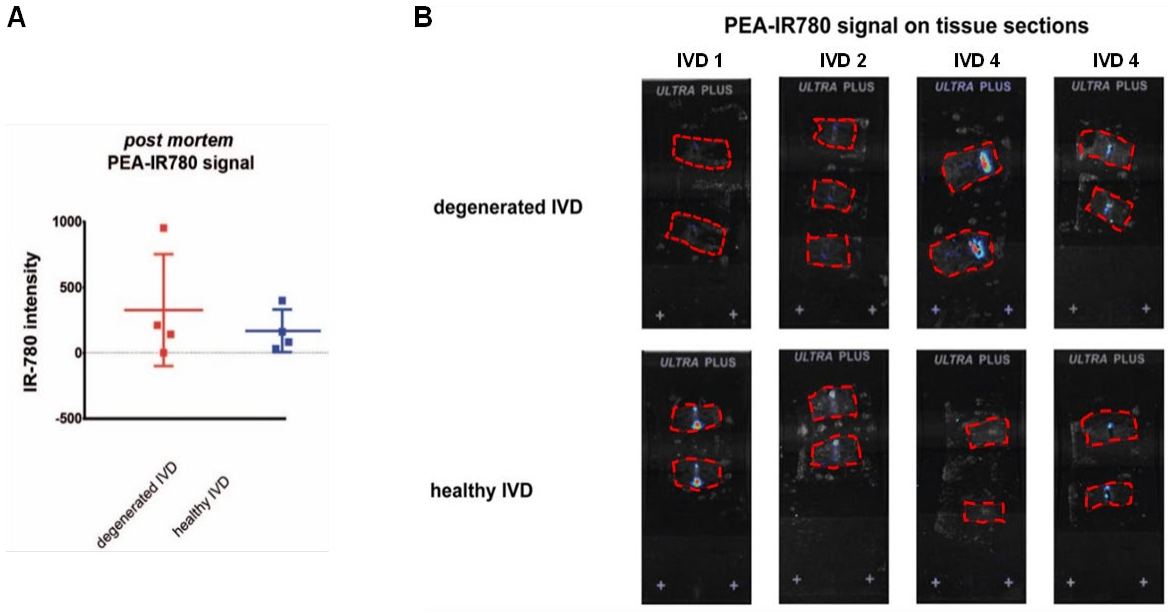

Supplementary figure 5. Post-mortem retention from controlled released IR-780 in healthy and degenerated IVD, 16 weeks post-injection.

A) Post-mortem IR-780 signal intensity, detected in healthy and degenerated skinned rat tail IVDs 16 weeks after intradiscal injection. Free IR-780 was undetectable. B) Post-mortem IR-780 signal intensity, detected in 5 µm thick histological IVD slides from formalin-fixed, EDTA-decalcified, paraffin embedded tissues. Free IR-780 was undetectable. The red dotted line indicates IVD tissue including rostral and caudal vertebrae. IVDs = intervertebral discs, PEA = polyesteramide.

References

[1] G.B.D. Disease, I. Injury, C. Prevalence, Global, regional, and national incidence, prevalence, and years lived with disability for 310 diseases and injuries, 1990-2015: a systematic analysis for the Global Burden of Disease Study 2015, Lancet 388(10053) (2016) 1545-1602.
[2] J.N. Katz, Lumbar disc disorders and low-back pain: socioeconomic factors and consequences, J Bone Joint Surg Am 88 Suppl 2 (2006) 21-4.
[3] J.W. Geurts, P.C. Willems, J.W. Kallewaard, M. van Kleef, C. Dirksen, The Impact of Chronic Discogenic Low Back Pain: Costs and Patients' Burden, Pain Res Manag 2018 (2018) 4696180.
[4] Y.G. Zhang, T.M. Guo, X. Guo, S.X. Wu, Clinical diagnosis for discogenic low back pain, Int J Biol Sci 5(7) (2009) 647-58.
[5] J. Antoniou, T. Steffen, F. Nelson, N. Winterbottom, A.P. Hollander, R.A. Poole, M. Aebi, M. Alini, The human lumbar intervertebral disc: evidence for changes in the biosynthesis and denaturation of the extracellular matrix with growth, maturation, ageing, and degeneration, J Clin Invest 98(4) (1996) 996-1003.
[6] P.J. Roughley, Biology of intervertebral disc aging and degeneration: involvement of the extracellular matrix, Spine (Phila Pa 1976) 29(23) (2004) 2691-9.
[7] H.E. Gruber, E.N. Hanley, Jr., Ultrastructure of the human intervertebral disc during aging and degeneration: comparison of surgical and control specimens, Spine (Phila Pa 1976) 27(8) (2002) 798-805.
[8] M. Molinos, C.R. Almeida, J. Caldeira, C. Cunha, R.M. Goncalves, M.A. Barbosa, Inflammation in intervertebral disc degeneration and regeneration, J R Soc Interface 12(104) (2015) 20141191.
[9] A.J. Freemont, T.E. Peacock, P. Goupille, J.A. Hoyland, J. O'Brien, M.I. Jayson, Nerve ingrowth into diseased intervertebral disc in chronic back pain, Lancet 350(9072) (1997) 178-81.
[10] J. Melrose, S. Roberts, S. Smith, J. Menage, P. Ghosh, Increased nerve and blood vessel ingrowth associated with proteoglycan depletion in an ovine anular lesion model of experimental disc degeneration, Spine (Phila Pa 1976) 27(12) (2002) 1278-85.
[11] W.T.M. Enthoven, P.D. Roelofs, B.W. Koes, NSAIDs for Chronic Low Back Pain, JAMA 317(22) (2017) 2327-2328.
[12] N.E. Foster, J.R. Anema, D. Cherkin, R. Chou, S.P. Cohen, D.P. Gross, P.H. Ferreira, J.M. Fritz, B.W. Koes, W. Peul, J.A. Turner, C.G. Maher, G. Lancet Low Back Pain Series Working, Prevention and treatment of low back pain: evidence, challenges, and promising directions, Lancet 391(10137) (2018) 2368-2383.
[13] P.D. Roelofs, R.A. Deyo, B.W. Koes, R.J. Scholten, M.W. van Tulder, Non-steroidal anti-inflammatory drugs for low back pain, Cochrane Database Syst Rev (1) (2008) CD000396.
[14] B.R. Whatley, X. Wen, Intervertebral disc (IVD): Structure, degeneration, repair and regeneration, Materials Science and Engineering: C 32(2) (2012) 61-77.
[15] M.A. Tryfonidou, G. de Vries, W.E. Hennink, L.B. Creemers, "Old Drugs, New Tricks" - Local controlled drug release systems for treatment of degenerative joint disease, Adv Drug Deliv Rev 160 (2020) 170-185.
[16] M. Muttenthaler, G.F. King, D.J. Adams, P.F. Alewood, Trends in peptide drug discovery, Nature Reviews Drug Discovery 20(4) (2021) 309-325.
[17] J.D. Glaeser, K. Salehi, L.E.A. Kanim, Z. NaPier, M.A. Kropf, J.M. Cuéllar, T.G. Perry, H.W. Bae, D. Sheyn, NF-κB inhibitor, NEMO-binding domain peptide attenuates intervertebral disc degeneration, The Spine Journal 20(9) (2020) 1480-1491.
[18] Effect of Synthetic Link N Peptide on the Expression of Type I and Type II Collagens in Human Intervertebral Disc Cells, 17(7-8) (2011) 899-904.
[19] Z. Wang, W.C. Hutton, S.T. Yoon, ISSLS Prize Winner: Effect of Link Protein Peptide on Human Intervertebral Disc Cells, Spine 38(17) (2013).

[20] F. Mwale, K. Masuda, M.P. Grant, L.M. Epure, K. Kato, S. Miyazaki, K. Cheng, J. Yamada, W.C. Bae, C. Muehleman, P.J. Roughley, J. Antoniou, Short Link N promotes disc repair in a rabbit model of disc degeneration, Arthritis Research & Therapy 20(1) (2018) 201.
[21] S.B. Blanquer, D.W. Grijpma, A.A. Poot, Delivery systems for the treatment of degenerated intervertebral discs, Adv Drug Deliv Rev 84 (2015) 172-87.
[22] M. Janssen, U.T. Timur, N. Woike, T.J. Welting, G. Draaisma, M. Gijbels, L.W. van Rhijn, G. Mihov, J. Thies, P.J. Emans, Celecoxib-loaded PEA microspheres as an auto regulatory drug-delivery system after intra-articular injection, J Control Release 244(Pt A) (2016) 30-40.
[23] A.R. Tellegen, I. Rudnik-Jansen, M. Beukers, A. Miranda-Bedate, F.C. Bach, W. de Jong, N. Woike, G. Mihov, J.C. Thies, B.P. Meij, L.B. Creemers, M.A. Tryfonidou, Intradiscal delivery of celecoxib-loaded microspheres restores intervertebral disc integrity in a preclinical canine model, J. Control. Release 286 (2018) 439-450.
[24] E. Botines, L. Franco, J. Puiggali, Thermal stability and degradation studies of alternating poly(ester amide)s derived from glycolic acid and omega-amino acids, Journal of Applied Polymer Science 102(6) (2006) 5545-5558.
[25] N. Willems, G. Mihov, G.C. Grinwis, M. van Dijk, D. Schumann, C. Bos, G.J. Strijkers, W.J. Dhert, B.P. Meij, L.B. Creemers, M.A. Tryfonidou, Safety of intradiscal injection and biocompatibility of polyester amide microspheres in a canine model predisposed to intervertebral disc degeneration, J Biomed Mater Res B Appl Biomater 105(4) (2017) 707-714.
[26] T. Wiersema, A.R. Tellegen, M. Beukers, M. van Stralen, E. Wouters, M. van de Vooren, N. Woike, G. Mihov, J.C. Thies, L.B. Creemers, M.A. Tryfonidou, B.P. Meij, Prospective Evaluation of Local Sustained Release of Celecoxib in Dogs with Low Back Pain, Pharmaceutics 13(8) (2021).
[27] J. Gaudreault, D. Fei, J. Rusit, P. Suboc, V. Shiu, Preclinical pharmacokinetics of Ranibizumab (rhuFabV2) after a single intravitreal administration, Invest Ophthalmol Vis Sci 46(2) (2005) 726-33.
[28] F. Cuyckens, Mass spectrometry in drug metabolism and pharmacokinetics: Current trends and future perspectives, Rapid Commun Mass Spectrom 33 Suppl 3 (2019) 90-95.
[29] G. Normand, M. Maker, J. Penraat, K. Kovach, J.G. Ghosh, C. Grosskreutz, S. Chandra, Non-invasive molecular tracking method that measures ocular drug distribution in non-human primates, Commun Biol 3(1) (2020) 16.
[30] M. Malet-Martino, V. Gilard, F. Desmoulin, R. Martino, Fluorine nuclear magnetic resonance spectroscopy of human biofluids in the field of metabolic studies of anticancer and antifungal fluoropyrimidine drugs, Clin Chim Acta 366(1-2) (2006) 61-73.
[31] G. Tsitlanadze, M. Machaidze, T. Kviria, N. Djavakhishvili, C.C. Chu, R. Katsarava, Biodegradation of amino-acid-based poly(ester amide)s: in vitro weight loss and preliminary in vivo studies, J Biomater Sci Polym Ed 15(1) (2004) 1-24.
[32] A.R. Tellegen, I. Rudnik-Jansen, B. Pouran, H.M. de Visser, H.H. Weinans, R.E. Thomas, M.J.L. Kik, G.C.M. Grinwis, J.C. Thies, N. Woike, G. Mihov, P.J. Emans, B.P. Meij, L.B. Creemers, M.A. Tryfonidou, Controlled release of celecoxib inhibits inflammation, bone cysts and osteophyte formation in a preclinical model of osteoarthritis, Drug Deliv 25(1) (2018) 1438-1447.
[33] J. Du, J.-J. Pfannkuche, G. Lang, S. Häckel, L.B. Creemers, M. Alini, S. Grad, Z. Li, Proinflammatory intervertebral disc cell and organ culture models induced by tumor necrosis factor alpha, 3(3) (2020) e1104.
[34] G. Lang, Y. Liu, J. Geries, Z. Zhou, D. Kubosch, N. Südkamp, R.G. Richards, M. Alini, S. Grad, Z. Li, An intervertebral disc whole organ culture system to investigate proinflammatory and degenerative disc disease condition, J Tissue Eng Regen Med 12(4) (2018) e2051-e2061.
[35] J. Du, J.P. Garcia, F.C. Bach, A.R. Tellegen, S. Grad, Z. Li, R.M. Castelein, B.P. Meij, M.A. Tryfonidou, L.B. Creemers, Intradiscal injection of human recombinant BMP-4 does not reverse intervertebral disc degeneration induced by nuclectomy in sheep, Journal of Orthopaedic Translation 37 (2022) 23-36.

[36] B. Han, K. Zhu, F.C. Li, Y.X. Xiao, J. Feng, Z.L. Shi, M. Lin, J. Wang, Q.X. Chen, A simple disc degeneration model induced by percutaneous needle puncture in the rat tail, Spine (Phila Pa 1976) 33(18) (2008) 1925-34.
[37] K. Masuda, Y. Aota, C. Muehleman, Y. Imai, M. Okuma, E.J. Thonar, G.B. Andersson, H.S. An, A novel rabbit model of mild, reproducible disc degeneration by an anulus needle puncture: correlation between the degree of disc injury and radiological and histological appearances of disc degeneration, Spine (Phila Pa 1976) 30(1) (2005) 5-14.
[38] H.E. Gruber, J. Ingram, E.N. Hanley, Jr., An improved staining method for intervertebral disc tissue, Biotech Histochem 77(2) (2002) 81-3.
[39] H.J. Mankin, L. Lippiello, Biochemical and metabolic abnormalities in articular cartilage from osteo-arthritic human hips, J Bone Joint Surg Am 52(3) (1970) 424-34.
[40] V. Krenn, L. Morawietz, G.R. Burmester, R.W. Kinne, U. Mueller-Ladner, B. Muller, T. Haupl, Synovitis score: discrimination between chronic low-grade and high-grade synovitis, Histopathology 49(4) (2006) 358-64.
[41] M. Ayoub, D.J.C.o. Scheidegger, Peptide drugs, overcoming the challenges, a growing business, 24(4) (2006) 46.
[42] H. Hu, N. Huang, P. Yi, Y.H. Hui, R.D. Dally, W.J. Ehlhardt, P. Kulanthaivel, Utilizing 19F NMR to investigate drug disposition early in drug discovery, Xenobiotica 45(12) (2015) 1081-91.
[43] E.K. Wagner, A. Vedadghavami, T.D. Jacobsen, S.A. Goel, N.O. Chahine, A.G. Bajpayee, Avidin grafted dextran nanostructure enables a month-long intra-discal retention, Sci Rep 10(1) (2020) 12017.
[44] H. Arakawa, H. Yamada, K. Arai, T. Kawanishi, N. Nitta, S. Shibata, E. Matsumoto, K. Yano, Y. Kato, T. Kumamoto, I. Aoki, T. Ogihara, Possible utility of peptide-transporter-targeting [(19)F]dipeptides for visualization of the biodistribution of cancers by nuclear magnetic resonance imaging, Int J Pharm 586 (2020) 119575.
[45] C. Gonzales, H.A. Yoshihara, N. Dilek, J. Leignadier, M. Irving, P. Mieville, L. Helm, O. Michielin, J. Schwitter, In-Vivo Detection and Tracking of T Cells in Various Organs in a Melanoma Tumor Model by 19F-Fluorine MRS/MRI, PLoS One 11(10) (2016) e0164557.
[46] S. Bo, Y. Yuan, Y. Chen, Z. Yang, S. Chen, X. Zhou, Z.X. Jiang, In vivo drug tracking with (19)F MRI at therapeutic dose, Chem Commun (Camb) 54(31) (2018) 3875-3878.
[47] B. Meng, S.L. Grage, O. Babii, M. Takamiya, N. MacKinnon, T. Schober, I. Hutskalov, O. Nassar, S. Afonin, S. Koniev, I.V. Komarov, J.G. Korvink, U. Strähle, A.S. Ulrich, Highly Fluorinated Peptide Probes with Enhanced In Vivo Stability for 19F-MRI, Small 18(41) (2022) 2107308.
[48] A. Reum Son, D.Y. Kim, S. Hun Park, J. Yong Jang, K. Kim, B. Ju Kim, X. Yun Yin, J. Ho Kim, B. Hyun Min, D. Keun Han, M. Suk Kim, Direct chemotherapeutic dual drug delivery through intra-articular injection for synergistic enhancement of rheumatoid arthritis treatment, Sci Rep 5 (2015) 14713.
[49] I. Rudnik-Jansen, S. Colen, J. Berard, S. Plomp, I. Que, M. van Rijen, N. Woike, A. Egas, G. van Osch, E. van Maarseveen, K. Messier, A. Chan, J. Thies, L. Creemers, Prolonged inhibition of inflammation in osteoarthritis by triamcinolone acetonide released from a polyester amide microsphere platform, J Control Release 253 (2017) 64-72.
[50] R. Weissleder, V. Ntziachristos, Shedding light onto live molecular targets, Nat Med 9(1) (2003) 123-8.
[51] D.J. Wilkinson, M.D.C. Arques, C. Huesa, A.D. Rowan, Serine proteinases in the turnover of the cartilage extracellular matrix in the joint: implications for therapeutics, Br J Pharmacol 176(1) (2019) 38-51.
[52] J. Salo, Z. Mackiewicz, A. Indahl, Y.T. Konttinen, A.K. Holm, A. Sukura, S. Holm, Plasmin-matrix metalloproteinase cascades in spinal response to an experimental disc lesion in pig, Spine (Phila Pa 1976) 33(8) (2008) 839-44.

[53] F.H. Meng, X.L. Shao, Y. Song, T. Zhang, Correlation between the Expression of High Temperature Requirement Serine Protease A1 in Nucleus Pulposus Tissue and the Degree of Intervertebral Disc Degeneration, Zhongguo Yi Xue Ke Xue Yuan Xue Bao 39(6) (2017) 737-742.
[54] A.N. Tiaden, M. Klawitter, V. Lux, A. Mirsaidi, G. Bahrenberg, S. Glanz, L. Quero, T. Liebscher, K. Wuertz, M. Ehrmann, P.J. Richards, Detrimental role for human high temperature requirement serine protease A1 (HTRA1) in the pathogenesis of intervertebral disc (IVD) degeneration, J Biol Chem 287(25) (2012) 21335-45.
[55] B. Sterner, M. Harms, S. Woll, M. Weigandt, M. Windbergs, C.M. Lehr, The effect of polymer size and charge of molecules on permeation through synovial membrane and accumulation in hyaline articular cartilage, Eur J Pharm Biopharm 101 (2016) 126-36.
[56] S. Roberts, J.P. Urban, H. Evans, S.M. Eisenstein, Transport properties of the human cartilage endplate in relation to its composition and calcification, Spine (Phila Pa 1976) 21(4) (1996) 415-20.
[57] A. Maroudas, Biophysical chemistry of cartilaginous tissues with special reference to solute and fluid transport, Biorheology 12(3-4) (1975) 233-48.
[58] C.J. Porter, S.A. Charman, Lymphatic transport of proteins after subcutaneous administration, J Pharm Sci 89(3) (2000) 297-310.
[59] J. Shi, Q. Liang, M. Zuscik, J. Shen, D. Chen, H. Xu, Y.J. Wang, Y. Chen, R.W. Wood, J. Li, B.F. Boyce, L. Xing, Distribution and alteration of lymphatic vessels in knee joints of normal and osteoarthritic mice, Arthritis Rheumatol 66(3) (2014) 657-66.
[60] K. Kliskey, K. Williams, J. Yu, D. Jackson, J. Urban, N. Athanasou, The presence and absence of lymphatic vessels in the adult human intervertebral disc: relation to disc pathology, Skeletal Radiol 38(12) (2009) 1169-73.
[61] M.H. Bonanomi, M. Velvart, M. Stimpel, K.M. Roos, K. Fehr, H.G. Weder, Studies of pharmacokinetics and therapeutic effects of glucocorticoids entrapped in liposomes after intraarticular application in healthy rabbits and in rabbits with antigen-induced arthritis, Rheumatol Int 7(5) (1987) 203-12.
[62] J.R. Fraser, W.G. Kimpton, B.K. Pierscionek, R.N. Cahill, The kinetics of hyaluronan in normal and acutely inflamed synovial joints: observations with experimental arthritis in sheep, Semin Arthritis Rheum 22(6 Suppl 1) (1993) 9-17.
[63] P.A. Simkin, J.E. Bassett, Pathways of microvascular permeability in the synovium of normal and diseased human knees, J Rheumatol 38(12) (2011) 2635-42.
[64] E. Selard, A. Shirazi-Adl, J.P. Urban, Finite element study of nutrient diffusion in the human intervertebral disc, Spine (Phila Pa 1976) 28(17) (2003) 1945-53; discussion 1953.
[65] Q. Zhu, X. Gao, W. Gu, Temporal changes of mechanical signals and extracellular composition in human intervertebral disc during degenerative progression, J Biomech 47(15) (2014) 3734-43.
[66] S. Li, J. Johnson, A. Peck, Q. Xie, Near infrared fluorescent imaging of brain tumor with IR780 dye incorporated phospholipid nanoparticles, J Transl Med 15(1) (2017) 18.
[67] T. Peters, S.W. Kim, V. Castro, K. Stingl, T. Strasser, S. Bolz, U. Schraermeyer, G. Mihov, M. Zong, V. Andres-Guerrero, R. Herrero Vanrell, A.A. Dias, N.R. Cameron, E. Zrenner, Evaluation of polyesteramide (PEA) and polyester (PLGA) microspheres as intravitreal drug delivery systems in albino rats, Biomaterials 124 (2017) 157-168.
[68] C.M.E. Rustenburg, K.S. Emanuel, M. Peeters, W.F. Lems, P.-P.A. Vergroesen, T.H. Smit, Osteoarthritis and intervertebral disc degeneration: Quite different, quite similar, JOR Spine 1(4) (2018) e1033.

Chapter 7

Summary and General Discussion

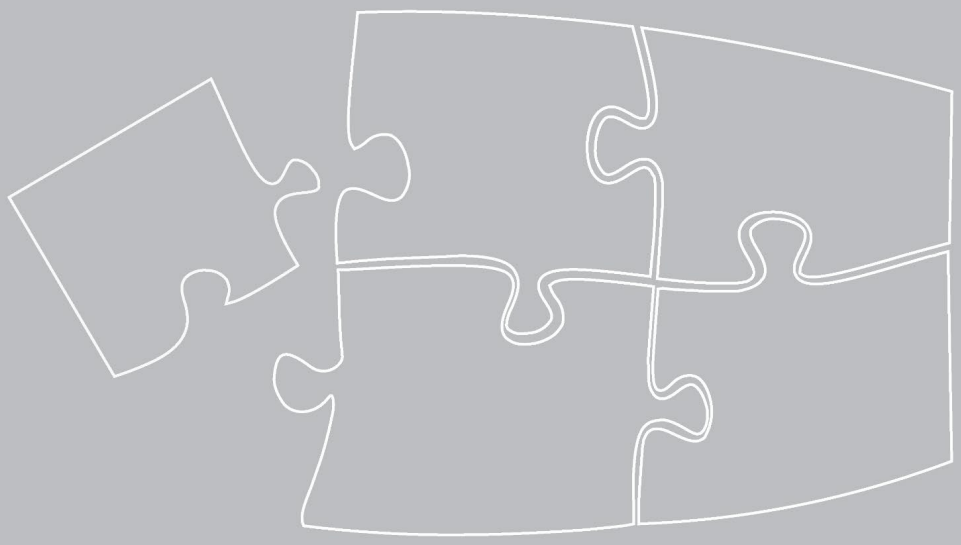

1. Summary and general discussion

1.1. Summary

Chronic low back pain (CLBP) affects more than 4% of the adult population and over 20% of the older population. It impairs the patient's quality of life and has a significant burden on the social and healthcare systems. Intervertebral disc (IVD) degeneration is a leading case of CLBP. To date, the clinical treatments are limited to pain relief strategies, and to date no efficient therapy was developed aiming at IVD regeneration. Hence, there is an unmet need for therapeutic strategies that are successful at alleviating pain, stopping disc degeneration, and inducing disc regeneration. This thesis aimed to understand degenerative processes of the IVD and propose potential therapeutic routes to halt degeneration and achieve regeneration.

It is widely accepted that inflammation plays a crucial role in IVD degeneration and discogenic low back pain. Hence, blocking inflammation is considered a viable strategy to relieve pain and delay disc degeneration. Drug development commonly starts *in vitro* and then moves to *in vivo*. A proper *ex vivo* model can bridge the gap between *in vitro* and *in vivo*, improve translatability and reduce animal use. Several pro-inflammatory cytokines have been shown to be associated with inflammation and pain in IVD degeneration, with TNF-α considered to be as one of the major regulators. Therefore, **in chapter 2**, a TNF-α-induced *ex vivo* IVD degenerative model was established on the bovine whole caudal IVD culture system under mechanical loading. Firstly, we confirmed that human recombinant TNF-α (hrTNF-α) has equal effects on bovine nucleus pulposus cells as bovine recombinant TNF-α. Then the intradiscal injection dose of hrTNF-α was optimized to induce sufficient inflammatory and pro-catabolic reaction demonstrated by increased release of inflammatory mediators and glycosaminoglycan (GAG) and upregulated degeneration-related genes. In addition, we found that the time point of anti-inflammatory treatment was crucial to achieving significant effects. This model can be used to further elucidate the mechanisms of TNF-α-induced IVD degeneration, and importantly, can serve as model for screening of bioactives targeting TNF-a inhibition.

A previous study reported that bone morphogenetic protein- 4 (BMP-4) has potent effects on NP matrix regeneration, as shown in a co-culture of human NP cells and mesenchymal stem cells. **In chapter 3**, the effects of BMP-4 on IVD regeneration were evaluated *in vitro* and *in vivo* on sheep models. *In vitro*, the regenerative effects of BMP-4 on NP and AF cells were shown by improved cell proliferation and ECM production. Interestingly, BMP-4 induced a phenotype shift in AF cells, as demonstrated by increased proteoglycans and collagen type II production, which is a characteristic of NP cells. However, upon intradiscal injection of BMP-4 in a nucleotomy-induced sheep lumbar IVD degeneration model, no regeneration in the NP nor AF was observed. Instead, side effects were found, including extradiscal new bone formation and Schmorl's node-like changes in the endplate. These results suggest that direct intradiscal injection of BMP-4 may not be a suitable strategy for IVD regeneration. More factors should be considered before attempting translation BMP-4 for IVD regeneration, for instance, the delivery method.

To restore the function of the IVD, keeping its structural integrity is essential. Although the AF is a crucial component of the IVD, this structure is often overlooked in therapy development.

Strategies to repair AF injuries and defects are important in preventing or halting IVD degeneration and promoting regeneration. **In chapter 4,** AF analog scaffolds were explored and evaluated *in vitro* and *ex vivo*. We found that pre-treating AF cells with TGF-β induced a functional AF phenotype, possibly promoting AF repair, which was demonstrated by upregulation of several functional genes and improved cell contractility. These pre-treated AF cells were encapsulated in a collagen I hydrogel supplemented with TGF-β, then seeded into a PU scaffold to build a tissue engineered AF construct. The collagen type I hydrogel helped maintain the AF functional phenotype, and the TGF-β supplement within the collagen type I hydrogel further promoted cell proliferation and matrix deposition *in vitro*. Implantation of this AF construct in a bovine caudal IVD organ culture model led to enhanced deposition of collagen. Our findings demonstrate that the combination of cellular, biomaterial and bioactive strategies has excellent potential for AF regeneration.

Characterization of cells is vital for cell-based therapies for AF regeneration. $CD146^+$ AF cells show a contractile phenotype, and TGF-β enhances this cellular phenotype by promoting CD146 upregulation. Altogether, it is suggested that CD146 might be a potential functional marker for AF tissue engineering cell sources. Understanding the role of CD146 in AF cells and the underlying mechanism of the regulation by TGF-β may facilitate using $CD146^+$ for AF regeneration. In this context, in **chapter 5**, we found that knockdown CD146 in human AF cells decreased contractility accompanied by down-regulation of smooth muscle protein 22α (SM22α). Furthermore, we demonstrated that TGF-β upregulated CD146 via ALK5 signaling cascade, partially through SMAD2/4 and AKT pathway, whereas ERK was shown to be a potential negative modulator. Hence, we partly elucidated the underlying signaling pathway of CD146 upregulation by TGF-β in AF cells and suggest that CD146 can potentially be used as a functional marker in AF repair strategies.

Intradiscal administration has been proposed as a desirable strategy for drug delivery to increase local drug concentration, prolong drug retention, and reduce systemic side effects because of the isolated nature of IVD. The pharmacokinetics of local delivery is fundamental knowledge to guide and design adequate drug administration. However, it was seldomly investigated for intradiscal administration. **In chapter 6**, a ^{19}fluorine- labelled peptide (^{19}F-P), used as a model for small-peptide drugs, was used to study drug retention in the IVD. In the *ex vivo* IVD culture model, little peptide remained in the IVD after one week of culture. *In vivo*, no signal was detected 3 months after intradiscal delivery in the sheep lumbar IVDs. This may indicate that the peptide was quickly cleared from the IVD after intradiscal bolus injection. In addition, a near-infrared (NIR) fluorescent dye, IR-780, was used to mimic hydrophobic small molecular drugs. IR-780 was loaded in polyesteramide microspheres (PEAMs) and studied in a rat IVD degeneration model. Intradiscal drug retention was studied in free and encapsulated IR-780 in both healthy and degenerated IVDs by using NIR imaging. In addition, encapsulated IR-780 was injected into subcutaneous, healthy and OA knee joints to investigate drug retention between those tissue. Notably, in the IVD drug retention was prolonged by PEAMs compared to bolus injection. Interestingly, retention of the loaded drug in PEAMs was further extended by IVD degeneration. Additionally, drug retention in the IVD was more extended than in the knee joint and subcutaneously. This study provides evidence of drug release and retention profiles in the IVD by using different methods and models. Results showed that drug retention in the IVD can be affected by degeneration, and that a proper

drug release system could prolong drug retention in IVD, which theoretically may improve treatment outcomes.

1.2. General discussion

Chronic low back pain (CLBP) affects a large part of the population worldwide and brings enormous direct and indirect economic costs to society. Currently, treatments are limited to efforts in relieving pain, and their outcomes are still unsatisfactory. Intervertebral disc (IVD) degeneration has been suggested as the most common source of CLBP. Several strategies have been investigated to halt the IVD degeneration and to restore the IVD functions, by IVD regeneration. However, the IVD is a complex cartilaginous tissue, and the pathology of disc degeneration is still not fully elucidated. Understanding the degenerative processes and cell biology of the IVD will guide and facilitate the development of therapeutic treatments. Therefore, the studies described in this thesis investigated multiple aspects of improving IVD degeneration treatment, including new strategies to regenerate the IVD (nucleus pulposus and annulus fibrosus), the role of inflammation in IVD degeneration, AF cell biology, and drug retention in IVD. Results, challenges, and future perspectives for IVD degeneration treatments are discussed below.

1.2.1. Inflammation and anti-inflammatory treatment in disc degeneration and chronic low back pain.

The function of inflammation is to eliminate the initial cause of infection and/or tissue damage and initiate repair. To date, it is widely accepted that inflammatory processes play a vital role in IVD degeneration and CLBP [1]. Upregulation of pro-inflammatory factors has been identified in degenerated IVDs, such as interleukins (ILs, IL-1β, IL-6, IL-8, IL-17), interferon-gamma (IFN-γ), and tumor necrosis factor-alpha (TNF-α) [2-5]. TNF-α is one of the most commonly used pro-inflammatory factors for inducing disc degeneration. TNF-α induces IVD degeneration through several processes, such as amplifying inflammation and inducing immune cell infiltration, promoting ECM degradation and decreasing its production, accelerating cell senescence and death, and inducing angiogenesis and reinnervation [6-9]. **Chapter 2** described two models of TNF-a-induced inflammation, *i)* an *in vitro* 2D monolayer culture model, and ii) an *ex vivo* whole bovine caudal IVD culture model. The 2D model is most commonly used because it is low-cost and convenient for large-scale cultures. The major disadvantage of 2D models is that isolated disc cells lose their native structural and biomechanical environment. In addition, the cell phenotype changes with cell expansion [10], which could affect experimental results and outcomes, therefore impairing and limiting clinical translation [11]. The 3D whole IVD culture model has been suggested as a better model to simulate *the in vivo* environment of IVD cells and reduce animal use as a preclinical model. Our *in vitro* results showed that TNF-α treatment promoted degeneration by upregulating pro-inflammatory cytokines, inducing ECM catabolism, and reducing ECM anabolism. TNF-α intradiscal injection in the *ex vivo* model promoted the release of inflammatory modulators and degradation of the ECM, but did not down-regulate ECM gene expression. These findings highlight the difference between *in vitro* and *ex vivo* models and suggests a protective effect of the IVD environment from inflammation. In addition, our results showed that the anti-inflammatory treatment at the early stage was crucial to achieve a significant effect in preventing further disc degeneration, as it was shown that TNF-α induced a non-

recoverable catabolic shift of NP cells [12], and even transient exposure to TNF-α results in lasting biophysical changes in NP cells [13]. This further indicated that a combination of anti-inflammation treatment with other strategies, such as inhibition of ECM catabolic enzymes, or supplementation of growth factors, which can reverse the functionality of NP cells likely could achieve better outcomes.

In the current study, we focused on evaluating the effect of TNF-α on ECM metabolism and inflammatory factor release. Besides, our *ex vivo* model can also be used to investigate the role of TNF-α in cell death, cell senescence, and innervation. Several studies have shown that culture of NP cells with TNF-α enhanced cell apoptosis [14, 15]. A previous study showed that injection of TNF-α in whole caudal bovine IVD and culturing with a physiological loading did not induce loss of cell viability compared with PBS injection [16]. In contrast, the combination of nutrient deficiency and overloading in the presence or absence of TNF-α significantly reduced cell viability in both the NP and AF [16]. This indicates that inflammation may not be the trigger of cell death at the early stage of IVD degeneration. Senescent cells are metabolically viable but arrest cell cycle transition, cease proliferation and exhibit altered expression of various catabolic cytokines and degrading enzymes [17]. Senescent cell accumulation in degenerative IVD has been reported [18, 19]. Therefore, acceleration of cell senescence could be another mechanism related to inflammation-induced IVD degeneration. TNF-α promotes cell senescence, which has been established in 2D cell culture models and IVD tissue culture [12, 20, 21]. Besides its role on IVD cell biology, inflammation is also associated with reinnervation, blood vessel ingrowth, and pain in the IVD. It has been reported that IL-1β and TNF-α stimulation promoted the gene expression of vascular endothelial growth factor (VEGF), nerve growth factor (NGF), and brain-derived neurotrophic factor (BDNF) in NP cells, resulting in angiogenesis and innervation [22]. Degenerative NP cells in alginate beads promoted neurite outgrowth of human SH-SY5Y neuroblastoma cells [23]. However, as behavior in isolated cells and explants is likely different from the native environment, the inflammatory whole bovine IVD culture system described **in chapter 2** could be a suitable and versatile model to explore the role of inflammation on innervation, and vessel ingrowth by developing proper co-culture models. This model could furthermore be used to develop new anti-inflammatory drugs that could prevent these processes. In the future, the *ex vivo* model described here, could be modified to better mimic *in vivo* conditions by, for instance, culturing the IVD with limited supply of nutrients and oxygen and multiaxial loading patterns [24, 25]. The IVD inflammation can also be induced by other pro-inflammatory factors like, IL1-β, lipopolysaccharide, or combinations [26]. In addition, including other degenerative triggers, such as, over loading and enzymatically digestion in the inflammatory ex *vivo* system can develop complex IVD degenerative models for investigation of IVD degeneration and regeneration [16, 27].

Given the vital role of inflammation in IVD degeneration and pain, anti-inflammatory treatments have been widely studied. Glucocorticoids are commonly used in the treatment of LBP by epidural injection and nerve root block [28, 29]. However, these therapies are usually short-term. Long-term glucocorticoid treatment risks bone loss and glucocorticoid-induced osteoporosis [30, 31]. Clinical studies showed that intradiscal glucocorticoid injection could reduce pain for 1 month but not 3, 6, and 12 months [32, 33]. Therefore, other types of anti-inflammatory drugs should be developed for CLBP treatment. A single injection of IVD cells overexpressing IL-1 receptor

antagonist (IL-1Ra) in IVD explants resulted in significant inhibition of all matrix degradation enzymes [34]. In *ex vivo* murine and human discs cultured with Atsttrin, an engineered antagonist of TNFR (TNF receptor) signaling, an effective inhibition of TNF-α-mediated catabolism and TNF-α-induced inflammatory cytokine release was observed in the murine and human discs, respectively [35, 36]. Intradiscal infliximab injection, an anti-TNF-α monoclonal antibody, alleviated pain in a puncture-induced disc degeneration model in rats [37]. In a clinical setting, intradiscal injection of a single dose of Etanercept (0.1-1.5 mg per disc) in patients with CLBP was unable to resolve chronic discogenic pain compared to placebo control [38]. However, a higher dose of Etanercept, 10 mg per disc combined with bupivacaine, alleviated intractable discogenic LBP for up to 8 weeks compared to bupivacaine alone [39]. Local sustained drug delivery has been proposed as a strategy to prolong drug effects in CLBP treatment due to the avascular nature of the IVD [40]. Local and controlled drug delivery allows for a prolonged bioactivity of drugs, minimizing side effects and improving efficacy. Indeed, intradiscal controlled release of celecoxib from polyesteramide microspheres prevented the progression of IVD degeneration both *in vitro* and *in vivo* [41]. Further, in a randomized prospective double-blinded placebo-controlled study, results showed improvement in pain in dog patients for 12 weeks [42].

Overall, anti-inflammation treatments could be an effective strategy for CLBP in relieving pain and delaying IVD degeneration. Initiating anti-inflammation treatment at an earlier stage of IVD degeneration could improve the final outcome. Nevertheless, it may not be sufficient to induce IVD regeneration in more degenerated stages and, in this regard, regenerative cues should be applied. As the excessive inflammatory environment can impede the disc regeneration process, anti-inflammatory treatment could be combined with a regeneration approach for achieving better IVD regeneration [43, 44].

1.2.2. Regeneration by growth factors

Several strategies have been applied to induce IVD regeneration, for instance by using growth factors, cells, biomaterials, and gene therapies or by combining these [45-47]. Growth factors promote anabolism and reduce catabolism by increasing cellular viability, cell proliferation, ECM production, and decreasing ECM degradation. Several growth factors have been widely studied for these purposes in the last decade, including insulin-like growth factor (IGF), epidermal growth factor (EGF), platelet-derived growth factor (PDGF), and transforming growth factor (TGF) superfamily members, TGF-β, bone morphogenetic proteins (BMPs) and BMP subfamilies, growth differentiation factors (GDF) [48]. In **chapter 3,** the regenerative potential of BMP-4 was confirmed on sheep IVD cells *in vitro,* as reported before on degenerated human NP cells [49]. However, no regeneration effects were observed *in vivo*. In contrast, side effects such as extradiscal bone formation and Schmorl's node-like changes were detected after intradiscal injection in degenerated sheep lumbar IVDs. Extradiscal bone formation has been reported when BMP-7 was injected intradiscally in a canine model of spontaneous IVD degeneration [50]. Ectopic bone in the spinal canal was also reported when using BMP-2 for spine fusion in the humans [51]. Thus far, BMP-2, BMP-7, PDGF-BB have been FDA-approved for bone regeneration [52].

Interestingly, many growth factors have been reported to promote both bone and IVD regeneration. For instance, IGF-1 promoted osteoblast differentiation [53, 54], and IGF-1 loaded

implants enhance bone regeneration [55, 56]. In addition, evidence showed that reducing the expression of IGF-1 receptor leads to accelerated IVD degeneration in mice [57]. Exogenous IGF-1 stimulated proteoglycan synthesis in bovine NP cells *in vitro* [58], and sustained delivery of IGF-1 increased cell proliferation and decreased apoptosis in a rat disc degeneration model [59]. Therefore, understanding the underlying mechanism of growth factors on bone and cartilage-like tissue generation will facilitate their use for IVD regeneration and eliminate or reduce the side effects of ectopic bone formation. To the best of our knowledge, this study is the first time a Schmorl's node-like change is reported after intradiscal growth factor delivery. Similar adverse effect has been reported after intradiscal delivery stromal vascular fraction, an adipose tissue-derived heterogeneous cell mixture containing, among others, multipotent adipose stromal cells and erythrocytes, into goat IVD degenerative models [60]. It may indicate that inducing endplate and vertebral bone resorption could be a potential side effect when using growth factors for IVD regeneration. The underly mechanism still needs to be further elucidated.

Relieving discogenic pain is one of the main purposes of IVD regeneration. Evidence shows that reinnervation and revascularization are related to disc degeneration and discogenic pain [22, 61, 62]. But the effects of growth factors on reinnervation and revascularization are rarely investigated when assessing growth factors for IVD regeneration. It is worth noting that several growth factors have the potential to promote nerve growth and angiogenesis by increasing the expression of neurotrophic and angiogenic factors, including NGF, BDNF, and VEGF in disc cells [63-65]. For instance, TGF-β was shown to promote angiogenesis by recruiting hematopoietic cells and inducing VEGF production in these cells [66]. Intraperitoneal injection of TGF-β elevated NGF expression in a mouse IVD injury model [63]. In this context, the potential side effects, especially on reinnervation and revascularization, should be addressed when assessing growth factors for IVD regeneration. GDF-6 injections positively affected disc degeneration, as demonstrated by partial restoration of disc height, improved MRI disc degeneration grades, decreased degeneration-associated *il-6*, *tnf-α*, *vegf*, *ngf*, and prostaglandin-endoperoxide synthase 2 expression in a rabbit annular-puncture model [67]. Similar results were reported in a rat posterior disc puncture model [68], altogether suggesting GDF-6 may be a better candidate. However, clinical trials using rhGDF-5 for the treatment of early-stage lumbar disc degeneration were discontinued (NCT01124006, NCT00813813, NCT01158924, NCT01182337). To date, a small number of growth factors were reported to have translation potential for IVD regeneration, therefore research into the effects of other growth factors or combinations of growth factors is warranted.

In vivo, the presence of proteolytic enzymes leads to poor stability and a short half-life of growth factors [69]. Therefore, multiple and/or supraphysiological doses are often necessary to sustain an effective concentration of growth factors at the delivery site, resulting in high cost and adverse effects [70]. In this context, several delivery systems have been developed for growth factor delivery to prolong the growth factor retention and mitigate the side effect, including natural materials, polymers, composites-based hydrogels, microspheres, and scaffolds [71, 72]. An appropriate drug delivery system could facilitate the successful clinical transformation of growth factor therapy for IVD regeneration. In addition, delivery of growth factors by gene-edited disc cells or stem cells could be a promising strategy and warrants further studies [73, 74]. The challenges that come with local drug delivery are further discussion in section 1.2.4.

1.2.3. Annulus fibrosus tissue engineering

In healthy conditions, the AF is critical for the function and mechanical properties of the IVD, therefore its structural integrity is crucial to achieving IVD regeneration and restoring the native function of the IVD. AF repair strategies could potentially be used to decrease the likelihood of re-herniation, prevent further IVD degeneration, and prevent leakage of intradiscal therapeutic agents [75, 76]. Tissue engineering could be an efficient strategy to achieve large AF defect repair because of the AF's complex structure and mechanical environment. Firstly, seeded cells may be a critical component in rebuilding the biological component of AF. Both AF cells and certain stem cell types are potential candidates. Although stem cells were shown to differentiate to an AF-like phenotype *in vitro*, producing collagen type I, proteoglycan, and collagen type II [77, 78], MSCs failed to produce matrix in an *ex vivo* bovine IVD culture model. However, they may positively affect the phenotype of host disc cells via paracrine signaling [79]. This suggests that mature AF cells might be better candidates to produce AF matrix and achieve fast AF repair in AF tissue engineering. Although autologous AF cells could be isolated from injured AF tissue, and harvesting AF cells from IVD is less invasive than NP cells, the cell yields are likely suboptimal. In the future, a stable AF-specific differentiation method should be established to solve this limitation by using stem cells. **In chapter 4**, the TGF-β pre-treated AF cells were used in an AF tissue engineered construct. These cells were shown to produce a new matrix after being implanted in a bovine IVD *ex vivo* culture model. In addition, TGF-β supplementation further improved matrix production. **In chapter 5**, we confirmed that TGF-β could induce a functional AF phenotype in AF cells and this phenotype was associated with CD146 upregulation [80]. CD146 was identified as a cell adhesion molecule, which is involved in the process of cell adhesion by binding to other cells or ECM [81, 82]. In addition, CD146 has been used as a marker for pericytes and vascular smooth muscle cells as well as endothelial cells, and identified as a tendon stem cell marker promoting tendon regeneration [83, 84]. Our results showed that CD146 played an important role in maintaining the cell contractility of AF cells and potentially regulated AF functional gene expression, altogether suggesting that CD146 could be a functional AF cell marker for AF repair strategies. Sorting or inducing best-performing AF cells may be a more effective strategy to reach tissue repair [85]. However, successful implementation of biomedical intervention therapy requires in-depth knowledge of IVD cells and molecular biology [86].

Understanding the underlying signaling of functional markers can be potentially critical to produce potent functional AF cells for AF tissue engineering and for guiding AF regeneration approaches. **In chapter 5,** our results elucidated that TGF-β upregulated CD146 via ALK5 signaling cascade, partially through SMAD2, SMAD4, and AKT pathway, whereas ERK was shown to be a potential negative modulator. Some other key factors have also been identified in AF development, maintenance, and regeneration, such as Mohawk (Mkx) and SCX [87, 88]. Mkx has been found mainly to be expressed in the outer AF of humans and mice, and it has been identified as a key transcription factor that regulates AF development, maintenance, and regeneration [87]. In tendon cells, Smad3 binds Mkx and positively regulates tendon matrix organization [89]. Wnt/β-catenin signaling inhibits Mkx and tenogenic gene expressions [90]. In a neonatal mice model of an AF defect, it was found that SCX-lineage AF cells lose SCX expression, adopt a stem/progenitor phenotype, proliferate, and then re-differentiate towards type I collagen-producing cells, but not

in adult mice [88]. SCX, but not Mkx, was upregulated by TGF-β in AF cells **in Chapter 5**. So far, this basic knowledge is deficient in the AF tissue and warrants further investigation.

Supporting scaffolds are crucial to provide a platform for seeded cells to grow, produce ECM, or differentiate in AF tissue engineering [91-93]. In addition, the scaffold should ideally mimic the native AF microstructure, be strong enough to sustain the complex mechanical loading the IVD is exposed to and be suitable for fixation [91]. Polyurethane (PU)-based materials are biocompatible and biodegradable and have high stiffness, excellent flexibility and processability, matching those requests [94]. **In chapter 4**, porous PU scaffolds supported AF cell growth and prevented NP herniation in the *ex vivo* IVD culture model of AF defect. In addition, electrospinning has been commonly used to simulate the microstructure of AF, therefore, mimicking its mechanical properties [95, 96]. Chemical surface modification by anionic dihydroxyl oligomer increases the surface polar chemistry of PU scaffolds, improving AF cell attachment and ECM retention on the scaffold [93, 97]. Besides PU, many other materials have been evaluated as scaffolds for AF tissue engineering. For instance, other i) synthetic polymers such as poly(Ɛ-caprolactone), poly (trimethylene carbonate), poly(lactide-co-glycolide), and ii) naturally-occurring biomaterials such as collagen, fibrin hydrogel crosslinked with genipin (FibGen), silk, and decellularized AF matrix [91, 98]. Interestingly, recent studies showed the combination of synthetic polymers and natural polymers could increase cell proliferation and AF matrix production in scaffolds [99, 100].

Incorporating bioactive molecules into the AF construct could facilitate AF repair and regeneration by promoting cell migration, proliferation, and ECM production [101]. Hydrogels are scaffolds that can be used to encapsulate and deliver bioactive molecules and cells [102-104]. **In chapter 4,** a collagen I hydrogel, one of the main components of AF ECM, has been used to encapsulate AF cells and TGF-β. Scaffolds with encapsulated TGF-β produced more ECM when compared with scaffolds with cells alone. Similarly, Chen Liu et al. (2019) reported that decellularized AF matrix/chitosan hybrid hydrogels loaded with basic fibroblast growth factor (bFGF) effectively promoted the production of AF tissue ECM [103]. Recently, a multifunctional nanofibrous scaffold was developed with angle-ply microstructure co-delivered with TGF-β and an anti-inflammation drug, ibuprofen [101]. Scaffolds presented good anti-inflammatory properties, enhanced ECM formation and maintained the mechanical properties in rat models of IVD defect and replacement [101]. Similar strategies showed encouraging effects also on cartilage regeneration and IVD regeneration. S.J. Lin et al. (2022) reported that sustained release of TGF-β3 by PLGA microspheres encapsulated in methoxypoly (ethylene glycol)-poly(alanine) hydrogels enhanced chondrogenesis *in vitro* [105]. An injectable hydrogel scaffold loaded with IL-4 and kartogenin sustained-release PLGA microspheres promoted IVD tissue regeneration by increasing the proportion of M2 macrophages, promoting ECM gene expression, and reducing *mmp-3* expression in a rat IVD degeneration model [106]. In the future, more delivery platforms, for instance, microspheres and nanoparticles, and other bioactive agents, including growth factors, anti-inflammation drugs, and therapeutic DNA/RNAs, should be developed and combined with AF constructs to facilitate AF repair and regeneration.

In recently studies, tissue engineering strategy for AF repair and regeneration achieved promising results [99, 101, 105]. However, to date, it is still at an early stage, and most of the studies evaluated the AF constructs *in vitro* or in small animal models where the mechanical environments

are significantly different to the human situation. A recently study showed that FibGen is better than poly(trimethylene carbonate) scaffolds for AF repair to seal AF tested on ovine AF injury model [107]. Therefore, better *ex vivo* and large animal models to mimic human-scale biomechanics should be used to design, develop and test potential AF repair strategies.

1.2.4. Drug retention in IVD

As mentioned previously, intradiscal controlled drug delivery could increase the local drug concentration and prolong drug exposure, thus improving efficacy and circumventing repeated administration and systemic side effects. Various drug delivery systems have been widely investigated to further enhance intradiscal administration's efficacy and safety [108], however there is little knowledge on drug retention and clearance profiles after intradiscal administration. In this context, a deeper insight into drug retention and clearance is crucial to optimize and predict drug efficacy and safety. **In Chapter 6,** drug retention in the IVD after intradiscal injection was evaluated using different drug mimics and experimental models. The majority of ^{19}F-P, soluble peptide, was cleared from the IVD after 1 week culture in the *ex vivo* IVD culture model. In contrast, the NIR dye, a hydrophobic small molecule, was detected after 2 months upon intradiscal injection into healthy and degenerated rat tail IVDs. Present results may suggest that hydrophobic materials probably remain longer in the IVD than soluble materials after intradiscal administration. These results may provide a potential explanation for clinical outcomes, in which CLBP patients with active discopathy were treated by intradiscal injection of insoluble prednisolone acetate and reported reduced pain intensity for 1 month but not at 3 months or longer [32, 33]. In addition, our results showed that a drug delivery system, polyesteramide (PEA) microspheres, could prolong the retention of NIR dye in rat tail IVDs, as the signal remained visible after 16 weeks of follow-up. These findings were partially corroborated in another study where celecoxib-loaded PEA microspheres were injected in dogs with low back pain. Celecoxib-loaded particles reduced pain interference with daily life activities when compared to placebo up to 6 and 12 weeks [42]. The PEA-based drug delivery system has been proposed to be superior over PLGA, an FDA-approved material, because PEA is broken down in non-toxic waste products by proteolytic enzymes [109]. A previous study showed that PLGA microspheres were still visible in the disc for 4 weeks after administration in rat caudal discs [110]. This may indicate that PEA microspheres could remain longer in the IVD compared to PLGA microspheres. However, this should be confirmed in further study. In addition, our results showed that drug release from PEA microspheres is degeneration-dependent, potentially due to their sensitivity to serine protease activity. Various serine proteinases have been described to play a role in IVD degeneration pathology, such as high temperature requirement serine protease A1 [111]. Therefore, using PEA-based drug delivery for intradiscal administration deserves further study.

In the current study, drug retention was assessed by using ^{19}F NMR and NIR fluorescence imaging. When compared to traditionally used methods, such as enzyme-linked immunosorbent assay (ELISA) and liquid chromatography/mass spectrometry (LC/MS), there are several advantages and disadvantages. The peptide-based therapeutic has become one of the fastest-growing classes of new drugs [112]. When using traditional methods to track peptides, the sensitivity and specificity of ELISA are determined by the antibody used, and both ELISA and LC/MS can interfere with endogenous peptides. In contrast, ^{19}F NMR is highly specific and can

exclude endogenous interference, although the peptide should be fluorine labeled. Additionally, the large chemical shift range of ^{19}F NMR responding to a chemical environment makes this method sensitive to detecting structural changes, possibly allowing the measurement of drug degradation. Several approaches have been used to improve the pharmacokinetic properties of peptides, including fluorinated amino acid replacement [113]. In addition, in recent years, approximately 20% of the marketed drugs have a least one fluorine atom [114]. Hence, ^{19}F NMR could be used to study the pharmacokinetics of these fluorine-containing drugs. However, this ^{19}F nuclear magnetic resonance-based approaches also present some drawbacks. For instance, this method is less sensitive than ELISA [115, 116], and the assessment can only be conducted at the endpoint. Although ^{19}F nuclear magnetic resonance imaging (^{19}F MRI) could be a further alternative to visualize fluorinated drugs *in vivo*, the resolution is still limited nowadays [117, 118]. NIR fluorescence imaging is a sensitive, noninvasive approach, and it can monitor drug release in real-time [119, 120]. Another advantage of using NIR imaging to assess local drug release over time is the minimal tissue autofluorescence in the NIR wavelength region [121]. However, noninvasive NIR fluorescence imaging of lumbar IVDs is currently difficult due to its limited tissue penetration [122, 123]. Therefore, cervical and caudal IVDs in animal models probably are better suited than the lumbar IVDs which are covered by bulky muscles. Otherwise, the assessment should be conducted on isolated and harvested tissue. However, it is worth noting that NIR fluorescence imaging can only track the NIR dye but not the drug itself. In the current study, ^{19}F-P and NIR were used as examples of soluble and insoluble drugs to demonstrate a general retention profile of these two types of drugs in the IVD, and confirmed that a proper drug delivery system could prolong their retention in IVD. However, the retention and clearance profile of different molecules varies according to their individual properties and the delivery system used. In future studies, more attention should be paid to the pharmacokinetics and pharmacodynamics of the drugs being tested. These will be different depending on the drug being tested, and can help designing optimal drug delivery systems with improved treatment efficacies.

2. Conclusions and future directions

CLBP is one of the most common musculoskeletal disorder diseases worldwide, and to date, treatments are only available to manage pain in the short term. CLBP is highly related to disc degeneration. Anti-inflammation strategies and regenerative medicine may provide prospective therapeutics to manage pain, halt disc degeneration, and promote disc regeneration. The present thesis contributes to the field with the following highlights.

- Compared to *in vitro* model, *ex vivo* whole IVD culture model is suggested as a better alternative to simulate the *in vivo* environment of IVD cells and bridge the gap between *in vitro* and *in vivo*, improve translatability and reduce animal use.
- IVD is a complex and well-organized tissue. Its structural integrity is necessary to maintain biological and mechanical functions of the IVD. Therefore, repairing the AF is a prerequisite for preventing further disc degeneration and achieving disc regeneration after surgery for disc herniation or AF injury. AF tissue engineering has been proposed a promising strategy for AF repair, and understanding the AF cell biology will facilitate the development of adequate regenerative therapies for AF.

- As the IVD is a relatively self-isolated tissue, treatments could benefit from local drug administration by using controlled drug delivery systems to prolong drug retention, promote therapeutic effects, and prevent systemic side effects.
- Disc degeneration is a multifactorial and complex disease, and the degenerated IVD is presented in a harsh microenvironment. Therefore, a single strategy may not be sufficient to achieve disc regeneration. Combining strategies that address the degenerative process at multiple levels, e.g. anti-inflammatory and anti-catabolic/pro-anabolic will be crucial for developing effective IVD regeneration therapies.

References

[1] D.J. Gorth, I.M. Shapiro, M.V. Risbud, A New Understanding of the Role of IL-1 in Age-Related Intervertebral Disc Degeneration in a Murine Model, J Bone Miner Res 34(8) (2019) 1531-1542.
[2] C. Weiler, A.G. Nerlich, B.E. Bachmeier, N. Boos, Expression and distribution of tumor necrosis factor alpha in human lumbar intervertebral discs: a study in surgical specimen and autopsy controls, Spine (Phila Pa 1976) 30(1) (2005) 44-53; discussion 54.
[3] C.L. Le Maitre, J.A. Hoyland, A.J. Freemont, Catabolic cytokine expression in degenerate and herniated human intervertebral discs: IL-1beta and TNFalpha expression profile, Arthritis Res Ther 9(4) (2007) R77.
[4] M.F. Shamji, L.A. Setton, W. Jarvis, S. So, J. Chen, L. Jing, R. Bullock, R.E. Isaacs, C. Brown, W.J. Richardson, Proinflammatory cytokine expression profile in degenerated and herniated human intervertebral disc tissues, Arthritis Rheum 62(7) (2010) 1974-82.
[5] M. Molinos, C.R. Almeida, J. Caldeira, C. Cunha, R.M. Goncalves, M.A. Barbosa, Inflammation in intervertebral disc degeneration and regeneration, J R Soc Interface 12(104) (2015) 20141191.
[6] Y. Wang, M. Che, J. Xin, Z. Zheng, J. Li, S. Zhang, The role of IL-1beta and TNF-alpha in intervertebral disc degeneration, Biomed Pharmacother 131 (2020) 110660.
[7] Z. Li, Y. Gehlen, F. Heizmann, S. Grad, M. Alini, R.G. Richards, D. Kubosch, N. Sudkamp, K. Izadpanah, E.J. Kubosch, G. Lang, Preclinical ex-vivo Testing of Anti-inflammatory Drugs in a Bovine Intervertebral Degenerative Disc Model, Front Bioeng Biotechnol 8 (2020) 583.
[8] X. Li, F. Lin, Y. Wu, N. Liu, J. Wang, R. Chen, Z. Lu, Resveratrol attenuates inflammation environment-induced nucleus pulposus cell senescence in vitro, Biosci Rep 39(5) (2019).
[9] H.E. Gruber, B. Jones, E. Marrero, E.N. Hanley, Jr., Proinflammatory Cytokines IL-1beta and TNF-alpha Influence Human Annulus Cell Signaling Cues for Neurite Growth: In Vitro Coculture Studies, Spine (Phila Pa 1976) 42(20) (2017) 1529-1537.
[10] T.T. Tsai, A. Guttapalli, E. Oguz, L.H. Chen, A.R. Vaccaro, T.J. Albert, I.M. Shapiro, M.V. Risbud, Fibroblast growth factor-2 maintains the differentiation potential of nucleus pulposus cells in vitro: implications for cell-based transplantation therapy, Spine (Phila Pa 1976) 32(5) (2007) 495-502.
[11] H.S. An, K. Masuda, Relevance of in vitro and in vivo models for intervertebral disc degeneration, J Bone Joint Surg Am 88 Suppl 2 (2006) 88-94.
[12] D. Purmessur, B.A. Walter, P.J. Roughley, D.M. Laudier, A.C. Hecht, J. Iatridis, A role for TNFalpha in intervertebral disc degeneration: a non-recoverable catabolic shift, Biochem Biophys Res Commun 433(1) (2013) 151-6.
[13] R. Maidhof, T. Jacobsen, A. Papatheodorou, N.O. Chahine, Inflammation induces irreversible biophysical changes in isolated nucleus pulposus cells, PLoS One 9(6) (2014) e99621.
[14] W. Yu, J. Fu, Y. Liu, Y. Wu, D. Jiang, Osteogenic protein-1 inhibits nucleus pulposus cell apoptosis through regulating the NF-kappaB/ROS pathway in an inflammation environment, Biosci Rep 38(6) (2018).
[15] H. Ishibashi, H. Tonomura, T. Ikeda, M. Nagae, M. Sakata, H. Fujiwara, T. Tanida, K. Mastuda, M. Kawata, T. Kubo, Hepatocyte growth factor/c-met promotes proliferation, suppresses apoptosis, and improves matrix metabolism in rabbit nucleus pulposus cells in vitro, J Orthop Res 34(4) (2016) 709-16.
[16] G. Lang, Y. Liu, J. Geries, Z. Zhou, D. Kubosch, N. Sudkamp, R.G. Richards, M. Alini, S. Grad, Z. Li, An intervertebral disc whole organ culture system to investigate proinflammatory and degenerative disc disease condition, J Tissue Eng Regen Med 12(4) (2018) e2051-e2061.
[17] F. Wang, F. Cai, R. Shi, X.H. Wang, X.T. Wu, Aging and age related stresses: a senescence mechanism of intervertebral disc degeneration, Osteoarthritis Cartilage 24(3) (2016) 398-408.
[18] S. Roberts, E.H. Evans, D. Kletsas, D.C. Jaffray, S.M. Eisenstein, Senescence in human intervertebral discs, Eur Spine J 15 Suppl 3 (2006) S312-6.
[19] H.E. Gruber, J.A. Ingram, H.J. Norton, E.N. Hanley, Jr., Senescence in cells of the aging and degenerating intervertebral disc: immunolocalization of senescence-associated beta-galactosidase in human and sand rat discs, Spine (Phila Pa 1976) 32(3) (2007) 321-7.

[20] P. Li, Y. Gan, Y. Xu, L. Song, L. Wang, B. Ouyang, C. Zhang, Q. Zhou, The inflammatory cytokine TNF-alpha promotes the premature senescence of rat nucleus pulposus cells via the PI3K/Akt signaling pathway, Sci Rep 7 (2017) 42938.
[21] S. Ashraf, P. Santerre, R. Kandel, Induced senescence of healthy nucleus pulposus cells is mediated by paracrine signaling from TNF-alpha-activated cells, FASEB J 35(9) (2021) e21795.
[22] J.M. Lee, J.Y. Song, M. Baek, H.Y. Jung, H. Kang, I.B. Han, Y.D. Kwon, D.E. Shin, Interleukin-1beta induces angiogenesis and innervation in human intervertebral disc degeneration, J Orthop Res 29(2) (2011) 265-9.
[23] S.M. Richardson, D. Purmessur, P. Baird, B. Probyn, A.J. Freemont, J.A. Hoyland, Degenerate human nucleus pulposus cells promote neurite outgrowth in neural cells, PLoS One 7(10) (2012) e47735.
[24] A. Secerovic, A. Ristaniemi, S. Cui, Z. Li, A. Soubrier, M. Alini, S.J. Ferguson, G. Weder, S. Heub, D. Ledroit, S. Grad, Toward the Next Generation of Spine Bioreactors: Validation of an Ex Vivo Intervertebral Disc Organ Model and Customized Specimen Holder for Multiaxial Loading, ACS Biomater Sci Eng (2022).
[25] S. Junger, B. Gantenbein-Ritter, P. Lezuo, M. Alini, S.J. Ferguson, K. Ito, Effect of limited nutrition on in situ intervertebral disc cells under simulated-physiological loading, Spine (Phila Pa 1976) 34(12) (2009) 1264-71.
[26] G.Q. Teixeira, A. Boldt, I. Nagl, C.L. Pereira, K. Benz, H.-J. Wilke, A. Ignatius, M.A. Barbosa, R.M. Gonçalves, C. Neidlinger-Wilke, A Degenerative/Proinflammatory Intervertebral Disc Organ Culture: An Ex Vivo Model for Anti-inflammatory Drug and Cell Therapy, Tissue Engineering Part C: Methods 22(1) (2015) 8-19.
[27] C.M. Rustenburg, J.W. Snuggs, K.S. Emanuel, A. Thorpe, C. Sammon, C.L. Le Maitre, T.H. Smit, Modelling the catabolic environment of the moderately degenerated disc with a caprine ex vivo loaded disc culture system, Eur Cell Mater 40 (2020) 21-37.
[28] L. Manchikanti, V. Pampati, J.A. Hirsch, Retrospective cohort study of usage patterns of epidural injections for spinal pain in the US fee-for-service Medicare population from 2000 to 2014, BMJ Open 6(12) (2016) e013042.
[29] G.R. Dhakal, P.K. Hamal, S. Dhungana, Y. Kawaguchi, Clinical Efficacy of Selective Nerve Root Block in Lumbar Radiculopathy due to Disc Prolapse, J Nepal Health Res Counc 17(2) (2019) 242-246.
[30] D.J. Baylink, Glucocorticoid-induced osteoporosis, N Engl J Med 309(5) (1983) 306-8.
[31] M.J. Seibel, M.S. Cooper, H. Zhou, Glucocorticoid-induced osteoporosis: mechanisms, management, and future perspectives, Lancet Diabetes Endocrinol 1(1) (2013) 59-70.
[32] C. Nguyen, I. Boutron, G. Baron, K. Sanchez, C. Palazzo, R. Benchimol, G. Paris, E. James-Belin, M.M. Lefevre-Colau, J. Beaudreuil, J.D. Laredo, A. Bera-Louville, A. Cotten, J.L. Drape, A. Feydy, P. Ravaud, F. Rannou, S. Poiraudeau, Intradiscal Glucocorticoid Injection for Patients With Chronic Low Back Pain Associated With Active Discopathy: A Randomized Trial, Ann Intern Med 166(8) (2017) 547-556.
[33] I. Tavares, E. Thomas, C. Cyteval, M.C. Picot, F. Manna, V. Macioce, I. Laffont, Y. Thouvenin, P. Viala, A. Larbi, A. Gelis, A. Dupeyron, Intradiscal glucocorticoids injection in chronic low back pain with active discopathy: A randomized controlled study, Ann Phys Rehabil Med 64(2) (2021) 101396.
[34] C.L. Le Maitre, J.A. Hoyland, A.J. Freemont, Interleukin-1 receptor antagonist delivered directly and by gene therapy inhibits matrix degradation in the intact degenerate human intervertebral disc: an in situ zymographic and gene therapy study, Arthritis Res Ther 9(4) (2007) R83.
[35] W. Tang, Y. Lu, Q.Y. Tian, Y. Zhang, F.J. Guo, G.Y. Liu, N.M. Syed, Y. Lai, E.A. Lin, L. Kong, J. Su, F. Yin, A.H. Ding, A. Zanin-Zhorov, M.L. Dustin, J. Tao, J. Craft, Z. Yin, J.Q. Feng, S.B. Abramson, X.P. Yu, C.J. Liu, The growth factor progranulin binds to TNF receptors and is therapeutic against inflammatory arthritis in mice, Science 332(6028) (2011) 478-84.
[36] H. Ding, J. Wei, Y. Zhao, Y. Liu, L. Liu, L. Cheng, Progranulin derived engineered protein Atsttrin suppresses TNF-alpha-mediated inflammation in intervertebral disc degenerative disease, Oncotarget 8(65) (2017) 109692-109702.

[37] T.W. Evashwick-Rogler, A. Lai, H. Watanabe, J.M. Salandra, B.A. Winkelstein, S.K. Cho, A.C. Hecht, J.C. Iatridis, Inhibiting tumor necrosis factor-alpha at time of induced intervertebral disc injury limits long-term pain and degeneration in a rat model, JOR Spine 1(2) (2018).
[38] S.P. Cohen, D. Wenzell, R.W. Hurley, C. Kurihara, C.C. Buckenmaier, 3rd, S. Griffith, T.M. Larkin, E. Dahl, B.J. Morlando, A double-blind, placebo-controlled, dose-response pilot study evaluating intradiscal etanercept in patients with chronic discogenic low back pain or lumbosacral radiculopathy, Anesthesiology 107(1) (2007) 99-105.
[39] T. Sainoh, S. Orita, M. Miyagi, G. Inoue, H. Kamoda, T. Ishikawa, K. Yamauchi, M. Suzuki, Y. Sakuma, G. Kubota, Y. Oikawa, K. Inage, J. Sato, Y. Nakata, J. Nakamura, Y. Aoki, T. Toyone, K. Takahashi, S. Ohtori, Single Intradiscal Administration of the Tumor Necrosis Factor-Alpha Inhibitor, Etanercept, for Patients with Discogenic Low Back Pain, Pain Med 17(1) (2016) 40-5.
[40] M.A. Tryfonidou, G. de Vries, W.E. Hennink, L.B. Creemers, "Old Drugs, New Tricks" - Local controlled drug release systems for treatment of degenerative joint disease, Adv Drug Deliv Rev 160 (2020) 170-185.
[41] A.R. Tellegen, I. Rudnik-Jansen, M. Beukers, A. Miranda-Bedate, F.C. Bach, W. de Jong, N. Woike, G. Mihov, J.C. Thies, B.P. Meij, L.B. Creemers, M.A. Tryfonidou, Intradiscal delivery of celecoxib-loaded microspheres restores intervertebral disc integrity in a preclinical canine model, J Control Release 286 (2018) 439-450.
[42] T. Wiersema, A.R. Tellegen, M. Beukers, M. van Stralen, E. Wouters, M. van de Vooren, N. Woike, G. Mihov, J.C. Thies, L.B. Creemers, M.A. Tryfonidou, B.P. Meij, Prospective Evaluation of Local Sustained Release of Celecoxib in Dogs with Low Back Pain, Pharmaceutics 13(8) (2021).
[43] G. Vadala, L. Ambrosio, F. Russo, R. Papalia, V. Denaro, Interaction between Mesenchymal Stem Cells and Intervertebral Disc Microenvironment: From Cell Therapy to Tissue Engineering, Stem Cells Int 2019 (2019) 2376172.
[44] Y. Ding, H. Wang, Y. Wang, L. Li, J. Ding, C. Yuan, T. Xu, H. Xu, H. Xie, N. Zhu, X. Hu, H. Fang, S. Tan, Co-delivery of luteolin and TGF-β1 plasmids with ROS-responsive virus-inspired nanoparticles for microenvironment regulation and chemo-gene therapy of intervertebral disc degeneration, Nano Research (2022).
[45] B. Costachescu, A.G. Niculescu, R.I. Teleanu, B.F. Iliescu, M. Radulescu, A.M. Grumezescu, M.G. Dabija, Recent Advances in Managing Spinal Intervertebral Discs Degeneration, Int J Mol Sci 23(12) (2022).
[46] B. Ashinsky, H.E. Smith, R.L. Mauck, S.E. Gullbrand, Intervertebral disc degeneration and regeneration: a motion segment perspective, Eur Cell Mater 41 (2021) 370-380.
[47] X.D. Gao, X.B. Zhang, R.H. Zhang, D.C. Yu, X.Y. Chen, Y.C. Hu, L. Chen, H.Y. Zhou, Aggressive strategies for regenerating intervertebral discs: stimulus-responsive composite hydrogels from single to multiscale delivery systems, J Mater Chem B 10(30) (2022) 5696-5722.
[48] A. Matta, W.M. Erwin, Injectable Biologics for the Treatment of Degenerative Disc Disease, Curr Rev Musculoskelet Med 13(6) (2020) 680-687.
[49] A. Krouwels, J.D. Iljas, A.H.M. Kragten, W.J.A. Dhert, F.C. Oner, M.A. Tryfonidou, L.B. Creemers, Bone Morphogenetic Proteins for Nucleus Pulposus Regeneration, Int J Mol Sci 21(8) (2020).
[50] N. Willems, F.C. Bach, S.G. Plomp, M.H. van Rijen, J. Wolfswinkel, G.C. Grinwis, C. Bos, G.J. Strijkers, W.J. Dhert, B.P. Meij, L.B. Creemers, M.A. Tryfonidou, Intradiscal application of rhBMP-7 does not induce regeneration in a canine model of spontaneous intervertebral disc degeneration, Arthritis Res Ther 17 (2015) 137.
[51] D.A. Wong, A. Kumar, S. Jatana, G. Ghiselli, K. Wong, Neurologic impairment from ectopic bone in the lumbar canal: a potential complication of off-label PLIF/TLIF use of bone morphogenetic protein-2 (BMP-2), Spine J 8(6) (2008) 1011-8.
[52] C.E. Gillman, A.C. Jayasuriya, FDA-approved bone grafts and bone graft substitute devices in bone regeneration, Mater Sci Eng C Mater Biol Appl 130 (2021) 112466.

[53] Y. Guo, C.Y. Tang, X.F. Man, H.N. Tang, J. Tang, C.L. Zhou, S.W. Tan, M. Wang, Y.Z. Feng, H.D. Zhou, Insulin-like growth factor-1 promotes osteogenic differentiation and collagen I alpha 2 synthesis via induction of mRNA-binding protein LARP6 expression, Dev Growth Differ 59(2) (2017) 94-103.
[54] Y. Yuan, R. Duan, B. Wu, W. Huang, X. Zhang, M. Qu, T. Liu, X. Yu, Gene expression profiles and bioinformatics analysis of insulin-like growth factor-1 promotion of osteogenic differentiation, Mol Genet Genomic Med 7(10) (2019) e00921.
[55] G.H. Choi, H.J. Lee, S.C. Lee, Titanium-adhesive polymer nanoparticles as a surface-releasing system of dual osteogenic growth factors, Macromol Biosci 14(4) (2014) 496-507.
[56] S. Vahabzadeh, A. Bandyopadhyay, S. Bose, R. Mandal, S.K. Nandi, IGF-loaded silicon and zinc doped brushite cement: physico-mechanical characterization and in vivo osteogenesis evaluation, Integr Biol (Camb) 7(12) (2015) 1561-73.
[57] B. Li, X.F. Zheng, B.B. Ni, Y.H. Yang, S.D. Jiang, H. Lu, L.S. Jiang, Reduced expression of insulin-like growth factor 1 receptor leads to accelerated intervertebral disc degeneration in mice, Int J Immunopathol Pharmacol 26(2) (2013) 337-47.
[58] R. Osada, H. Ohshima, H. Ishihara, K. Yudoh, K. Sakai, H. Matsui, H. Tsuji, Autocrine/paracrine mechanism of insulin-like growth factor-1 secretion, and the effect of insulin-like growth factor-1 on proteoglycan synthesis in bovine intervertebral discs, J Orthop Res 14(5) (1996) 690-9.
[59] V. Price, P. Wells, M. Tucci, J.A. Cameron, A. Ragab, H. Benghuzzi, Effects of sustained delivery of IGF-1 in a rat degenerative disc model, Biomed Sci Instrum 43 (2007) 384-9.
[60] S.E. Detiger, M.N. Helder, T.H. Smit, R.J. Hoogendoorn, Adverse effects of stromal vascular fraction during regenerative treatment of the intervertebral disc: observations in a goat model, Eur Spine J 24(9) (2015) 1992-2000.
[61] P. Lama, C.L. Le Maitre, I.J. Harding, P. Dolan, M.A. Adams, Nerves and blood vessels in degenerated intervertebral discs are confined to physically disrupted tissue, J Anat 233(1) (2018) 86-97.
[62] M. Stefanakis, M. Al-Abbasi, I. Harding, P. Pollintine, P. Dolan, J. Tarlton, M.A. Adams, Annulus fissures are mechanically and chemically conducive to the ingrowth of nerves and blood vessels, Spine (Phila Pa 1976) 37(22) (2012) 1883-91.
[63] Y. Yokozeki, K. Uchida, A. Kawakubo, M. Nakawaki, T. Okubo, M. Miyagi, G. Inoue, M. Itakura, H. Sekiguchi, M. Takaso, TGF-beta regulates nerve growth factor expression in a mouse intervertebral disc injury model, BMC Musculoskelet Disord 22(1) (2021) 634.
[64] A. Ding, Y.Y. Bian, Z.H. Zhang, SP1/TGFbeta1/SMAD2 pathway is involved in angiogenesis during osteogenesis, Mol Med Rep 21(3) (2020) 1581-1589.
[65] E. Gratacos, N. Checa, E. Perez-Navarro, J. Alberch, Brain-derived neurotrophic factor (BDNF) mediates bone morphogenetic protein-2 (BMP-2) effects on cultured striatal neurones, J Neurochem 79(4) (2001) 747-55.
[66] S. Fang, N. Pentinmikko, M. Ilmonen, P. Salven, Dual action of TGF-beta induces vascular growth in vivo through recruitment of angiogenic VEGF-producing hematopoietic effector cells, Angiogenesis 15(3) (2012) 511-9.
[67] S. Miyazaki, A.D. Diwan, K. Kato, K. Cheng, W.C. Bae, Y. Sun, J. Yamada, C. Muehleman, M.E. Lenz, N. Inoue, R.L. Sah, M. Kawakami, K. Masuda, ISSLS PRIZE IN BASIC SCIENCE 2018: Growth differentiation factor-6 attenuated pro-inflammatory molecular changes in the rabbit anular-puncture model and degenerated disc-induced pain generation in the rat xenograft radiculopathy model, Eur Spine J 27(4) (2018) 739-751.
[68] H. Cui, J. Zhang, Z. Li, F. Chen, H. Cui, X. Du, H. Liu, J. Wang, A.D. Diwan, Z. Zheng, Growth differentiation factor-6 attenuates inflammatory and pain-related factors and degenerated disc-induced pain behaviors in rat model, J Orthop Res 39(5) (2021) 959-970.
[69] A.C. Mitchell, P.S. Briquez, J.A. Hubbell, J.R. Cochran, Engineering growth factors for regenerative medicine applications, Acta Biomater 30 (2016) 1-12.

[70] X. Ren, M. Zhao, B. Lash, M.M. Martino, Z. Julier, Growth Factor Engineering Strategies for Regenerative Medicine Applications, Front Bioeng Biotechnol 7 (2019) 469.
[71] L.M. Caballero Aguilar, S.M. Silva, S.E. Moulton, Growth factor delivery: Defining the next generation platforms for tissue engineering, J Control Release 306 (2019) 40-58.
[72] K.L. Spiller, Y. Liu, J.L. Holloway, S.A. Maher, Y. Cao, W. Liu, G. Zhou, A.M. Lowman, A novel method for the direct fabrication of growth factor-loaded microspheres within porous nondegradable hydrogels: controlled release for cartilage tissue engineering, J Control Release 157(1) (2012) 39-45.
[73] S.H. Moon, K. Nishida, L.G. Gilbertson, H.M. Lee, H. Kim, R.A. Hall, P.D. Robbins, J.D. Kang, Biologic response of human intervertebral disc cells to gene therapy cocktail, Spine (Phila Pa 1976) 33(17) (2008) 1850-5.
[74] O. Krupkova, E. Cambria, L. Besse, A. Besse, R. Bowles, K. Wuertz-Kozak, The potential of CRISPR/Cas9 genome editing for the study and treatment of intervertebral disc pathologies, JOR Spine 1(1) (2018) e1003.
[75] W.C. Watters, 3rd, M.J. McGirt, An evidence-based review of the literature on the consequences of conservative versus aggressive discectomy for the treatment of primary disc herniation with radiculopathy, Spine J 9(3) (2009) 240-57.
[76] E.J. Carragee, M.Y. Han, P.W. Suen, D. Kim, Clinical outcomes after lumbar discectomy for sciatica: the effects of fragment type and anular competence, J Bone Joint Surg Am 85(1) (2003) 102-8.
[77] D.A. Frauchiger, S.R. Heeb, R.D. May, M. Woltje, L.M. Benneker, B. Gantenbein, Differentiation of MSC and annulus fibrosus cells on genetically engineered silk fleece-membrane-composites enriched for GDF-6 or TGF-beta3, J Orthop Res 36(5) (2018) 1324-1333.
[78] Y. Zhou, X. Hu, X. Zheng, Y. Wu, N. Tian, H. Xu, X. Zhang, Differentiation Potential of Mesenchymal Stem Cells Derived from Adipose Tissue vs Bone Marrow Toward Annulus Fibrosus Cells In vitro, Curr Stem Cell Res Ther 12(5) (2017) 432-439.
[79] T. Pirvu, S.B. Blanquer, L.M. Benneker, D.W. Grijpma, R.G. Richards, M. Alini, D. Eglin, S. Grad, Z. Li, A combined biomaterial and cellular approach for annulus fibrosus rupture repair, Biomaterials 42 (2015) 11-9.
[80] T. Nakai, D. Sakai, Y. Nakamura, T. Nukaga, S. Grad, Z. Li, M. Alini, D. Chan, K. Masuda, K. Ando, J. Mochida, M. Watanabe, CD146 defines commitment of cultured annulus fibrosus cells to express a contractile phenotype, J Orthop Res 34(8) (2016) 1361-72.
[81] J.M. Lehmann, B. Holzmann, E.W. Breitbart, P. Schmiegelow, G. Riethmuller, J.P. Johnson, Discrimination between benign and malignant cells of melanocytic lineage by two novel antigens, a glycoprotein with a molecular weight of 113,000 and a protein with a molecular weight of 76,000, Cancer Res 47(3) (1987) 841-5.
[82] M. Trzpis, P.M. McLaughlin, L.M. de Leij, M.C. Harmsen, Epithelial cell adhesion molecule: more than a carcinoma marker and adhesion molecule, Am J Pathol 171(2) (2007) 386-95.
[83] C.H. Lee, F.Y. Lee, S. Tarafder, K. Kao, Y. Jun, G. Yang, J.J. Mao, Harnessing endogenous stem/progenitor cells for tendon regeneration, J Clin Invest 125(7) (2015) 2690-701.
[84] J. Chen, Y. Luo, H. Hui, T. Cai, H. Huang, F. Yang, J. Feng, J. Zhang, X. Yan, CD146 coordinates brain endothelial cell-pericyte communication for blood-brain barrier development, Proc Natl Acad Sci U S A 114(36) (2017) E7622-E7631.
[85] S. Wangler, U. Menzel, Z. Li, J. Ma, S. Hoppe, L.M. Benneker, M. Alini, S. Grad, M. Peroglio, CD146/MCAM distinguishes stem cell subpopulations with distinct migration and regenerative potential in degenerative intervertebral discs, Osteoarthritis Cartilage 27(7) (2019) 1094-1105.
[86] G.G. van den Akker, D.A. Surtel, A. Cremers, S.M. Richardson, J.A. Hoyland, L.W. van Rhijn, J.W. Voncken, T.J. Welting, Novel Immortal Cell Lines Support Cellular Heterogeneity in the Human Annulus Fibrosus, PLoS One 11(1) (2016) e0144497.

[87] R. Nakamichi, Y. Ito, M. Inui, N. Onizuka, T. Kayama, K. Kataoka, H. Suzuki, M. Mori, M. Inagawa, S. Ichinose, M.K. Lotz, D. Sakai, K. Masuda, T. Ozaki, H. Asahara, Mohawk promotes the maintenance and regeneration of the outer annulus fibrosus of intervertebral discs, Nat Commun 7 (2016) 12503.
[88] O.M. Torre, V. Mroz, A.R.M. Benitez, A.H. Huang, J.C. Iatridis, Neonatal annulus fibrosus regeneration occurs via recruitment and proliferation of Scleraxis-lineage cells, NPJ Regen Med 4 (2019) 23.
[89] E. Berthet, C. Chen, K. Butcher, R.A. Schneider, T. Alliston, M. Amirtharajah, Smad3 binds Scleraxis and Mohawk and regulates tendon matrix organization, J Orthop Res 31(9) (2013) 1475-83.
[90] Y. Kishimoto, B. Ohkawara, T. Sakai, M. Ito, A. Masuda, N. Ishiguro, C. Shukunami, D. Docheva, K. Ohno, Wnt/beta-catenin signaling suppresses expressions of Scx, Mkx, and Tnmd in tendon-derived cells, PLoS One 12(7) (2017) e0182051.
[91] G. Chu, C. Shi, H. Wang, W. Zhang, H. Yang, B. Li, Strategies for Annulus Fibrosus Regeneration: From Biological Therapies to Tissue Engineering, Front Bioeng Biotechnol 6 (2018) 90.
[92] M. Yeganegi, R.A. Kandel, J.P. Santerre, Characterization of a biodegradable electrospun polyurethane nanofiber scaffold: Mechanical properties and cytotoxicity, Acta Biomater 6(10) (2010) 3847-55.
[93] L. Yang, R.A. Kandel, G. Chang, J.P. Santerre, Polar surface chemistry of nanofibrous polyurethane scaffold affects annulus fibrosus cell attachment and early matrix accumulation, J Biomed Mater Res A 91(4) (2009) 1089-99.
[94] L.D. Agnol, F.T. Gonzalez Dias, N.F. Nicoletti, A. Falavigna, O. Bianchi, Polyurethane as a strategy for annulus fibrosus repair and regeneration: a systematic review, Regen Med 13(5) (2018) 611-626.
[95] K.G. Turner, N. Ahmed, J.P. Santerre, R.A. Kandel, Modulation of annulus fibrosus cell alignment and function on oriented nanofibrous polyurethane scaffolds under tension, Spine J 14(3) (2014) 424-34.
[96] L. Koepsell, L. Zhang, D. Neufeld, H. Fong, Y. Deng, Electrospun nanofibrous polycaprolactone scaffolds for tissue engineering of annulus fibrosus, Macromol Biosci 11(3) (2011) 391-9.
[97] M. Attia, J.P. Santerre, R.A. Kandel, The response of annulus fibrosus cell to fibronectin-coated nanofibrous polyurethane-anionic dihydroxyoligomer scaffolds, Biomaterials 32(2) (2011) 450-60.
[98] A.P. Peredo, S.E. Gullbrand, H.E. Smith, R.L. Mauck, Putting the Pieces in Place: Mobilizing Cellular Players to Improve Annulus Fibrosus Repair, Tissue Eng Part B Rev 27(4) (2021) 295-312.
[99] A. Dewle, P. Rakshasmare, A. Srivastava, A Polycaprolactone (PCL)-Supported Electrocompacted Aligned Collagen Type-I Patch for Annulus Fibrosus Repair and Regeneration, ACS Appl Bio Mater 4(2) (2021) 1238-1251.
[100] C. Liu, Y. Li, Y. Zhang, H. Xu, The experimental study of regeneration of annulus fibrosus using decellularized annulus fibrosus matrix/poly(ether carbonate urethane)urea-blended fibrous scaffolds with varying elastic moduli, J Biomed Mater Res A 110(5) (2022) 991-1003.
[101] F. Han, Q. Yu, G. Chu, J. Li, Z. Zhu, Z. Tu, C. Liu, W. Zhang, R. Zhao, H. Mao, F. Han, B. Li, Multifunctional Nanofibrous Scaffolds with Angle-Ply Microstructure and Co-Delivery Capacity Promote Partial Repair and Total Replacement of Intervertebral Disc, Adv Healthc Mater (2022) e2200895.
[102] M. Alini, W. Li, P. Markovic, M. Aebi, R.C. Spiro, P.J. Roughley, The potential and limitations of a cell-seeded collagen/hyaluronan scaffold to engineer an intervertebral disc-like matrix, Spine (Phila Pa 1976) 28(5) (2003) 446-54; discussion 453.
[103] C. Liu, Z. Jin, X. Ge, Y. Zhang, H. Xu, Decellularized Annulus Fibrosus Matrix/Chitosan Hybrid Hydrogels with Basic Fibroblast Growth Factor for Annulus Fibrosus Tissue Engineering, Tissue Eng Part A 25(23-24) (2019) 1605-1613.
[104] C. Yan, X. Wang, C. Xiang, Y. Wang, C. Pu, L. Chen, K. Jiang, Y. Li, Applications of Functionalized Hydrogels in the Regeneration of the Intervertebral Disc, Biomed Res Int 2021 (2021) 2818624.
[105] Q. Yu, F. Han, Z. Yuan, Z. Zhu, C. Liu, Z. Tu, Q. Guo, R. Zhao, W. Zhang, H. Wang, H. Mao, B. Li, C. Zhu, Fucoidan-loaded nanofibrous scaffolds promote annulus fibrosus repair by ameliorating the inflammatory and oxidative microenvironments in degenerative intervertebral discs, Acta Biomater 148 (2022) 73-89.

[106] H. Cheng, Q. Guo, H. Zhao, K. Liu, H. Kang, F. Gao, J. Guo, X. Yuan, S. Hu, F. Li, Q. Yang, Z. Fang, An Injectable Hydrogel Scaffold Loaded with Dual-Drug/Sustained-Release PLGA Microspheres for the Regulation of Macrophage Polarization in the Treatment of Intervertebral Disc Degeneration, Int J Mol Sci 24(1) (2022).
[107] R.G. Long, S.J. Ferguson, L.M. Benneker, D. Sakai, Z. Li, A. Pandit, D.W. Grijpma, D. Eglin, S. Zeiter, T. Schmid, U. Eberli, D. Nehrbass, T. Di Pauli von Treuheim, M. Alini, J.C. Iatridis, S. Grad, Morphological and biomechanical effects of annulus fibrosus injury and repair in an ovine cervical model, JOR SPINE 3(1) (2020) e1074.
[108] F. Colella, J.P. Garcia, M. Sorbona, A. Lolli, B. Antunes, D. D'Atri, F.P.Y. Barre, J. Oieni, M.L. Vainieri, L. Zerrillo, S. Capar, S. Hackel, Y. Cai, L.B. Creemers, Drug delivery in intervertebral disc degeneration and osteoarthritis: Selecting the optimal platform for the delivery of disease-modifying agents, J Control Release 328 (2020) 985-999.
[109] E. Botines, L. Franco, J. Puiggali, Thermal stability and degradation studies of alternating poly(ester amide)s derived from glycolic acid and omega-amino acids, Journal of Applied Polymer Science 102(6) (2006) 5545-5558.
[110] D.J. Gorth, J.T. Martin, G.R. Dodge, D.M. Elliott, N.R. Malhotra, R.L. Mauck, L.J. Smith, In vivo retention and bioactivity of IL-1ra microspheres in the rat intervertebral disc: a preliminary investigation, J Exp Orthop 1(1) (2014) 15.
[111] A.N. Tiaden, M. Klawitter, V. Lux, A. Mirsaidi, G. Bahrenberg, S. Glanz, L. Quero, T. Liebscher, K. Wuertz, M. Ehrmann, P.J. Richards, Detrimental role for human high temperature requirement serine protease A1 (HTRA1) in the pathogenesis of intervertebral disc (IVD) degeneration, J Biol Chem 287(25) (2012) 21335-45.
[112] P. Vlieghe, V. Lisowski, J. Martinez, M. Khrestchatisky, Synthetic therapeutic peptides: science and market, Drug Discov Today 15(1-2) (2010) 40-56.
[113] S. Huhmann, B. Koksch, Fine-Tuning the Proteolytic Stability of Peptides with Fluorinated Amino Acids, 2018(27-28) (2018) 3667-3679.
[114] M. Inoue, Y. Sumii, N. Shibata, Contribution of Organofluorine Compounds to Pharmaceuticals, ACS Omega 5(19) (2020) 10633-10640.
[115] R. Martino, V. Gilard, F. Desmoulin, M. Malet-Martino, Fluorine-19 or phosphorus-31 NMR spectroscopy: a suitable analytical technique for quantitative in vitro metabolic studies of fluorinated or phosphorylated drugs, J Pharm Biomed Anal 38(5) (2005) 871-91.
[116] S. Zhang, A. Garcia-D'Angeli, J.P. Brennan, Q. Huo, Predicting detection limits of enzyme-linked immunosorbent assay (ELISA) and bioanalytical techniques in general, Analyst 139(2) (2014) 439-45.
[117] H. Arakawa, H. Yamada, K. Arai, T. Kawanishi, N. Nitta, S. Shibata, E. Matsumoto, K. Yano, Y. Kato, T. Kumamoto, I. Aoki, T. Ogihara, Possible utility of peptide-transporter-targeting [(19)F]dipeptides for visualization of the biodistribution of cancers by nuclear magnetic resonance imaging, Int J Pharm 586 (2020) 119575.
[118] C. Gonzales, H.A. Yoshihara, N. Dilek, J. Leignadier, M. Irving, P. Mieville, L. Helm, O. Michielin, J. Schwitter, In-Vivo Detection and Tracking of T Cells in Various Organs in a Melanoma Tumor Model by 19F-Fluorine MRS/MRI, PLoS One 11(10) (2016) e0164557.
[119] A. Reum Son, D.Y. Kim, S. Hun Park, J. Yong Jang, K. Kim, B. Ju Kim, X. Yun Yin, J. Ho Kim, B. Hyun Min, D. Keun Han, M. Suk Kim, Direct chemotherapeutic dual drug delivery through intra-articular injection for synergistic enhancement of rheumatoid arthritis treatment, Sci Rep 5 (2015) 14713.
[120] I. Rudnik-Jansen, S. Colen, J. Berard, S. Plomp, I. Que, M. van Rijen, N. Woike, A. Egas, G. van Osch, E. van Maarseveen, K. Messier, A. Chan, J. Thies, L. Creemers, Prolonged inhibition of inflammation in osteoarthritis by triamcinolone acetonide released from a polyester amide microsphere platform, J Control Release 253 (2017) 64-72.

[121] R. Weissleder, V. Ntziachristos, Shedding light onto live molecular targets, Nat Med 9(1) (2003) 123-8.
[122] N. Kosaka, M. Ogawa, P.L. Choyke, H. Kobayashi, Clinical implications of near-infrared fluorescence imaging in cancer, Future Oncol 5(9) (2009) 1501-11.
[123] L. Xiao, M. Ding, Y. Zhang, M. Chordia, D. Pan, A. Shimer, F. Shen, D. Glover, L. Jin, X. Li, A Novel Modality for Functional Imaging in Acute Intervertebral Disk Herniation via Tracking Leukocyte Infiltration, Mol Imaging Biol 19(5) (2017) 703-713.

Appendices

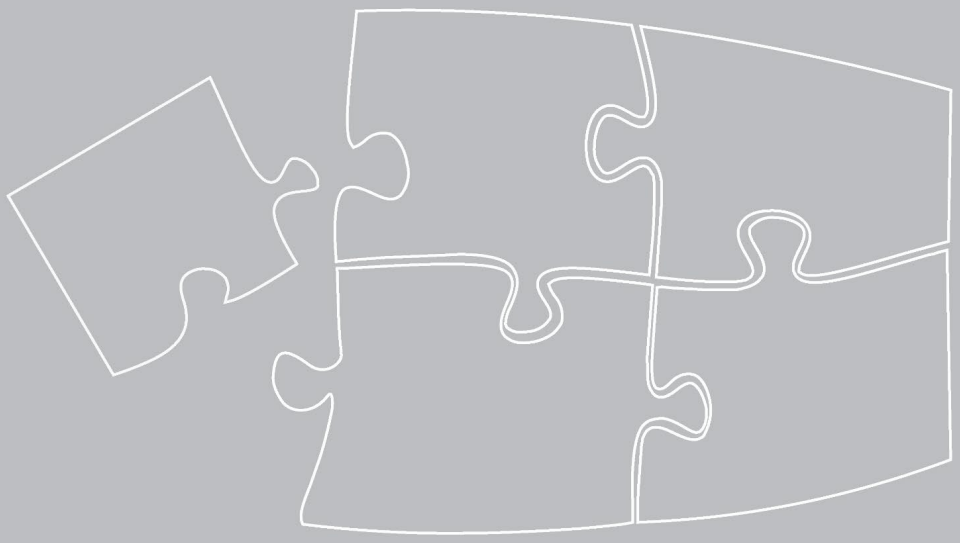

Nederlands Samenvatting

Meer dan 4% van de volwassen bevolking heeft chronisch lage rugpijn (CLR) en dit is zelfs 20% in ouderen. CLR reduceert de kwaliteit van leven en belast de gezondheids- en maatschappelijke zorgvoorziening. Tussenwervelschijfslijtage (TWSS) is de belangrijkste oorzaak van CLR. Tot op heden is de behandeling beperkt tot manieren om de pijn te verminderen, en is er geen behandeling die de TWS regenereert. Er is dus een dringende noodzaak om medische behandelingen te ontwikkelen die niet alleen de pijn remmen, maar ook de slijtage stoppen en herstel van de TWS teweegbrengen. In dit proefschrift worden de achterliggende processen van TWSS verder opgehelderd en mogelijkheden therapeutische strategieën om slijtage te stoppen en regeneratie te bewerkstelligen.

Het is een geaccepteerd gegeven dat ontsteking een cruciale rol speelt in TWSS en discogene lage rugpijn. Daarom wordt het remmen van ontsteking gezien als een zinvolle aanpak om pijn te verlichten en TWSS te remmen. De ontwikkeling van nieuwe medicijnen start meestal in vitro waarmee deze in vivo worden getest. Een goed ex vivo model kan het gat dichten tussen in vitro en in vivo onderzoek, de translatie naar de klinische praktijk verbeteren en het gebruik van proefdieren verminderen. Van diverse ontstekingsmediatoren is het aangetoond dat ze een rol spelen in de ontsteking en pijn in TWSS, waarbij TNF-α als een van de belangrijkste spelers wordt gezien. Daarom is een model van TNF-α-geïnduceerde TWSS ontwikkeld op basis van complete caudale TWS uit de koe, gekweekt in een bioreactor met biomechanische belasting. Daarbij stelden we eerst vast dat humaan recombinant TNF-α (hr TNF-α) dezelfde effecten op nucleus pulposuscellen heeft als runder-TNF-α. Vervolgens werd de optimale dosis van hrTNF-α bepaald voor intradiscale injectie die voldoende ontsteking en afbraak induceerde, zoals vastgesteld aan de hand van de verhoogde afgifte van ontstekingsmediatoren, glycosaminoglycanen (GAGs) en de verhoogde expressie van genen die gerelateerd zijn aan slijtage. Daarbij vonden we dat het tijdstip van ontstekingsremming cruciaal was bij het efficiënt interveniëren in ontsteking en afbraak. Dit model kan gebruikt worden om de mechanismen van TNF-α-geïnduceerde TWSS op te helderen, en daarnaast voor het testen van nieuwe therapeutica die op de TNF-α aangestuurde mechanismen aangrijpen.

Een eerder studie liet zien dat “bone morphogenetic protein”-4 (BMP-4) een potent effect hadden op weefselregeneratie door NP cellen, aangetoond in cokweek met mesenchymale stamcellen en NP cellen. In hoofdstuk 3 werden de effecten van BMP-4 op schapencellen in vitro en in vivo bestudeerd. In vitro werd aangetoond dat BMP-4 celdeling en extracellulaire matrix (ECM) productie door NP en annulus fibrosuscellen (AF) verhoogd was. Opvallend was dat BMP-4 een fenotypeverandering in AF cellen teweegbracht, zoals aangetoond door een verhoogde proteoglycaan- en collageen II productie, componenten die karakteristiek zijn voor de NP. Na intradiscale injectie van BMP-4 in een schapenmodel van TWSS geïnduceerd door een steekwond, werd echter regeneratie van NP noch AF gezien. IN plaats daarvan werd extradiscale botvorming gezien en Schmorl’s node-achtige afwijkingen in de eindplaat. Deze resultaten suggereren dat directe injectie van BMP-4 mogelijk geen valide aanpak is voor het behandelen van TWSS. Meer aspecten moeten onderzocht worden om BMP-4 voor klinische behandeling van TWSS, bijvoorbeeld de manier van toedienen.

Om de functie van de TWS te herstellen is het behoud van zijn structurele integriteit belangrijk. Hoewel de AF een cruciale component is van de TWS, wordt het belang van deze structuur vaak over het hoofd gezien in de ontwikkeling van nieuwe behandelingen. Manieren om AF-schade en defecten te herstellen zijn belangrijk in het voorkomen of tegenhouden van TWSS and voor het bevorderen van regeneratie. In hoofdstuk 4 werden mogelijke AF-achtige scaffolds onderzocht voor hun functionaliteit in vitro en in vivo. We ontdekten dat het voorbehandelen van AF-cellen met TGF- β een functioneel AF-fenotype induceerden die mogelijk AF herstel kan bevorderen, hetgeen werd aangetoond door de verhoging van expressie van diverse relevante genen en een verhoogde contractiliteit. Deze voorbehandelde cellen werden opgenomen in een collageen I hydrogel met toevoeging van TGF-β, wat vervolgens werd geladen op een polyurethaanscaffold om een AF weefselconstruct te bouwen. De collageen I hydrogel ondersteunde het AF fenotype en de TGF-β in de hydrogel bevorderde celdeling en ECM afzetting in vitro. Implantatie van dit construct in een caudale runder-TWS in een bioreactor leidde tot de afzetting van collageen. Deze bevindingen laten zien dat de combinatie van cellen, biomaterialen en bioactieve stoffen veel potentieel heeft voor AF regeneratie.

Karakterisatie van cellen is van vitaal belang voor celgebaseerde behandelingen voor AF regeneratie. CD146 positieve cellen hebben een contractiel fenotype, en TGF-β versterkt dit celfenotype door CD146 expressie te verhogen. Bij elkaar genomen suggereert dit dat CD146 mogelijk een functionele marker is voor het gebruik van cellen in AF weefseltechnologie. Meer kennis van de rol van CD146 in AF cellen en het mechanisme dat ten grondslag ligt aan de regulatie door TGF-β zou het gebruik van deze marker in AF regeneratie kunnen verder brengen. In dit verband vonden we in hoofdstuk 5 dat het uitzetten van de expressie van CD146 in humane AF-cellen contractiliteit verminderde, vergezeld van een remming van expressie van smooth muscle protein 22α (SM22α). Verder hebben we laten zien dat de stimulatie van CD146 expressie door TGF-β via de ALK signaalroute loopt, deels via de SMAD2/4 en AKT pathway, terwijl ERK een remmende werking had. We hebben dus deels de signaalcascades die ten grondslag liggen aan de opregulatie van CD146 door TGF-β in AF cellen opgehelderd die suggereren dat CD146 mogelijk gebruikt kan worden als functionele marker in strategieën voor AF herstel.

Door de geïsoleerde aard van de TWS wordt intradiscale toediening voorgesteld als een wenselijke aanpak om de lokale concentratie en retentie van farmaca te verhogen, en tegelijkertijd systemische bijwerkingen te voorkomen. Kennis van de farmacokinetiek na plaatselijke toediening is van fundamenteel belang om intradiscale toediening te sturen en te ontwikkelen. Echter is dit zelden onderzocht. In hoofdstuk 6 wordt een 19fluorine gelabeld peptide (19F-P) gebruikt als een modelpeptide om retentie in de TWS te bestuderen. In het ex vivo TWS bioreactormodel was er weinig peptide over na een week kweken. In vivo was het peptide niet detecteerbaar 3 maanden na injectie in lumbale TWS' in schapen. Dit duidt erop dat het peptide relatief snel geklaard werd uit de TWS na intradiscale injectie. Daarnaast is IR-780 gebruikt, een molecuul dat fluoresceert in het nabij-infrarode spectrum, als model voor hydrofobe laagmoleculaire farmaca. IR-780 werd geladen in polyesteramide microsferen (PEAM) en toegepast in een rattenmodel van TWSS. Intradiscale retentie werd onderzocht door het NIR signaal te meten, na bolusinjectie en injectie in microsferen in een zowel gezonde als versleten TWS'. Daarnaast werd de afgifte van IR-780 uit PEAMs ook na injectie in de huid en gezonde en artrotische rattenknieën onderzocht. Deze studie heeft afgifte en retentieprofielen in de TWS

bepaald door gebruik te maken van verschillende methodes en modellen. De resultaten lieten zien dat retentie in de TWS kan aangetast worden door slijtage en dat goede medicijnafgiftesystemen retentie in de TWS kunnen verlengen, wat in principe de uitkomsten van behandelingen kan verbeteren.

Abbreviations

^{19}F	^{19}Fluorine
^{19}F MRI	^{19}Fluorine nuclear magnetic resonance imaging
^{19}F NMR	^{19}Fluorine nuclear magnetic resonance spectrum
^{19}F-P	A random peptide was labelled with ^{19}fluorine at N-terminal
AB/PR	Alcian blue and picrosirius red
ACAN	Aggrecan
ADAMTS	A disintegrin and metalloproteinase with thrombospondin motifs
AF	Annulus fibrosus
AKT	Protein kinase B (PKB)
ALK5	Activin receptor-like kinases 5
ANOVA	Analysis of variance
APC	Allophycocyanin
bFGF	Basic fibroblast growth factor
BMPs	Bone morphogenetic proteins
BSA	Bovine serum albumin
CAM	Cell adhesion molecule
CCL4	Hemokine (C-C motif) ligands 4
CD146	Cluster of differentiation 146
CLBP	Chronic low back pain
COL1A1	Collagen type I alpha 1
COL1A2	Collagen type I alpha 2
COL2A1	Collagen type II alpha 1
COX-2	Cyclooxygenase-2
DAPI	4′,6-diamidino-2-phenylindole
DDS	Drug delivery system
DHI	Disc height index
DMEM	Dulbecco's Minimum Essential Medium
DMMB	1,9-dimethyl-methylene blue
DMSO	Dimethyl dulfoxide
DNA	Deoxyribonucleic acid
ECM	Extracellular matrix
EDTA	Ethylenediaminetetraacetic acid
EGFP	Enhanced green fluorescent protein
ELISA	Enzyme-linked immunosorbent assay
ELN	Elastin
EPs	Endplates
ERK	Extracellular signal-regulated kinase
FACS	Fluorescence-activated cell sorting
FAM	Carboxyfluorescein
FBS	Fetal bovine serum

FCS	Foetal calf serum
GAG	Glycosaminoglycan
GAPDH	Glyceraldehyde-3-phosphate dehydrogenase
GDF-8	Growth and differentiation factor-8
H&E	Hematoxylin and eosin
HMDI	1,6-hexamethylene diisocyanate
iAF	Inner AF tissue
IFN-γ	Interferon gamma
IL	Interleukin
ISO	1,4,3,6-dianhydro-D-sorbitol (isosorbide diol)
IVDD	Intervertebral disc degeneration
IVD	Intervertebral disc
JNK	C-Jun N-terminal kinase
Ki-67	Nuclear Ki-67 protein
LBP	Low back pain
MCAM	Melanoma cell adhesion molecule
Micro-CT	Micro-computed tomography
MKX	Mohawk homeobox
MMP	Matrix metalloproteinase
MRI	Magnetic resonance imaging
MSC	Mesenchymal stem cells
NEAA	Nonessential amino acid
NF-κB	Nuclear factor κB
NIR	Near-infrared
NO	Nitric oxide
NP	Nucleus pulposus
OA	Osteoarthritis
oAF	Outer Annulus fibrosus
PBS	Phosphate-buffered saline
PCL	Poly(ε-caprolactone)
PCR	Polymerase chain reaction
PEA	Polyesteramide
PG	Proteoglycan
PU	Polyurethane
qRT-PCR	Quantitative real-time polymerase chain reaction
RNA	Ribonucleic acid
ROCK	Rho-associated protein kinase
RPL19	Ribosomal protein L19
RPLP0	Ribosomal protein lateral stalk subunit P0
Saf-O FG	Safranin-O and fast green
SCX	Scleraxis
SDS-PAGE	Sodium dodecyl-sulfate polyacrylamide gel electrophoresis
shRNA	Short hairpin RNA

SM22α	Smooth muscle protein 22-alpha
SOX-9	SRY-box transcription factor-9
TAMRA	Tetramethylrhodamine
TFA	Trifluoroacetic acid
TGF-β	Transforming growth factor-beta
TNF-α	Tumor necrosis factor-alpha
TRAP	Tartrate-resistant acid phosphatase
VCAN	Versican
αMEM	Alpha minimum essential medium

List of Publications and Manuscripts

Included in this thesis:

Du J, Long RG, Nakai T, Sakai D, Benneker LM, Zhou G, Li B, Eglin D, Iatridis JC, Alini M, Grad S, Li Z. Functional cell phenotype induction with TGF-β1 and collagen-polyurethane scaffold for annulus fibrosus rupture repair. Eur Cell Mater. 2020 Jan 3;39:1-17. doi: 10.22203/eCM.v039a01.

Du J, Pfannkuche JJ, Lang G, Häckel S, Creemers LB, Alini M, Grad S, Li Z. Proinflammatory intervertebral disc cell and organ culture models induced by tumor necrosis factor alpha. JOR Spine. 2020 Jun 19;3(3):e1104. doi: 10.1002/jsp2.1104.

Du J, Guo W, Häckel S, Hoppe S, Garcia JP, Alini M, Tryfonidou MA, Creemers LB, Grad S, Li Z. The function of CD146 in human annulus fibrosus cells and mechanism of the regulation by TGF-β. J Orthop Res. 2022 Jul;40(7):1661-1671. doi: 10.1002/jor.25190.

Du J, Garcia JP, Bach FC, Tellegen AR, Grad S, Li Z, Castelein RM, Meij BP, Tryfonidou MA, Creemers LB. Intradiscal injection of human recombinant BMP-4 does not reverse intervertebral disc degeneration induced by nuclectomy in sheep. J Orthop Translat. 2022 Sep 23;37:23-36. doi: 10.1016/j.jot.2022.08.006.

Jansen IR, **Du J**, Degen NK, Tellegen AR, Wadhwani P, Zuncheddu D, Meij BP, Thies J, Emans P, Mihov G, Garcia JP, Ulrich AS, Grad S, Tryfonidou MA, Ingen H, Creemers LB. Drug retention after intradiscal administration. Manuscript prepared.

Not included in this thesis:

Garcia JP, Utomo L, Rudnik-Jansen I, **Du J**, Zuithoff NPA, Krouwels A, van Osch GJVM, Creemers LB. Association between Oncostatin M Expression and Inflammatory Phenotype in Experimental Arthritis Models and Osteoarthritis Patients. Cells. 2021 Feb 27;10(3):508. doi: 10.3390/cells10030508.

Hu P, **Du J**, Zhang S, Wang T, Li J, Chen G, Zhou G. Oral Administration of Strontium Gluconate Effectively Reduces Articular Cartilage Degeneration Through Enhanced Anabolic Activity of Chondrocytes and Chondrogenetic Differentiation of Mesenchymal Stromal Cells. Biol Trace Elem Res. 2020 Feb;193(2):422-433. doi: 10.1007/s12011-019-01711-9.

Luo L, Zhou Y, Zhang C, Huang J, **Du J**, Liao J, Bergholt NL, Bünger C, Xu F, Lin L, Tong G, Zhou G, Luo Y. Feeder-free generation and transcriptome characterization of functional mesenchymal stromal cells from human pluripotent stem cells. Stem Cell Res. 2020 Oct;48:101990. doi: 10.1016/j.scr.2020.101990.

Zhou Z, Cui S, **Du J**, Richards RG, Alini M, Grad S, Li Z. One strike loading organ culture model to investigate the post-traumatic disc degenerative condition. J Orthop Translat. 2020 Oct 20;26:141-150. doi: 10.1016/j.jot.2020.08.003.

Häckel S, Zolfaghar M, **Du J**, Hoppe S, Benneker LM, Garstka N, Peroglio M, Alini M, Grad S, Yayon A, Li Z. Fibrin-Hyaluronic Acid Hydrogel (RegenoGel) with Fibroblast Growth Factor-18 for In Vitro 3D Culture of Human and Bovine Nucleus Pulposus Cells. Int J Mol Sci. 2019 Oct 11;20(20):5036. doi: 10.3390/ijms20205036.

Xiao T, Zhu JJ, Huang S, Peng C, He S, **Du J**, Hong R, Chen X, Bode AM, Jiang W, Dong Z, Zheng D. Phosphorylation of NFAT3 by CDK3 induces cell transformation and promotes tumor growth in skin cancer. Oncogene. 2017 May 18;36(20):2835-2845. doi: 10.1038/onc.2016.434.

Zhu J, He S, **Du J**, Wang Z, Li W, Chen X, Jiang W, Zheng D, Jin G. Local administration of a novel Toll-like receptor 7 agonist in combination with doxorubicin induces durable tumouricidal effects in a murine model of T cell lymphoma. J Hematol Oncol. 2015 Mar 4;8:21. doi: 10.1186/s13045-015-0121-9.

Acknowledgements (致谢)

Time goes fast, my PhD study is coming to an end. I am lucky because of you, my supervisors, colleagues, friends, and family. My thesis would never have been completed without your help, support, and encouragement. I would like to thank all of you, and a few in particular.

Promotors

My deepest gratitude goes to my promotors, Prof. dr. Marianna A. Tryfonidou, Dr. Laura B. Creemers, Dr. Sibylle Grad. Thank you for your support over these years and your efforts on manuscripts and this thesis. Marianna, you always give me useful comments. Although you are quite busy, you can reply to questions quickly with every detail. I still remember that you helped me to harvest sheep spines which is impressive.
Dear Laura, thank you for offering me the position as a PhD student in your group and extending me many times until finishing this thesis. I learned a lot from you not only the knowledge from our field, but your attitude toward scientific research. It is impressive that you can manage to supervise so many students in our group on different research topics. I really enjoyed all discussions with you about solving scientific questions and appreciated that you would support my ideas and give me the freedom to try. You have been an excellent scientist and supervisor and are making a strong team in our field.
Dear Sibylle, first of all, thank you for all the efforts on this PhD position. Without your support, the position would never have existed. 'Good job' is the most frequent word heard from you. Even though I know it was not such good, it gives me the energy to become better. Although you have been an incredible scientist, you are working hard almost every day. I am pleasantly surprised that there is a person who always gets off later than me when I see the night still on through the window.

Colleagues & friends

I would like to thank all my colleagues at OA Research Institute Davos, the Department of Orthopedics, and RMCU, and a few in particular.

My PhD work started at OA Research Institute Davos. It was an impressive journey at the beginning of my PhD working and living in Davos. Robert, Ursula, and Nora thank you for teaching me lab techniques and keeping the lab well-organized and running smoothly. Thank you, our 'family leaders' Prof. Mauro Alini and Prof. R Geoff Richards, you are not only supporting our scientific research but together us like a family. Thank you Prof. Martin Stoddart for your suggestions on TGF-β signaling. Congratulation for you became our new family leader. Thank you, Prof. David Eglin and your group, for providing me polyurethane scaffolds, hope Marianna and your kids doing well in France. Thanks, Sonja, Judith, and Sebastian, nice to work with you and I am pretty sure you will become excellent doctors. Letizia, Valentina, and Graziana thank you for helping in the lab, I hope you enjoyed your new career in a new environment. Yann, you are so funny, but I enjoyed solving the technic problem of DMMB with you. Thank you for enduring my poor English and for your kind encouragement. Your brain is such active. I believe you will get great achievements in your new career. Daniele, I did not work with you at AO, thank you for your

help in IVD tissue culture, and all the best for your PhD. I enjoyed a lot for our annual group activities, and it is a wonderful and unforgettable memory in my mind.

The TargetCaRe team, it was a pleasure to be one member of you, Andrea, Bernardo, Bradley, Fabio, Federico, Florian, Jacopo, Letizia, Luana, Lucia, Serdar, Yunpeng, Domenico, Sonja, Joao, even only see some of you once during TargetCaRe meeting in Israel. All the best wishes to all of you.

Last four years, I worked at RMCU, Orthopedics. Firstly, I would like to thank our support team and lab technicians Mattie, and Anneloes for offering our nice work environment and keeping the lab running smoothly. Mattie, there is no way to hide from me. Thanks a lot for your help on technical problems, ordering things, and everything I do not know in the lab. Hope you are always 'young'.

As a member of RECUE PhDs. I would like to thank our PhD program managers, Paul and Keon for organizing courses and activities. Thanks to all the RESCUE PhDs, I'm honored to be one of you. Nada, Madison, Leonardo, and Paree thank you for your help and ideas. All the best to all of your work and/or your PhD careers.

Joao, my colleague, and good friend, I met you at TargetCaRe meeting but did not know we would work together at RMCU for years. You are always the first person I go to when I need to help in the lab, also moving places ^_^, sorry about that. You are very smart and always find a solution to a problem. I really appreciate you for the time we were working and talking together. Thank you for liking my cooking and allowing me to thank your help. I remembered that you brought me chocolate when I said I felt depressed. You let me think that you are a big bother of mine, although I am older than you. You have lots of new ideas. I'm still working on one of them. I hope you can achieve outstanding in producing artificial meat, and one day I can have a try. Also thank your brother, Luis, for helping the thesis cover design.

Our Dream Team, it's a pleasure to work with you. Katrin, thank you for your help in the lab and for organizing our team activities and all the chats in the lab, coffee, and lunch time. Yeter, thanks for sharing your traditional food and the cell isolation work from IVDs ^_^. I'm glad you shared your experience with me. You can trust everything will be fine in the end. Jaqueline, you are the only postdoc in our group. Thank you for arranging lots of things. We are proud that you can be an assistant professor at UMC. Carla, I will miss nice parties in your nice house. Remei, thank you for your nice cakes. And Adriano, Chingting, Oscar, Fiona, and Stijn. Thank you for sharing your excellent work and your interesting discussions and feedback on the group meeting. All the best to all of you, and I hope one day can meet somewhere in the world again.

Thank you to all the colleagues from Marianna's group, Saskia, Frances, Lizette, Amir, and Depani, for your help and all the interesting discussions and feedback during the cartilage meetings. Anna, Thank you for your help with MRI scoring.

Hugo, thanks a lot for your help and comments on the ^{19}F NMR project and the manuscript. I said many times, 'It must be the last run', however, the last run is on the way.

时光荏苒，六年的海外博士生涯即将画上句号。我无疑是幸运的，一路走来有老师，同事，朋友和家人的帮助，支持和鼓励。没有你们，这段历程将必然不会如此顺利和充实。在此，向你们表示诚挚的感谢！

在求学的道路上我应该算不上一个好学生。能走到今天离开老师们，耐心，细致，负责的教育和指导，同时也感谢你们对我的包容。“‘野心’是一步一步形成的” 这是我高中班主任黄毅老师说的。这句话里包含这许多层次的含义，我现在的理解是只有你达成现在的目标，才知道未来的目标在哪儿。它能帮我在有些迷茫的时候找到方向。有了方向也未必就能往前多踏一步，毕竟自己的实力还是不允许。所以，庆幸能在研究生阶段郑多教授课题组学到扎实的实验技能，和辩证的科研思维。也感谢毕业后能够加入周光前老师课题组，从事软骨相关研究，能够有更多机会培养研究的自主性。 对于一个英文很少及格的学生来说，应该不会去想有一天要去国外求学并用英文完成自己的学位论文。 “Your English is disqualified as a PhD student.” 这是李真老师改我的第一篇文章的时候说的。我很能理解您当时的感受。 I’m so sorry. 遇到你应该是我能够开始这段博士经历最大的幸运。感谢您能提供给我去 AO 的机会。同时也感谢你在 AO 对我生活上的帮助，研究上的耐心指导，对论文的逐字修改和宝贵的建议。 我知道没有您的帮助和在 AO 的训练，我不可能拿到现在的博士职位。希望您在 AO 工作顺利！替我向刘浩教练问好！也祝福小岸雅，健康快乐成长！

“海内存知己” 在海外也能认识到很多朋友。也有可能是长辈。周治宇博士，现在应该您叫周教授。感谢你在 AO 的照顾，你的经历给了我许多激励。希望你的课题组越来越壮大。马俊轩博士你踏实，认真的态度是我们的榜样。希望你在 AO 能够有更好的发展。郭玮感谢你对我实验的帮助，也感谢你能欣赏的油泼辣子面。很怀恋有你，徐易驰一起徒步，旅游的时光，还有姜楠一起聊天，聚餐，火锅的日子。你们都是医生，让我很羡慕的职业，希望你们都能有很好的职业发展。
来到荷兰实验室最早认识的李洋博士，很高兴能向你请教一些材料和组织芯片领域的知识。更重要的是，感谢你介绍我去乌特华人足球队让我认识了更多的朋友，让我这个伪球迷得以体验足球的乐趣，让训练慢慢成了每周工作之余的期待。 祝你在新的岗位有新的收获。说到球队就不得不感谢我们队长，教练（毅哥）感谢你组织这只球队，为我们带许多欢乐。也感谢你的关怀，让我们的球队更有温度。希望我们的球队越来越来好！也希望你的自己的日子也过得红红火火，多姿多彩！刘超，感谢你在每周五晚带我回家，让我不用担心踢完球还能不能等到公车。祝你们一家人在荷兰，事事顺利！吕俊，我们也是因为踢球认识的， 然后我也聊科研，事业，家庭。虽然也说不上是无话不谈，但也算多了一个谈天论地，吃鸡翅的朋友。希望你回国后有更好的发展，家庭幸福，闺女无忧无虑，健康成长！还有桃子，瑞学，杨超，向辉，阿秋，王豪，Gray,曦晨 以及其它球队的伙伴，感谢你们包容我这个基本规则都不懂的小白。我明白三十岁才开始踢球，应该在球技上没啥希望了^_^。但我知道在球场上你们是认真，所以我需要拼尽全力不能掉链子。祝大家万事顺利，事事顺心！

同在 RMCU 的刘庆武，没少耽误你的时间，和白嫖你们组的试剂。希望你能找到满意的岗位，是金子在哪儿都会发光。叶石成，很高兴能有机会和你交流对科研和事业的想法，有志向的少年，加油！祝福你和王梦，也希望你们家闺女健健康康，快乐成长！还有小乐，智明，正清，谢谢的

帮助和浪费时间陪我漫无边际的闲聊，祝你们早日完胜学业！小乐，替我向张楠问好，很喜欢你们的泡菜锅，还有可爱的芒果。

为学习带娃经验认识了杨超&闪闪，陶卫阳&李伯会，首先感谢你们的答疑解惑，让乐知能平安健康成长，不至于被我们玩坏。同时也感谢你们在事业发展上的经验分享，希望你们在各自的研究领域都有所建树，也祝你们家庭美满，小朋友们茁壮成长！说到遛娃就不得不感谢何桂卫师兄，现在应该叫你何老板。很抱歉在你不知情的情况给你起了外号。从你回国后每个周末的遛娃时间变得格外漫长，很怀恋一起遛娃聊天的日子。希望回深圳后，有更多一起遛娃的自由时间。祝你的课题组壮大，多发好文章，我也得以有机会沾沾光。还有一起组织各种活动，遛娃的黄玲杰&胡聿帅一家，黄艳丽&付世珍一家，曹晶月&郭宗一家，张瑜&殷海涵一家，祝你们在荷兰万事如意，小朋友们都健健康康，开开心心！

最后，当然要感谢我的亲人。我的爸爸，妈妈是你们把我带到这个世界上，养育我，鼓励我走到现在。爸爸你不幸的离开了我们，是我这辈子最大的遗憾。在我的记忆里我们的相处总是短暂的，你一直在四处奔波，支撑起我们的家。但你一直是我内心深处那个最可靠支柱。是你的朴实，善良，鼓励和笑容，影响激励了我。没有文字能够表达我的感激，只希望往后的日子能更多的陪伴妈妈。妈妈你也年纪大了，希望你能够开开心心，少为这个家操劳，我会撑起这个家。也要感谢阳叔陪伴妈妈，为这个家的付出，有你们的地方就是家。祝你们笑口常开，越活越年轻！在我有记忆以来主要爷爷，奶奶，外公，外婆陪伴我长大的。我深知你们这一辈人的艰辛，你们为我们付出的太多，太多。到你们晚年，你们生病的时候，我并没又能够像你们在儿时照顾我一样照顾您，对不起！外婆，祝你健健康康，长命百岁！还有我的岳父，岳母，感谢你们的支持，和鼓励。以后乐知应该不会少烦你们。祝你们，和和睦睦，健健康康！

我的妻子莫翠萍女士，感谢你的付出和陪伴，感谢你能容忍我的坏脾气，想尽办法满足我的四川胃，有你在的日子从来都不至于单调和乏味。结婚以来也并没有给你过上好日子，总是四处奔波。希望以后我们的日子能够更稳定，也有更多精力去实现一些奇思妙想，而不总是受困于柴米油盐。感谢你把乐知带到我们的世界，也感谢你对她的付出。我爱你们♡。小乐知，你已经不是小 baby 了，是大姐姐了。你的到来为我的生活增加多了一份期盼，也多了一份牵挂。感谢你占据了我这三年几乎所有的业余时间，让我发现一个人的时候其实是多么的无聊和没有意义。 爸爸不知道能给你什么，只是希望能花尽可能多的时间陪你长大，你也陪我慢慢变老，然后你能够自由的飞翔。成长是快乐的，是痛苦的，是值得回味的。希望你以后能有更多选择的权力，同时做出正确选择的能力，活出自己精彩的人生。在任何时候爸爸，妈妈都会支持你，我们永远都爱你♡。不过现在你应该什么也不懂，只记得好好玩就好^_^。

Jie DU (杜杰)
April 2023, Utrecht

Curriculum Vitae

Jie Du was born on October 21st 1989, in Yingshan, Sichuan, China. He graduated from high school in 2008. In the same year, he moved to Mianyang to start his bachelor's studies in Biotechnology at the Faculty of Life Science and Technology at Mianyang Normal University. After graduating in 2012, he enrolled as a master's student in Oncology at Medical School at Shenzhen University. He finished his master's study under the supervision of Prof. Dr. Duo Zheng and worked on molecular signaling pathways in lung cancer. After graduating in 2015, he worked in developing *in vitro* diagnostic reagents based on next-generation sequencing in companies. In 2016, he was hired as a research assistant in the Prof. Dr. Guangqian Zhou group at Shenzhen University and worked on osteoarthritis research.

In July 2017, he moved to Switzerland and worked as a research fellow at AO Research Institute, Davos, financially supported by TargetCaRe. In AO, he started working on developing strategies for intervertebral disc (IVD) regeneration, supervised by Dr Sibylle Grad. In June 2019, he moved to The Netherlands to finish his work and pursue a PhD degree in Regenerative Medicine at the Department of Orthopedics at the University Medical Centre Utrecht under the supervision of Prof. Dr. Marianna A. Tryfonidou and Dr. Laura B. Creemers, financially supported by CoFund. His PhD thesis included these two parts of work involved in IVD inflammation, annulus fibrosus repair, growth factor for IVD regeneration, and drug retention in IVD. The results were presented and discussed in this thesis.

Afterward, he wants to go back to Shenzhen, China, to find a postdoc and continually work in academia.